INFORMATION TO USERS

This manuscript has been reproduced from the microfilm master. UMI films the text directly from the original or copy submitted. Thus, some thesis and dissertation copies are in typewriter face, while others may be from any type of computer printer.

The quality of this reproduction is dependent upon the quality of the copy submitted. Broken or indistinct print, colored or poor quality illustrations and photographs, print bleedthrough, substandard margins, and improper alignment can adversely affect reproduction.

In the unlikely event that the author did not send UMI a complete manuscript and there are missing pages, these will be noted. Also, if unauthorized copyright material had to be removed, a note will indicate the deletion.

Oversize materials (e.g., maps, drawings, charts) are reproduced by sectioning the original, beginning at the upper left-hand corner and continuing from left to right in equal sections with small overlaps. Each original is also photographed in one exposure and is included in reduced form at the back of the book.

Photographs included in the original manuscript have been reproduced xerographically in this copy. Higher quality 6" x 9" black and white photographic prints are available for any photographs or illustrations appearing in this copy for an additional charge. Contact UMI directly to order.

UMI

A Bell & Howell Information Company
300 North Zeeb Road, Ann Arbor MI 48106-1346 USA
313/761-4700 800/521-0600

SPECTRAL, TEMPORAL AND VECTORIAL PROPERTIES OF ULTRAFAST OPTICAL PULSE PROPAGATING IN OPTICAL FIBERS

by

QINGDE LIU

A dissertation submitted to the Graduate faculty in Engineering in partial fulfillment of the requirements for the degree of Doctor of Philosophy, The City University of New York

——— 1996 ———

This manuscript has been read and accepted for the Graduate Faculty in Electrical Engineering in satisfaction of the dissertation requirement for the degree of Doctor in Philosophy

3/13/96
Date:

Chairman of the Examining Committee:
Dr. Robert R. Alfano, Distinguished Professor of Science and Engineering, Department of Physics and Electrical Engineering, The City College of The City University of New York.

3/13/96
Date:

Co-Chairman of the Examining Committee:
Dr. Ping P. Ho, Professor, Department of Electrical Engineering, The City College of The City University of New York.

3/25/96
Date:

Executive Officer:
Dr. Gerard Lowen

Dr. Joel Gersten	Professor, Chairman of the Department of Physics, The City College of The City University of New York.
Dr. Yao Li	Adjunct Doctoral Faculty of E.E., CUNY and NEC Research Company.
Dr. Fred Moshary	Associate Professor, Department of Electrical Engineering, The City College of The City University of New York.

Supervisory Committee

The City University of New York

ABSTRACT

SPECTRAL, TEMPORAL AND VECTORIAL PROPERTIES OF ULTRAFAST OPTICAL PULSE PROPAGATING IN OPTICAL FIBERS

by

QINGDE LIU

Thesis Advisors: Prof. R. R. Alfano and Prof. P. P. Ho

The polarization state of light is important for applications and experimental work of the light propagating in optical fibers. In this thesis, a theoretical model for intense laser light pulses propagating in nonbirefringent single-mode optical fibers has been proposed for the first time. Polarization stabilities of linearly and circularly polarized laser pulses propagating in nonbirefringent single-mode optical fibers are analyzed. Nonlinear depolarization and polarization rotation for linearly polarized laser pulses in optical fibers are calculated. The changes of the temporal properties of the propagating laser pulses in single-mode optical fibers are also discussed.

The polarization stabilities for linearly and circularly polarized ultrashort laser pulses propagating in nonbirefringent single-mode fibers were measured. The experimental results and analytical conclusions are in good agreement. Picosecond laser pulses with a duration of 35 ps were used to observe the polarization stabilities of linearly and circularly polarized light pulses.

Nonlinear polarization twisting (NPT) of linearly polarized laser light pulses has been studied using picosecond and femtosecond laser plight pulses propagating in nonbirefringent single-mode optical fibers. The theoretical simulation of the NPT are in

good agreement with the measured results. Nonlinear polarization rotation and depolarization which occurred due to the NPT of linearly polarized light pulses were measured using femtosecond laser light pulses propagating in nonbirefringent single-mode optical fibers. The femtosecond light pulses from a Ti:sapphire laser system had a pulse duration of 120 fs at the wavelength of 780 nm..

The single pulse degenerate cross-phase modulation (DXPM) was measured for its two circularly polarized components of ultrashort laser pulses in single-mode optical fibers. The experimental results has shown that the DXPM process should be considered even for a single laser pulse propagating in an single-mode optical fiber. This result is quiet different with the conventional understanding on XPM in which XPM was thought only to occur between two separated laser pulses.

The DXPM of two physically separated light pulses was investigated for different time delays and pulse intensities in a nonbirefringent single-mode optical fiber. Considering the nonlinear polarization stability of circularly polarized light, two opposite-rotating circularly polarized light pulses were used in the experiment. The DXPM process for light in different modes in a multi-mode optical fiber was also studied in the thesis work. Laser light was coupled into the lowest two propagation modes in a multi-mode fiber (LP_{01} and LP_{11}). Different spectral broadening of LP_{01} and LP_{11} mode at high light intensity was attributed to DXPM process between these two fiber modes. The measured results are in good agreement with the theoretical simulations.

DEDICATION

This thesis is dedicated to my dear wife, Weil Sha

ACKNOWLEDGMENTS

I have been receiving much encouragement, support, and help from many people during my thesis work. I would like deeply to acknowledge and thank them.

My thesis advisors, Professor R. R. Alfano, Distinguished Professor of Science and Engineering, and Professor Ping-pei Ho, have been not only out-standing teachers and capable directors of our large world-renowned institute, but also distinguished scientists with capabilities to search out the frontier research area of nonlinear optics (NLO). It is a great pleasure to acknowledge my deep appreciation for their patient guidance, rigorous training, continued encouragement, numerous invaluable suggestions and discussions during the course of this thesis. I would like to express my special thanks to them for their help in defining this thesis project, correcting the thesis manuscript, and the financial support during this thesis work.

I wish to thank Dr. L. Shi and Dr. S. K. Gayen for their helps and useful discussions. I would like to acknowledge Dr. G. P. Agrawal and Dr. R. -J. Essiambre of Rochester University for their help for simulating the spectra of femtosecond light pulses in a single-mode fiber. I would like also to acknowledge professors J. Gersten, Y. Li, F. Moshary, and Dean G. Lowen for serving on my graduate committee. It is also with great pleasure to acknowledge all colleagues in the Institute of Ultrafast Spectroscopy and Lasers at The City College of New York for their cooperation, kindness, friendship, and help.

I am grateful to Dr. Brian Hendrickson of ARPA & Rome Airforce Development Center and The Center for Advanced Technology (CAT) of New York State for making

this research possible by providing the financial support, suggestions, directions, and enthusiastically following the developments of this research.

I wish to give my special thanks to my dear wife for her love, patience, and help. These help are not only her contribution to my experimental work; but also her understanding and new ideas to my whole research field. Without her tremendous sacrifices and her strong support in the background, I would not have been able to finish this thesis work. I also wish to thank my younger brother for his understanding and considerations which enabled me to pay more attention to this work. I would like to express my sincere appreciation to my mother, my father, and my mother and father in law for their encouragement and support on each step of my career. Especially, it is of great pleasure to thanks my mother and father in law for their love, fondness, and help during their short visit to us.

TABLE OF CONTENTS

LIST OF FIGURES

Chapter I
INTRODUCTION

I.1. Historical Review

An optical fiber confines light into a cylindrical tube. It consists of a central core surrounded by a cladding layer whose refractive index is slightly lower than that of the core. Optical waves can be guided in the optical fiber using the principle of total internal reflection[1-3]. The early optical fibers were extremely lossy (typical loss ~1000 dB/km) and impossible for most practical applications. During the past two decades, the processes in the fabrication technology[4-6] have brought optical fibers having a loss of about 0.2 dB/km near the 1.55 μm wavelength, a loss level limited mainly by the fundamental process of Rayleigh scattering. Such low-loss optical fibers has led to a revolution in the field of optical fiber communications and data transmission[7-10].

The availability of low-loss optical fibers has led not only a revolution in the field of optical fiber communication and high speed data transmission[11-14], but also the advent of a new field of nonlinear fiber optics. Using these optical fibers, nonlinear optical processes[15] have also been investigated extensively because high intensity light can propagate a long distance in the fibers without tremendous attenuation. Nonlinear optical processes are important for ultrashort laser pulses in the fibers because these processes will affect the spectral, temporal, and vector properties of the propagating ultrashort laser pulses. Among several major nonlinear optical processes in the optical fibers, self-phase modulation (SPM) and cross-phase modulation (XPM) are the most important. Since the first observation of supercontinuum generation of picosecond optical pulses by Alfano and Shapiro[16-17], the SPM and XPM processes have been studied for

various types of applications and in different media. In optical fibers, the SPM and XPM processes are particularly important because the light is confined and guided within the core of fibers. The spectral changes induced by SPM have been measured for different type of fibers and wavelengths[18]. XPM processes have been observed by using two optical pulses having the same polarization at different wavelengths[19-20] or the same wavelengths but different polarization states[21]. The latter process is known as degenerate-cross-phase modulation (DXPM).

Other nonlinear optical processes such as Stimulated Raman Scattering (SRS), Four Wave Mixing (FWM), and Stimulated Brillouin Scattering (SBS) in single-mode optical fibers have also been studied both experimentally[22-23] and theoretically[24]. This work stimulated the study of other nonlinear phenomena such as optically induced birefringence[25], parametric four-wave mixing[26-27], and optical soliton[28]. Nonlinear polarization effects in single-mode optical fibers has been studied through the nonlinear induced birefringence[29-31]. Optical solitons have been observed and led to a number of advances in the generation and control of ultrafast optical pulses[32-37].

The research of nonlinear optical processes in fibers has progressed enormously in last two decades. It has led a number of important advances from the understanding of fundamental principles as well as applications. In future, the interest in nonlinear fiber optics is expected to continue on the development of the photonics-based technologies for ultrafast computation, information systems and high-speed data transmission.

I.2. Fundamental of Optical Fibers

The fundamental material of low-loss optical fibers is silica glass formed by fusing SiO_2 molecules. The refractive-index difference between the core and the cladding is realized by the selective use of dopants during the fabrication process. Dopants such as GeO_2 and P_2O_5 increase the refractive index of pure silica and are suitable for the core, while fluorine is primarily used for the cladding because it decreases the refractive index of silica glass.

The basic fiber structure is a central core surrounded by a cladding layer and the refractive index of the cladding is slight lower than that of the core[38]. Two types of the refractive index profiles are used for optical fibers: step-index fibers in which the refractive index has a sudden change from the core to the cladding layer and graded-index fibers in which the refractive index of the core decreases gradually from the center the core boundary. Figure I.1 shows schematically the cross section and the refractive profile of a step-index fiber. Two important parameters which characterize an optical fiber are the numerical aperture NA defined by

$$NA = (n_1^2 - n_2^2)^{1/2}, \tag{I.1}$$

where n_1 and n_2 are the refractive index of the core and the cladding of a fiber, respectively. The normalized frequency V defined by

$$V = k_0 a (n_1^2 - n_2^2)^{1/2}, \tag{I.2}$$

where $k_0 = 2\pi/\lambda$, a is the core radius, and λ is the wavelength of the light. The numerical aperture determines the coupling efficiency of light into an optical fiber. For most of the

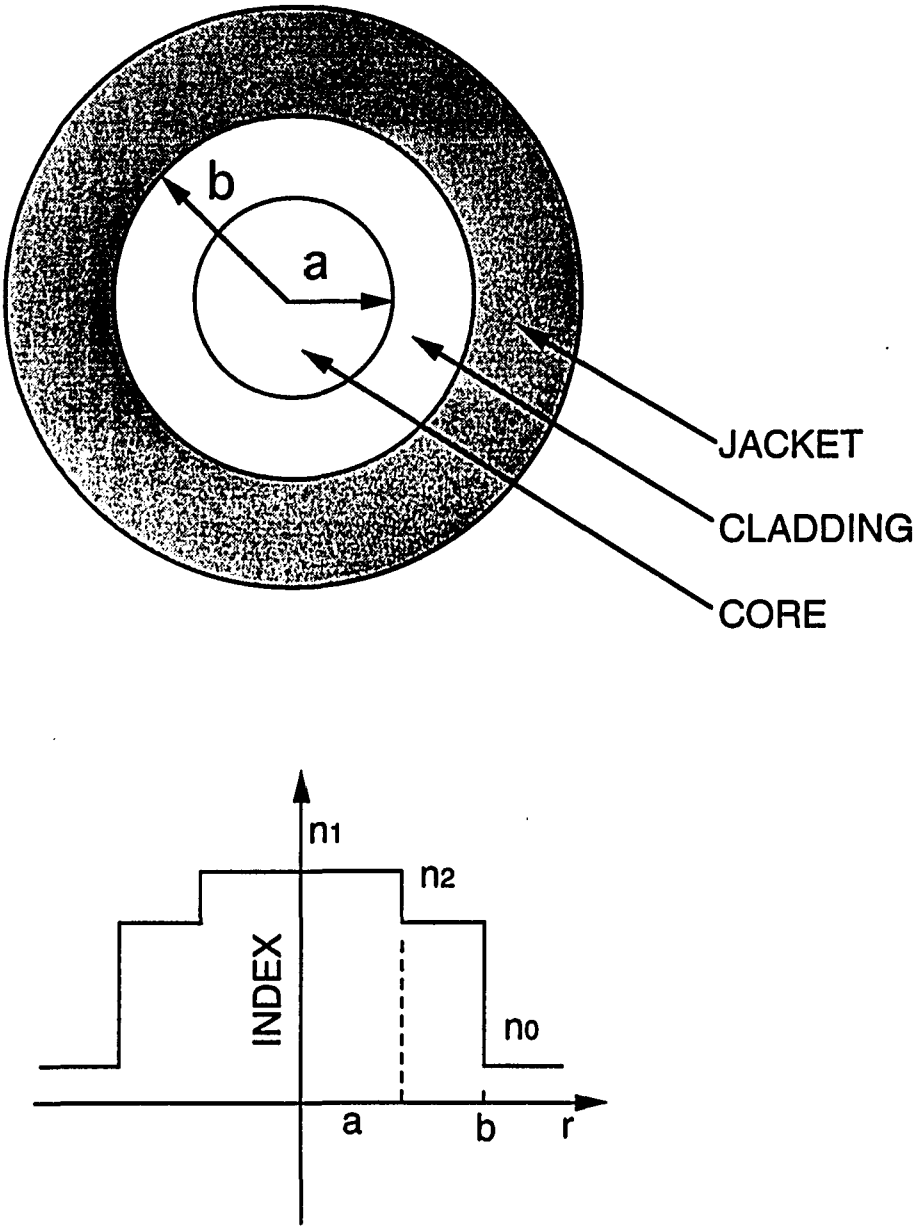

Figure. I.1 Schematic digram of the cross section of the refractive index profile of a step-index optical fiber.

optical fibers, the values of NA is more or less 0.1. The parameter V determines the number of the optical modes propagating in the fiber. For a step-index optical fiber, it will be single-mode if $V < 2.405$. The main difference between single- and multi-mode fiber is the core size. The core size is usually 25~30 μm for typical multi-mode optical fibers. Single-mode optical fiber has a typical core size of 2~4 μm.

From Eqs. (I.1) and (I.2), the light propagation mode in an optical fiber depends on the normalized frequency V. When V increases, the number of the modes propagating in the fiber also increases. The normalized frequency V is a function of the fiber diameter and the numerical aperture (NA). To increase the fiber diameter or the numerical aperture, the value of V will be increased. Therefore, the number of the propagation mode in a fiber will be increased accordingly. For $V<2.405$, there only one lowest propagation mode allowed in the fiber and this type of fiber is called single-mode optical fiber. The cross-section light intensity distribution in this fiber is a typical Gaussian distribution around the center of the fiber. For a multi-mode optical fiber which possess a $V>2.405$, many propagation modes can exist simultaneously in a fiber depending the value of V. Each propagation mode has different cross-section intensity distribution. The output intensity distribution of light will be a superposition of all allowed propagation modes

When light wave propagates in an optical fiber, several dispersions from different sources will affect the property of the light. One most important is the group-velocity dispersion (GVD) which is the refractive index as a function of the light wavelength as shown in Figure I.2. This kind of dispersion is extremely critical for ultrashort laser pulses because it will affect the pulse shape and duration. Mathematically, the light propagation constant β can be expanded in a Taylor series about the center frequency ω_0:

$$\beta(\omega) = n(\omega)\frac{\omega}{c} = \beta_0 + \beta_1(\omega - \omega_0) + \frac{1}{2}\beta_2(\omega - \omega_0)^2 + \ldots, \qquad \text{(I.3)}$$

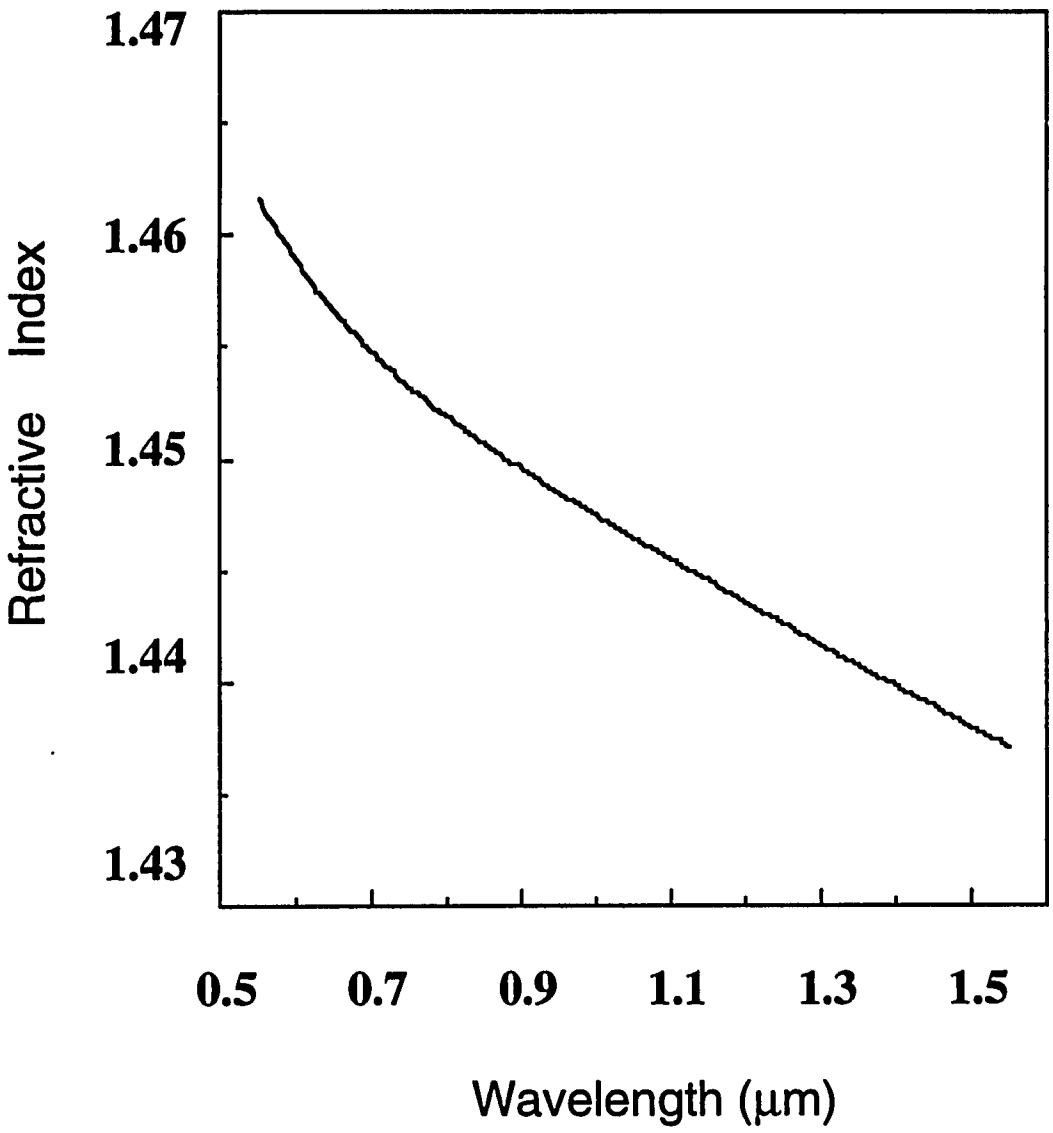

Figure I.2 The refractive index n as afunction of wavelength for fused siliuca glass.

where $1/\beta_1$ is the group velocity, β_n ($n > 2$) are the high order dispersion. If the optical fibers are multi-mode, some other kind of dispersion such as inter-mode dispersion and waveguide dispersion will be introduced[38]. The dispersions for different wavelength and different modes of optical waves propagating in optical fibers will affect the temporal properties of the light and are specially important for ultrashort laser pulses.

Many applications of optical fibers require the preservation of the polarization state of the input optical wave. The optical fiber having a core shape of circular cross section can not maintain the input polarization state for a long distance because the fluctuation of core shape, the stress-induced anisotropy, a twist, and the scattering from a defect will change the polarization state of the optical wave. The optical fibers with intrinsic birefringence have been developed. This kind of optical fiber is anisotropic. The mode-propagation constants β become slightly different for the modes polarized in the x and y directions. The degree of modal birefringence B is given[39-40] by:

$$B = \frac{|\beta_x - \beta_y|}{k_o} = |n_x - n_y|, \qquad \text{(I.4)}$$

where n_x and n_y are the effective indices in the two orthogonal polarization states. The refractive index of silica glass which is used as the fundamental material of most optical fibers is about 1.5 and will change slightly with the concentration of dopants. The axis along which the effective index is smaller is called fast axis as the group velocity is larger for light propagating in that direction. Likewise, the axis with the larger index is called the slow axis. When the light propagates along the fiber, the polarization state will change periodically in the propagation. The length of period is generally referred as the beat length L_B. The beat length can be obtained as:

$$L_B = \frac{2\pi}{|\beta_x - \beta_y|} = \frac{\lambda}{B}, \qquad \text{(I.5)}$$

This length (L_B) means the periodical distance of the change of polarization state for light propagating in the birefringent fiber. Figure I.3 shows schematically the evolution of polarization over one beat length of a birefringent fiber. The state of polarization changes over half of the beat length from linear to elliptic, elliptic to circular, circular to elliptic, and then back to linear but rotated by 90o from the incident linear polarization. The process is repeated over the remaining half of the beat length such that the initial state is recovered at $z=L_B$ and its multiples. The beat length is ~1cm for a strongly birefringent fiber with $B=10^{-4}$.

Another important parameter is a measure of power loss during transmission of optical wave inside a fiber. If P_o is the power coupled into an optical fiber with a length of L, the transmitted power P_T is given by:

$$P_T = P_o \exp(-\alpha L), \qquad \text{(I.5)}$$

where α is the attenuation constant referred to the fiber loss. A more popular expression for the fiber loss is the unit of dB/km by using the relation[38]:

$$\alpha_{dB} = -\frac{10}{L}\log[\frac{P_T}{P_o}] = 4.343\alpha. \qquad \text{(I.6)}$$

The fiber loss is a function of light wavelength. As shown in Figure I.4, it is a typical loss curve in single-mode optical fibers. The solid curve in Figure I.4 is the measured loss profile and the dashed curve is the intrinsic loss profile of the fused silica. Several factors

contribute to the loss spectrum, material absorption and Rayleigh scattering are dominant. Impurity such as OH enhances the fiber absorption, and loss. This effect causes a peak for the fiber loss at the light wavelength of 1.4 μm as shown in Figure I.4. The two minimum loss wavelength of around λ_1=1.3 μm and λ_2=1.5 μm are important in the applications such as the transmission of the light signal over a long distance for communication in an optical fiber. As a matter of fact, most fiber communication systems are working at the either one of these two wavelengths considering the fiber loss and the fiber dispersion.

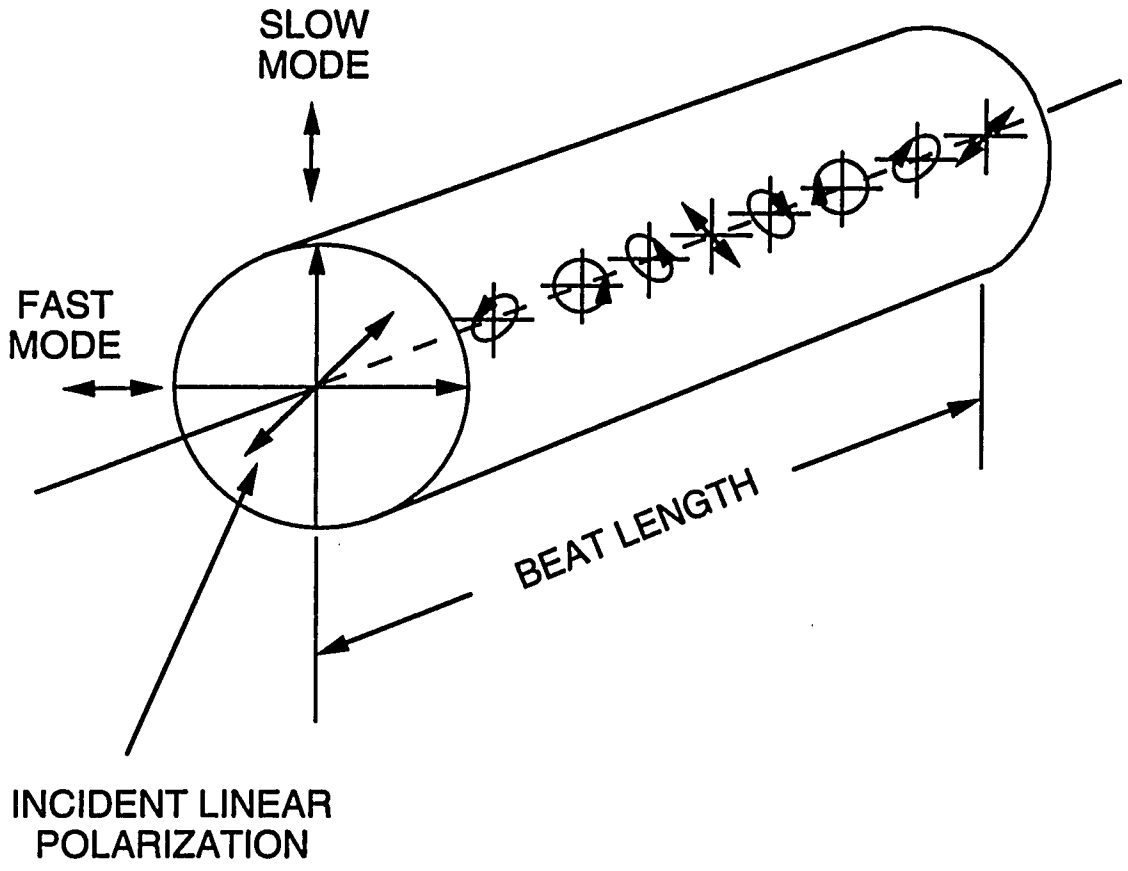

Figure I.3 Schematic illustration of the evolution of light polarization along a birefringent fiber when the input beam is linearly polarized at 45 degree with respect to the slow and fast axes.

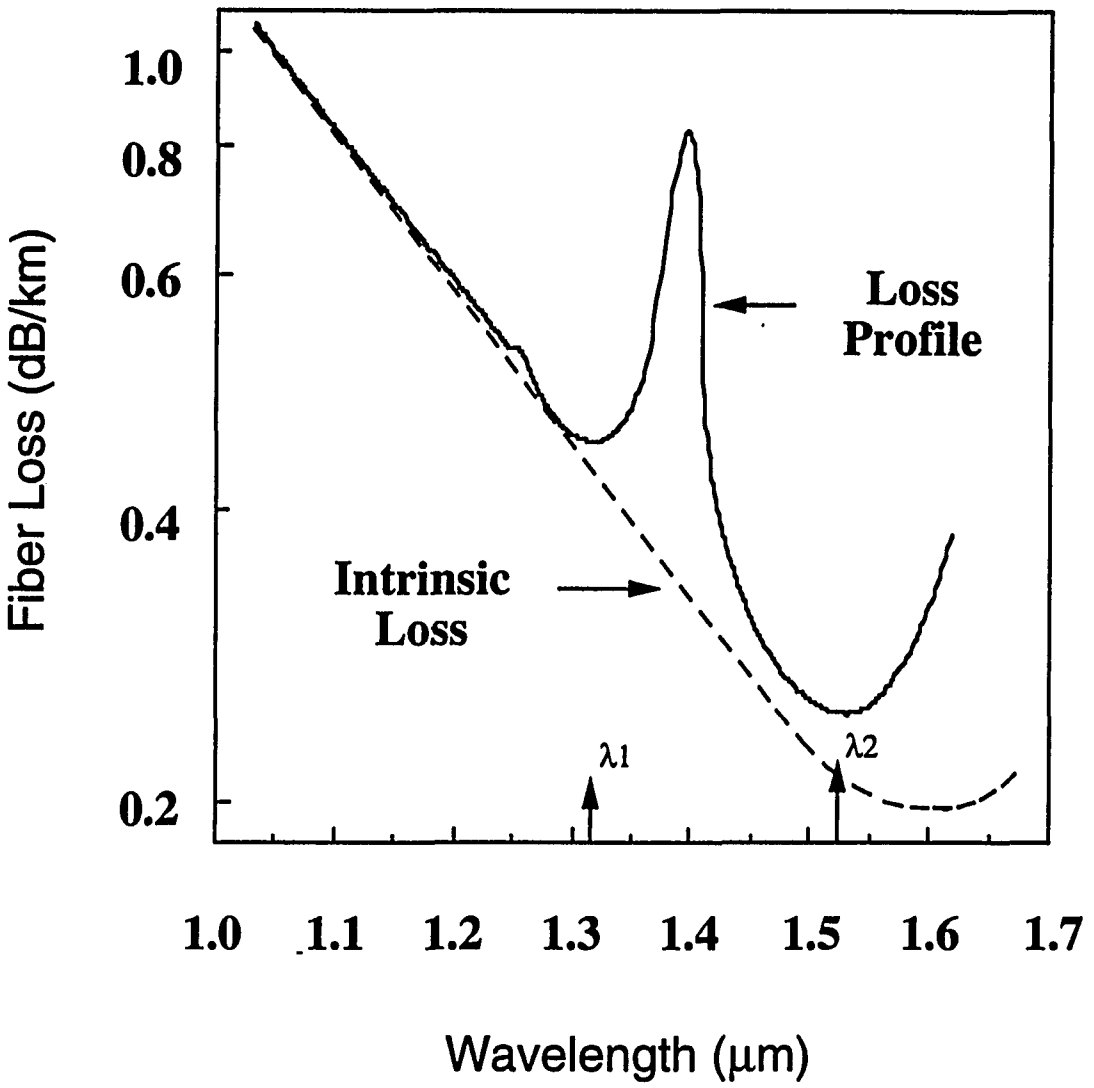

Figure I.4 The loss measured profile of a single-mode optical fiber. Dash curve shows the intrinsic loss profile resulting from Rayleigh scattering and absorption in pure silica glass.

I.3. Nonlinear Processes and Applications in optical fibers

The response of optical fibers to light becomes nonlinear for intense electromagnetic field. Basically, the nonlinear response is resulted from the distortion of the electronic structure in the material under the influence of an intense optical field. The induced polarization **P** of the electric dipoles is not linear to the applied electric field **E** and can be expressed as[1]:

$$\vec{P} = \varepsilon_0(\chi^{(1)}.\vec{E} + \chi^{(2)}.\vec{E}\vec{E} + \chi^{(3)}.\vec{E}\vec{E}\vec{E} + \ldots), \qquad \text{(I.7)}$$

where ε_0 is the vacuum permittivity and $\chi^{(i)}$(i = 1, 2, 3 ,...) is the ith order susceptibility. To account for the light polarization effect, $\chi^{(i)}$ is a tensor of rank $i+1$. The linear susceptibility $\chi^{(1)}$ represents the dominant contribution to $\vec{P}$. Its effects are included through the refractive index n and the attenuation coefficient α. The second-order susceptibility $\chi^{(2)}$ is responsible for nonlinear effects such as second-harmonic generation and parametric oscillation. It is non zero only for the media that lack an inversion symmetry at the molecular level. Since SiO2 is a symmetric molecular, $\chi^{(2)}$ vanishes for silica glasses. As a result, optical fibers made of fused silica glasses do not normally show second-order nonlinear effects. The lowest-order nonlinear effects in optical fiber originate from the third-order susceptibility $\chi^{(3)}$ which is responsible for phenomena such as third-harmonic generation, four-wave mixing, and nonlinear refraction. However, unless special efforts are made to achieve phase matching, the nonlinear processes which involve the generation of new frequencies(e. g. third-harmonic generation or four-wave mixing) are not efficient in optical fibers. Most of the nonlinear effects in optical fibers therefore are from nonlinear refraction, a phenomenon that refers to the intensity dependence of the refractive index resulting from the contribution of $\chi^{(3)}$. The refractive index of an isotropic material possessing nonlinearity can be written as:

$$n(\omega) = [\varepsilon(w)]^{1/2} = n_0(\omega) + n_2 I, \qquad (I.8)$$

where $n_0(\omega)$ is the linear refractive index and n_2 is nonlinear refractive index.

The refractive index change, $n_2 I$, imposes a phase modulation on the laser pulses which causes spectral broadening. When the phase modulation happens to the laser pulse itself, the process is called self-phase-modulation (SPM). When the phase modulation occurs to the copropagating pulses, the process is called cross-phase-modulation (XPM). SPM and XPM cause the spectral broadening of the propagating laser pulses[41]. This spectral broadening also change the temporal profiles of the laser pulses through the chromatic dispersion. Another effect of these phase modulations is the intensity-dependent polarization states of the propagating laser pulses. This nonlinear polarization change has been investigated in nonbirefringent single-mode optical fibers[42].

Using third-order nonlinear processes, light can be used to control light for the ultrafast optical signal processing. Some application such as switches[43], logic-gates[44-45], amplifiers[46-47], and multiplexer/demultiplexer[48] based on the optical Kerr effect in nonlinear waveguides. As the development of optical communication and information technology, high speed optical analog to digital (A/D converter) converter has been drawing considerable interests. Due to its intrinsic parallel and high speed characteristics, all optical A/D converter has wide range of potential applications in optical computation. They are also needed to handle real-time data for signal processing applications such as spread spectrum communication, lidar, fiber-optic sensors, etc. Because of the increased use of fiber-optic sensors and fiber-optic communications, signals applied to an optical signal processor are often optical, and thus optical A/D converter should handle optical input signals directly and be very fast.

For an all-optical A/D converter, an input light intensity analog signal is first converted into changes in certain light properties, such as the spectral distribution, through the nonlinear light-medium interaction. An encoder is then used to encode the property changes into the digital signal. Among several types of A/D converters based on different mechanism and techniques[49-53], an all-optical A/D converter using the cross-phase modulation (XPM) for the spectral encoding is a promising one for the ultrafast applications[54]. In an XPM based A/D converter, carrier and signal light waves interact in a third-order nonlinear medium causing the phase structure of the carrier beam changed. This phase structure change imposes a change in its spectrum, or spatial distribution by a grating or a prism. This spatial distribution has the characteristics of monotonously-varying according to the light intensity with some modulation structure. A binary encoder is used to convert the spatial distribution into binary codes for A/D processing.

Another application of the nonlinear optical processes in the fibers is the all-optical amplifier. Because of the increasing uses of optical waves in communication and computation technologies, the processing signals are often optical. All-optical devices have stimulated great interests in many application fields. One important device is the direct optical amplification that is all-optical amplifier. The all-optical amplifiers are needed to handle the real-time data in optical signal processing applications such as spread-spectrum communication, lidar, computation and fiber-optical sensors. Several different type of all-optical amplifications such as Stimulated-Raman amplifiers[55], diode-laser amplifiers[56] and erbium-doped fiber amplifiers[57-48] have been developed. Using optical Kerr effect in a low-birefringent single-mode optical fiber, a modulational gain at the perpendicularly polarizing direction of linearly polarized laser pulses has been

observed at high input laser intensity. A broadband all-optical amplifier has been proposed using the optical Kerr effect[59].

I.4. Thesis Statement

The thesis research has focused on measuring and modeling the spectral, vectorial and temporal properties of ultrafast optical pulses propagating in non-birefringent single-mode optical fibers for understanding and improving the spectral encoding of intensity of an optical pulse using $\chi^{(3)}$ processes for an ultrafast optical A/D converter. The accuracy of the XPM spectral encoding will be measured and theoretically modeled based on nonlinear vector rotation and depolarization. The following five topics have been investigated to accomplish my goal in this thesis work:

(1). Nonlinear polarization stabilities of linearly and circularly polarized ultrashort laser pulse propagating in short non-birefringent single-mode optical fibers;

(2). Nonlinear polarization rotation and depolarization of ultrashort optical pulses propagating in single-mode optical fibers;

(3). Nonlinear polarization twisting of ultrashort laser pulses in non-birefringent single-mode optical fibers;

(4). Single-pulse degenerate-cross-phase modulation (DXPM) in single-mode optical fibers for ultrashort circularly and linearly polarized laser pulses;

(5). Two-pulses DXPM processes in single-mode optical fibers by using two circularly polarized optical pulses with different time delays and laser intensities;

In Chapter II, the conventional theories for self-phase modulation (SPM) and cross-phase modulation (XPM) are discussed under different polarization bases. A theoretical model for ultrashort laser pulses propagating in nonbirefringent single-mode optical is proposed. The spectral broadening caused by SPM and XPM is simulated in optical fibers. Polarization stabilities of linearly and circularly polarized laser pulses propagating in nonbirefringent single-mode optical fiber are analyzed. Nonlinear

depolarization and polarization rotation for linearly polarized laser pulses in optical fibers are calculated. The changes of the temporal properties of the propagating laser pulses in single-mode optical fibers are also discussed.

The experimental methods and set-ups are described in Chapter III. Ultrashort laser pulses with pulse durations of 35 ps and 100 fs are used in the investigations. Streak camera and cross correlator are used to measure the temporal profiles of the laser pulses. The spectral measurements are carried out using spectrometers and CCD cameras. The optical fibers had an attenuation of 20 dB/km which can be neglected for short optical fibers (~1m) in the experiment.

The polarization stabilities for linearly and circularly polarized ultrashort laser pulses propagating in nonbirefringent single-mode fibers were measured. The experimental results and analytical conclusions were described in Chapter IV. Picosecond laser pulses with a duration of 35 ps were used to observe the polarization stabilities of linearly and circularly polarized pulses.

Nonlinear polarization twisting (NPT) of linearly polarized laser light pulses was studied in Chapter V. Picosecond and femtosecond laser plight pulses were used to demonstrate NPT in nonbirefringent single-mode optical fibers. The theoretical simulation of the NPT are in good agreement with the measured results. Nonlinear polarization rotation and depolarization of linearly polarized light pulses was investigated in Chapter VI using femtosecond laser light pulses propagating in nonbirefringent single-mode optical fibers. The femtosecond light pulses from a Ti:sapphire laser system had a pulse duration of 120 fs at the wavelength of 780 nm..

In Chapter VII, the single pulse degenerate cross-phase modulation (DXPM) of ultrashort laser pulse in single-mode optical fibers was measured. The experimental results has shown that the DXPM process should be considered even for a single laser pulse propagating in an single-mode optical fiber. This result is quiet different with the conventional understanding on XPM in which XPM was thought only to occur between two separated laser pulses. To observe the single light pulse DXPM process, picosecond light pulses were coupled into a nonbirefringent single-mode optical fiber. Using femtosecond light pulses, DXPM processes were observed in high-birefringent and nonbirefringent single-mode optical fibers. The DXPM of two physically separated light pulses was investigated for different time delays and pulse intensities in a nonbirefringent single-mode optical fiber. Considering the nonlinear polarization stability of circularly polarized light, two opposite-rotating circularly polarized light pulses were used in the experiment. The DXPM process for light in different modes in a multi-mode optical fiber was also studied in this chapter. Laser light was coupled into the lowest two propagation modes in a multi-mode fiber (LP_{01} and LP_{11}). Different spectral broadening of LP_{01} and LP_{11} mode at high light intensity was attributed to DXPM process between these two fiber modes. The measured results are in good agreement with the theoretical simulations.

The future research directions related to this thesis work are discussed in Chapter VIII. An all-optical amplifier is proposed. Using SPM and XPM in a nonbirefringent single-mode optical fiber, all-optical amplification system is possible. The characteristic curves and gain of this optical amplifier was calculated. An all-optical amplifier may be needed in the optical communication and computation system in the future.

References

[1]. A. C. S. Van Heel, Nature **173**, 39 (1954).

[2]. N. S. Kapany, J. Opt. Soc. Am. **49**, 779 (1959).

[3]. N. S. Kapany, *Fiber Optics: Principles and Applications* (Academic, New York, 1967)

[4]. D. N. Payne and W. A. Gambling, Electron. Lett., **10**, 289 (1974).

[5]. W. G. French, J. B. McChesney, P. B. O'Connor and G. W. Tasker, Bell Sys. Tech. J., **53**, 951 (1974).

[6]. T. Miya, Y. Terunuma, T. Hosaka and T. Miyoshita, Electron. Lett., **15**, 106 (1979).

[7]. Y. Suematsu, Proc. IEEE **71**, 692 (1983).

[8]. T. Li, IEEE J. Sel. Areas Commun. **SAC-1**, 356 (1983).

[9]. E. E. Basch, ed., *Optical Fiber Transmission* (Sams, Indianapolis, 1986).

[10]. S. E. Miller and I. P. Kaminow, eds., *Optical Fiber Telecommunications II* (Academic, Boston, 1989).

[11]. Y. Suemastu, Proc. IEEE, **71**, 692 (1983).

[12]. T. Li, IEEE, J. Sel. Areas Commun., **SAC-1**, 356 (1983).

[13]. E. E. Basch, ed., *Optical Fiber Transmission*, (Sams, Indianapolis, 1986).

[14]. S. E. Miller, and I. P. Kaminow, eds., *Optical Fiber Telecommunication II*, (Academic, Boston, 1988).

[15]. G. P. Agrawal, ed., *Nonlinear Fiber Optics* (Academic Press, New York, 1989).

[16]. R. R. Alfano and Shapiro, Phys. Rev. Lett. **24**, 584, (1970).

[17]. R. R. Alfano and Shapiro, Phys. Rev. Lett. **24**, 592, (1970).

[18] Q. Z. Wang, Q. D. Liu, P. P. Ho and R. R. Alfano, J. Opt. Soc. Am. B **11**, 1084 (1994).

[19]. M. N. Islam, L. F. Mollenauer, R. H. Stolen, J. R. Simpson, H. T. Shang, Opt. Lett. **12**, 625 (1987).

[20]. P. L. Baldeck, R. R. Alfano and G. P. Agrawal, Appl. Phys. Lett. **52**, 1939 (1988).

[21]. Q. Z. Wang, P. P. Ho and R. R. Alfano, Opt. Lett. **15**, 1023 (1990).

[22]. R. H. Stolen, E. P. Ippen and A. R. Tynes, Appl. Phys. Lett., **20**, 62 (1972).

[23]. E. P. Ippen and R. H. Stolen, Appl. Phys. Lett., **21**, 539 (1972).

[24]. R. G. Smith, Appl. Opt., **11**, 2489 (1972).

[25]. R. H. Stolen and A. Ashkin, Appl. Phys. Lett., **22**, 294 (1973).

[26]. R. H. Stolen, J. E. Bjorkholm and A. Ashkin, Appl. Phys. Lett., **24**, 308 (1974).

[27]. R. H. Stolen, IEEE J. Quantum Electron. **QE-11**, 100 (1975).

[28]. L. F. Mollenauer, R. H. Stolen and J. P. Gordon, Phys. Rev. Lett., **45**, 1095 (1980).

[29]. H. G. Winful, Opt. Lett., **11**, 33 (1986).

[30]. S. F. Feldman, D. A. Weinberger, and H. G. Winful, Opt. Lett., **15**, 311 (1990).

[31]. S. Trillo, S. Wabnitz, R. H. Stolen, G. Assanto, C. T. Seaton, and G. I. Stegeman, Appl. Phys. Lett., **49**, 1224 (1986).

[32]. L. F. Mollenauer, R. H. Stolen, and J. P. Gordon, Phys. Rev. Lett., **45**, 1095 (1980).

[33]. L. F. Mollenauer, and R. H. Stolen, Opt. Lett., **9**, 13 (1984).

[34]. L. F. Mollenauer, J. P. Gordon, and M. N. Islam, IEEE J. Quantum Electron., **QE-22**, 157 (1986).

[35]. M. N. Islam, L. F. Mollenauer, R. H. Stolen, and J. R. Simpson, and H. T. Shang, Opt. Lett., **12**, 814 (1987).

[36]. A. S. Gouveia-Neto, A. S. L. Gomes, and J. R. Taylor, Opt. Quantum Electron., **20**, 165 (1988).

[37]. J. D. Kafka, and T. Baer, Opt. Lett., **12**, 181 (1987).

[38]. P. J. Dean ed., *Optical Communication Systems* (Prentice Hall International, UK, 1984)

[39]. R. H. Stolen, V. Ramaswamy, P. Kaiser and W. Pleibel, Appl. Phys. Lett., **33**, 699 (1978).

[40]. I. P. Kaminow, IEEE J. Quantum Electron. **QE-17**, 15 (1981).

[41]. Q. Z. Wang, Q. D. Liu, P. P. Ho and R. R. Alfano, Opt. Lett. **19**, 1636 (1994).

[42]. Q. D. Liu, J. T. Chen, Q. Z. Wang, P. P. Ho and R. R. Alfano, IEEE Photon. Tech. Lett., 7, 517 (1995).

[43]. M. J. LaGasse, D. Liu-wong, J. G. Fujimoto and H. A. Haus, Opt. Lett. **14**, 311 (1989).

[44]. Y. Kimura, K. I. Kitayama, N. Shibata and S. Seikai, Electron. Lett. **22**, 277 (1986).

[45]. J. -M. Jeong and M. E. Marhic, Opt. Comm. **85**, 430 (1991).

[46]. A. S. Davison and I. H. White, Opt. Lett. **14**, 802 (1988).

[47]. M. E. Marhic, C. H. Hsia and J. -M. Jeong, Electron. Lett. **27**, 27 (1991).

[48]. T. Morioka, M. Saruwatari and A. Takada, Electron. Lett. **27**, 210 (1991).

[49]. J. -M. Jeong and M. E. Marhic, Opt. Comm. **91**, 115 (1992).

[50]. A. M. Weiner, J. P. Heritage and J. A. Salehi, Opt. Lett. **13**, 300 (1988).

[51]. M. A. Flavin and J. L. Horner, Appl. Opt. **28**, 1692 (1989).

[52]. B. L. Shoop and J. W. Goodman, Appl. Opt. **31**, 5654 (1992).

[53]. P. P. Ho, Q. Z. Wang, Q. D. Liu , Disa Liu, and R. R. Alfano, Optoelectronic Signal Processing for Phased-array Antennas IV, SPIE Proc. Vol. **2155**, 157 (1994).

[54]. P. P. Ho, Q. Z. Wang, Q. D. Liu , Disa Liu, and R. R. Alfano, Optoelectronic Signal Processing for Phased-array Antennas IV, SPIE Proc. Vol. **2155**, 37 (1994).

[55]. N. Nakazawa, Appl. Phys. Lett., **46**, 628 (1985).

[56]. M. J. Mohony, in Digest of Conference on Integrated Optics and Optical Fiber Communication (Istituto Internazionale Delle Conmmunicazioni, Venice, Italy, 1985).

[57]. R. J. Mears, L. Reekie, I. M. Jauncey and D. N. Payne, Electron. Lett., **23**, 1026 (1987).

[58]. M. Nakazawa, K. Kurokawa, H. Kubota, K. Suzuki and Y. Kimura, Appl. Phys. Lett., 57, 653 (1990).

[59]. A. S. Davison and I. H. White, Opt. Lett., **14**, 802 (1989).

Chapter II
THEORY OF NONLINEAR EFFECTS OF LASER PULSES PROPAGATING IN OPTICAL FIBERS

II.1 Introduction

The nonlinear processes in optical fibers affect the spectral, temporal, and vectorial properties of the ultrashort laser pulses propagating in materials. Self-phase modulation (SPM) occurs when the refractive index of the nonlinear material depends on the intensity of the laser pulses itself. Cross-phase modulation (XPM) occurs when the refractive index of the material depends on the intensity of another copropagating laser pulse. These nonlinear phase modulations cause the spectral broadening of the propagating laser pulses, change the polarization states, and also affect the pulse duration. Many applications can be created in optical communication and computation using XPM and SPM.

SPM and XPM processes in nonlinear media have been intensively investigated by many researchers in the past decade, especially by R. R. Alfano and P. L. Baldeck group[1-10]. The generation and compression of femtosecond supercontinuum light using single-mode optical fibers and high-refractive index prisms has been studied[1-3]. The spectral and temporal effects of XPM on the propagation of interacting ultrashort light pulses in optical fibers have been theoretically and experimentally investigated[4-8]. In addition, the spatial effects on the nonlinear propagation of picosecond pulses in multimode optical fibers were also studied. A self-focusing effect has been demonstrated in multimode optical fibers[9-10].

In this chapter, the nonlinear time-dependent wave equations of electric-magnetic field in a nonlinear medium will be derived from Maxwell's equation first. The standard theories for self-phase modulation (SPM) and cross-phase modulation (XPM) are discussed under different polarization bases. A new theoretical model for ultrashort laser pulses propagating in nonbirefringent single-mode optical is proposed. The spectral broadening caused by SPM and XPM is simulated in optical fibers. Polarization stabilities of linearly and circularly polarized laser pulses propagating in nonbirefringent single-mode optical fiber are analyzed. Nonlinear polarization twisting (NPT) of linearly polarized optical pulses propagating in optical fibers will be theoretically investigated. Nonlinear depolarization and polarization rotation for linearly polarized laser pulses in optical fibers are calculated. The changes of the temporal properties of the propagating laser pulses in single-mode optical fibers are also discussed.

II.2. Nonlinear Time-dependent Wave Equations

The response of a nonlinear medium to an intense electric and magnetic fields of a high intensity laser field will cause nonlinear polarization. This nonlinear polarization will generate new optical frequencies. The propagation of such intense field leads to various nonlinear optical phenomena. SPM and XPM are two important nonlinear phenomena. The nonlinear wave equations can give a very good quantitative description of SPM and XPM effects. In this section, the nonlinear wave equations will be derived from Maxwell's equations.

From the Maxwell's equations, we can find the wave equations that governs optical wave propagation in a medium:

$$\nabla \times \nabla \times \vec{E}(r,t) + \frac{1}{c^2}\frac{\partial^2}{\partial t^2}\vec{D}(r,t) = 0, \tag{II.1}$$

since the electric displacement is

$$\vec{D} = \vec{E} + 4\pi\vec{P}, \tag{II.2}$$

we can obtain

$$\nabla \times \nabla \times \vec{E} + \frac{1}{c^2}\frac{\partial^2}{\partial t^2}\vec{E} = -\frac{4\pi}{c^2}\frac{\partial^2}{\partial t^2}\vec{P}. \tag{II.3}$$

This equation is the most general form of the wave equation. Under certain conditions it can be simplified. For example, by using an identity from vector calculus, the first term on the left-handed side of Eq. (II.3) can be written as

$$\nabla \times \nabla \times \vec{E} = \nabla(\nabla \bullet \vec{E}) - \nabla^2 \vec{E}, \qquad \text{(II.4)}$$

In the linear optics of isotropic source-free media, the first term on the right-handed side of this identity vanishes because the Maxwell's equation $\nabla \bullet \vec{D} = 0$ implies that $\nabla \bullet \vec{E} = 0$. However, in nonlinear optics this term in general is nonvanishing even for isotropic materials, since the more general relation between $\vec{D}$ and $\vec{E}$ is much more complicated than a linear proportion. Fortunately, in nonlinear optics the first term on the right-handed side of Eq. (II.4) can usually be dropped. For example, if $\vec{E}$ is of the form of a transverse, infinite plane wave, $\nabla \bullet \vec{E}$ vanishes identically. More generally, the first term on the right-handed side of Eq. (II.4) can often be shown to be very small, even when it does not vanish, especially when the slowly-varying amplitude approximation is valid.

It is convenient to split $\vec{P}$ into its linear and nonlinear parts as

$$\vec{P} = \vec{P}_L + \vec{P}_{NL}, \qquad \text{(II.5)}$$

where $\vec{P}_L$ is proportional to the electric field $\vec{E}$. Hence Eq. (II.2) can be written as

$$\vec{D} = \vec{E} + 4\pi\vec{P}_L + 4\pi\vec{P}_{NL} = \vec{D}_L + 4\pi\vec{P}_{NL}, \qquad \text{(II.6)}$$

where $\vec{D}_L = \varepsilon \cdot \vec{E}$ is the linear electric displacement vector, ε is the linear dielectric tensor which reduce to a real scalar quantity for the case of an isotropic, and lossless material. Substituting Eqs. (II.4) and (II.6) into Eq. (II.3), and using the approximation $\nabla \bullet \vec{E} = 0$. We have the wave equation

$$\nabla^2 \vec{E}(r,t) - \frac{1}{c^2}\frac{\partial^2}{\partial t^2}\vec{D}_L(r,t) = \frac{4\pi}{c^2}\frac{\partial^2}{\partial t^2}\vec{P}_{NL}(r,t), \qquad \text{(II.7)}$$

Since both SPM and XPM processes involve propagating waves with time varying amplitudes, we need to find the time-dependent nonlinear wave equations in dispersive media. In general, the electric field of a linearly polarized laser pulse can be approximately expressed as a quasi-monochromatic plane wave when the change along the transverse coordinates are negligible

$$\vec{E}(r,t) = \vec{e}\,E(z,t) = \vec{e}\,A(z,t)\exp[i(k_0 z - \omega_0 t)], \qquad \text{(II.8)}$$

where $\vec{e}$ is the unit vector of the polarizing direction of the electric field, ω_0 is the carrier frequency, k_0 is the carrier wave number, and $A_{(z,t)}$ is the slowly varying amplitude of the electric field.

In this case, the electric field depends only on the spatial coordinate z, we can replace ∇ by $\partial / \partial z$ in Eq. (II.7), and we have

$$\nabla^2 E(z,t) = \{\frac{\partial^2 A(z)}{\partial z^2} + 2i k_0 \frac{\partial A(z)}{\partial z} - k_0^2 A(z)\}\exp[i(k_0 z - \omega_0 t)], \qquad \text{(II.9)}$$

when solving the wave equations, several simplifying approximations are often made[11, 16]. Among them is the slowly varying amplitude approximation, which is valid for many nonlinear effects. Since the energy among waves usually travels over a distance much longer than their wavelength, we expect

$$\left|\frac{\partial^2 A(z)}{\partial z^2}\right| << \left|k_0 \frac{\partial A(z)}{\partial z}\right|, \qquad \text{(II.10)}$$

So we have

$$\nabla^2 E_{(z,t)} = \{2i k_0 \frac{\partial A_{(z)}}{\partial z} - k_0^2 A_{(z)}\} \exp[i(k_0 z - \omega_0 t)], \qquad \text{(II.11)}$$

From Alfano *et al*[16], this electric field E(z,t) is expressed in terms of the Fourier integral

$$E_{(z,t)} = \int_{-\infty}^{\infty} E_{(z,\omega)} \exp(i\omega t) d\omega. \qquad \text{(II.12)}$$

Then we have

$$D_{(z,t)} = \int_{-\infty}^{\infty} n_0^2(\omega) E_{(z,\omega)} \exp(-i\omega t) d\omega, \qquad \text{(II.13)}$$

where $n_{0(\omega)} = \sqrt{\varepsilon}$ is the linear index of refraction which is frequency dependent. The linear polarization term on the left side of Eq. (II.7) can be expressed as

$$\begin{aligned} -\frac{1}{c^2}\frac{\partial^2}{\partial t^2} D_{(z,t)} &= -\frac{1}{c^2} \int_{-\infty}^{\infty} n_0^2(\omega) E_{(z,\omega)} \frac{\partial^2}{\partial t^2} \exp(-i\omega t) d\omega \\ &= \int_{-\infty}^{\infty} \frac{\omega^2 n_0^2(\omega)}{c^2} E_{(z,\omega)} \exp(-i\omega t) d\omega \\ &= \frac{1}{2\pi} \int_{-\infty}^{\infty} \int_{-\infty}^{\infty} k^2(\omega) A(z,t') \exp[i\omega(t-t')] \\ &\qquad \times \exp[i(k_0 z - \omega_0 t)] d\omega dt'. \end{aligned} \qquad \text{(II.14)}$$

The derivative of the wave equation then proceeds by expanding $k^2_{(\omega)}$ about the carrier frequency ω_0 in the form of

$$k^2(\omega) = k_0^2 + k_0 k_0^{(1)}(\omega - \omega_0) + k_0 k_0^{(2)}(\omega - \omega_0)^2 + \cdots, \qquad \text{(II.15)}$$

where $k_0=k(\omega_0)$ is the propagation constant, $k_0^{(1)} = (\partial k/\partial\omega)_{\omega=\omega 0} = 1/\upsilon_g$ is the inverse of the group velocity, and $k_0^{(2)} = (\partial^2 k/\partial\omega^2)_{\omega=\omega 0}$ is the group velocity dispersion.

It is possible to evaluate the integral of Eq. (II.14) by using the convenient delta function identities

$$\frac{1}{2\pi}\int_{-\infty}^{\infty} \exp[i(\omega - \omega_0)(t' - t)]d\omega = \delta(t' - t), \qquad \text{(II.16)}$$

as well as

$$\frac{1}{2\pi}\int_{-\infty}^{\infty} (\omega - \omega_0)\exp[i(\omega - \omega_0)(t' - t)]d\omega = i\delta^{(1)}(t' - t), \qquad \text{(II.17)}$$

and

$$\frac{1}{2\pi}\int_{-\infty}^{\infty} (\omega - \omega_0)^2\exp[i(\omega - \omega_0)(t' - t)]d\omega = i\delta^{(2)}(t' - t), \qquad \text{(II.18)}$$

In these expressions, $\delta^{(n)}(t' - t)$ is the nth-order derivative of the Dirac delta function, with the property of that

$$\int_{-\infty}^{\infty}\delta^{(n)}(t-t_0)f(t)dt=\left(\frac{\partial^n f(t)}{\partial t^n}\right)_{t=t_0}, \tag{II.19}$$

when applied to a function f(t). Substituting Eq. (II.15) into Eq. (II.14) and using Eqs. (II.16) to (II.19), the second term on the left side of Eq. (II.7) becomes

$$\begin{aligned}
&-\frac{1}{c^2}\frac{\partial^2}{\partial t^2}D(z,t)\\
&\quad=\frac{1}{2\pi}\int_{-\infty}^{\infty}\int_{-\infty}^{\infty}(k_0^2+k_0k_0^{(1)}(\omega-\omega_0)+k_0k_0^{(2)}(\omega-\omega_0)^2)A(z,t')\\
&\qquad\times\exp[i\omega(t'-t)]\exp[i(k_0z-\omega_0t)]d\omega dt'\\
&\quad=\int_{-\infty}^{\infty}[k_0^2\delta(t'-t)+i2k_0k_0^{(1)}\delta^{(1)}(t'-t)+k_0k_0^{(2)}\delta^{(2)}(t'-t)]A(z,t')\\
&\qquad\times\exp[i(k_0z-\omega_0t)]dt'\\
&\quad=[k_0^2A(z,t)+i2k_0k_0^{(1)}\frac{\partial A(z,t)}{\partial t}-k_0k_0^{(2)}\frac{\partial^2A(z,t)}{\partial t^2}]\\
&\qquad\times\exp[i(k_0z-\omega_0t)].
\end{aligned} \tag{II.20}$$

Inserting Eqs. (II.13) and (II.20) into Eq. (II.7) with the approximation of

$$\frac{\partial^2P_{NL}(z,t)}{\partial t^2}=-\omega_0^2P_{NL}(z,t), \tag{II.21}$$

finally, yields the time-dependent nonlinear wave equation:

$$\begin{aligned}
i\left(\frac{\partial A(z,t)}{\partial z}+\frac{1}{v_g}\frac{\partial A(z,t)}{\partial t}\right)-\frac{1}{2}k_0^{(2)}\frac{\partial^2A(z,t)}{\partial t^2}&=-\frac{2\pi\omega_0}{k_0c^2}P_{NL}(z,t)\\
&\quad\times\exp[-i(k_0z-\omega_0t)].
\end{aligned} \tag{II.22}$$

where υ_g is the group velocity. In Eq. (II.22), the first two terms on the left side describes the developing propagation at the group velocity; the third term determines the temporal pulse broadening due to the group velocity dispersion; and the terms on the right side characterizes the nonlinear polarization which is responsible for different kinds of nonlinear phenomena. This equation is frequently used in later sections. The nonlinear polarization P_{NL} in Eq. (II.22) depends on the different conditions such as for SPM and XPM under different polarization bases. More details of the nonlinear wave equations for SPM and XPM can be found in Appendix.

II.3 Self-phase Modulation (SPM)

SPM was first proposed by Shimisu[17] to explain the observed spectral broadening of the self-focused Q-switched nanosecond laser pulse in liquid with large optical Kerr constants. In this case, the spectral broadening was relatively small (~100 cm^{-1}). Alfano and Shapiro showed that with picosecond laser pulses, it is possible to generate by SPM spectrally broadened output extending over 10,000 cm^{-1} in almost any transparent condensed medium[18, 19]. In order to study a pure SPM process, one would like to keep the beam cross section constant over the entire propagation distance in the medium. A single-mode optical fiber is ideal since the beam cross section of a guided wave should be constant. Stolen and Lin found that the observed spectral broadening of a laser pulse propagating through a long fiber can be well explained by the simple SPM theory[20]. Recently the fine structures of the SPM spectral broadening have been measured and were in good agreement with the theoretical expectations[21].

The nonlinear wave equation (II.22) can be used to describe SPM. For one optical wave, Eq. (II.22) can be further reduced by neglecting the group-velocity dispersion and expressed as:

$$\frac{\partial A}{\partial z}+\frac{1}{v_g}\frac{\partial A}{\partial t}=i\frac{\omega_o n_2}{c}|A|^2 A, \qquad \text{(II.23)}$$

where $n_2 = 3\chi^{(3)}_{1111}/8n_o$ is the nonlinear refractive index coefficient and n_o is the linear refractive index. Eq. (II.23) was derived using the following approximations: (1) a single linearly polarized electric field; (2) slowly varying pulse envelope; (3) isotropic and homogenous medium; (4) frequency independent nonlinear susceptibility $\chi^{(3)}$; (5) negligible Raman effect; and (6) neglecting the group velocity dispersion, absorption,

self-steeping. The basic mechanism and properties of SPM can be explained using Eq. (II.23) which is from reference [16]. By changing the variables with:

$$\tau = t - z / \upsilon_g, \quad \text{and} \quad z=z, \tag{II.24}$$

where t is real time, and τ is defined as the pulse local time. Denoting by $a_{(z,\tau)}$ and $\alpha_{(z,\tau)}$ the amplitude and the phase of the electric envelope of the laser pulse, respectively, the pulse slowly varying profile $A_{(z,t)}$ can be written as

$$A_{(z,\tau)} = a_{(z,\tau)} \exp[i\,\alpha_{(z,\tau)}]; \tag{II.25}$$

therefore, Eq. (II.23) reduces to

$$\frac{\partial a}{\partial z} = 0, \tag{II.26a}$$

$$\frac{\partial \alpha}{\partial z} = \frac{\omega_o n_2}{c} \alpha^2. \tag{II.26b}$$

The analytical solutions of Eqs. (II.26) for the nonlinear phase modulation and the slowly changing amplitude of a light pulse can be obtained as

$$a_{(z,\tau)} = a_0 F_{(\tau)}, \tag{II.27a}$$

$$\alpha_{(z,\tau)} = \frac{\omega_o n_2}{c} a_o^2 z F_{(\tau)}^2. \tag{II.27b}$$

where a_o is the peak amplitude of the laser pulse and $F_{(\tau)}$ is the envelope of the light pulse.

From the solution (II.27), the main physics of SPM is that the phase of an optical pulse propagating in a nonlinear medium becomes time dependent in the pulse profile, and results in SPM. The frequency of the electric field will be continuously shifted in time. This process is the most important in the supercontinuum generation of femtosecond laser pulses. Because the pulse duration is much larger than the optical period $2\pi/\omega_0$ (slowly varying approximation), the electric field at each given t within the pulse has a specific local instantaneous frequency that is given by

$$\omega_{(\tau)} = \omega_0 + \delta\omega_{(\tau)}, \tag{II.28}$$

where

$$\delta\omega_{(\tau)} = -\frac{\partial\alpha}{\partial\tau} = -\frac{\omega_o n_2}{c} a_o^2 \frac{\partial F_{(\tau)}^2}{\partial\tau}. \tag{II.29}$$

where $\delta\omega(\tau)$ is the frequency shift generated at a particular local time τ within the pulse envelope. This frequency shift is proportional to the derivative of the pulse envelope with respect to τ, the nonlinear index, and the intensity of the pulse. The frequency shift will generate a wider spectrum of the laser pulse. This mechanism is schematically shown in Figure II.1. The nonlinear index change is shown in Figure II.1(a) vs the local time. This nonlinear index change has the same profile with the propagating optical pulse for the nonlinear medium having instantaneous response. The time rate of the index change is shown in Figure II.1(b) and the frequency change at different local time is shown in Figure II.1(c). The frequency of the leading edge of the laser pulse (near τ_1) shows a shift to Stokes side (red-shift) and the frequency of the tailing edge of the laser pulse (near τ_2) shows a shift to anti-Stokes side (blue-shift). In some nonlinear medium having a large nonlinear refractive index n_2 [18, 19], these frequency broadening in the ultrashort laser

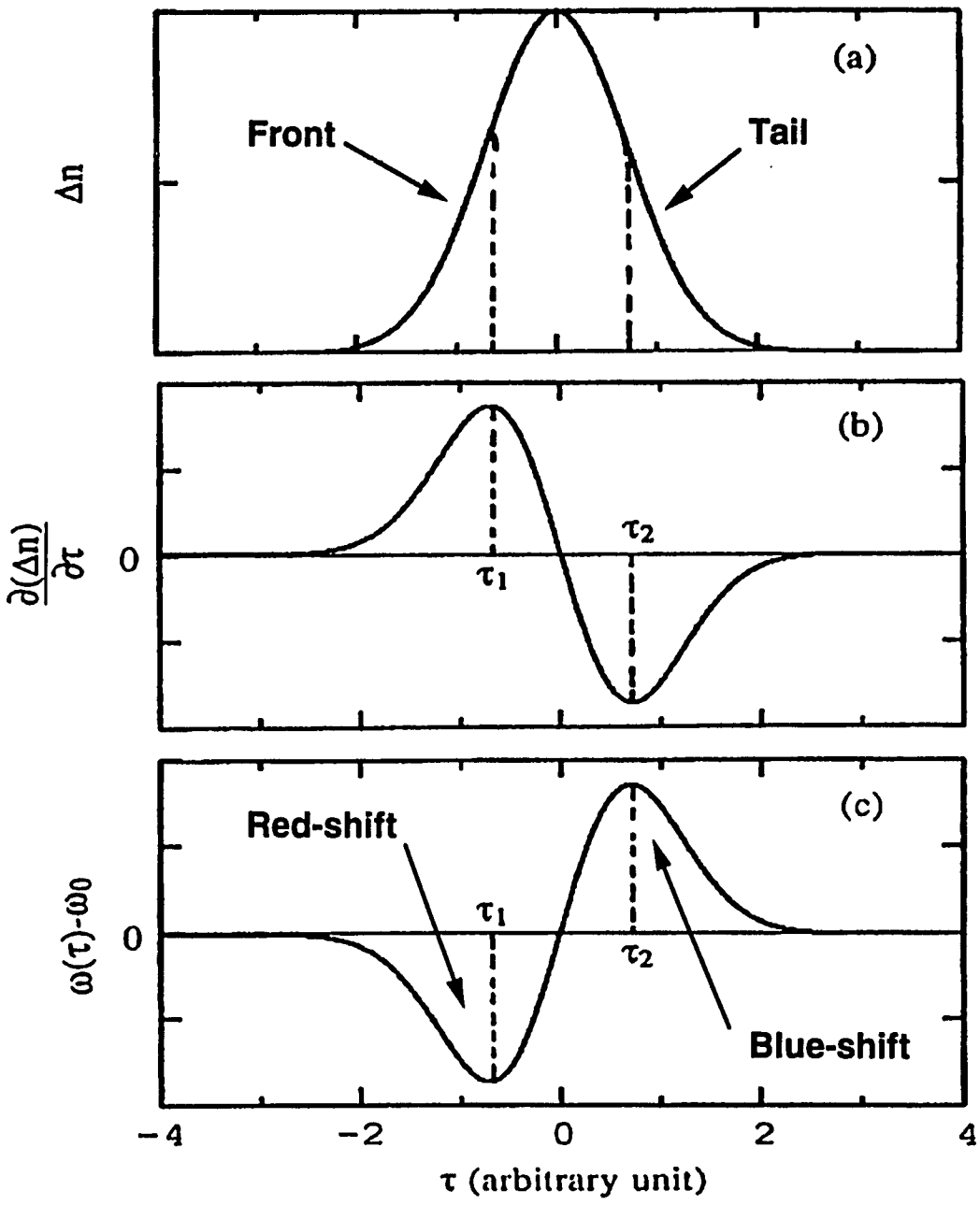

Figure II. 1 Time dependent index, phase, and frequency shift generated by self-phase modulation (SPM). (a). time-dependent nonlinear index change; (b). time rate of index change; and (c). time distribution of SPM frequency shift $\omega(\tau)$-ω_0.

pulse profile can be tremendously large to produce the ultrashort white light pulses. This process is defined as supercontinuum generation.

Ultrashort optical pulses having correspondingly broad spectral profiles are therefore sensitive to dispersion phenomenon. The group-velocity dispersion (GVD) is that the different frequency components of optical pulses will propagate at different speeds through a dispersive medium. One observable consequence of GVD is the temporal broadening of he propagating optical pulses. For ultrashort laser pulses without passing through any nonlinear medium, their spectral bandwidths are usually narrow and the distribution of all the spectral components are uniform in the pulse temporal profiles. When these laser pulses propagate in a nonlinear medium, SPM causes the spectral broadening as we discussed. There will be a resulting distribution of frequency components throughout the temporal envelope which is described as 'chirped' [22,23]. A positive chirp corresponds to an increase in frequency with time and a negative chirp corresponds to a decrease in frequency with time. Figure II.2(a) shows the electric field of an optical pulse without any chirp. The frequency distribution is uniform throughout the pulse temporal profile. Figure II.2(b) shows the electric field of a pulse with a positive chirp or up-chirp. Figure II.2(c) shows the electric field of a pulse with a negative chirp or down-chirp.

It should be understood that the GVD changes the temporal profile the optical pulses, it does not change the spectral profiles. It merely adjust the relative temporal positions of the spectral components. Silica glass, the standard optical medium, is said to exhibit 'normal' dispersion for visible light. This corresponds to the situation where the higher frequencies travel slower than lower frequencies. An initially unchirped optical pulse will therefore become positively chirped after propagating through a medium with normal dispersion. Conversely, the situation where the higher frequencies travel faster

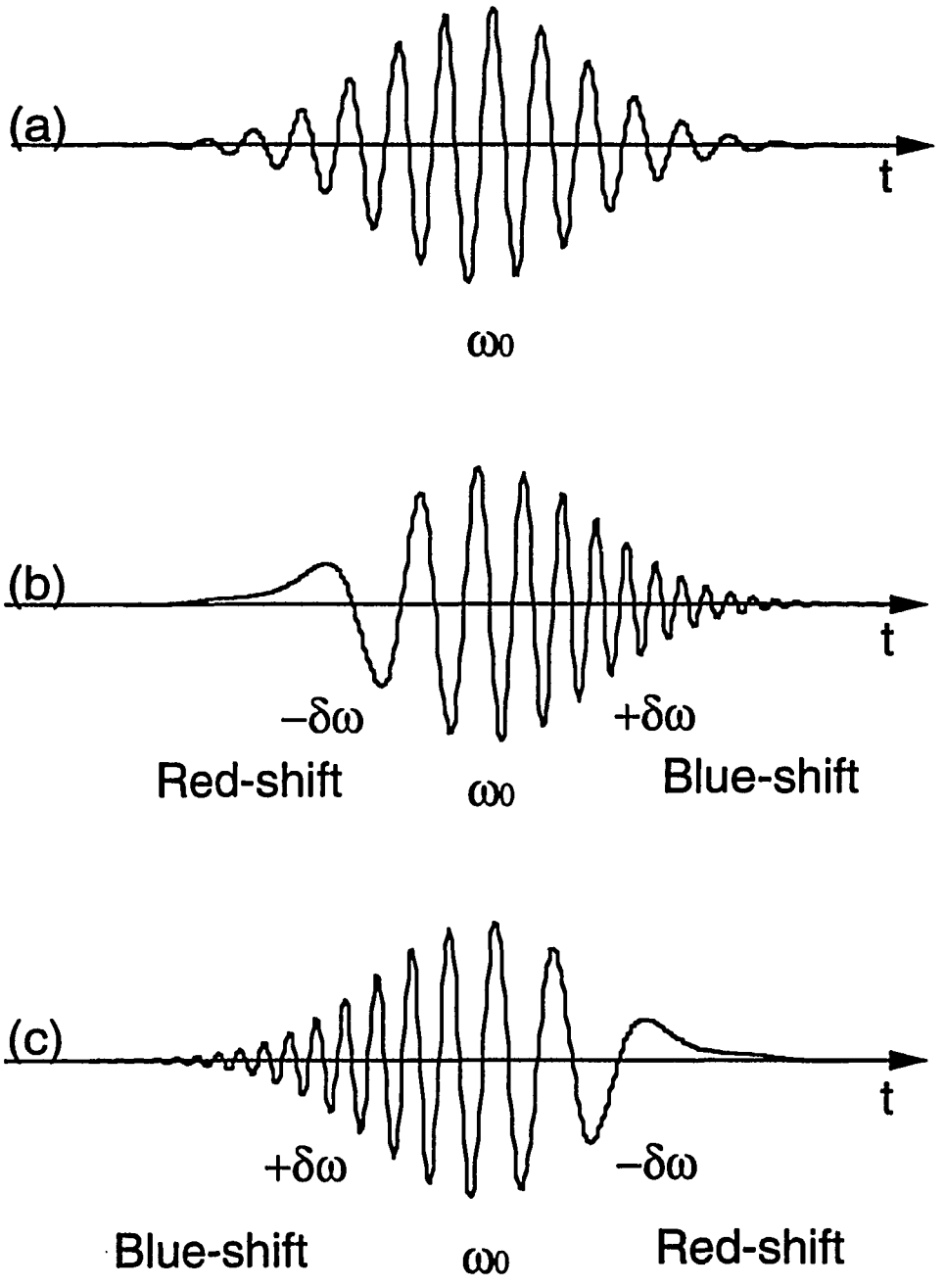

Figure II.2 Schematic of the electric field of an optical pulse with (a) no frequency chirp, (b) positive frequency chirp, and (c) negative frequency chirp.

than lower frequencies is described as anomalous dispersion. Propagation of a unchirped pulse through such a medium will produce a negative frequency chirp. Note that in principle the effect of propagation through a dispersive medium can be reversed by propagation through a medium of the opposite dispersion. This phenomenon has been used as a standard technique of pulse compression[23-27].

The complex-field spectral profiles $E(z, \omega-\omega_o)$ of the optical pulse after SPM process can be obtained by computing the Fourier transformation of its temporal pulse distribution as

$$E(z,\ \omega-\omega_o)=\frac{1}{2\pi}\int A(\tau,z)\exp(-i\omega_o\tau)\exp(-i\omega\tau)d\tau$$
$$=\frac{1}{2\pi}\int a(\tau,z)\exp[i\alpha(\tau,z)]\exp[i(\omega-\omega_o)\tau]d\tau. \qquad \text{(II.30)}$$

The spectral intensity distribution of the pulse is given by

$$|E_{(z,\omega-\omega_o)}|^2. \qquad \text{(II.31)}$$

The maximum frequency spread can be estimated by[16]

$$\Delta\omega_{(z)max}=\frac{\omega_o n_2}{c}z a_o^2\left(\frac{\partial F^2_{(\tau)}}{\partial\tau}|_{\tau_2}-\frac{\partial F^2_{(\tau)}}{\partial\tau}|_{\tau_1}\right), \qquad \text{(II.32)}$$

where τ_1 and τ_2 are the pulse envelope inflection points as depicted in Figure II.1. For a Gaussian laser pulse given by

$$F_{(\tau)}=\exp(-\tau^2/2\tau_0^2), \qquad \text{(II.33)}$$

where τ_0 is the 1/e pulse duration, the maximum frequency extent is

$$\Delta\omega_{(z)max} = \frac{\omega_o n_2}{c\tau_0} z a_o^2. \qquad \text{(II.33)}$$

An example of SPM is shown in Figure II.3. A 4.5 ps full-width at half-maximum (FWHM) Gaussian laser pulse is assumed to propagate in a nonlinear medium that gives a modulated SPM spectral output. The nonlinear phase change has an analytical solution such as Eq. (II.27) and then the complex electric field of the spectral profile of the optical pulse is calculated using Eq. (II.30) numerically. Finally, the spectrum intensity distribution is calculated using Eq. (II.31). The spectrum of the output shows a broadening of several hundreds cm^{-1} with quasi-periodic oscillation. It is symmetric with respect to the incoming laser frequency because the SPM pulse is symmetric. The leading half of the $\Delta\phi$ pulse is responsible for the Stokes broadening and the lagging half for the anti-Stokes broadening. The peaks and valleys in the spectrum are from the interference of the new generated frequencies. The broadened spectrum has Stokes to anti-Stokes symmetry because $\Delta\phi(t)$ is directly proportional to the intensity and the laser pulse is symmetric. For an asymmetrical laser pulse, meaning that the leading and tailing edges of the laser pulse have different time, the nonlinear phase change $\Delta\phi(t)$ will be asymmetrical too. Its time rate is also different between the leading and tailing edge. The spectral broadening is asymmetrical for red and blue shifts.

If the response of the medium to the laser pulse is not instantaneous. The spectral broadening will be also asymmetric. In this case, the Eq. (II.27b) which is valid for an instantaneous medium will have to be modified for the transient response medium[16]. The nonlinear phase change therefore is

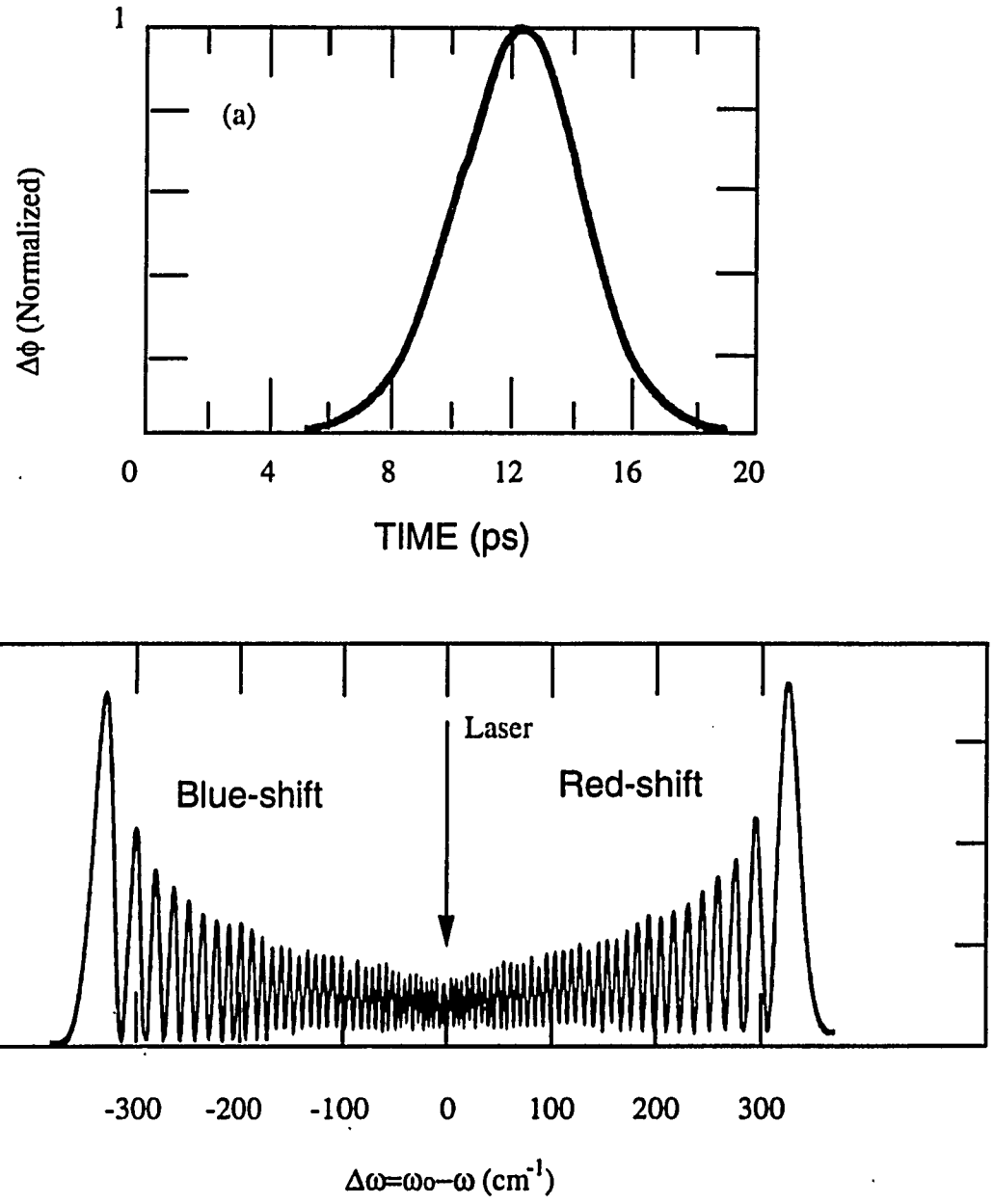

Figure II.3 Theoretical spectral distribution obtained by assuming an instaneous respones of Δn to the intensity, so that the phase modulation $\Delta\phi$ is propotional to laser intensity. (a). $\Delta\phi$ versus t ;and (b). spectral distribution of the phase modulated pulse.

$$\alpha_{(z,\tau)}=\frac{\omega_0}{c} a_0^2 \int_0^z \int_{-\infty}^{\tau} n_{2(z,\tau-t)} F_{(\tau)}^2 dtdz. \qquad \text{(II.34)}$$

where $n_{2(z,\ \tau-t)}$ is the time dependent nonlinear refractive index. This nonlinear phase change has to be calculated numerically. Then by the time rate of the nonlinear phase change, the SPM spectral intensity distribution can be calculated numerically. A calculation of the spectral intensity distribution of a laser pulse is shown in Figure II.4 for a transient response medium. Because of the finite response time of the medium, the leading part of the $\Delta\phi(t)$ curve always see a larger portion of the pulse intensity. Therefore, the Stokes side of the spectrum is always stronger.

The SPM induced spectra broadening has been measured for different wavelengths in various of materials. Figure II.5 displays an experimental arrangement of measuring the spectral broadening of picosecond laser pulse propagating in single optical fibers. The laser pulses at 1064 nm and 532 nm were generated from a Nd:YAG laser system. The 1/e pulse durations were 39 ps and 28 ps, respectively, and the pulse energies were approximately 2 μJ and 200 nJ for 1064 nm and 532 nm, respectively. A set of color filters were used to select the wavelength of the laser pulses. The laser pulses were coupled into a 1-meter single-mode optical fiber with a 10x micro-objective lens. A set of neutral density filters was used in front of the micro-objective lens to control the pulse energy coupled into the optical fiber. The optical signal pulse from the optical fiber was collected with another 10x micro-objective lens. The beam was then split into two. On beam was used to monitor the intensities of the pulses coupled into the optical fiber by a photomultiplier tube. The other beam passed through a spectral analysis system and the spectrum was recorded by a computer controlled charge-coupled-device (CCD) camera. This system had a dispersion of 0.005 nm/pixel at the wavelength of 532 nm and 0.01 nm

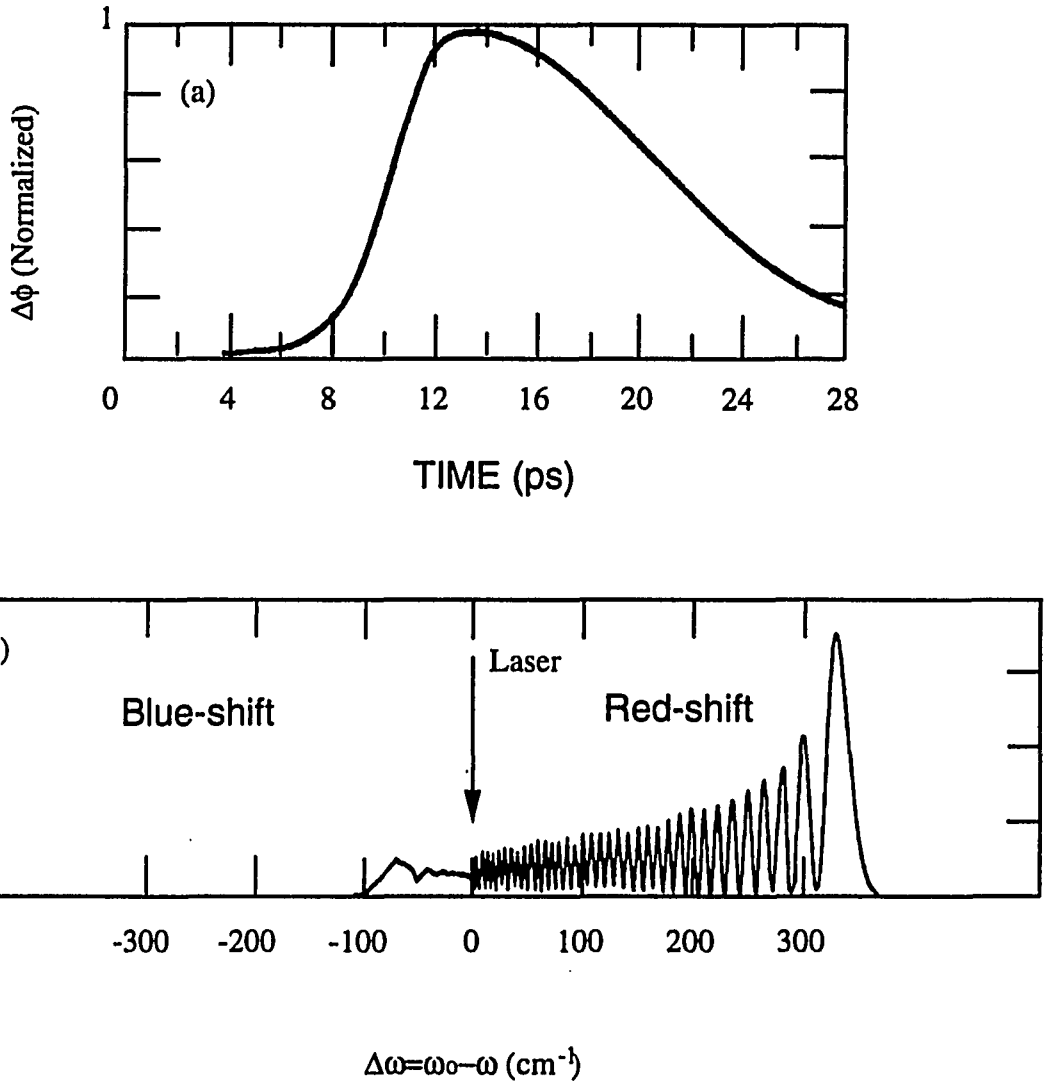

Figure II.4 Theoretical spectral distribution obtained by assuming a transient response of Δn to the laser intensity, so that $\Delta\phi$ is no longer proportional to the intensity. The nonlinear phase change is similar to that of an asymmetric laser pulse in an instaneouse respones medium. (a). $\Delta\phi$ vs. t; and (b). spectrum of the phase modulated pulse.

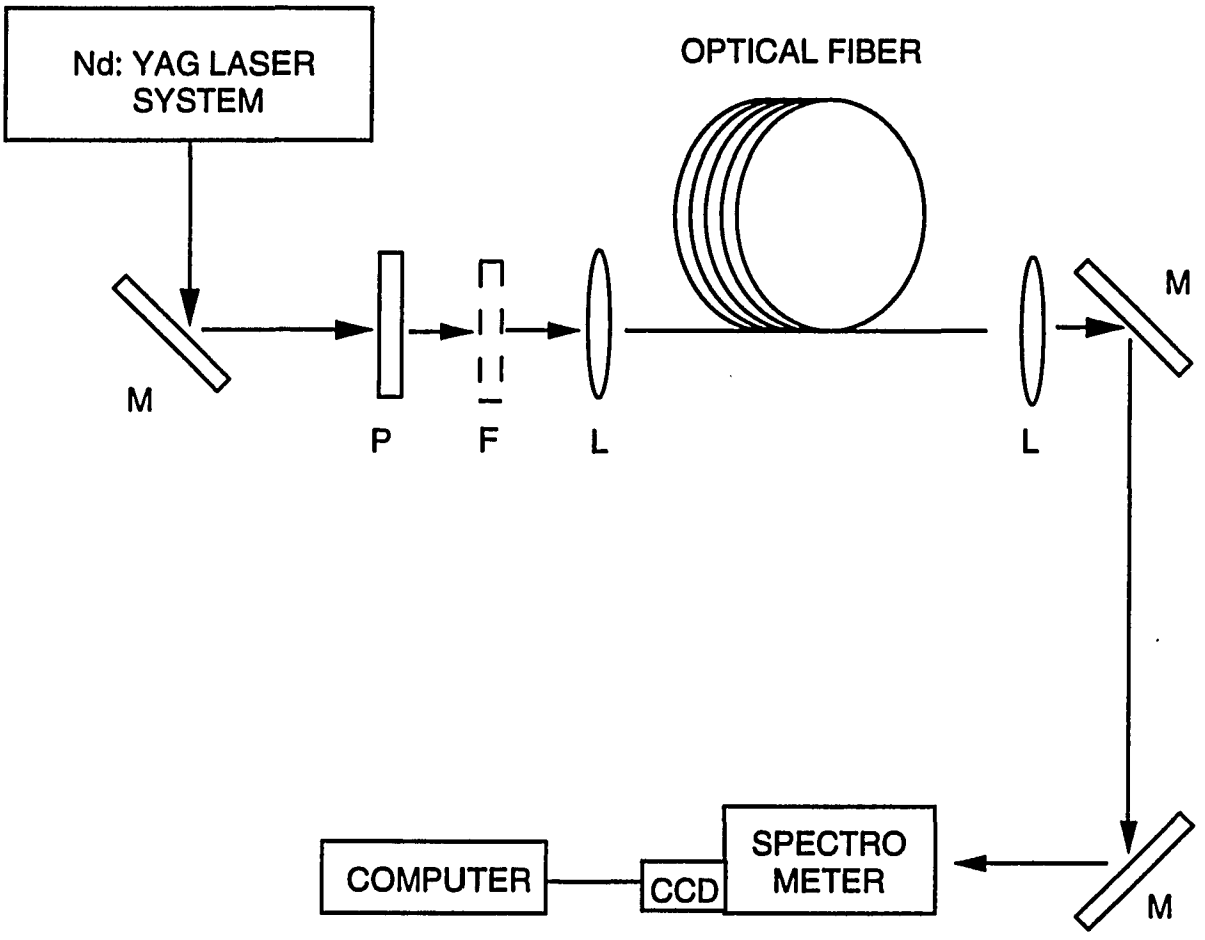

Figure II.5 The experiemntal setup to observe the SPM induced spectral broadening picosecond laser pulses propagating in nonbirefringent single-mode optical fibers. M: mirror; P: polarizer; F: color filter; L: micro-objective lens.

at 1064 nm. The single-mode optical fibers had core diameters of 2.5 μm and 4 μm for 532 nm and 1064 nm laser light, respectively, and the same cladding diameter of 125 μm.

The measure spectra broadening of SPM are displayed in the right columns in Figure II.6 and 7 for 532 nm and 1064 nm, respectively. The left-columns of Figure II.6 and 7 shows the numerical solutions of expression (II.31) for laser pulses at 532 nm and 1064, respectively. The calculations and measurements are in good agreement. In calculation, the initial pulse shape at 532 nm is assumed Gaussian. The spectral bandwidth of the input laser for 532 nm pulse is smaller than 0.1 nm as shown in Figure II.7(a). The length of the optical fiber used in the calculation is 1 meter which is the same as used in experiment. As the intensity of the input laser pulse increases, the spectrum of the output signal broadens. Large-intensity oscillations occur at the same time because of the interference[11]. In the same spectrum the width of the maxim near the input laser frequency is smaller than that farther away from the input laser frequency. The most outside maxims have the largest widths. For different spectra the widths of the maxim at the same wavelength of the spectra of higher-intensity laser pulses are smaller than those for lower-intensity pulses. The peak intensities of the outermost maxim for all the different intensities remain the largest, as can be seen in Figures II. 6(b) to 6(f).

The SPM spectral broadening for laser pulses at 1064 nm are displayed in the left column of Figure II.7. The results are similar to those displayed in the left column of Figure II. 6 for laser pulse at the wavelength of 532 nm. The measured SPM spectral profiles on the right columns of Figure II. 6 and 7 are in good agreement with the calculations. The modulation structures of the central regions of the measured spectra are not clear. This is believed due to the limited resolution of the spectral detection system.

The frequency extent of SPM is inversely proportional to the pump pulse duration as shown in Eq. (II.33). The shorter the incoming pulse, the greater the frequency extent[28,29]. The first white light broadening supercontinuum pulses were generated using picosecond laser pulses. The spectral broadening is proportional to the nonlinear refraction index n_2. The supercontinuum generation can be enhanced by using the material having a high nonlinear refractive index[30,31]. The spectral broadening is also proportional to w_0, medium length z, and the intensity a_0^2.

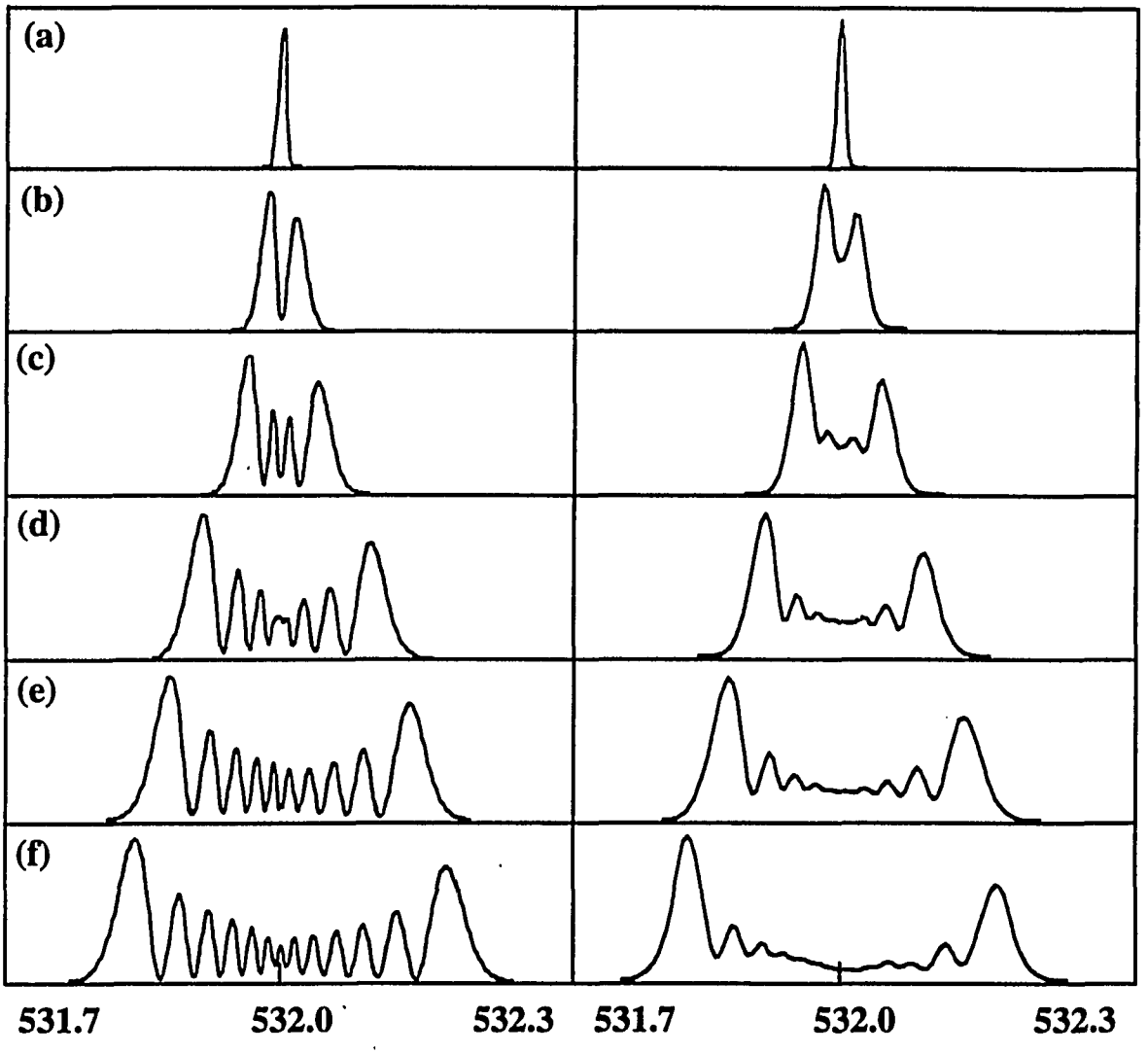

Figure II.6 Left column: Calculated SPM spectra of 532-nm laser pulses propagating in a 1-m optical fiber. Right column: Measured SPM specrtral curves of 532-nm laser pulse propagating in a 1-m 2.5 μm-core single-mode optical fiber with different input peak powers. (a). Input laser; (b). P_0= 110 w; (c). P_0= 225 w; (d). P_0= 460 w; (e). P_0= 630 w; (f). P_0= 790 w.

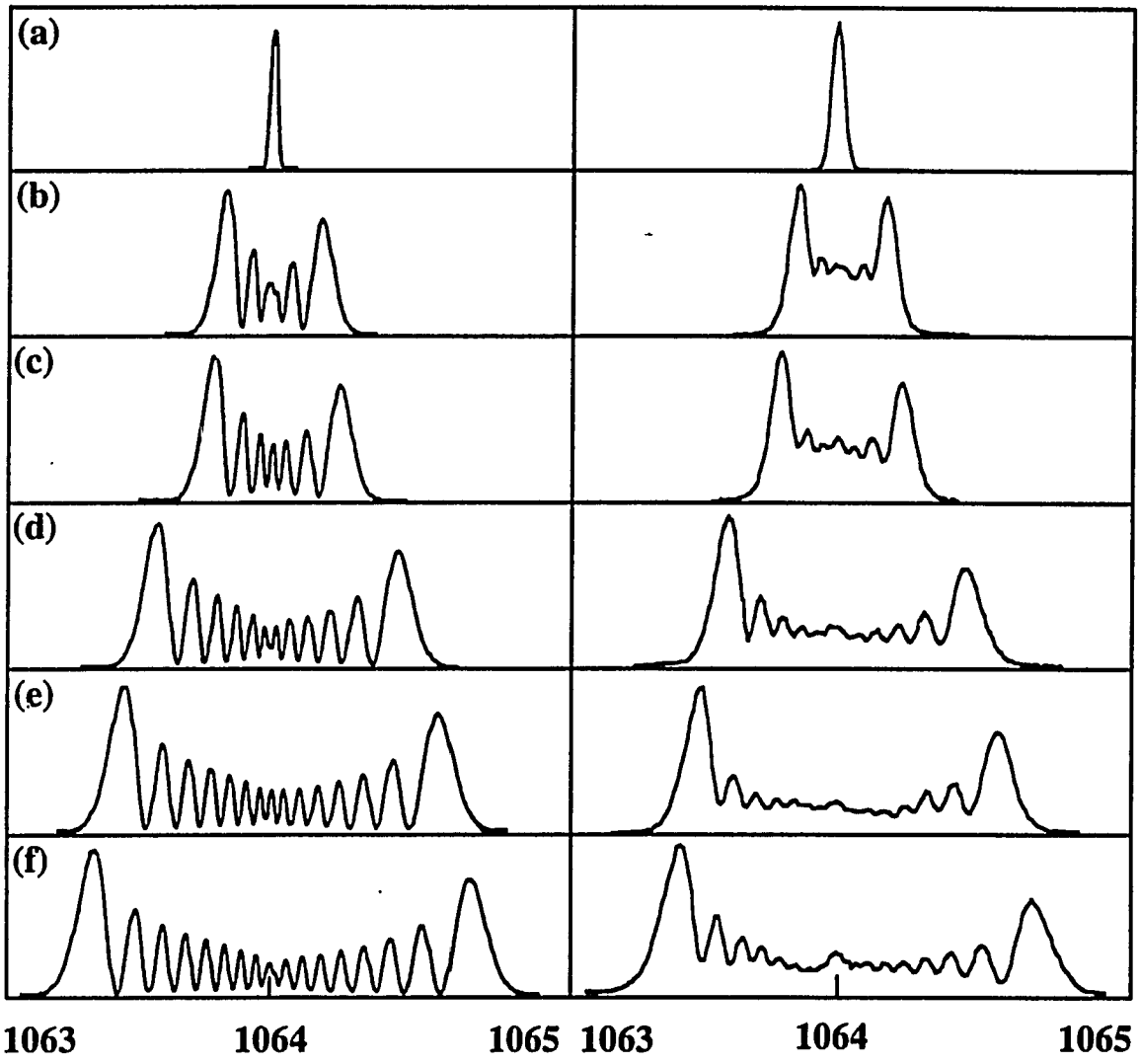

Figure II.7 Left column: Calculated SPM spectra of 1064-nm laser pulses propagating in a 1-m optical fiber. Right column: Measured SPM specrtral curves of 1064-nm laser pulse propagating in a 1-m 4 μm-core single-mode optical fiber with different input peak powers. (a). Input laser; (b). P_0= 1800 w; (c). P_0= 2300 w; (d). P_0= 3900 w; (e). P_0= 4900 w; (f). P_0= 5700 w.

II.4 Cross-phase Modulation (XPM)

When two or more optical waves copropagate inside a fiber, they can interact with each other through the fiber nonlinearity. Under appropriate conditions, such interactions can generate new optical waves through a variety of nonlinear phenomena such as four-wave mixing, stimulated Raman and Brillouin scattering, and third harmonic generation. However, the most important third order nonlinear phenomena in optical fibers is referred as cross-phase modulation (XPM). XPM is always accompanied by SPM and occurs because the effective refractive index of an optical wave depends on the not only the intensity of this wave but also the intensity of other coprpagating optical waves[4-8, 32-39].

The spectral broadening due to XPM is sketched in Figure II.8. An intense laser pulse at the frequency of ω_1 is used to induce the time-dependent nonlinear index change and dynamically alter the phase and frequency of a weak probe pulse at ω_2. Without ω_1, the spectrum of the weak laser pulse will be broadened through the SPM process of this weak pulse its own. This broadening is usually very small because of the low intensity of the weak pulse. With an intense ω_1, the spectral broadening the weak pulse will be much enhanced depending on the intensity of the pump pulse and the time delay between the two laser pulses. The spectral shift of XPM which is controlled by the time delays is illustrated in Figure II.9. When the pump and probe pulses overlap totally, the probe pulse has a frequency shift similar to that of the pump pulse. The leading edge of the probe pulse is red-shifted and the trailing edge is blue-shifted. When the probe pulse overlaps with the leading edge of the pump pulse, the phase of the probe pulse is modulated by the index change caused by the leading edge of the pump pulse and its frequency is red-shifted. When the probe pulse overlap with the trailing edge of the pump pulse, the phase of the probe pulse is modulated by the index change caused by the tailing edge of the pump pulse and its frequency is blue-shifted.

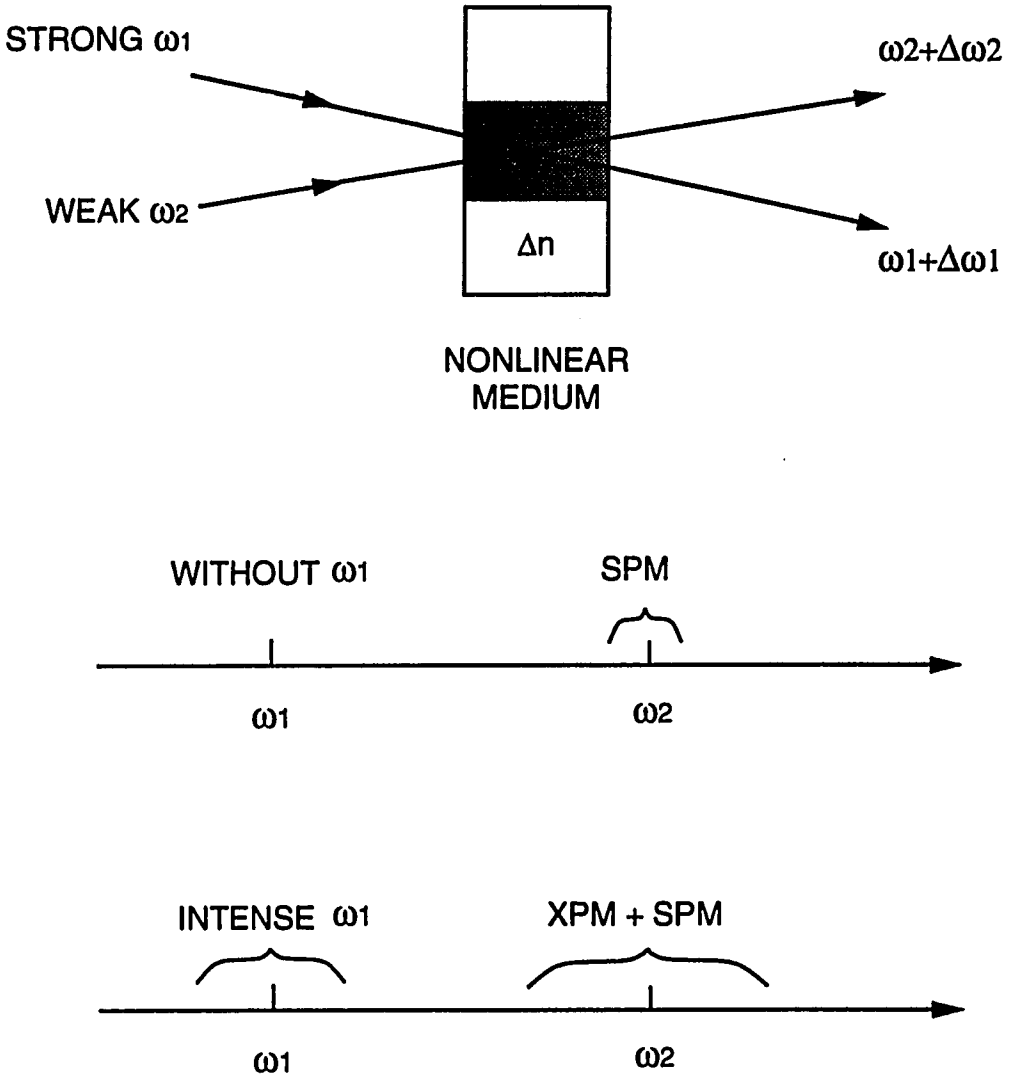

Fgiure II.8 A schematic of XPM process. The induced spectral broadening of a weak probe pulse at ω2 modulated by an intense laser pulse at ω1.

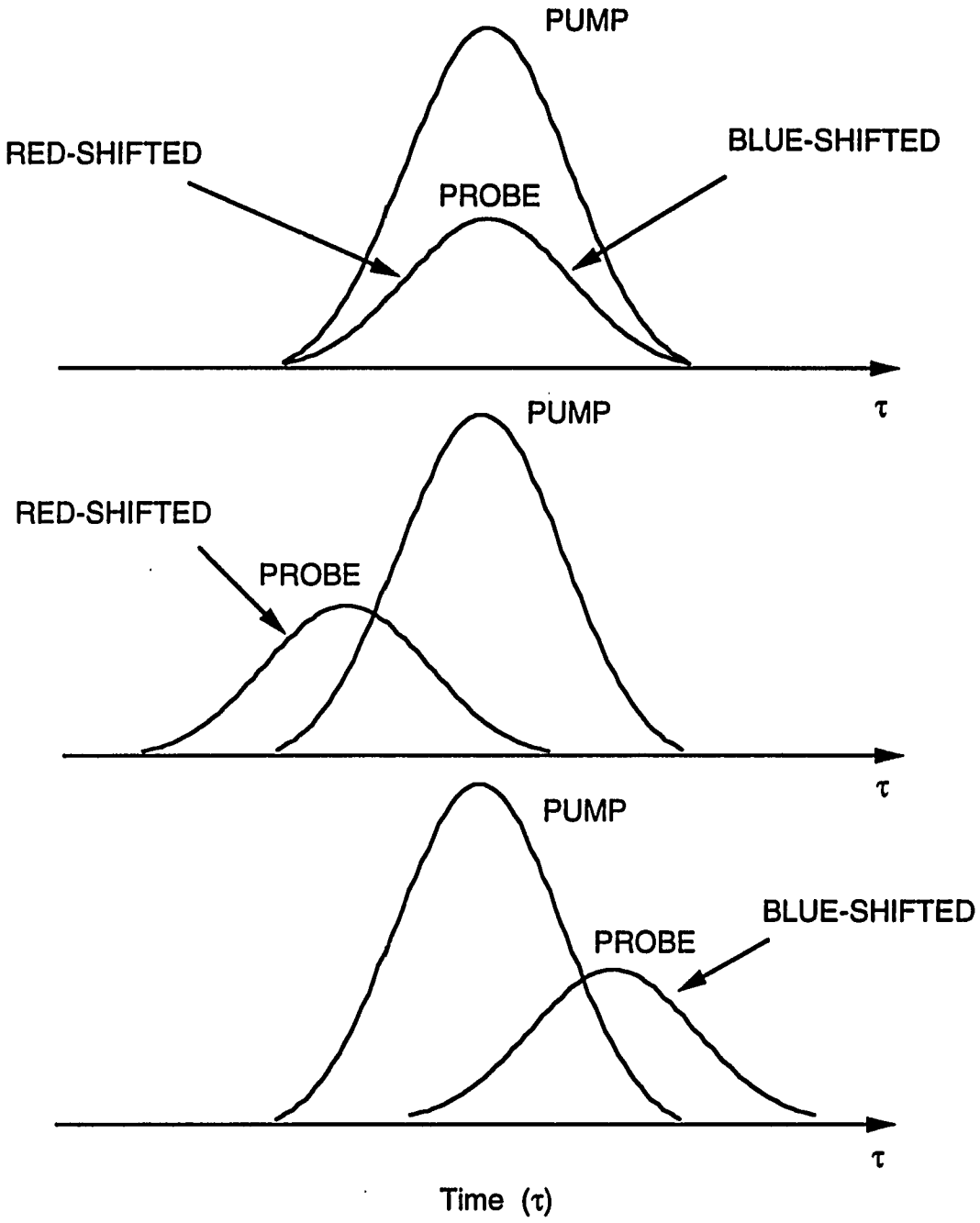

Figure II.9 XPM with different time delays between the strong pump and weak probe pulses. (a) when the probe pulse and pump pulse totally overlap, the leading edge of the probe pulse is red-shifted and the trailing edge is blue-shifted; (b) when the weak probe pulse overlaps with the leading edge of the pump pulse, its frequency is red-shifted; and (c) when the probe pulse overlaps with the trailing edge of the pump pulse, its frequency is blue-shifted.

XPM processes have been investigated in optical fibers for different conditions. Two typical arrangements are for two waves with the same polarization but different frequencies and for two wave with the same frequency but different polarizations, the latter case is called degenerate cross-phase modulation (DXPM)[36, 40]. For polarization, different polarization bases can be selected for different optical fiber by considering the propagating stability of the laser pulses. Usually, linear polarization bases are used to discuss two optical wave having the same linear polarization but at different wavelength. Using the quasi-monochromatic approximation, the total electric field can be written as the rapidly varying part and the amplitude envelope part and can be expressed as:

$$\vec{E}(r,z,t) = \frac{1}{2}\vec{e}_x\{A_1(r,z,t)e^{i(\omega_1 t-\beta_1 z)} + A_2(r,z,t)e^{i(\omega_2 t-\beta_2 z)} + c.c.\}, \qquad \text{(II.35)}$$

where $\vec{e}_x$ is the polarization unit vector, ω_1 and ω_2 are the center frequencies of the two optical waves, β_1 and β_2 are propagating constants, A_1 and A2 are the slowly varying amplitude envelopes of them. Assuming that the nonlinear response is instantaneous and no attenuation in the isotropic medium. and no wavelength dependence for the nonlinear susceptibility $\chi^{(3)}$, the nonlinear polarization reduce to

$$\vec{P}^{nl}(r,z,t) = \chi^{(3)}E^3(r,z,t), \qquad \text{(II.36)}$$

Substituting the total electric field in Eq. (II.35) into (II.36) and keeping only the terms synchronized with ω_1 and ω_2, one obtains

$$\vec{P}^{nl}(r,z,t) = \vec{P}_1^{nl}(r,z,t) + \vec{P}_2^{nl}(r,z,t), \qquad \text{(II.37a)}$$

$$\vec{P}_1^{nl}(r,z,t) = \frac{3}{8}\chi^{(3)}(|A_1|^2 + 2|A_2|^2)A_1 e^{i(\omega_1 t-\beta_1 z)}, \qquad \text{(II37b)}$$

$$\vec{P}_2^{nl}(r,z,t) = \frac{3}{8}\chi^{(3)}(|A_2|^2 + 2|A_1|^2)A_2 e^{i(\omega_1 t-\beta_1 z)}, \qquad \text{(II.37c)}$$

where $\vec{P}_1^{nl}$ and $\vec{P}_2^{nl}$ are the nonlinear polarizations at frequencies ω_1 and ω_2, respectively. Substituting Eqs. (II.37) into Eq. (II.22) and separating the equations which describe the propagation of the laser pulses at different frequencies ω_1 and ω_2, one obtains the nonlinear wave equations that govern the propagation of the optical pulses:

$$\frac{\partial A_1}{\partial z} + \frac{1}{v_{g1}}\frac{\partial A_1}{\partial t} + \frac{i}{2}k_1^{(2)}\frac{\partial^2 A_1}{\partial t^2} = i\frac{\omega_1 n_2}{c}(|A_1|^2 + 2|A_2|^2)A_1, \qquad \text{(II.38a)}$$

$$\frac{\partial A_2}{\partial z} + \frac{1}{v_{g2}}\frac{\partial A_2}{\partial t} + \frac{i}{2}k_2^{(2)}\frac{\partial^2 A_2}{\partial t^2} = i\frac{\omega_2 n_2}{c}(|A_2|^2 + 2|A_1|^2)A_2, \qquad \text{(II.38b)}$$

where v_{gi} is the group velocity for the wave i, $k_i^{(2)}$ is the group velocity dispersion for the wave i, and $n_2=3\chi^{(3)}/8n$ is the nonlinear refractive index. The first terms in the right sides of Eqs. (II.38) are SPM terms and the second terms are the XPM terms. Eqs. (II.38) also show that XPM terms are twice larger than SPM terms for two optical waves at the same linear polarization state.

Similarly, the nonlinear coupling equations for two laser pulses having different linear polarization states can be obtained. The wavelengths of the laser pulses can be either the same or different. The total electric field can be expressed as

$$\vec{E}(r,z,t) = \frac{1}{2}\{\vec{e}_x A_x(r,z,t)e^{i(\omega_x t-\beta_x z)} + \vec{e}_y A_y(r,z,t)e^{i(\omega_y t-\beta_y z)} + c.c.\}, \qquad \text{(II.39)}$$

where $\vec{e}_x$, and $\vec{e}_y$ are the unit vectors of the two perpendicular linear polarizations. The nonlinear coupling equations can be obtained as

$$\frac{\partial A_x}{\partial z}+\frac{1}{v_{gx}}\frac{\partial A_x}{\partial t}+\frac{i}{2}k_x^{(2)}\frac{\partial^2 A_x}{\partial t^2}=i\frac{\omega_x n_2}{c}$$

$$x\ [(|A_x|^2+\frac{2}{3}|A_y|^2)A_x+\frac{1}{3}A_y{}^2A_x{}^*\exp(-i2\Delta\beta z)], \qquad \text{(II.40a)}$$

$$\frac{\partial A_y}{\partial z}+\frac{1}{v_{gy}}\frac{\partial A_y}{\partial t}+\frac{i}{2}k_y^{(2)}\frac{\partial^2 A_y}{\partial t^2}=i\frac{\omega_y n_2}{c}$$

$$x\ [(|A_y|^2+\frac{2}{3}|A_x|^2)A_y+\frac{1}{3}A_x{}^2A_y{}^*\exp(i2\Delta\beta z)], \qquad \text{(II.40b)}$$

where $\Delta\beta=\beta_x-\beta_y$ is the wave vector mismatch for the two optical waves. The first and second terms in the right sides of Eqs. (II.40) are the SPM and XPM, respectively, such as in the Eqs. (II.38) except that XPM here is smaller (only 2/3) than SPM. The third terms in the right sides of Eqs. (II.40) are known as the degenerate four-wave mixing (DFWM) terms. When the frequencies of the two optical waves are not equal, means $\omega_x \neq \omega_y$ and the wave vector mismatch $\Delta\beta>>0$, these terms will oscillate and then vanish. There is no net effect in this case. When two optical wave are at these same frequency which is called degenerate case. The DFWM terms is steady because of the wave vector mismatch $\Delta\beta=0$. DFWM processes will modulate the phase and cause the amplitudes of the two optical waves coupling with each other during nonlinear interactions of the optical waves.

XPM phenomenon in a nonlinear medium can be discussed using different polarization bases. Two perpendicular linear polarization bases have been used in Eqs. (II.38) and (II.40). Mathematically, any two orthogonally polarized unit vectors can be selected as the polarization bases to describe the propagation of optical waves in optical fibers. Another well-known polarization bases are two opposite rotating circularly polarized unit vectors. They can be expressed using linear polarization bases as:

$$\vec{e}_R = \frac{1}{\sqrt{2}}(\vec{e}_x - i\vec{e}_y), \tag{II.41a}$$

$$\vec{e}_L = \frac{1}{\sqrt{2}}(\vec{e}_x + i\vec{e}_y), \tag{II.41b}$$

where $\vec{e}_R$, and $\vec{e}_L$ are the right- and left-handed unit vectors, respectively. The nonlinear coupling equations between two **opposite-rotating** circularly polarized optical waves with ω_R and ω_L for the right- and left- handed, respectively, can be obtained by calculating the nonlinear polarization P_{NL}under circular polarization basis and substituting P_{NL} into Eq. (II.22). The nonlinear wave equations are

$$\frac{\partial A_R}{\partial z} + \frac{1}{v_{gR}}\frac{\partial A_R}{\partial t} + \frac{i}{2}k_R^{(2)}\frac{\partial^2 A_R}{\partial t^2} = i\frac{\omega_R n_2}{c}\left(\frac{2}{3}|A_R|^2 + \frac{4}{3}|A_L|^2\right)A_R, \tag{II.42a}$$

$$\frac{\partial A_L}{\partial z} + \frac{1}{v_{gL}}\frac{\partial A_L}{\partial t} + \frac{i}{2}k_L^{(2)}\frac{\partial^2 A_L}{\partial t^2} = i\frac{\omega_L n_2}{c}\left(\frac{2}{3}|A_L|^2 + \frac{4}{3}|A_R|^2\right)A_L, \tag{II.42b}$$

where $A_R(z,t)$ and $A_L(z,t)$ are the amplitude envelopes of the laser pulses for right- and left- handed wave, respectively. For two circularly polarized optical waves at the **same rotating** direction (right- or left-handed). Th e nonlinear coupling equations are

$$\frac{\partial A_1}{\partial z} + \frac{1}{v_{g1}}\frac{\partial A_1}{\partial t} + \frac{i}{2}k_1^{(2)}\frac{\partial^2 A_1}{\partial t^2} = i\frac{\omega_1 n_2}{c}\left(\frac{2}{3}|A_1|^2 + \frac{1}{3}|A_2|^2\right)A_1, \tag{II.43a}$$

$$\frac{\partial A_2}{\partial z} + \frac{1}{v_{g2}}\frac{\partial A_2}{\partial t} + \frac{i}{2}k_2^{(2)}\frac{\partial^2 A_2}{\partial t^2} = i\frac{\omega_2 n_2}{c}\left(\frac{2}{3}|A_2|^2 + \frac{1}{3}|A_1|^2\right)A_2, \tag{II.43b}$$

where $A_1(z,t)$ and $A_2(z,t)$ are the amplitude envelopes of the laser pulses, and ω_1, ω_2 are their frequencies. The first and second terms in the right sides of the Eqs. (II.42) and (II.43) are SPM and XPM processes, respectively.

The nonlinear interactions of two optical waves have been shown theoretically in the nonlinear coupling equations (II.38), (II.40), (II.42), and (II.43) for different configuration. By using linear and circular polarization bases, many interesting properties can be demonstrated. For two linearly polarized optical waves, XPM is twice large than SPM in Eqs. (II.38) if they are in the parallel linear polarization; but XPM is 2/3 of SPM as shown in Eqs. (II.40) for two optical waves at perpendicular linear polarizations. However, these characteristics are different for two circularly polarized optical waves. XPM is only half of SPM if two optical waves are at the same circularly polarized state (right-handed or left-handed); and XPM is twice of SPM for two optical waves at opposite circularly polarized states. In additional, the DWFM terms does not appear under the circular polarization bases. There is no amplitude coupling during the nonlinear interaction of two circularly polarized optical waves.

In the most general case, numerical methods have to be used to solve these nonlinear coupling equations. However, the analytical solutions can be obtained when the group velocity dispersion temporal broadening can be neglected. As an example, the typical nonlinear wave equation (II.38) will be solved to demonstrate the spectral modulations caused by XPM processes. Eq. (II.38) is almost the same as Eqs. (II.42) and (II.43) except their coefficients are different. They have similar properties and cause same spectral broadening structures. By denoting the slowly changing envelope and phase of the pulses with A and α, we obtain:

$$A_1(\tau,z) = a_{1(\tau,z)}e^{i\alpha_1(\tau,z)} \quad \text{and} \quad A_2(\tau,z) = a_{2(\tau,z)}e^{i\alpha_2(\tau,z)} \qquad \text{(II.44)}$$

and assuming $k_1^{(2)}=k_2^{(2)}=0$, Eqs. (II.38) reduce to

$$\frac{\partial a_1}{\partial z} = 0, \tag{II.45a}$$

$$\frac{\partial \alpha_1}{\partial z} = i\frac{\omega_1}{c} n_2 [a_1^2 + 2a_2^2], \tag{II.45b}$$

$$\frac{\partial a_2}{\partial z} + (\frac{1}{v_{g2}} - \frac{1}{v_{g2}})\frac{\partial a_2}{\partial \tau} = 0, \tag{II.45c}$$

$$\frac{\partial \alpha_2}{\partial z} = i\frac{\omega_2}{c} n_2 [a_2^2 + 2a_1^2], \tag{II.45d}$$

where $\tau = (t - z/v_{g1})/\tau_0$ is the local time and τ_0 is the 1/e pulse duration. In addition, Gaussian pulse shapes are chosen at the input z=0:

$$A_{1(\tau, z=0)} = A_{10} e^{-\tau^2/2}, \tag{II.46a}$$

$$A_{2(\tau, z=0)} = A_{20} e^{-(\tau-\tau_d)^2/2}, \tag{II.46a}$$

where A_{10} and A_{20} is the input peak amplitudes of the laser pulses, and $\tau_d = t_d/\tau_o$ is the normalized time delay between pulses at z=0. With these initial conditions, the solutions for the amplitudes and phases of the optical pulses after propagating in an optical fiber with length z are

$$A_{1(\tau,z)} = A_{10} e^{-\tau^2/2} e^{i\alpha_1(\tau,z)}, \tag{II.47a}$$

$$A_{2(\tau,z)} = A_{20} e^{-(\tau-\tau_d-z/L_w)^2/2} e^{i\alpha_2(\tau,z)}, \tag{II.47b}$$

$$\alpha_1(\tau, z) = \frac{\omega_1}{c} n_2 z I_{10} e^{-\tau^2} + 2\sqrt{\pi}\frac{\omega_1}{c} n_2 L_w I_{20} * [\mathrm{erf}(\tau - \tau_d) - \mathrm{erf}(\tau - \tau_d - \frac{z}{L_w})], \tag{II.47c}$$

$$\alpha_2(\tau, z) = \frac{\omega_2}{c} n_2 z I_{20} e^{-(\tau-\tau_d-z/L_w)^2} + 2\sqrt{\pi}\frac{\omega_2}{c} n_2 L_w I_{20}, * [\mathrm{erf}(\tau) - \mathrm{erf}(\tau - \frac{z}{L_w})], \tag{II.47d}$$

where I_{10} and I_{20} are the input intensities of the laser pulses, and $L_w=\tau_o/(1/v_{g1}-1/v_{g2})$ is defined as the walk-off length. Eqs. (II.47) give the nonlinear phase changes for laser pulses propagating in a nonlinear medium. This phase modulation will generate new frequencies as SPM does. The first terms on the right-handed side of Eqs. (II.47c and 47d) are the SPM induced phase changes which will broaden the spectrum of the optical pulse itself. The second terms on the right-handed side of Eqs. (II.47c and 47d) are the XPM induced phase changes which will broaden the spectrum of the other copropagating optical pulse. The nonlinear phase change coefficient of XPM is twice of the SPM. One can also find that XPM induced phase changes are sensitive to optical delay τ_d between the two optical pulses and the walk-off distance L_w. The instantaneous nonlinear frequency changes are obtained by differentiating the phase changes in (II.47c) and (II.47d) according to the formula $\delta\omega_{(\tau)} = -\partial\alpha / \partial\tau$. The instantaneous nonlinear frequency changes are:

$$\Delta\omega_1(\tau, z) = 2\frac{\omega_1}{c} n_2 I_{10} \frac{z}{\tau_0} \tau e^{-\tau^2} + 4\frac{\omega_1}{c} n_2 I_{20} \frac{L_w}{\tau_o}$$
$$* [(\tau - \tau_d) e^{-(\tau-\tau_d)^2} - (\tau - \tau_d - z/L_w) e^{-(\tau-\tau_d-z/L_w)^2}], \qquad \text{(II.48a)}$$
$$\Delta\omega_2(t, z) = 2\frac{\omega_2}{c} n_2 I_{20} \frac{z}{\tau_0} (\tau - \tau_d - z/L_w) e^{-(\tau-\tau_d-z/L_w)^2}$$
$$+4\frac{\omega_2}{c} n_2 I_{20} \frac{L_w}{\tau_o} [\tau e^{-\tau^2} - (\tau - z/L_w) e^{-(\tau-z/L_w)^2}], \qquad \text{(II.48b)}$$

where $\Delta\omega_1=\omega-\omega_1$ and $\Delta\omega_2=\omega-\omega_2$. The first and second terms on the right-handed side of Eqs. (II.48) are the contributions of SPM and XPM, respectively. The XPM induced frequency change is twice of that induced by SPM. The XPM induced frequency shift also depends on the initial optical delay τ_d and the walk-off distance L_w. Finally, the

spectral profiles can be studied by computing the Fourier transform as shown in Eqs. (II.30).

A calculation of the DXPM spectra is shown in Figure II.10 for two parallely linearly polarized 30-ps laser pulses at the wavelength of 532 nm propagating in an optical fiber. The length of the optical fiber is 1 meter. The energy of the intense laser pulse (pump) is 30 nJ. The energy of the weak laser pulse (probe) is small enough and can be neglected. The optical delay between two laser pulses is also set to zero. There is no walk-off because these laser pulses are at the same wavelength and the nonlinear medium is assumed to be isotropic. Figure II.10(a) and (b) is the spectrum of the pump and probe laser pulse, respectively. The broadening of the pump spectrum is caused by SPM of the pump pulse itself. The broadening of the Figure 10 probe spectrum is caused by the DXPM between the two laser pulses. It has been found that the modulated spectral structure of DXPM spectrum has similar oscillating properties to the SPM spectrum. The broadening of the DXPM spectrum is twice larger than that of the SPM. This can be understood by checking the nonlinear coupling equations (II.38) in which the coefficient of DXPM is two times of SPM.

Nondegenerate XPM spectra have also been calculated for two laser pulses propagating in an optical fiber with the same parallel linear polarization and different wavelengths. The calculated results are shown in Figure II.11 for laser pulses at the wavelengths of 1064 nm and 532 nm as pump and probe, respectively. The spectral bandwidths of the input two laser pulses are both less than 0.1 nm. The pulse durations of these two laser pulses are assumed to be 35 ps and 50 ps for 532 nm and 1064 nm laser pulses, respectively (In experiment, 532 nm pulse is the second harmonic of the 1064 nm laser pulse, the 532 nm pulse is shorter than 1064 nm pulse). The spectral broadening of the pump pulse is because of the SPM of pump pulse itself as shown in Figure II.11(a).

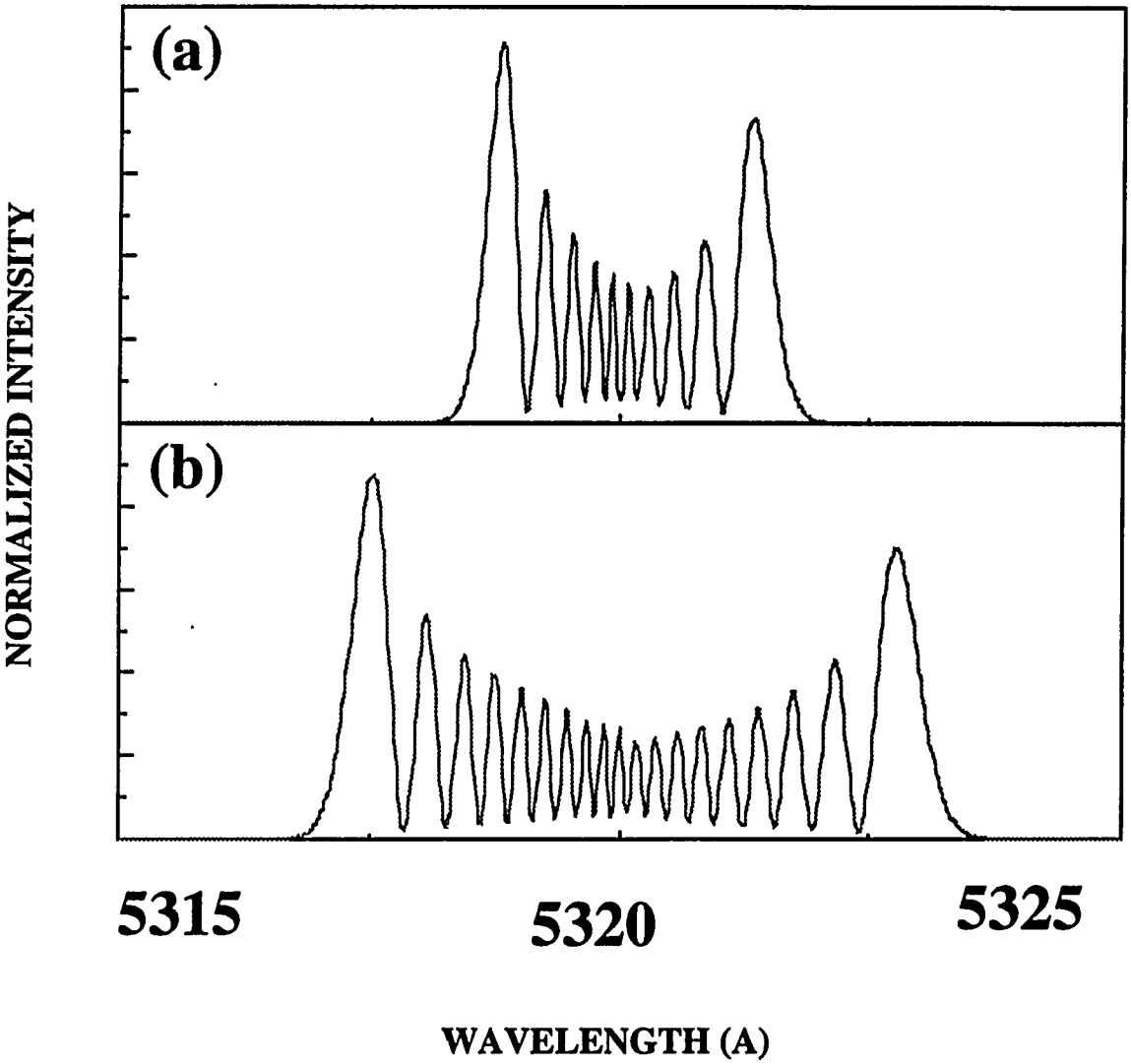

Figure II.10 Theoretical spectra of DXPM of 30-ps laser pulses at wavelength of 532 nm propagating in a 1-m optical fiber. Time delay between two pulse is zero. (a). SPM spectum distribution of the pump (intense) pulse; and (b). XPM spectral profile of the probe (weak) pulse. Note the broadening of XPM spectrum is twice larger than that of SPM.

The XPM induced spectral broadening is displayed from Figure II.11(b) to (d) for different initial time delays. The walk-off distance of the two laser pulses is about 1 meter which is the same as the fiber length used in the calculation. In Figure II.10(b), the initial time delay is t_d=0 ps. The XPM spectrum broadened to only anti-Stokes side. This can be explained as a result of walk-off. The pump pulse at the wavelength 1064 nm propagates faster than the probe pulse in optical fibers. The probe pulse sees only the tail of the pump and the probe shifted only one side. Using the same model, the XPM spectrum broadened to both Stokes and anti-Stokes side for the initial delay of t_d=31 ps as shown in Figure II.11(c) and the XPM spectrum broadened to only Stokes side for the initial delay of t_d=61 ps as shown in Figure II.11(d).

The XPM effects have been theoretically studied for many different conditions[16,33]. Experimental observation of XPM processes has been made in optical fibers[32]. The XPM effect can cause the pulse spectral broadening, it can also cause the pulse polarization properties of the propagating laser pulse in an optical fiber. In next section, the effect of XPM process on polarization state of a laser pulse propagating in an single-mode nonbirefringent optical fiber will be discussed. A model of XPM induced polarization change of a linearly polarized laser pulse will be proposed.

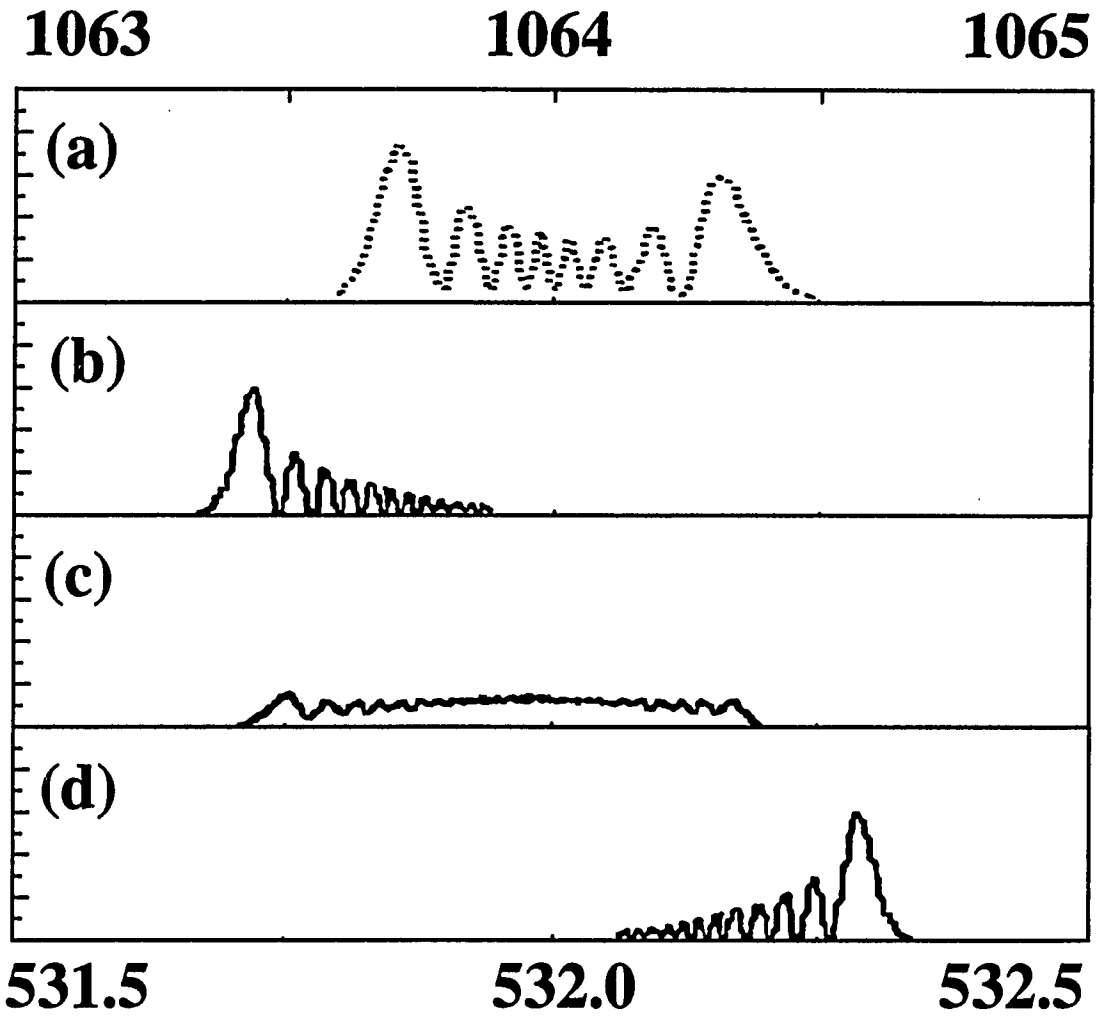

Figure II.11 Theoretical spectra of XPM of two laser pulses at the wavelengths of 1064 nm and 532 nm propagating in a 1-m optical fiber. The pump pulse is at 1064 nm and 532 nm pulse is probe. The XPM spectra are calculated for different initial time delay and the same pump intensity. (a).The SPM spectrum of pump pulse; (b). The XPM spectrum at initial time delay of t_d=0 ps; (c). The XPM spectrum at t_d=31 ps; (d). The XPM spectrum at t_d=63 ps.

II.5 Nonlinear Polarization Stability of Laser Pulse Propagating in Optical Fibers

The polarization state of the optical waves propagating in an optical fiber is important to many applications[41-42]. A single-mode optical fiber with birefringence can preserve the polarization state of the optical waves[43-46]. When a single-mode optical fiber is non-birefringent, the polarization state of the propagating optical waves will be scrambled. Many effects in optical fibers can change the polarization states of the propagating optical waves. The defects and strains that exist either randomly or are introduced by bending or twisting in optical fibers will scatter the light between orthogonal polarization modes. In addition, bending or twisting can also cause local fiber birefringence which transfers the light to different polarization states. Linear effects cause depolarization even when optical pulses are weak. Nonlinear effects may effect the polarization state at high intensity.

The nonlinear processes in optical fibers such as SPM and XPM affect not only the spectral properties of the propagating optical pulses, but also their temporal and vectorial properties. The intensity-induced polarization changes of an optical wave propagating in low-birefringent single-mode optical fibers have been intensively investigated in past two decades. The polarization instabilities caused by intensity-induced birefringence have been observed in birefringent optical fibers[47-49]. The polarization characteristics for ultrashort optical pulses propagating in non-birefringent single-mode optical fibers has not been experimentally observed and the mechanism for the intensity-induced depolarization has not been described.

Another important nonlinear phenomena on the polarization state of an optical wave propagating in wave guides are the nonlinear-optical polarization rotation. Theoretically, the intensity-induced polarization rotation of elliptically polarized optical

waves propagating in single-mode optical fibers was first studied by Crosignani *et al*[50]. They also developed a model for the nonlinear depolarization of a perfect linear polarization state because of optical Kerr effect in low-birefringent optical fibers[51]. Self-induced polarization changes in optical fiber and the polarization instabilities in birefringent media were studied by Winful[48,52] based on the intensity-induced vector rotation model.

Experimentally, nonlinear-optical polarization rotation was first observed in liquids by Maker *et al* [53]. It was shown that when high-intensity elliptically polarized light is focused into a liquid cell, the state of polarization of the light at the output is altered as a result of optically induced birefringence. In solid material, the measurements of intensity-induced polarization rotation (ellipse rotation) were first made by Owyoung *et al*[54]. The results were used to calculate the nonlinear susceptibility values of the glass. In optical wave guides, nonlinear polarization coupling and instabilities has been experimentally demonstrated by Kashyap *et al*[55] in a short single-mode liquid-cored weakly birefringent fiber made of nitrobenzene-filled silica capillary. The results indicate a possible application in nonlinear optical switching at low power. It also has been found that the nonlinear effect caused the polarization instability[47,56], induced cross-polarization changes[57] in low-birefringent single-mode glass fiber.

For the propagation of an optical wave in a low-birefringent single-mode optical fiber, the nonlinear polarization instabilities were attributed to that the intensity-induced index change of the optical fibers tends to cancel the natural low birefringence of the fiber. At certain high intensity, the optical wave propagates equivalently in a non-birefringent single-mode optical fiber. In order to well understand the propagation of a laser pulse in optical fibers, the nonlinear effect of an optical wave in non-birefringent single-mode optical fibers should be considered. When a weak laser pulse propagates in a

non-birefringent single-mode optical fiber, the polarization state of the pulse will not change if the defects of the fiber can be neglected. This is true for a short optical fiber. At high pulse intensity, nonlinear effects will dominate the polarization state of the laser pulse. Nonlinear polarization rotation and depolarization for linearly polarized ultrashort laser pulses in a short non-birefringent single-mode optical fiber can be modeled using SPM and XPM theories.

To describe the polarization state of a laser pulse propagating in a non-birefringent single-mode optical fiber, any two orthogonally polarized unit vector can be selected as a set polarization bases. Under this set of polarization bases, any polarization state of light can be a superposition of the two orthogonally polarized components. Two most useful sets of polarization bases are the two perpendicular linearly polarized unit vectors such as $\vec{e}_x$ and $\vec{e}_y$ and the two opposite rotation circularly polarized unit vectors such as $\vec{e}_R$ and $\vec{e}_L$. These two sets of polarization unit vectors can be transferred to each other through the relation

$$\vec{e}_R = \frac{1}{\sqrt{2}}(\vec{e}_x - i\vec{e}_y), \tag{II.49a}$$

$$\vec{e}_L = \frac{1}{\sqrt{2}}(\vec{e}_x + i\vec{e}_y). \tag{II.49b}$$

From Eqs. (II.49), the circular polarization bases itself are the superposition of the linear polarization bases. The right-handed polarization base $\vec{e}_R$ is the superposition of two equal perpendicular linear polarization with a phase difference of $\pi/2$. The left-handed polarization base $\vec{e}_L$ is the superposition of two equal perpendicular linear polarization with a phase difference of $-\pi/2$. On the other hand, the two linear polarization bases can

also treated as the superpositions of the equal two circular polarization with some phase differences.

For a given polarization state, the amplitudes of these two components depends on the different polarization bases. For example, an elliptically polarized light with an eccentricity of ~0 (almost circularly polarized) can be treated as two linearly polarized states with a phase difference of $\pi/2$ and almost the same amplitudes, or equivalently it can be treated as two circularly polarized components with zero phase difference and a large disparity of amplitudes. Another example is slightly depolarized linearly polarized laser light, this polarization state can be described as the superposition of the two perpendicular linearly polarized components with a large amplitude difference and a phase difference of $\pi/2$ using linear polarization bases. It can also be described as a superposition of the two opposite rotating circularly polarized components with almost equal amplitude and a phase difference of zero under circular polarization bases.

In the principle of XPM, when the two laser pulses have the same wavelength but different polarization states, this case was referred as the degenerate cross-phase modulation (DXPM). These two laser pulse having the same wavelength and different polarization states do not have to come from two physically separated pulses. They can be the two polarization components from one single laser pulse[58]. These two polarization components of a laser pules can act as two laser pulses copropagate with certain phase and amplitude differences. The intense component is the pump pulse and the weak component is the probe pulse. A key point which should be considered is the stability of the polarization of these two components in the pulse propagation in a nonlinear medium. If these two component are stable, meaning that their amplitudes do not change and they do not transfer energy from each other, the DXPM spectral broadening can be observed at the output signal[58]. If these two components are not

stable in propagation, meaning that they will coupled to each other, their spectra will mixed up at the output. Therefore, the DXPM spectral broadening can not be observed in this case. We will discuss the nonlinear wave equations under different polarization bases to find the polarization stability of the ultrashort laser pulses propagating in non-birefringent single-mode optical fibers.

The nonlinear wave equations for two linearly polarized laser pulses or the two linearly polarized components of a single laser pulse is the equations (II.40) which is also listed here

$$\frac{\partial A_x}{\partial z}+\frac{1}{v_{gx}}\frac{\partial A_x}{\partial t}+\frac{i}{2}k_x^{(2)}\frac{\partial^2 A_x}{\partial t^2}=i\frac{\omega_x n_2}{c}$$
$$x\ [(|A_x|^2+\frac{2}{3}|A_y|^2)A_x+\frac{1}{3}A_y{}^2A_x{}^*\exp(-i2\Delta\beta z)], \qquad \text{(II.40a)}$$
$$\frac{\partial A_y}{\partial z}+\frac{1}{v_{gy}}\frac{\partial A_y}{\partial t}+\frac{i}{2}k_y^{(2)}\frac{\partial^2 A_y}{\partial t^2}=i\frac{\omega_y n_2}{c}$$
$$x\ [(|A_y|^2+\frac{2}{3}|A_x|^2)A_y+\frac{1}{3}A_x{}^2A_y{}^*\exp(i2\Delta\beta z)]. \qquad \text{(II.40b)}$$

where A_x and A_y are the slowly changing pulse envelopes of the two linearly polarized components of a single pulse or for two linearly polarized separated laser pulses. There are three terms on the left-handed side. The first and second terms represent for SPM and DXPM, respectively. The coefficient of DXPM is 2/3 of SPM and so the DXPM spectral broadening is 2/3 of that of SPM. The third term is the degenerate four-wave-mixing (DWFM) term. SPM and DXPM terms will affect the phase of the two laser pulse and so generate new optical frequencies, but they do not cause their amplitudes change in propagation. The DWFM term will directly modulate the amplitudes of these laser pulses. It will cause the energy of these two optical pulses coupled to each other. In experiment,

the energies of the observed two linearly polarized optical pulses are not stable and their spectra do not show a broadening ratio of 2/3 because of the mixing up of the two pulses.

This DWFM process is important for the optical pulses propagating in nonbirefringent medium because of the wave vector mismatch $\Delta\beta=0$ which will lead the DWFM terms to be steady ones. In birefringent medium, two optical pulses have a wave vector mismatch of $\Delta\beta \neq 0$. The terms of DWFM process are oscillating ones. When these pulses propagate a distance long enough in the medium, the effect can be neglected. As a matter of fact, these pulse will be spatially separated if they propagate in a medium long enough with different wave vectors.

Similar discussion can be applied to two circularly polarized optical pulses. In fact the nonlinear wave equations for two linearly polarized optical pulse can be easily transferred into those for two circularly polarized optical pulses. Under linear and circular polarization bases, the slowly changing pulse electric field envelope can be expressed as:

$$\vec{A} = A_x \vec{e_x} + A_y \vec{e_y} = A_R \vec{e_R} + A_L \vec{e_L}, \qquad \text{(II.50)}$$

substituting Eqs. (II.49) into Eq. (II.50), one can expect

$$A_R = \frac{1}{\sqrt{2}}(A_x + i A_y), \qquad \text{(II.51a)}$$

$$A_L = \frac{1}{\sqrt{2}}(A_x - i A_y). \qquad \text{(II.51b)}$$

From the nonlinear wave equations (II.40a) and (II.40b) for $\Delta B=0$ and $\omega_x=\omega_y=\omega$, we have

$$\{\frac{\partial}{\partial z}+\frac{1}{v_{gx}}\frac{\partial}{\partial t}+\frac{i}{2}k_x^{(2)}\frac{\partial^2}{\partial t^2}\}(A_x-iA_y)$$
$$=i\frac{\omega n_2}{c}\{[(|A_x|^2+\frac{2}{3}|A_y|^2)A_x+\frac{1}{3}A_y{}^2A_x{}^*]$$
$$-i[(|A_y|^2+\frac{2}{3}|A_x|^2)A_y+\frac{1}{3}A_x{}^2A_y{}^*]\}$$

$$=i\frac{\omega n_2}{c}\{\frac{2}{3}(|A_x|^2+|A_y|^2)(A_x-iA_y)$$
$$+\frac{1}{3}(|A_x|^2A_x-i|A_y|^2A_y)+\frac{1}{3}A_y{}^2A_x{}^*-i\frac{1}{3}A_x{}^2A_y{}^*\}$$

$$=i\frac{\omega n_2}{c}\{\frac{2}{3}(|A_x|^2+|A_y|^2)(A_x-iA_y)$$
$$+\frac{1}{3}(|A_x|^2+|A_y|^2)(A_x+iA_y)^*\}. \qquad \text{(II.52)}$$

From Eq. (II.50) we have

$$|A_x|^2+|A_y|^2=|A_R|^2+|A_L|^2. \qquad \text{(II.53)}$$

and from Eq. (II.51) we have

$$A_x{}^2+A_y{}^2=2A_RA_L. \qquad \text{(II.54)}$$

Substituting Eq. (II.53) and (II.54) into Eq. (II.52)

$$\{\frac{\partial}{\partial z}+\frac{1}{v_{gx}}\frac{\partial}{\partial t}+\frac{i}{2}k_x^{(2)}\frac{\partial^2}{\partial t^2}\}(A_x-iA_y)$$
$$=i\frac{\omega n_2}{c}\{\frac{2}{3}(|A_R|^2+|A_L|^2)(A_x-iA_y)$$

$$+\frac{2}{3}A_R A_L (A_x + iA_y)^*\}. \qquad \text{(II.55)}$$

Putting Eqs. (II.51) into Eq. (II.55), we have the nonlinear wave equation for two circularly polarized optical pulses with amplitudes of A_R and A_L for right-handed component which is listed here again:

$$\frac{\partial A_R}{\partial z} + \frac{1}{v_{gR}}\frac{\partial A_R}{\partial t} + \frac{i}{2}k_R^{(2)}\frac{\partial^2 A_R}{\partial t^2} = i\frac{\omega_R n_2}{c}\left(\frac{2}{3}|A_R|^2 + \frac{4}{3}|A_L|^2\right)A_R, \quad \text{(II.42a)}$$

by similar calculation, the nonlinear wave equation for left-handed component is

$$\frac{\partial A_L}{\partial z} + \frac{1}{v_{gL}}\frac{\partial A_L}{\partial t} + \frac{i}{2}k_L^{(2)}\frac{\partial^2 A_L}{\partial t^2} = i\frac{\omega_L n_2}{c}\left(\frac{2}{3}|A_L|^2 + \frac{4}{3}|A_R|^2\right)A_L. \quad \text{(II.42b)}$$

Where A_R and A_L are the slowly changing pulse envelopes of the two circularly polarized components of a single pulse or for two circularly polarized separated laser pulses. The first and second terms on the left-handed side of these equations are represent for SPM and DXPM, respectively. The coefficient of DXPM which is 3/4 is twice of that for SPM which is 2/3. The spectral broadening of the DXPM of two circularly polarized optical pulses is also twice of the spectral broadening of SPM. Interestingly enough in Eqs. (II.42), the DWFM terms disappear, meaning that the nonlinear interactions between two circularly polarized optical pulses are pure phase modulations. These phase modulation processes just change the phase of the optical pulses. The amplitudes and so the pulse envelopes do not change in these processes. This salient feature is different with the nonlinear interactions of the two linearly polarized optical pulses where the DWFM terms will cause the energies of the pulses transferring with each other.

The nonlinear wave equations have different forms under different polarization bases as shown in equations (II.40) and (II.42). The DXPM spectral broadening in linear polarization bases which is 2/3 SPM broadening is smaller than that in circular polarization bases which is 2 times of SPM broadening. The DWFM terms disappear under circular polarization bases. From Eq. (52) to Eq. (55), it is clear that the DWFM terms of linear polarization combine with part of SPM and become DXPM processes for circular polarization. This indicates that the DWFM not only modulate the amplitudes of the two optical pulses, but also modulate the phase of these pulses. Furthermore, SPM spectral broadening is (3/2) lager than that of DXPM for linear polarizations, but part of SPM in linear polarization becomes DXPM for circular polarizations and cause the DXPM broadening is twice larger than that of SPM.

The physics essences of these equations are the same because these nonlinear coupling equations (II.40) and (II.42) can be transferred to each other by using the relations of the polarization bases for linear and circular polarization. When any light is coupled into an optical fiber, the polarization state of the light can be descried by using either two perpendicular linear polarization bases or two opposite rotating circular polarization bases. Both nonlinear coupling equations (II.40) and (II.42) can be used to describe to the light propagation. Experimentally, there are different ways of observation at the fiber output, different polarizing components can be measured such as two linearly or circularly polarized components. When two circularly polarized components are measured at the fiber output and Eqs. (II.42) are used in analyses, the results of these equations are quite straight forward. In contrast, if two linearly polarized components are observed but circularly polarized components are still used in the analyses of Eqs. (II.42), these linearly polarized components have to be calculated by the superposition of the circularly polarized components according to Eqs. (II.49) for the relations of unit vectors.

The solutions of these nonlinear coupling equations will give the self-induced nonlinear effects on the spectrum and polarization state for a single laser pulse in single-mode optical fibers. As discussed before, the first and second terms in the right side of these equation are SPM and XPM processes, respectively. The third terms in the right side of Eqs. (II.41) are known as degenerate four wave mixing (DWFM). These DWFM processes are important in the single pulse propagation in nonbirefringent single-mode optical fibers because of the wave vector mismatch $\Delta\beta=0$ which will lead the DWFM terms to be steady ones. The DWFM processes will cause the amplitudes of the two linear components coupled to each other, means the amplitudes of both linear components of the laser pulse are not stable in the propagation. In opposite, the nonlinear interactions of the circularly polarized laser pulses (or two circular components of a single laser pulse) are pure phase modulation processes such as SPM and DXPM. The amplitudes of the two circular components dose not change during the SPM and DXPM processes, means that these circular polarization states are stable at high intensity.

The nonlinear wave equations describing by Eqs. (II.40) for two linearly polarized components can be solved only by using numerical method because of the DWFM terms. The Eqs. (II.42) which give the same results as of Eqs. (II.40) for two circularly polarized components can be analytically solved using some approximations. Assuming that the third terms of the right sides of Eqs. (II.41) are small enough, meaning that the group velocity dispersion temporal broadening can be neglected. By denoting the slowly changing envelope and phase of the pulse with A and α, we obtain:

$$A_R(\tau,z) = a_{R(\tau,z)} e^{i\alpha_R(\tau,z)}, \qquad \text{(II.56a)}$$

$$A_L(\tau,z) = a_{L(\tau,z)} e^{i\alpha_L(\tau,z)}, \qquad \text{(II.56b)}$$

Eqs. (II.42) reduce to

$$\frac{\partial a_R}{\partial z} = 0, \tag{II.57a}$$

$$\frac{\partial a_L}{\partial z} = 0, \tag{II.57b}$$

$$\frac{\partial \alpha_R}{\partial z} = i\frac{\omega}{c} n_2 [\frac{2}{3} a_R^2 + \frac{4}{3} a_L^2], \tag{II.57c}$$

$$\frac{\partial \alpha_L}{\partial z} = i\frac{\omega}{c} n_2 [\frac{2}{3} a_L^2 + \frac{4}{3} a_R^2], \tag{II.57d}$$

where $\tau = (t - z/\upsilon_{gl})/\tau_0$ is defined as the pulse local time and τ_0 is the 1/e pulse duration. From these equations, one can find that the envelopes of the two circular components do not change when the optical pulse propagates in a fiber as shown by Eqs. (II.57a and b). The phases of the two components change with the intensities of these components. Furthermore, the phase induced by DXPM on the second terms of Eqs. (II.57c and d) is twice of that induced by SPM. In addition, Gaussian pulse shapes are chosen at the input z=0:

$$A_R(\tau, z = 0) = a_{R0} e^{-\tau^2/2}, \tag{II.58a}$$

$$A_L(\tau, z = 0) = a_{L0} e^{-\tau^2/2}, \tag{II.58b}$$

where a_{10} and a_{20} is the input peak amplitudes of the laser pulses. With these initial conditions, the solutions for the amplitudes and phases of the pulse after propagating in optical fiber with length z are

$$a_{R(\tau,z)} = a_{R0}, \tag{II.59a}$$

$$a_{L(\tau,z)} = a_{L0}, \tag{II.59b}$$

$$\alpha_R(\tau, z) = \frac{\omega}{c} n_2 z(\frac{2}{3} I_{R0} + \frac{4}{3} I_{L0}) e^{-\tau^2}, \quad \text{(II.59c)}$$

$$\alpha_L(\tau, z) = \frac{\omega}{c} n_2 z(\frac{2}{3} I_{L0} + \frac{4}{3} I_{R0}) e^{-\tau^2}, \quad \text{(II.59d)}$$

where I_{10} and I_{20} are the intensities of the two circular components of input laser pulse. Eqs. (II.59) give the amplitudes and phases caused by SPM and DXPM processes for a single laser pulse propagating in an optical fiber or any other nonlinear medium. As expected, the amplitudes of the two circular components remain stable during the propagation from the solution (II.59a and b), while the phases depend on the intensities of right- and left-handed components. The nonlinear phases which are time-dependent are responsible for the nonlinear polarization change in the pulse profile and new frequency generation.

The stability of circularly polarized laser pulse has been displayed from the solution (II.59a and b) of the nonlinear coupling equations. When a laser pulse is coupled into optical fibers, its two circularly polarized components are stable during the nonlinear interactions. The amplitudes of the two circular components are the same as the input initial amplitudes. If the energies of the two circular components are measured at the fiber output, the ratio of them is stable and dose not depend on the pulse intensity. The nonlinear phases do not affect the output amplitudes of the two circular components. The frequencies of the two circular components will be chirped through the nonlinear phase modulation. The leading edges of the components will be shifted to Stokes side and the tailing edges of the components will be shifted to anti-Stokes side. The spectral shifts depends on the intensities of the two components through Eqs. (II.59c and d).

For a perfect circularly polarized laser pulse which has only one component (such as A_R or A_L only). From Eqs. (II.59), the amplitude of the component remains stable and

the nonlinear phase reduces to have only one SPM term. For a circularly polarized laser pulse which has two components, the amplitudes still remain stable, the nonlinear phases contain two terms of SPM and DXPM. In both cases, the circular polarizations are stable in the pulse propagation. There is no energy coupling between two circularly polarized components.

An interesting case is for a perfect linearly polarized laser pulse. This linearly polarized optical pulse is coupled into an optical fiber. At the fiber output, the linearly polarized components are observed. In analysis, the circularly polarized components are used again. This perfect linearly polarized optical pulse can be regarded as superposition of two circularly polarized components with the same amplitude and zero phase difference. At the output, the linearly polarized components are calculated through the two circular components. The amplitudes of the two components remain to be equal in propagation. Since the intensities of the two components are equal, the nonlinear phase in solution (II.51c and d) will also remain exactly the same. At the output of optical fiber, the result of the superposition of the two circular polarization states is the original linear polarization state. Therefore, the input perfect linear polarization state does not change at all after nonlinear interactions.

In any real experimental conditions, the linearly polarized optical pulses are not perfect linearly polarized. They always are slightly depolarized. The depolarization happens when the light passes through the surfaces of optical components such as lens, filters, and mirrors, the light will be scattered between the two perpendicular polarization modes by the defects on the surfaces. These slightly depolarized optical pulses are defined as quasi-linearly polarized optical pulses. For a quasi-linearly polarized optical pulse, the amplitudes of its two circularly polarized components are not equal with a slight difference. The amplitudes of the two circular components are still stable, but the

nonlinear phase are not equal after SPM and XPM processes. There will be a nonlinear phase shift between these two circular components. The nonlinear phase shift can be calculated using Eqs. (II.59 c and d) and expressed as:

$$\Delta\alpha(\tau,z)=|\alpha_R-\alpha_L|=\frac{4\pi}{3\lambda}n_2 z\Delta I e^{-\tau^2}=2ke^{-\tau^2}, \qquad \text{(II.60)}$$

where $\Delta I=|I_{R0}-I_{L0}|$ is the input intensity difference between the right- and left-handed components, and $k=2\pi n_2 z\Delta I/3\lambda$ is a nonlinear phase parameter. The nonlinear phase shift is a function of time due to its dependence on pulse local time τ. At the output, the superposition of the two circular components is not the input pulse polarization state because of this nonlinear phase shift $\Delta\alpha$.

For more details, lets see the superposition of two circular components with a given phase difference of $\Delta\alpha$ and the same amplitude. The superposition can be expressed as:

$$\vec{A}=A_R\vec{e}_R+A_L\vec{e}_L e^{i\alpha}=A_R(\vec{e}_R+\vec{e}_L e^{i\Delta\alpha}), \qquad \text{(II.61)}$$

substituting the expression (II.41) into (II.61), one can have:

$$E_X/E_Y=[\tan(\Delta\alpha/2)]^{-1}, \qquad \text{(II.62)}$$

this always represents a linear polarization state rotated with an angle of $\alpha/2$ relative to x-axis($\Delta\alpha$=0). For a quasi-linearly polarized laser pulse with a nonlinear phase shift of $\Delta\alpha(\tau,z)$, the linearly polarized output will rotate by an angle of ϕ which can be given by

$$\phi(\tau)=\Delta\alpha(\tau,z)/2=k e^{-\tau^2}. \qquad \text{(II.63)}$$

The nonlinear polarization rotation angle $\phi(\tau)$ is a function of the pulse local time τ. Therefore, a quasi-linearly polarized laser pulse will keep linearly in the propagation in optical fibers, the linear polarization directions change at different local times.

For input Gaussian pulse shape at the fiber input z=0 which is quasi-linearly polarized at x-direction, the electric field envelope is:

$$\vec{A} = A_x \vec{e}_x + A_y \vec{e}_y, \qquad \text{(II.64)}$$

where A_X and A_Y are amplitude polarized at x- and y-direction, respectively, and can be expressed as:

$$A_{X(\tau,z=0)} = a_{xo} e^{-\tau^2/2}, \qquad \text{(II.65a)}$$
$$A_{Y(\tau,z=0)} = a_{yo} e^{-\tau^2/2}, \qquad \text{(II.65b)}$$

where a_{xo}, a_{yo} ($a_{xo} >> a_{yo}$) are the input amplitudes of the two linear components of the optical pulse. Note this optical pulse linearly polarized at x-direction. After the pulse propagates in a fiber with the length of z, the polarization direction rotates an angle of $\phi(\tau)$ which depends on the pulse local time. The amplitudes of the components polarized at x- and y-direction are

$$A_{x(\tau,z)} = a_{xo} e^{-\tau^2/2}\cos[\phi(\tau)] = a_{xo} e^{-\tau^2/2}\cos(k e^{-\tau^2}), \qquad \text{(II.66a)}$$
$$A_{y(\tau,z)} = a_{xo} e^{-\tau^2/2}\sin[\phi(\tau)] = a_{xo} e^{-\tau^2/2}\sin(k e^{-\tau^2}), \qquad \text{(II.66b)}$$

where $k=2\pi n_2 z\Delta I/3\lambda$ is the nonlinear phase parameter. Note that a_{yo} is neglected since it is much smaller than a_{xo}. Substituting Eqs. (II.66) into Eq. (II.64), the electric field of the optical pulse can be expected

$$\vec{A}_{(\tau)} = \{\cos(k e^{-\tau^2})\vec{e}_x + \sin(k e^{-\tau^2})\vec{e}_y\} a_{xo} e^{-\tau^2/2}. \qquad \text{(II.67)}$$

From Eq. (II.67), it is clearly shown that the polarization direction of the optical pulse at the output of a fiber is a function of the pulse local time. At the pulse front ant tail edge, the electric field is at the input polarization direction since the pulse instantaneous intensity is low. At the central region of the optical pulse, the electric field of the optical pulse rotates an angle of k due to the high instantaneous intensity. The polarization change in the pulse temporal profiles are shown in Figure II.12 as three dimensional displays. The input quasi-linearly polarized optical pulse is shown in Figure II.12(a), the optical pulse is linear polarized in x-direction. The components at y-direction is very small and so not shown in this Figure. Figure II.12(b) shows the output optical pulse after experiencing a certain nonlinear phase shift. The arrows show the directions of the electric field of the optical pulse at different local times. This is a twisting of polarization. The curve of pulse envelope is used to show the direction of linear polarization in the pulse profile. The arrows show the direction of electric field as a function of the pulse instantaneous intensity. There is a polarization rotation effect in pulse profile. The central region of the pulse (τ~0) has the maximum rotation angle.

For the linearly polarized optical pulses experienced different nonlinear phase shifts, the three dimensional polarization structures have been displayed in Figure II.13 using $A_{x(\tau)}$, $A_{y(\tau)}$, and local time τ of Eq. (II.67). Figure II.13(a) is the input pulse temporal distribution without nonlinear effect for k=0, it is linearly polarized in x-direction. In Figure II.13(b) for k=2, the optical pulse remains linearly polarized at the

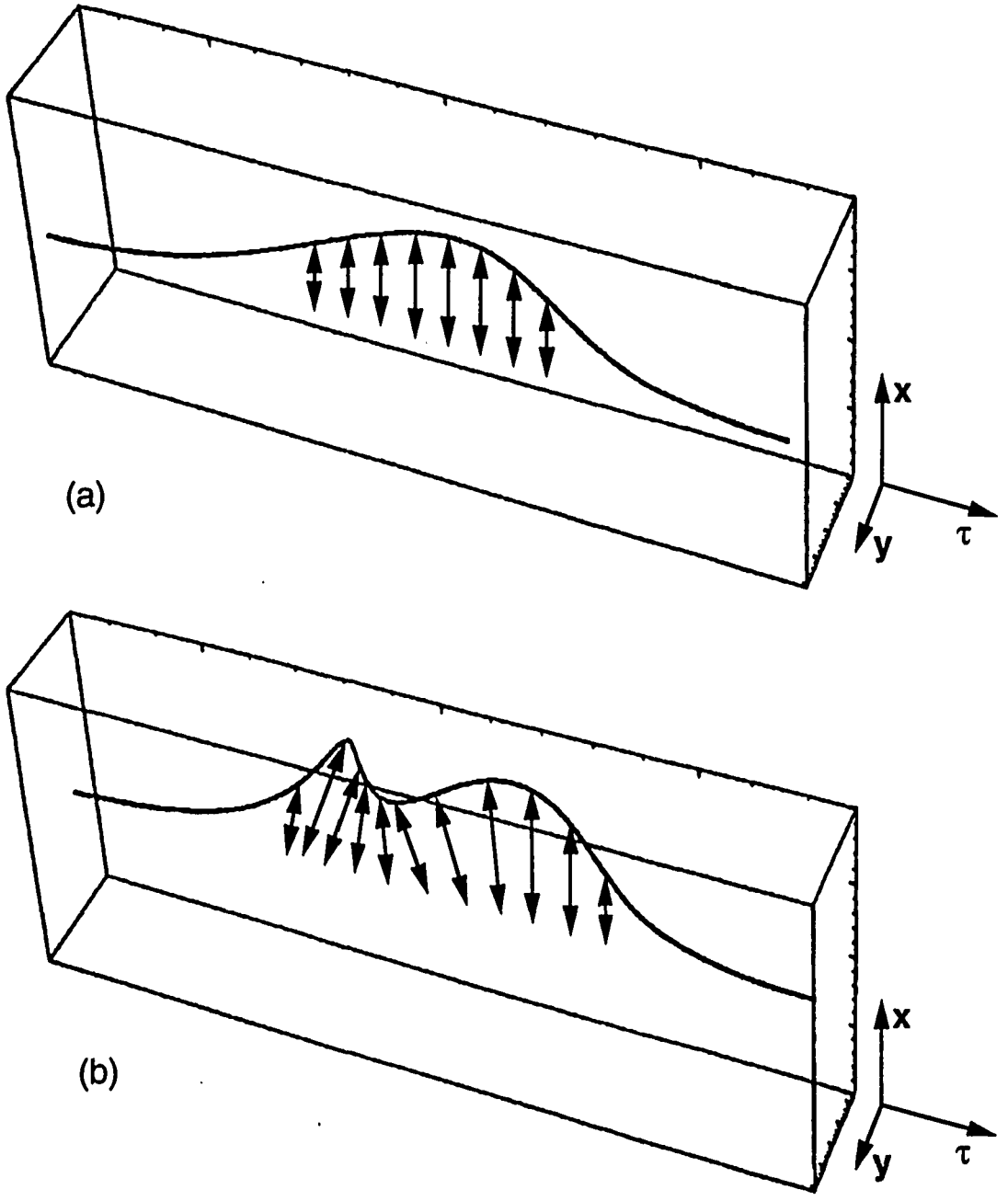

Fig II.12 Schematic of the direction the electric field of a linearly polarized optical pulse, (a) initial optical pulse which is linearly polarized at x-axis direction, (b) after propagating in a nonlinear medium, the linear polarization direction rotates and the degree of rotation depends on the instantaneous intensity of the optical pulse. Three dimensional curves are the traces of the direction of linear polarization.

input linear polarization direction for the leading and tailing edges of the pulse due to the low instantaneous intensity. The linear polarization direction at the central region of the optical pulse first shows polarization direction rotation from x- to y- direction because of the high instantaneous intensity. This polarization rotation will cause the pulse energy coupled from x-direction linear polarization mode to y-direction mode. In Figure II.13(c) for k=4, the direction of the linear polarization in the central region of the pulse profile rotates further and energy of this part is coupled into x-direction again. From Figure II.13(d) to (f), the linear polarization direction rotates more for larger nonlinear phase shift k values. Since the linear polarization direction rotates gradually from x-polarization mode to y-polarization at different local time in the pulse temporal profiles. The linear polarization of the output optical pulse develops to be twisted polarization structures. This polarization dependence on the instantaneous intensity in the pulse profile is defined as nonlinear polarization twisting (NPT) of the linearly polarized optical pulse. The twisting occurs because of the dependent of nonlinear polarization rotation on the instantaneous intensity of the optical pulse.

These twisted structures give a group of dynamic pictures of the change of polarization states for propagating laser pulse in a nonlinear medium. At any local time, the electric field is linearly polarized, but the polarization direction changes at different local time. The output laser pulse will appear to be depolarized when two linearly polarized components are observed. From the electric field of the output optical pulse in Eq. (II.67), the intensity distributions of the two linearly polarized components of the output laser pulse as a function of local times are:

$$I_{x(\tau)} = I_o e^{-\tau^2} \cos^2(k e^{-\tau^2}), \qquad \text{(II.68a)}$$

$$I_{y(\tau)} = I_o e^{-\tau^2} \sin^2(k e^{-\tau^2}), \qquad \text{(II.68b)}$$

Electric Field Direction Curves of Linearly Polarized Optical Pulses for Different Nonlinear Phase Shift $k=2\pi n_2 z\Delta I/3\lambda$

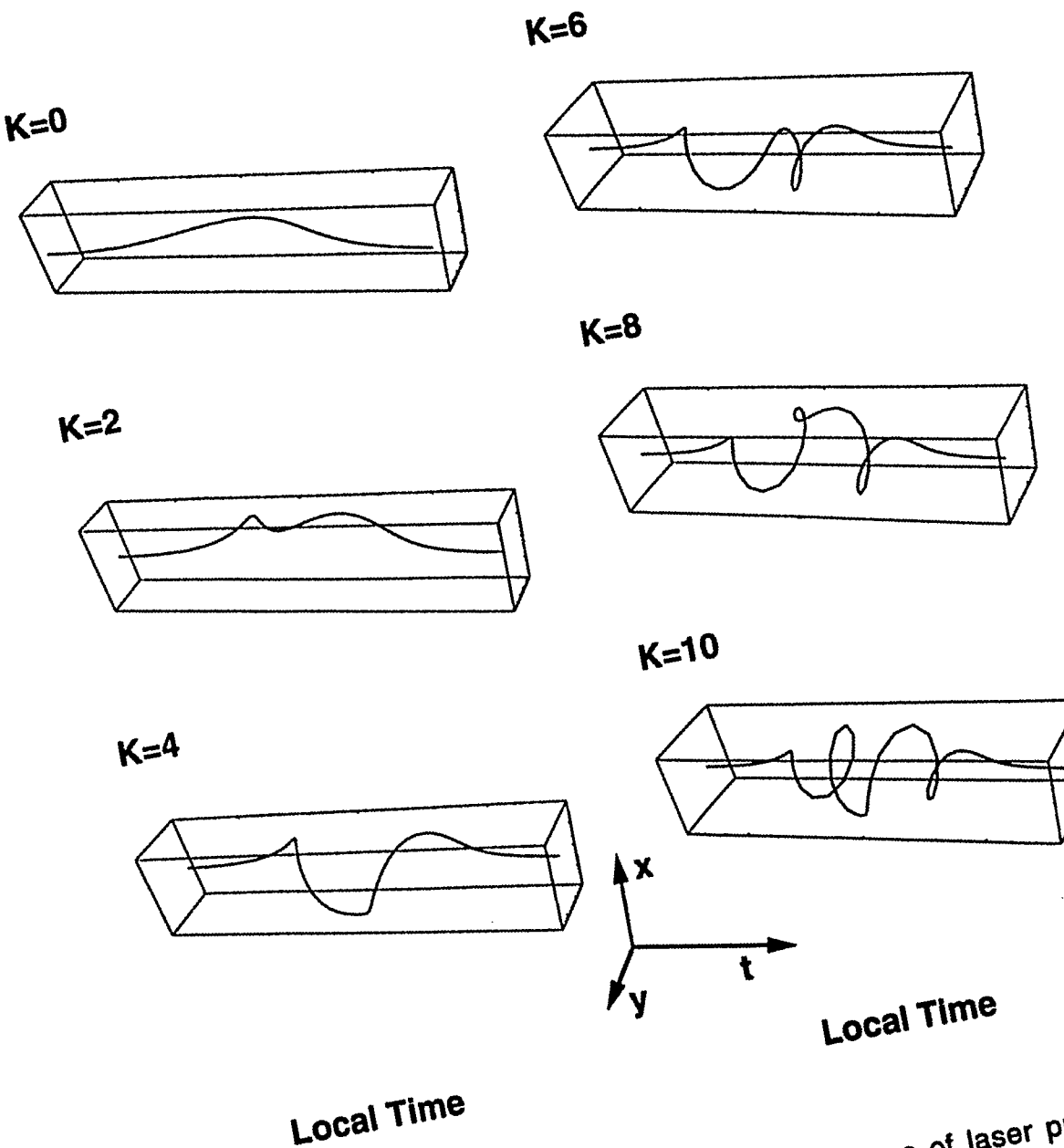

Fig II.13 Three dimensional polarization structures of laser pulses experienced different nonlinear phase shift. The laser pulse is linearly polarized at any local time, but the direction of linear polarization is different at different local time.

where I_0 is the input pulse intensity and $k=2\pi n_2 z\Delta I/3\lambda$ is the nonlinear phase parameter. At high intensity and large value of k, the $Sin^2(x)$ and $Cos^2(x)$ functions will give rise to a high frequency oscillation within the exponential profile. Hence, the input ultrafast laser pulse will be splitted into many small pulses with different intensities and pulse durations in the input pulse temporal profile.

The calculation results of normalized intensity distributions are shown in Figure II.14 and II.15 for parallel (I_x) and perpendicular (I_y) components, respectively. The input pulse is assumed to have a Gaussian intensity distribution. Without nonlinear phase shift, the output parallel component has the same Gaussian pulse shape as shown in Figure II.14(a), the perpendicular component in this case is shown in Figure II.15(a) where the intensity is assumed to be very small and can be neglected. For k=2, the parallel component in Figure II.14(b) splits into three pulses, but their intensities are relatively small. The perpendicular component in Figure II.15(b) is one pulse with a little dip on the top and most of the pulse energy is coupled into the perpendicular component. The parallel component has almost four small pulses with different intensities in Figure II.14(c) for k=4. And the perpendicular component in Figure II.15(c) has three small pulses. The energies of these two components are impending with each other. When k is increased further, two linear components develop into pulse trains with small laser pulses in the input pulse profile. For a large value of k, the pulse energy has a tendency of to be equally distributed into the two perpendicular polarization modes at the output optical pulse.

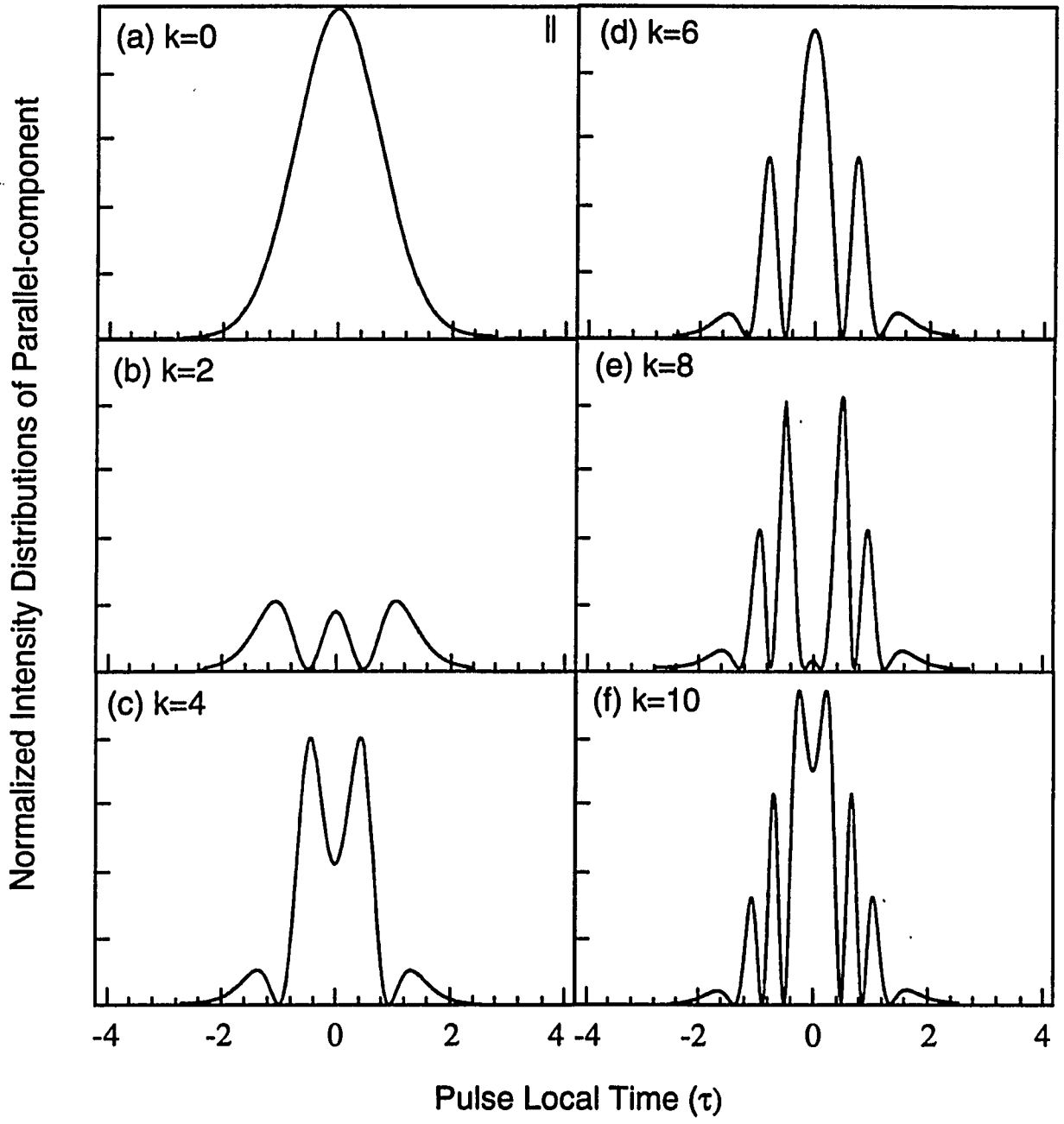

Figure II.14 The intensity distribution of the parallel component as a function of local time for different nonlinear phase shifts. The input laser pulse as shown in (a) for k=0 has Gaussian distribution. This pulse is splitting into pulse trains in the parallel linear component due to polarization twisting.

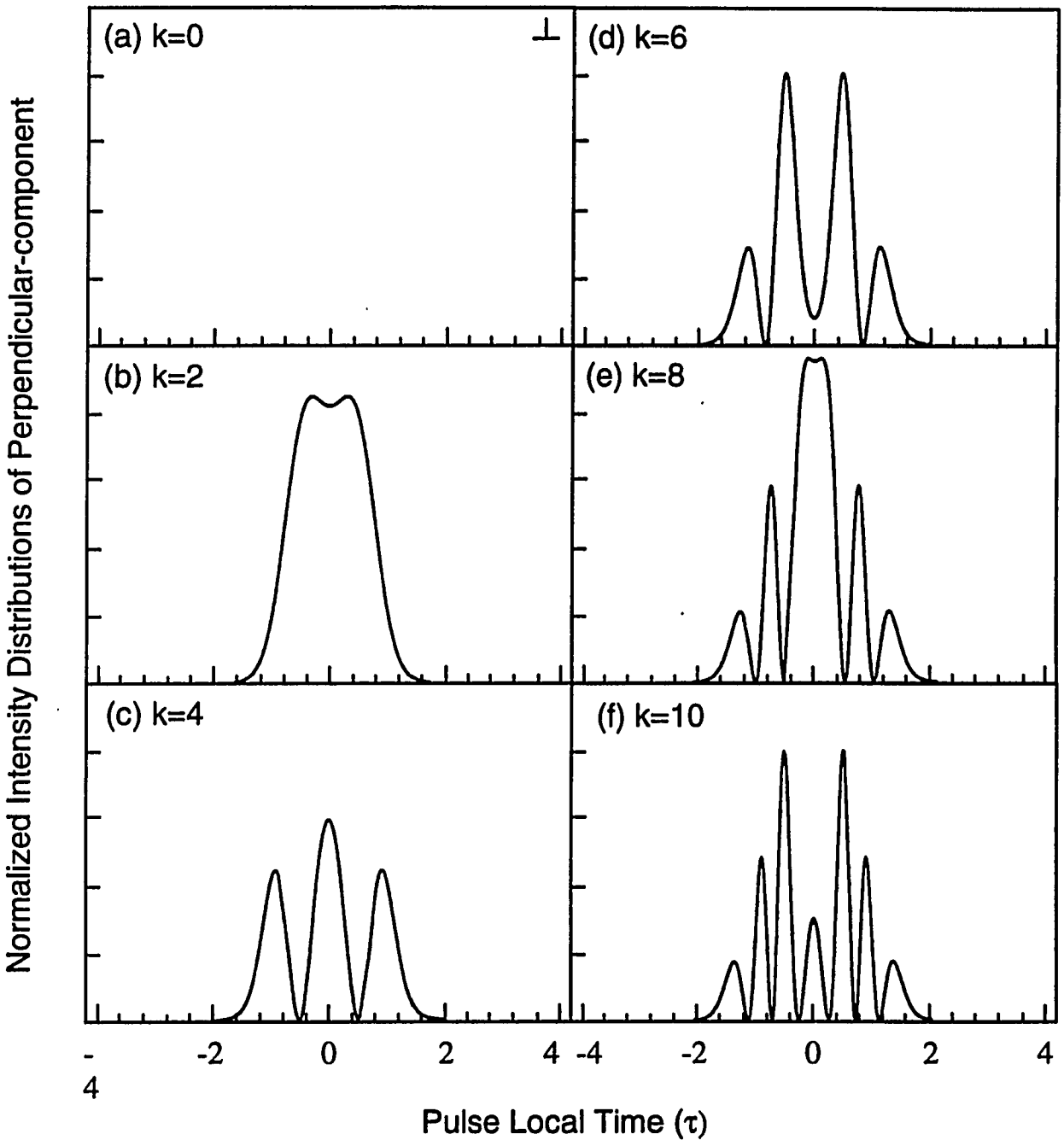

Figure II.15 The intensity distribution of the perpendicular component as a function of local time for different nonlinear phase shifts. There is no output at the direction for input laser pulse as shown in (a). The output are pulse trains for the perpendicular linear component due to polarization twisting.

To observe the polarization state of the input linearly polarized optical pulses propagating through a nonbirefringent single-mode optical fiber, the energy of the two linearly polarized components are usually measured. The degree of the polarization of the output optical pulse is calculated through the energies of the two perpendicularly polarized components. Theoretically, the energies of these two linearly polarized components can be calculated using the integrals of Eq. (II.68) and one can expect:

$$P_x = \int_{-\infty}^{\infty} I_o e^{-\tau^2} cos^2(k e^{-\tau^2}) d\tau, \tag{II.69a}$$

$$P_y = \int_{-\infty}^{\infty} I_o e^{-\tau^2} sin^2(k e^{-\tau^2}) d\tau, \tag{II.69b}$$

where Px and Py are the energy of the linearly polarized components at x- and y-direction, respectively. The degree of polarization of the output optical pulse can be calculated by

$$\rho = \frac{|P_x - P_y|}{(P_x + P_y)}, \tag{II.70}$$

Substituting Eq. (II.69) into Eq. (II.70), we have

$$\rho = \frac{\int_{-\infty}^{\infty} I_o e^{-\tau^2} \{\cos^2(k e^{-\tau^2}) - \sin^2(k e^{-\tau^2})\} d\tau}{\int_{-\infty}^{\infty} I_o e^{-\tau^2} \{\cos^2(k e^{-\tau^2}) + \sin^2(k e^{-\tau^2})\} d\tau}$$

$$= \frac{\int_{-\infty}^{\infty} e^{-\tau^2} \cos(2k e^{-\tau^2}) d\tau}{\int_{-\infty}^{\infty} e^{-\tau^2} d\tau}, \tag{II.71}$$

by using the error function integration which is

$$\int_{-\infty}^{\infty} e^{-\tau^2} d\tau = \sqrt{\pi}, \tag{II.72}$$

the degree of polarization of the output optical pulse is,

$$\rho = \frac{1}{\sqrt{\pi}} \int_{-\infty}^{\infty} e^{-\tau^2} \cos(2k e^{-\tau^2}) d\tau. \tag{II.73}$$

The calculating results of the degree of polarization is displayed in Figure II.16 for different nonlinear phase shift which is proportional to the pulse intensity. The oscillation characters of the degree of polarization shows that the pulse energy is coupled into x- any y-direction depending on the pulse intensity. It is important to show that the degree of polarization of a quasi-linearly polarized laser pulse is a function of the pulse intensity which is different for the circularly polarized laser pulse that the degree of polarization does not depends on the pulse intensity.

We have discussed the nonlinear polarization twisting (NPT) and nonlinear depolarization of the linearly polarized optical pulses propagating in single-mode nonbirefringent optical fibers. When intense linearly polarized optical pulses propagate in an optical fiber, the nonlinear phase shift will cause the linear polarization twisting. The linearly polarized optical pulses will appear to be overall depolarized. If two linearly polarized components are observed, the temporal profiles and the energies of these two linearly polarized components depend on the pulse intensity. Although the output optical pulse is depolarized, the angular distribution of the pulse energy is not uniform. By rotating the polarizer after the fiber with an angle of θ to the input linear polarization direction, the energy of the linearly polarized component at this direction can be

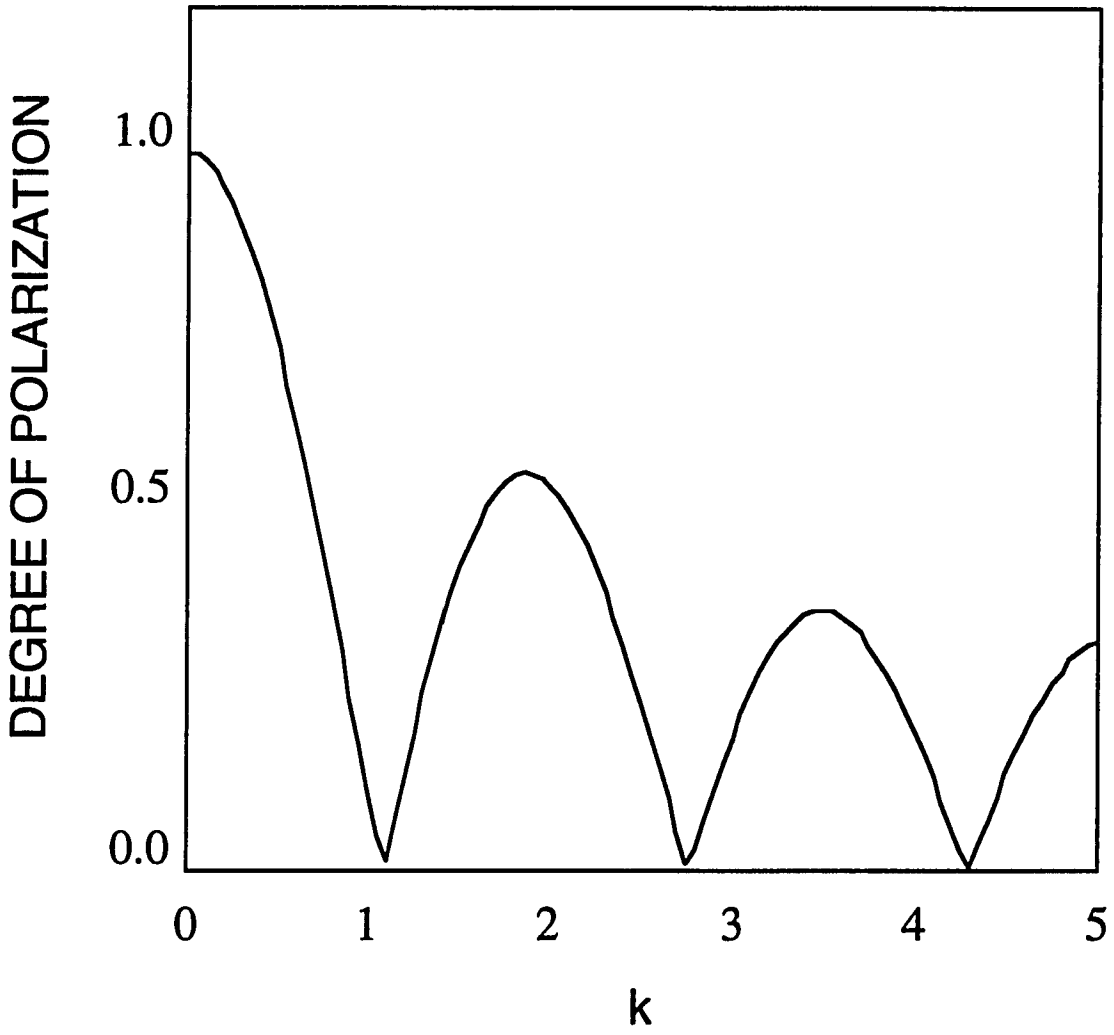

Figure II.16 The degree of polarization as a function of nonlinear phase shift (pulse intensity). At low intensity, the ouput pulse is quasi-linearly polarized. For high intensity, the degree of polarization oscilates and indicates that the pulse energy is coupled into different linearly polarized compnents at different pulse intensity.

calculated. Considering the nonlinear polarization rotation angle of $\phi(\tau)$ at local time τ within the pulse temporal profile, the angle between the polarizer and the output linear polarization at local time τ is $\phi(\tau)$-θ. For input Gaussian optical pulses, the energy of the output linearly polarized component at this direction is an integral of the instantaneous intensity to pulse local time τ and can be given by

$$P_{(\theta)} = \int_{-\infty}^{\infty} I_o e^{-\tau^2} \cos^2[\phi(\tau) - \theta] d\tau, \tag{II.74a}$$

and meanwhile the energy of the linearly polarized component at the perpendicular to this θ angle direction is expressed as

$$P_{(\theta+90^o)} = \int_{-\infty}^{\infty} I_o e^{-\tau^2} \sin^2[\phi(\tau) - \theta] d\tau. \tag{II.74b}$$

Using Eq. (II.63), the energies of these two linear components are

$$P_{(\theta)} = \int_{-\infty}^{\infty} I_o e^{-\tau^2} \cos^2(k e^{-\tau^2} - \theta) d\tau, \tag{II.75a}$$

$$P_{(\theta+90^o)} = \int_{-\infty}^{\infty} I_o e^{-\tau^2} \sin^2(k e^{-\tau^2} - \theta) d\tau. \tag{II.75b}$$

To find out the maximum of $P_{(\theta)}$ for a given intensity, we have to solve the following equation:

$$\frac{\partial P_{(\theta)}}{\partial \theta}\Big|_{\theta=\theta_{opt}} = 0, \tag{II.76}$$

substituting Eq. (II.75) into Eq. (II.76), we have

$$\int_{-\infty}^{\infty} e^{-\tau^2} \sin(2k e^{-\tau^2} - 2\theta_{opt}) d\tau = 0. \qquad \text{(II.77)}$$

The solution, θ_{opt}, of Eq. (II.77) is the angle at which the maximum energy of the output linear component can be observed. This angle gives an overall nonlinear rotation angle for input Gaussian pulses at a given intensity. Numerical method has to be used to solve the Eq. (II.77). The calculated results is shown in Figure II.17 as a function nonlinear phase parameter k which is proportional to the pulse intensity. Not surprisingly, it is easy to recognize that the rotation angle has almost a linear relation to the pulse intensity.

When the rotation angle of the output polarization state is found, the degree of polarization at that rotation angle can also be calculated through :

$$\rho = \frac{|P_{(\theta)} - P_{(\theta+90^0)}|}{P_{(\theta)} + P_{(\theta+90^0)}}|_{\theta=\theta_{opt}}, \qquad \text{(II.78)}$$

where θ_{opt} is the solution of Eq. (II.77) for a given k. The calculation of Eq. (II.78) is shown in Figure II.18 also as a function of k. At low pulse intensity (small k), the degree of polarization is near one (almost linearly polarized). When intensity is increased, the degree of polarization decreased linearly to about 0.3 at k=3. Then the degree of polarization starts to slightly oscillate and decrease for higher intensities.

In this section, the propagation of optical pulses in nonbirefringent single-mode optical fibers has been theoretically investigated considering the SPM and DXPM processes for a single laser pulse. The solutions of the nonlinear coupling equations have shown that circularly polarized laser pulses can stably propagate through a nonlinear medium. The DXPM and SPM processes do not affect the amplitudes of the circularly

polarized laser pulses. For linearly polarized laser pulses, the SPM and DXPM will introduce nonlinear phase shift between the two circularly polarized components. This nonlinear phase shift will change the output polarization state of the laser pulses. The linearly polarized laser pulses are not stably at high intensity. The nonlinear polarization twisting (NPT) and nonlinear depolarization have been discussed. The degree of polarization is a function of the input pulse intensity for linearly polarized optical pulses. The nonlinear polarization rotation and depolarization for Gaussian laser pulses are also calculated. The relation between the nonlinear depolarization and polarization rotation has been first investigated.

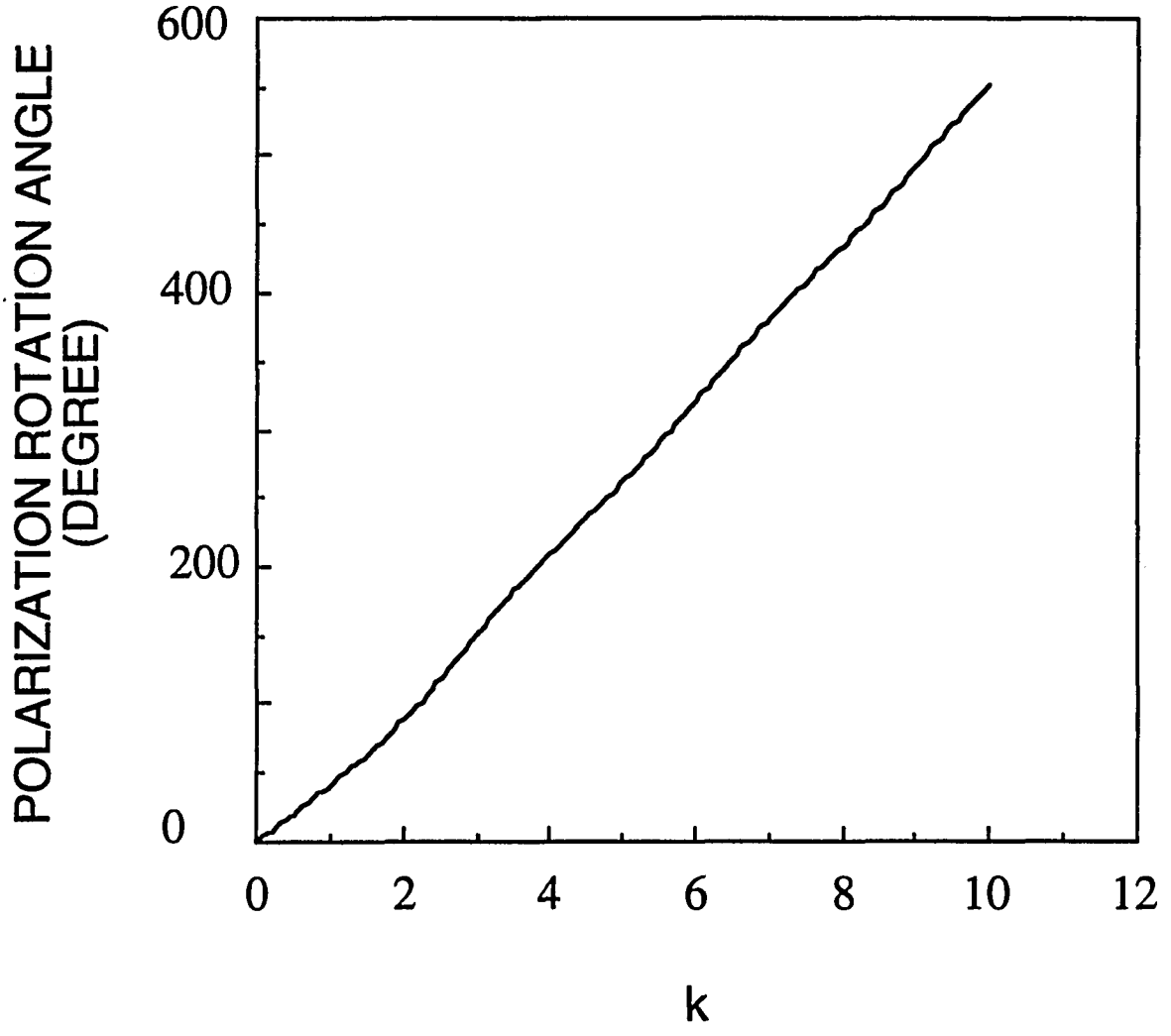

Figure II.17 The angle of nonlinear polarization rotation as a function of nonlinear phase shift k (pulse intensity).

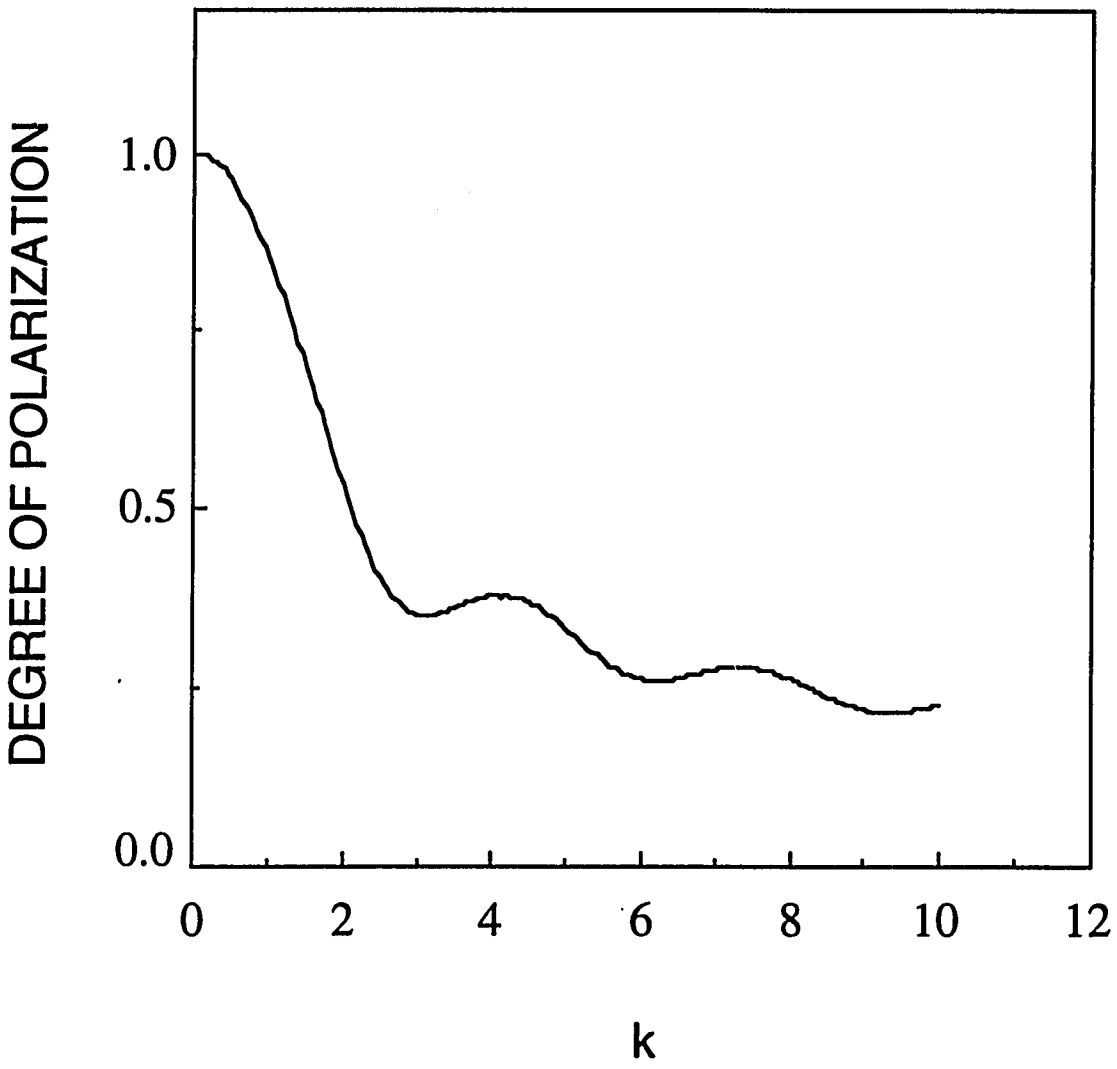

Figure II.18 The degree of polarization at an rotation angle as a function of nonlinear phase shift k (pulse intensity).

References:

[1]. P. L. Baldeck, R. R. Alfano, and G. P. Agrawal, Ultrafast Phenomena **6**, p 53-55 (Springer-Verlag, Berlin, Heilderberg 1988).

[2]. J. T. Manassah, P. L. Baldeck, and R. R. Alfano, Opt. Lett., **13**, 1090 (1988).

[3]. P. L. Baldeck, P. P. Ho, and R. R. Alfano, Rev. Phys. Appl., **22**, 1677 (1987).

[4]. R. R. Alfano, P. L. Baldeck, and P. P. Ho, J. Opt. Soc. Am **B 6**, 824 (1989).

[5]. P. L. Baldeck, P. P. Ho, and R. R. Alfano, *The Supercontinuum Laser Source*, pp 117, chapter 4 (Springer-Verlag, Berlin, 1989).

[6]. P. L. Baldeck, R. Garuthara, F. Raccah, and R. R. Alfano, Proceeding paper #TuC4, ILS-III, Atlantic City, N. J. (1987).

[7]. P. L. Baldeck, R. R. Alfano, and G. P. Agrawal, Appl. Phys. Lett., **52**, 1939 (1988).

[8]. R. R. Alfano, P. L. Baldeck, F. Raccah, and P. P. Ho, Appl. Opt., **26**, 3491 (1987).

[9]. J. T. Manassah, P. L. Baldeck, and R. R. Alfano, Appl. Opt., **27**, 3586 (1988).

[10]. P. L. Baldeck, F. Raccah, and R. R. Alfano, Opt. Lett., **12**, 588 (1987).

[11]. Y. R. Shen, *The Principles of Nonlinear Optics*, (Wiley, New York, 1971).

[12]. J. A. Amstrong, N. Bloembergen, J. Ducuining, and P. S. Pershan, Phys. Rev., **127**, 1918 (1962).

[13]. N. Bloembergen, *Nonlinear Optics* (Benjamin, New York, 1965).

[14]. N. Bloembergen, P. S. Pershan, Phys. Rev., **128**, 606 (1965).

[15]. S. A. Akmanov, A. S. Chirkin, K. N. Drabovich, A. I. Kovrigin, R. V. Khokholov, and A. P. Sukhorukov, IEEE J. Quantum Electron., **QE-4**, 598 (1968).

[16]. R. R. Alfano ed., *The Supercontinuum Laser Source*, chapter 2 (Springer-Verlag, New York, 1990).

[17]. F. Shimisu, Phys. Rev. Lett., **19**, 1097 (1967).

[18]. R. R. Alfano, and S. L. Shapiro, Phys. Rev. Lett., **24**, 584, 592, and 1219 (1970).

[19]. R. R. Alfano, Interaction of picosecond pulses with matter, GTE Technical Report TR-72-330.1 (1972) and Ph. D. Thesis, New York University (1972).

[20]. R. H. Stolen, and C. Lin, Phys. Rev., A **17**, 1448 (1978).

[21]. Q. Z. Wang, Q. D. Liu, Disa Liu, P. P. Ho, and R. R. Alfano, J. Opt. Soc. Am., B **11**, 1084 (1994).

[22]. S. De Silvestri, P. Laporta, and O. Svelto, IEEE, J. Quantum Electron., **QE-20**, 533 (1984).

[23]. W. Rudolph, and B. Wilhelmi, ed., *Light Pulse Compression*, (Char: Harwood), (1989).

[24]. W. J. Tomlinson, R. H. Stolen, and C. V. Shank, J. Opt. Soc. Am. B, **1**,139 (1984).

[25]. A. S. L. Gomes, A. S. Gouveia-Neto, and J. R. Taylor, Opt. Quantum Electron., **20**, 95 (1988).

[26]. H. Nakatsuka, D. Grischkowsky, and A. C. Balant, Phys. Rev. Lett., **47**, 1910 (1988).

[27]. C. V. Shank, R. L. Fork, R. Yen, R. H. Stolen, Appl. Phys. Lett., **40**, 761 (1982).

[28]. R. Fork, C. Shank, C. Hirliman, and R. Yen, Opt. Lett., **8**, 1 (1983).

[29]. G. Yang, and Y. R. Shen, Opt. Lett., **9**, 510 (1984).

[30]. T. Jimbo, V. L. Caplan, Q. X. Li, Q. Z. Wang, P. P. Ho, and R. R. Alfano, Opt. Lett., **12**, 477 (1987).

[31]. T. K. Gustafson, J. Taran, P. Kelley, and R. Chiao, Opt. Commun., **2**, 17 (1970).

[32]. R. R. Alfano, Q. X. Li, T. Jimbo, T. Manassah, and P. P. Ho, Opt. Lett., **11**, 626 (1986).

[33]. R. R. Alfano, P. L. Baldeck, F. Raccah, and P. P. Ho, Appl. Opt., **26**, 3491 (1987).

[34]. P. L. Baldeck, R. R. Alfano, and G. P. Agrawal, Appl. Phys. Lett., **52**, 1939 (1988).

[35]. R. R. Alfano, Q. Z. Wang, T. Jimbo, and P. P. Ho, Phys. Rev., A **35**, 459 (1987).

[36]. J. E. Rothenberg, Opt. Lett., **15**, 495 (1990).

[37]. J. Gersten, R. R. Alfano, and M. Beli, Phys. Rev., A **21**, 1222 (1980).

[38]. Q. Z. Wang, Q. D. Liu, P. P. Ho, E. K. Walge, and R. R. Alfano, Opt. Lett., **19**, 1638 (1994).

[39]. P. P. Ho, and R. R. Alfano, IEEE J. Quantum Electron., **24**, 351 (1988).

[40]. Q. Z. Wang, P. P. Ho, and R. R. Alfano, Opt. Lett., **15**, 1023 (1990).

[41]. I. P. Kaminow, IEEE J. Quantum Electron., QE-**17**, 15 (1981).

[42]. N. G. Walker and G. R. Walker, J. of Lightwave Tech., LT-**8**, 438, (1990).

[43]. R. H. Stolen, V. Ramaswamy, P. Kaiser, and W. Pleibel, Appl. Phys. Lett., **33**, 699 (1978).

[44]. F. M. Sears, J. Lightwave Tech., **8**, 684 (1990).

[45]. D. N. Payne, A. J. Barlow, and J. R. Ramskov, IEEE J. Quantum Electron., QE-**18**, 477 (1982).

[46]. J. I. Sakai, S. Machida, and T. Kimura, IEEE J. Quantum Electron., QE-**18**, 488 (1982).

[47]. S. F. Feldman, D. A. Weinberger, and H. G. Winful, Opt. Lett., **15**, ,311 (1990).

[48]. H. G. Winful, Opt. Lett., **11**, 33 (1986).

[49]. F. Matera, and S. Wabnitz, Opt. Lett., **11**, 467 (1986).

[50]. B. Crosignani, P. D Porto, Opt. Acta, **32**, 1251 (1985).

[51]. B. Crosignani, B. Daino, P. D. Porto, J. Opt. Am. B, **3**, 1120 (1986).

[52]. H. G. Winful, Appl. Phys. Lett. **47**, 213 (1985).

[53]. P. D. Maker, R. W. Terhune, and C. M. Savage, Phys. Rev. Lett. **12**, 507 (1964).

[54]. A. Owyoung, R. W. Hellwarth, and N. George, Phys. Rev. B, **5**, 628 (1972).

[55]. R. Kashyap, and N. Finlayson, Opt. Lett. **17**, 405 (1992).

[56]. S. Trillo, S. Wabnitz, R. H. Stolen, G. Assanto, C. T. Seaton, and G. I. Stegeman, Appl. Phys. Lett. **49**, 1224 (1986).

[57]. E. Lichtman, R. G. Waarts, A. A. Friesem, and S. Tang, Appl. Opt. **28**, 4056 (1988).

[58]. Q. D. Liu, J. T. Chen, Q. Z. Wang, P. P. Ho, and R. R. Alfano, Opt. Lett., **20**, 542 (1995).

Chapter III
EXPERIMENTAL METHODS

III.1 Introduction

In the various experiments, high intensity ultrashort optical pulses are coupled into single-mode optical fibers. At the output of an optical fiber, the spectral, temporal, and vectorial properties of the optical pulses are measured and analyzed. The measured results will be compared with the calculations using the proposed model of the ultrashort optical pulses propagating in single-mode optical fibers in Chapter 2.

In this chapter, the ultrashort laser systems and the optical components for the spectral and temporal measurements will be introduced. They will be used in the experiments later. The ultrashort laser sources include picosecond and femtosecond ultrashort laser systems . A Nd:YAG laser system which generates 30 ps laser light pulses will be described in this chapter. A Titanium:sapphire laser which outputs 100 fs laser light pulse train will also be discussed.

Laser light pulses are coupled into optical fibers. The core of the fiber is small enough so that the optical fibers are referred as single-mode optical fibers. Since the length and the attenuation coefficient of the optical fibers both can be neglected. The light pulse energy remains unattenuated while the light pulse propagates through the fibers. The spectral distributions of the output optical signals from an optical fiber are measured using a spectral analysis system consists of a grating spectrometer and a computerized charge-coupled-device (CCD) camera. The spectral analysis system will be discussed.

A polarizer and beam displacement prism (BDP) are used to select different polarization components of laser light. Quarter wave plates and rotators are used to changes the polarization state of the laser light. These polarization components will also be introduced in this chapter. For the measurements of the temporal distribution of the output optical signal, a single shot streak camera is used to measured the ultrashort optical pulse in picosecond range and an auto- and cross- correlator are used to measure the ultrashort optical pulses in femtosecond range.

III.2 Nd: YAG Laser and Its Amplifier System

A active-passive mode-locked neodymium-doped yttrium aluminum garnet (Nd:YAG) laser is shown schematically in Figure III.1 which consists of an laser oscillator and an amplifier. In oscillator, the laser cavity is TEM_{00} mode between the mirror within the dye cell (1) and the etalon within the acoustic-optical mode-locker (5). The mirror is immersed in a dye cell containing a liquid saturable absorber which causes the oscillator cavity to mode-lock. Lens (2) increases the beam diameter before impinging on the dye cell, thus reducing the risk of damage. The pinhole (3) forces the cavity to oscillate in a TEM_{00} mode and contribute to beam lean up. Laser oscillator (4) contains a 7 mm diameter YAG laser rod. The acoustic-optical mode-locker (5) will greatly enhances the stability of the oscillator output. The pumping light from a flash lamp is focused on the YAG laser rod and provides the optical energy necessary to excite the laser-active ions in the rod. The active and passive mode-locked mechanisms are achieved by an acoustic-optical mode-locker and a saturable absorber dye (Kodak dye #9470; Solvent: 1,2 dichloroethane)[1-2], respectively. The ends of the laser rod are cut at Brewster's angle to prevent subcavities, feedback, and reflection losses from the surfaces.

The output of a mode-locked oscillator consists of a train of individual pulses as shown in Figure III. 2(a). The temporal interval between pulses is the time of the light propagates a round trip in the cavity. The pulse selector (8) in Figure III.1 is used to extract one pulse from this pulse train and to suppress all the others. The pulse selector is preceded by a telescope (6) in order to reduce the power density on its optical elements. The selected output picosecond laser pulse is shown in Figure III. 2(b).

The output single picosecond laser pulse from the pulse selector is vertically polarized. The beam passes through a half-wave plate (9a) which is alignmented at 45^{o}

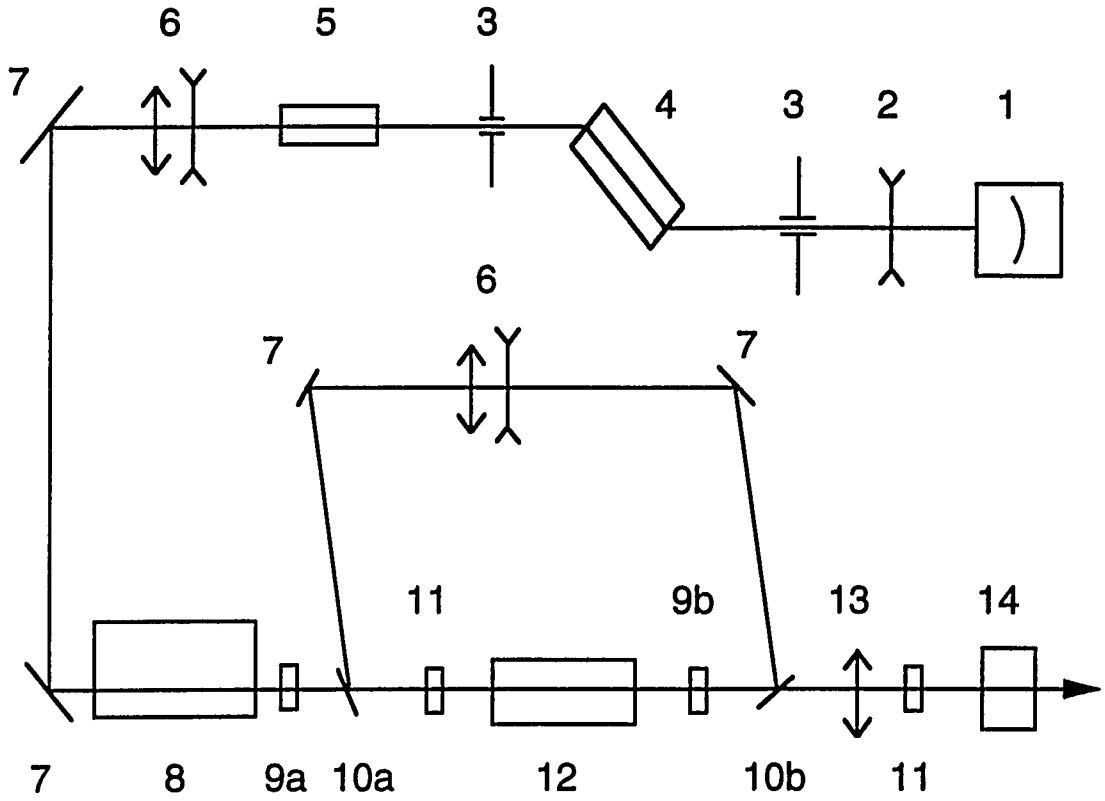

Figure III. 1 YAG401C Laser Configuration

(1). Mode-locking dye cell
(2). Diverging lens
(3). Pinhole
(4). Oscillator (Brewster angle/Brewster angle)
(5). Acousto-optical mode-locker
(6). Beam expanding telescope
(7). Reflecting mirror (45°)
(8). Pulse selector
(9). Half-wave plate
(10). Dielectric polarizer
(11). Quarter-wave plate
(12). Amplifier head
(13). Converging lens
(14). Second harmonic generator

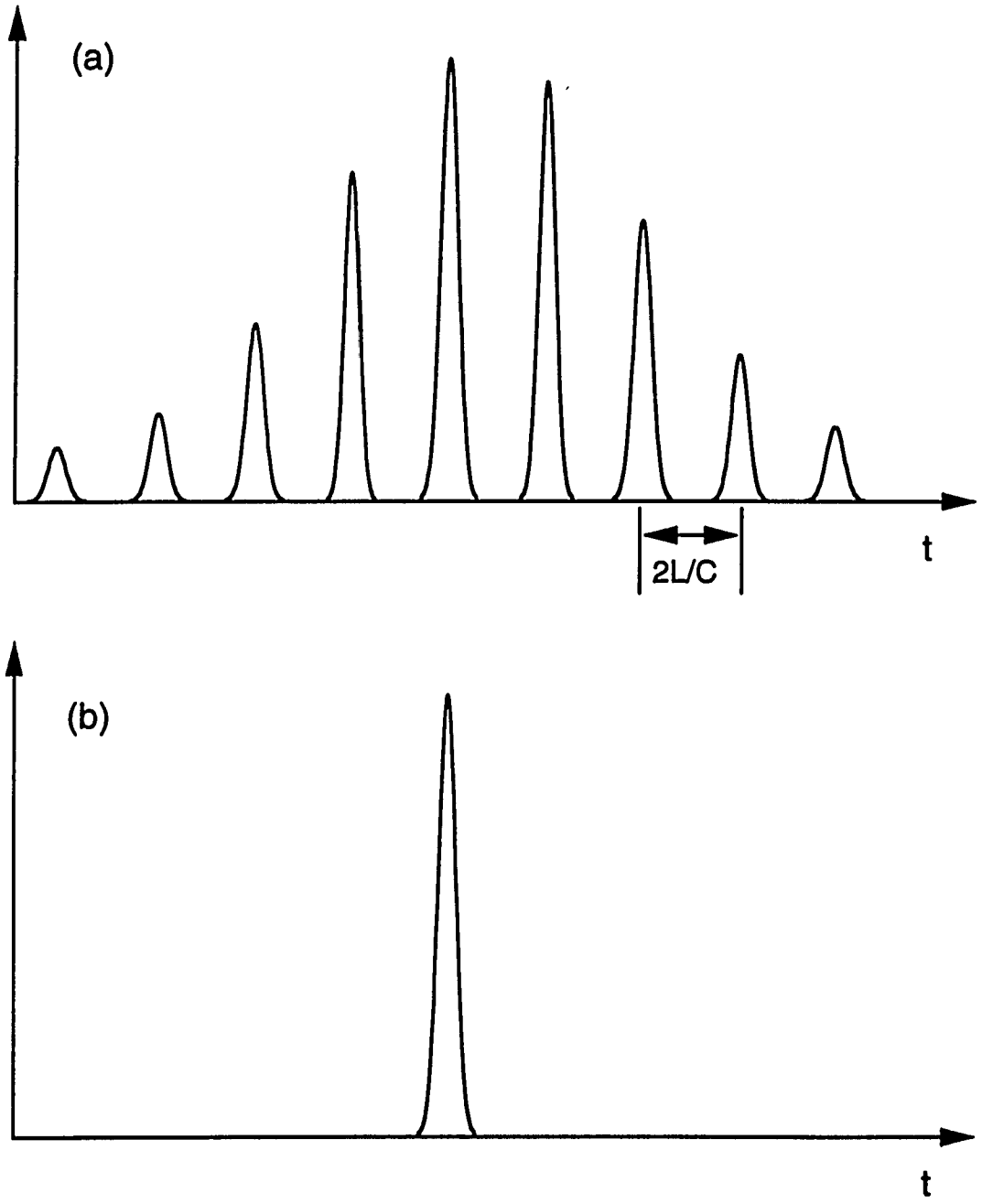

Figure III.2 (a) Ultrashort laser pulse train output from the oscillator. The time interval between pulses is the time of the light propagates around trip in the cavity. L is the cavity length. (b) The extracted picosecond laser pulse after the pulse selector.

and is thus horizontally polarized. This beam is then transmitted through the dielectric polarizer (10a). The energy of the laser pulse is amplified up to 10 mJ by the amplifying rod (12) and then sees the second half-wave plate (9b) which is alignmented parallel to (9a) and the laser beam is vertically polarized again. Now the vertically polarized beam is rejected by the second dielectric polarizer (10b). This beam is recollimated by the telescope assembly (6). Still vertically polarized, this beam is reflected from dielectric polarizer (10a) through the amplifier rod again and back through half-wave plate (9b). Now this beam is horizontally polarized, it is transmitted through (10b) to the output. The output laser pulse energy after amplification can be as high as 30 mJ at the wavelength of 1064 nm. Finally, the horizontally polarized output laser pulse is sent to the second harmonic generator (14) which is a type I KDP crystal. The polarization of the 532 nm output is vertical. This laser setup can generate 10 laser pulses per second (10 Hz).

The output beam after the second-harmonic crystal has two laser pulses at the different wavelengths of 1064 nm and 532 nm, respectively. The pulse energies of the laser light pulses at the wavelength of 1064 nm and its second harmonic wave at the wavelength of 532 nm are up to 55 mJ and 5 mJ, respectively. The spatial profiles of the laser pulses are Gaussian shapes since this laser is working at zero-order transverse mode. The temporal profiles of these ultrashort laser pulse can be measured with a streak camera. Figure III. 3 displays an output laser pulse at 532 nm measured with a Hamamatsu 2-ps streak camera. The dot curve is the measured result. The laser pulse is slightly asymmetric. The leading edge is shorter than the trailing edge. The pulse duration for the pulse at 532 nm is 35 ps. The solid curve is the theoretical fit to the laser pulse. Because the 532 nm pulse is the second-harmonic generation of the laser pulse at 1064 nm, the pulse width of the 1064 nm pulse is $\sqrt{2}$ times that of 532 nm pulse. The temporal shapes of these pulses are similar[3].

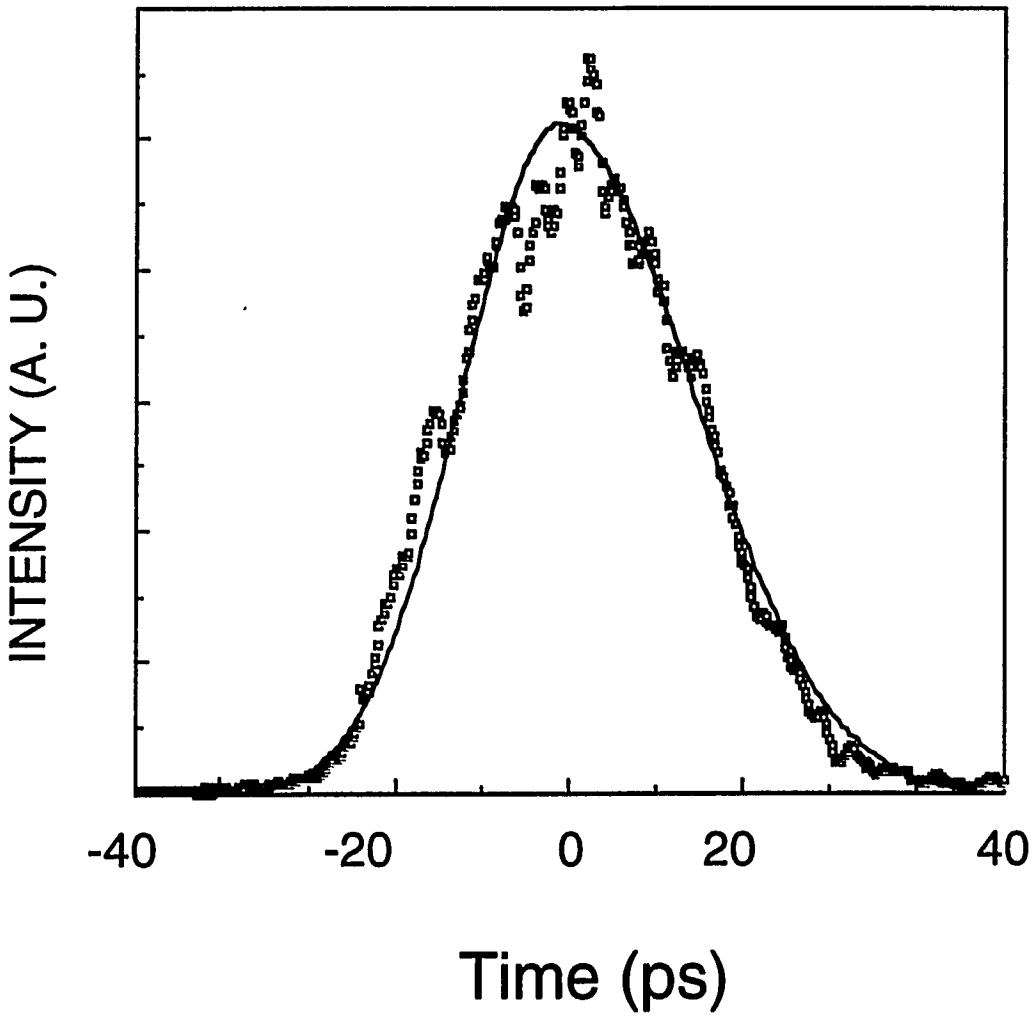

Figure III.3 The temporal profile of a 35-ps laser pulse at 532 nm. Dot curve is the measured result and the solid curve is the theoretical fit. The pulse is slightly asymmetric. The leading edge is shorter than that of the trailing edge.

III.3 Ti: sapphire Laser System

A Coherent Mira 900-B Titanium:sapphire laser is schematically displayed in Figure III.4. This laser is pumped using argon ion laser emitting a variety of wavelengths from 457 nm to 514 nm with the power of about 12w. The gain medium is tunable from 710 nm to 910 nm. In laser cavity, It is required that each lasing wavelength must satisfy the condition that precisely an integral number of half wavelengths must "fit" between the mirrors (M1 and M7). Since the integer is not specified there can be many wavelength which satisfy this criterion. Each of the wavelength is referred to as a laser longitudinal mode of the laser cavity. The overlap of tunable range of the gain medium and the cavity mode gives the lasing wavelengths. Continuous optical wave will be generated without mode-locking[4-5].

To get an ultrashort laser pulse output, some mode-locking mechanism must be introduced to the laser system. A passive mode-locking is used in this laser. The Mira cavity has been designed so that the beam diameter within the cavity changes by a small amount as the intensity of the light changes. More specifically, the beam diameter at certain locations within the cavity is large when the laser is operating continuously (CW) but become smaller when the laser is producing high intensity mode-locked pulses. A slit is now placed at the appropriate location, and its width is adjusted so that the large diameter laser beam associated with continuous operation will be interrupted at its edges. A high intensity laser pulse, however, will pass uninterrupted through the slit, since the beam is smaller as shown in Fig III.5(a) and (b). Such a slit in the Mira system will function as saturable absorber because it let the high intensity pulse pass through and introduce losses for low intensity laser light. Modelocking can be achieved through this high intensity induced change of beam diameter. Figure III. 5(c) displays the beam geometries for CW and mode-locked laser beams.

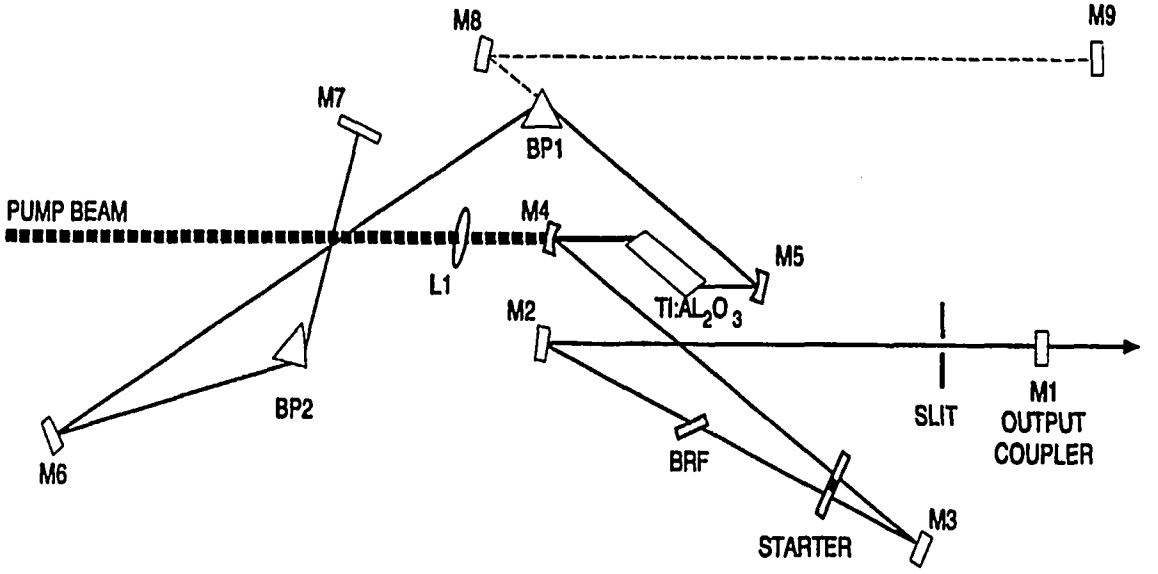

Figure III.4 Optical schematic of the Ti:sapphire laser

BP: Brewster Prism
BRF: Birefringent Filter
BS: Beamsplitter
L: Lens

M1: Mirror (partial reflection)
M2~M7: Mirrors (all reflection)
M8~M9: Mirrors (auxiliary)
TiAl2O3: Titanium:sapphire crystall

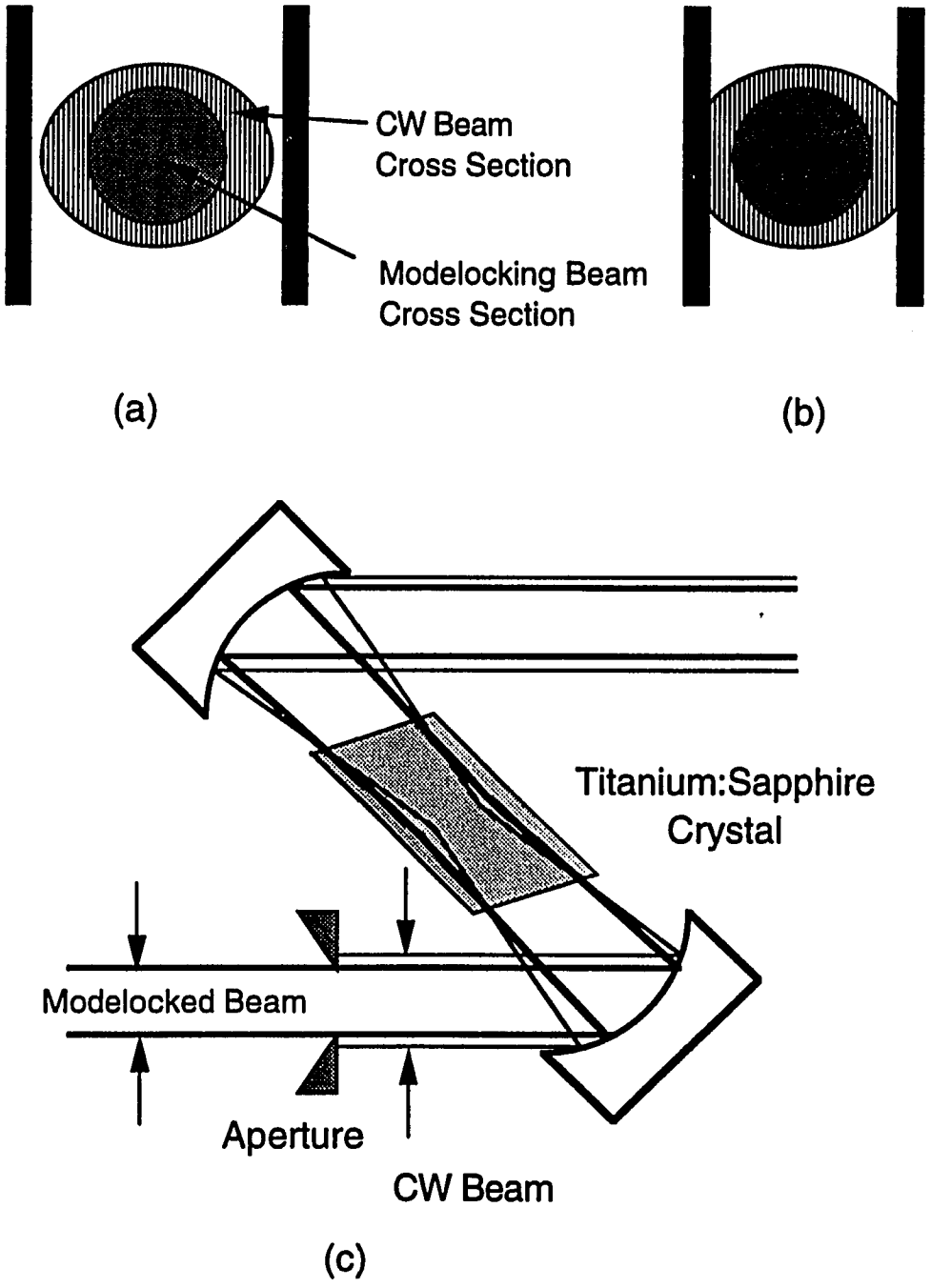

Figure III.5 (a). Slit open, no loss for either modelocking or CW; (b). Slit adjusted for modelocking and more loss for CW; (c) Beam geometry

This phenomenon is known as self-focus effect which is one of the third-order nonlinear processes. At sufficiently high intensity, the electric fields associated with the light can actually distort the atoms of the material and alter its index. This is called self-focus effect since the beam is less intense at its edges as compared to the center, the index at the center will be different, and a gradient index lens is formed. Since it is the optical Kerr effect which alter the index, the lens is also referred as a Kerr lens. The Kerr lens is formed only when the intensity of the light is extremely high. The instantaneous intensity of modelocked light pulses are sufficient to form this lens, but the weak intensity of the laser which is operating CW is not. Hence the lens is only formed upon the arrival of a modelocked pulse. It is this lens which narrows the laser beam. A slit to allow only narrow beams to pass unattenuated now forms a complete saturable absorber system which will provide a real driving force for modelocking.

Normally, the laser will operate in the CW mode with minor power fluctuations none of which cause, even instantaneously , powers which are sufficiently high to cause a Kerr lens to form. Hence, some mechanism must be introduced to create a sufficiently high peak power to open the saturable absorber system. By changing the cavity length at the proper speed, very high power fluctuations can be induced. Once the instantaneous power in one of these fluctuations becomes sufficiently high, a Kerr lens is formed, the beam is narrowed and can pass unattenuated through the slit. This pulse will become amplified and become the dominant pulse which will form the modelocked output.

In a laser such as Titanium:Sapphire[6-9], only one or two longitudinal modes operate simultaneously. This is due to the fact that all atoms within the lasing medium are considered to be equivalent and capable of emitting light over a range of frequencies and will emit at the same frequency as the stimulating light. Hence, the earliest light to reach high intensity through the amplification process will establish the frequency for

subsequent light. No atoms will remain in their upper state to amplify light at another frequency. In reality, two modes can operate simultaneously due to the spatial hole burning phenomenon.

From the principle if the mode-locking, the random fluctuations caused by only two modes do not cause very high instantaneous powers. A prerequisite for high intensity fluctuations is that the laser be encouraged to simultaneously operate with as many longitudinal modes as possible. Of all the longitudinal modes that can laser, there are a few that are more likely than others. This is due to the fact that any wavelength selecting element, will cause more losses on either side of the selected wavelength. As the wavelength selector, in our case the BRF, is changed, some modes are discouraged and others are encouraged. Alternately, the modes themselves can be shifted in wavelength by changing the cavity length, so that a different set of wavelengths satisfy the "integral half waves between reflectors" criterion. If the cavity length is changed rapidly enough, the freshly discouraged modes (previously oscillating modes) will be dying out, leaving atoms available for the new modes and there will be a period during which both can be lasing simultaneously. Thus we have created a transient condition under which the output of the laser contains more longitudinal modes than normally possible. Once a larger number of modes are lasing, peak intensities are produced to initiate Kerr lens formation and the modelocking process begins. Figure III.6 shows the pictures of the modelocked signal for different slit widths. A CW signal with slit open is shown in Figure III. 6(a). The CW laser wave has minor power fluctuation. But it can not produce high intensity modelocked pulses. When the slit is optimized, high intensity mode-locked pulse train is generated. This pulse train is shown in Figure III. 6(b) with a repetition rate of 76 MHz. The interval between pulses is the time of the light travel a round trip inside the laser cavity.

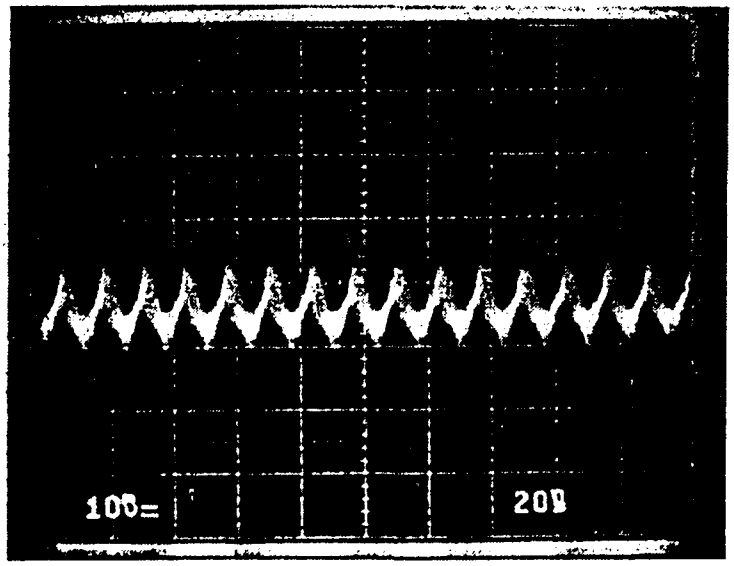

(a)

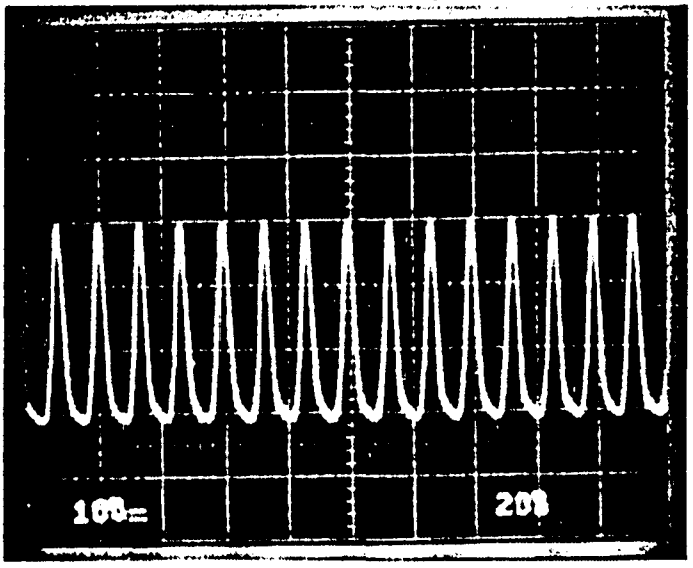

(b)

Figure III.6 (a). CW signal with slit open; (b). Modelocked signal with slit optimized.

It is important to mention that once modelocking starts, it will continue without the need of the starting mechanism. The rapid length variation can be halted. The length of the cavity is changed, not by increasing the distance between the mirrors, but by tipping the angle of a glass plate through which the beam must travel. As the plate is tipped, more glass must be traversed, and since light travels slower in glass than in air, it is entirely equivalent to increasing the distance between the mirrors. Both increase the time necessary to traverse the distance between the mirrors.

By tuning the BRF, different wavelengths can be selected. The modelocked output power of this Ti:sapphire laser is depends on the wavelength. The tuning range of this laser is designed between 710 nm and 910 nm. The calibrated output modelocked laser power as a function of the wavelength is displayed in Figure III.7. The maximum mode-locked average output power is 1.5 w at the wavelengths from 780 nm to 810 nm, corresponding to the pulse energy of 20 nJ for 76 MHz laser pulse train. The average output laser power is relatively low at the side wavelengths.

The mode-locked laser pulse duration from this Ti:sapphire laser can be measured with an auto-correlator. A measured curve is shown in Figure III. 8. The auto-correlation curve has a width of 230 femtosecond (fs). Assuming the laser pulse has a square hyperbolic secant temporal profile, the pulse width is the auto-correlation trace width divided by 1.55. Therefore, the laser pulse duration can be calculated to be 148 fs.

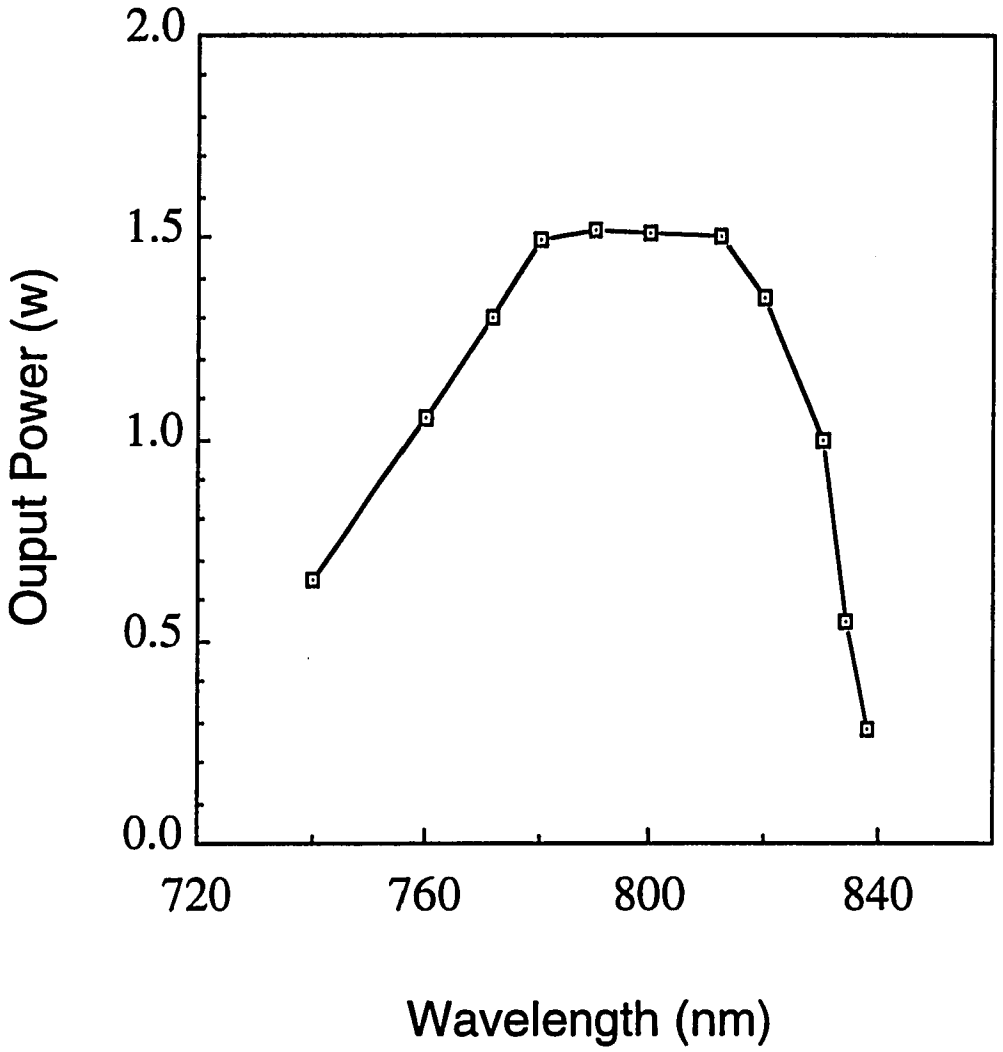

Figure III.7 The ouptut power of the mode-locked Ti:sapphire laser as afunction of wavelength.

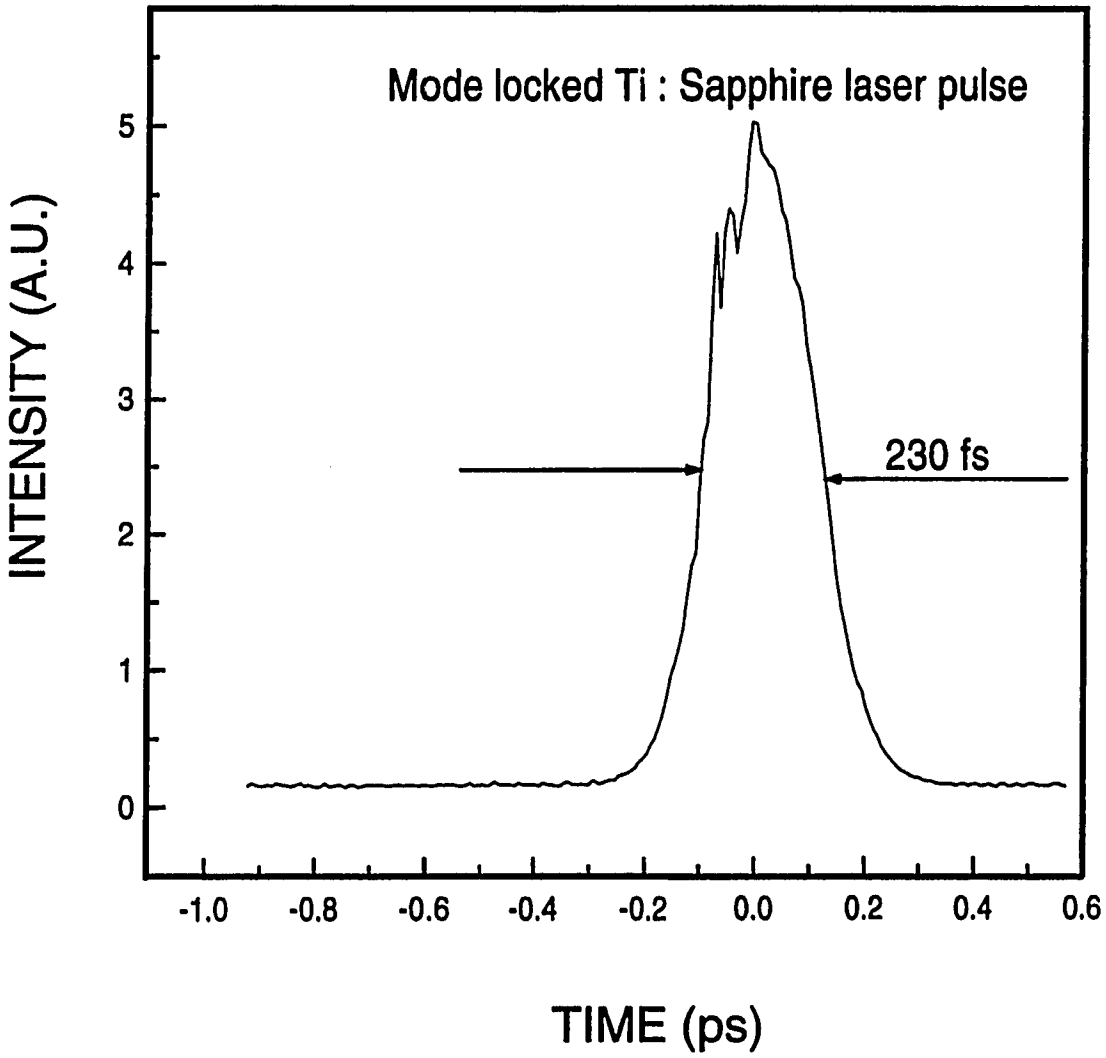

Figure III.8 The auto-correlation trace of the femtosecond laser light pulses from a Ti:sapphire laser system.

III. 4 Spectral Analysis Systems

The spectral analysis system is composed of a spectrometer and a computer controlled CCD (coupled charge device) camera. For high resolution measurements, a 1-meter Czerny-Turner Spectrometer (Model 78-460) is used to measure the spectra of the laser pulses after the nonlinear processes such as SPM and XPM in the optical fibers. A schematically diagram of this spectrometer is shown in Figure III.9. The light to be measured enters the slit S_1 and pass to the reflecting mirror M_1 where it is collimated and reflected as parallel light to the plane grating G. The dispersed light which is still parallel but with separate wavelength diverging is reflected back to the exit beam mirror M_2. Here the reflection is focused as monochromatic light at the exit slit S_2. The wavelength of the output monochromatic light at the exit slit is changed simply by rotating the grating about its center. As an alternate, with the flat mirror deflector M_3 in position, the exit beam can be focused on a CCD camera. The image of the spectrum will be recorded by the CCD camera. The focal length of the spectrometer is 1 meter. The grating is rectangular with a size of 5 cm by 5 cm and the grating spacing is a 1200 graves/mm. When incident light beams containing two different wavelengths such as at 1064 nm and its second harmonic wave at 532 nm are diffracted from the grating, the first order diffraction of light at 1064 nm is at the same direction with the second order diffraction of the light at the wavelength of 532 nm. Therefore, the light at these different wavelength regions can be measured at the same time.

The CCD camera system used in experiments is an Nu:200 type from Photometrics Ltd.. The CCD imager is a metal-oxide-semiconductor (MOS) optical detector that is composed of up to several million independent sites where photo-induced charge is store. These photosites are called picture pixels. When pixels that are closely arranged in a rectangle are exposed to light, a charge pattern accumulates that

corresponds to an illumination pattern. CCD pixels are rectangular and range from 6 to 30 micros in size. The CCD camera which is used in our experiments has 512x512 pixels with 20 micro in size.

In experiments, the laser light output from optical fibers is coupled into this spectral analysis system. For laser light at 1064 nm region, the dispersion of this system is 0.01 nm per pixel at the first order of diffraction from the grating. At the laser wavelength of 532 nm region, the dispersion of the system is 0.005 nm per pixel for the second order diffraction from the grating. The resolution of the spectral analysis system strongly depends on the width of the slit S_1. Some other parameters such as the size of the grating also affect the system resolution. This system has a resolution of 0.05 nm at the slit width of 0.03 mm.

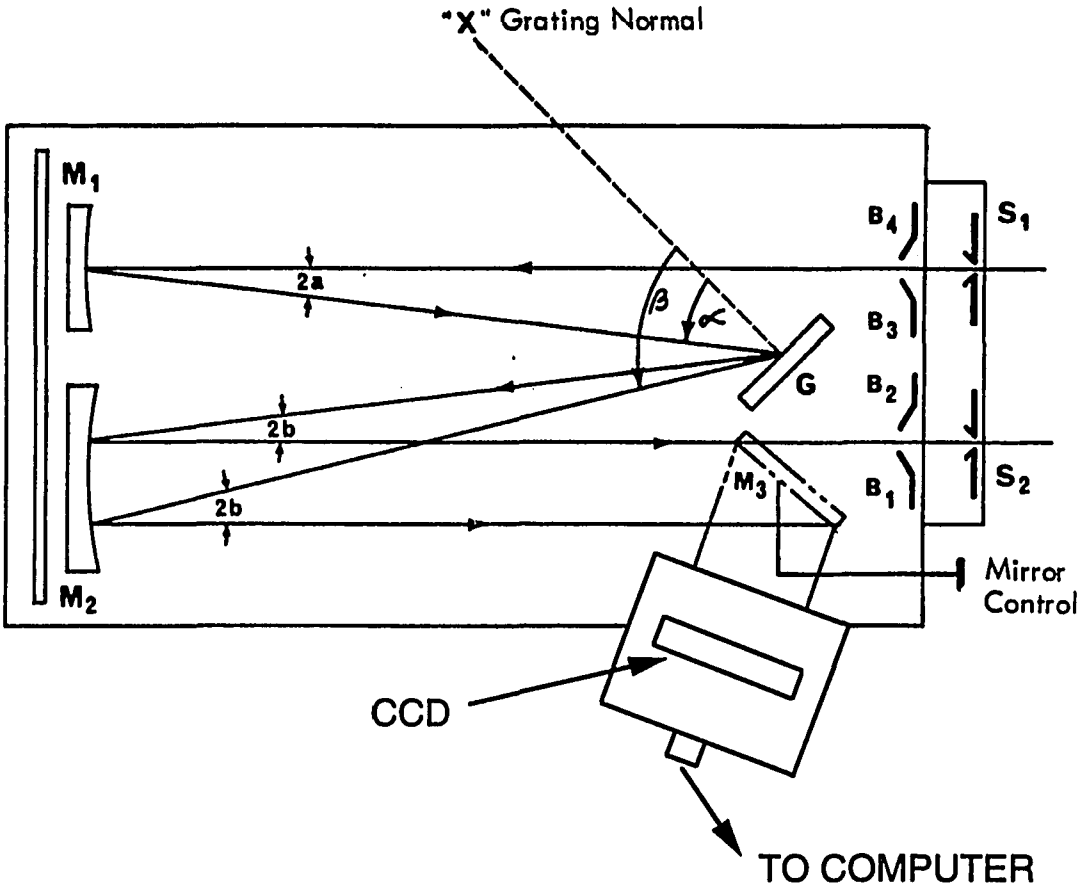

Figure III. 9 The schematical diagram of the spectral analysis system consisting of a spectrometer and a computer controlled CCD camera. S, slit; G, grating; M, mirror.

IV. 5 Optical Fibers and Light Coupler

The basic features of optical fibers has been discussed in Chapter I. An optical fiber consists of a core with very small diameter (usually 2~4 μm for single-mode fiber) surrounded by a layer of cladding. The refractive of the core is slightly larger than that of the cladding, that is why the light can be guided in the fiber. For all the commercial optical fibers, there is a plastic jacket outside of an optical fiber for protecting the fibers from any possible damages.

Two types of optical fibers are used in the experiments which are non-birefringent and high-birefringent single mode optical fibers. The non-birefringent single-mode optical fiber has a circular symmetrical core cross section without optical birefringence. There are some residual birefringence in the fiber during the fabricating processes. But the beat-length of the kind of birefringence is much longer than the length of the fibers used in the experiment. Hence, these fibers can be treated as non-birefringent single-mode fibers. Single-mode optical fibers are sensitive to optical wavelength since the different dispersion characteristics of the core and cladding materials. For example, the non-birefringent single-mode fiber which is designed for the wavelength of 514 nm can support a single mode at the wavelength of 532 nm. It does not support any propagation mode at the wavelength of 1064 nm. Conversely, the single-mode fiber which is designed working at the wavelength of 1064 nm will support multi-mode at the wavelength of 532 nm, meaning that it is not a single-mode fiber at this wavelength.

For high-birefringent single-mode optical fibers, the fiber core has a birefringence induced by the asymmetric tension between the fiber cladding and the fiber core. There are two optical axes which are perpendicular. When the linearly polarized light is coupled into such a fiber along one of the optical axis, the light will stay at the coupled linear

polarization state and will not transfer to the perpendicular polarization state. Since the optical fiber has birefringence, the light which is coupled into different polarization states has different propagating speed. The difference of their speeds is proportional to the birefringence and can be expressed as a beat-length as in Chapter I. The high-birefringent single-mode optical fiber designed for the wavelength of 532 nm has a typical beat-length of 2 mm. The high-birefringent single-mode optical fibers are also sensitive to the optical wavelength. For example, the high-birefringent single-mode fiber for the wavelength of 532 nm does not support any propagation mode at the wavelength of 1064 nm.

Two couplers are used for the light coupling into and out of an optical fiber. The coupler consists of a micro-objective lens held by frame with positioning screws which can make very small three dimensional position adjustment. The micro-objective lens focus the input light to a very small spot at the focus point (diffraction limit). The input tip of the optical fiber is also located at this focus point for light coupling. Part of the input light will be coupled into the fiber and propagate to the other end. The other micro-objective lens is used to collect and collimate the light at the output end of the optical fiber.

IV.6 Poalrizer, Quarter-wave Plate, and Beam Displacement Prism

To observe the polarization state of the laser light input to and output from optical fibers, one needs polarizers and wave-plates. A calcite crystal polarizer shown in Figure III.10(a) is used to make sure that the input laser light to an optical fiber is at a satisfactory linear polarization state. The extinction ratio of this calcite polarizer is lager than 10^6. Plastic polarizers are also used which has an extinction of 400.

Based on birefringence, the change in refractive index with the polarization of light, quarter-wave plates are used to tune linearly polarized light into circularly polarized light and vice versa. To do this, one must orient the wave plate so that equal amounts of fast and slow waves are excited such as orienting an incident linearly polarized light at 45^o to the fast (or slow) axis as shown in Figure III.10(b). If the incident linearly polarized light is not oriented at this angle, the output light from this wave plate will be elliptically polarized instead of circularly polarized.

A beam displacement prism (BDP) depicted in Figure III.10(c) is also an optical component using birefringence. A BDP has two optical axles. When light propagates in BDP, the light polarized along different optical axis will 'see' different refractive index of the BDP and will propagate at different refraction angle. Hence, the light at different polarization modes will propagate in the BDP at different direction. Two perpendicular linearly polarized components will be spatially separated after the light propagates certain distance in the BDP. At the end of the BDP the two separated linearly polarized components leave the BDP and propagates parallel because of the refraction at the rear surface. The basic function of the BDP is just like a polarizer which gives only one linearly polarized component, while BDP gives two perpendicular linearly polarized components at the same time.

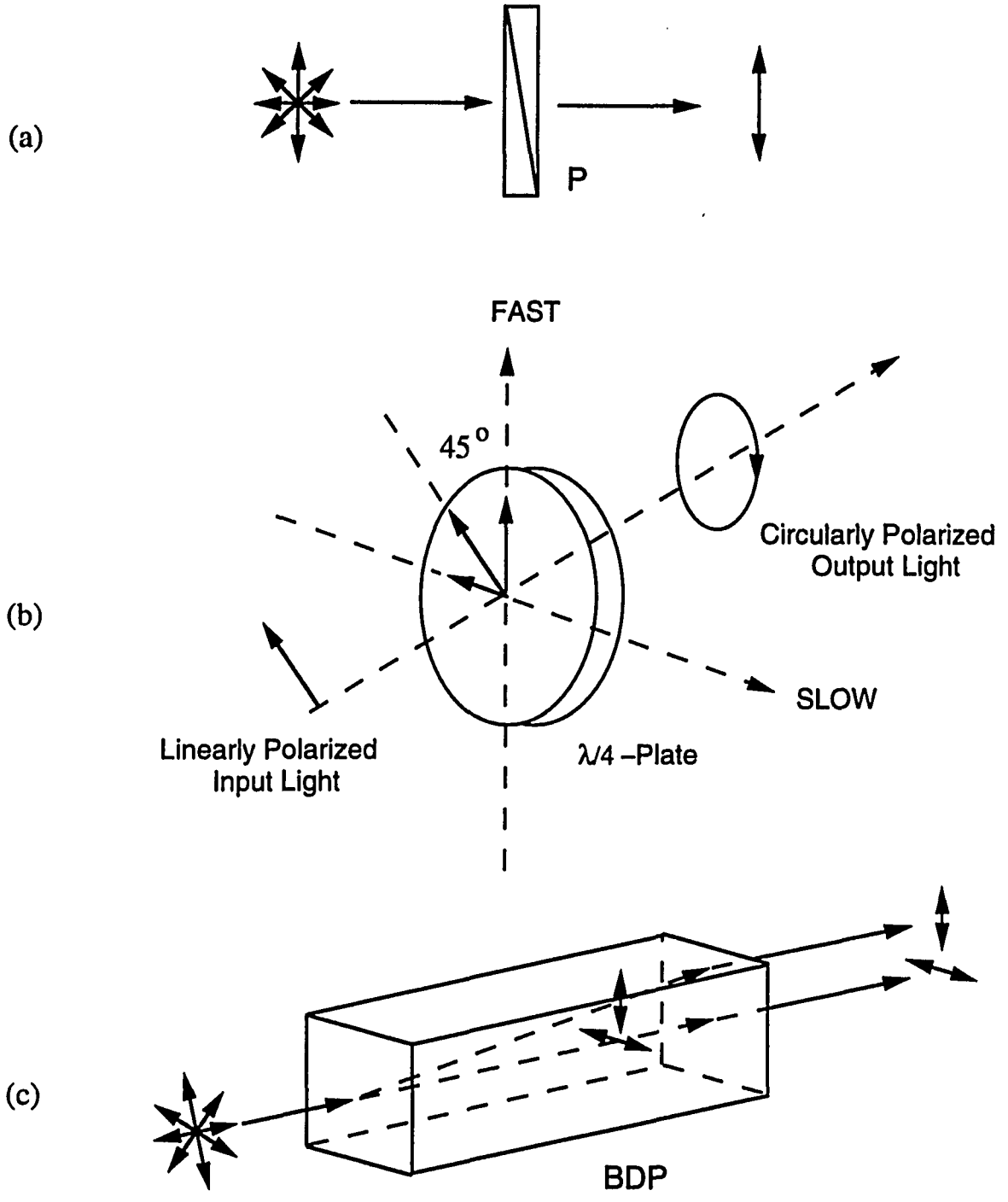

Figure III.10 (a) A polarizer (P) with the optical axis in vertical direction, the output light is linearly polarized in vertical direction; (b) A quarter-wave plate, the input linearly polarized light is at 45 degree to the fast axis, the ouput light is circularly polarized; (c) A beam displacement Prism (BDP), two perpendicular linearly polarized components of the input light are separated at the output of this BDP.

IV.7 Single Shot Streak Camera System for Time-resolved Measurements in Pico-second Regime

A streak camera is most widely used for the measurement of ultrafast temporal property such as the pulse profile of pico-second laser pulses and time-resolved luminescence. It converts the temporal characters of ultrafast processes into spatial information, and enable one to study the processes which occur on a picosecond scale.

A streak camera system consists of a streak tube[10-11], imaging optics, fast sweeping electrodes, and video display/computer equipment. The principle of the streak tube is schematically shown in Figure III.11. An ultrashort light pulse emitted from a laser or exit from an optical fiber is focused onto the potocathode of a streak tube at a given time. The number of the photoelectrons coming from the photocathode is proportional to the intensity of the incident light hitting the photocathode at that time. These photoelectrons are accelerated and deflected across a phosphor screen by a voltage ramp applied by a pair a electrodes. Since the incident light has a temporal intensity profile, the electrons released from the photocathode at different times have different intensities. These electrons are deflected linearly with time and strike the phosphor screen at different positions. This produces a streak, which has a spatial intensity profile directly proportional to the incident temporal intensity profile of the input light pulse. The phosphorescent track is analyzed electronically using a direct readout system including a silicon intensified target (SIT) vidicon camera, a temporal analyzer, and a TV monitor. This displayed profile transforms the temporal information into spatial information.

Since the picosecond laser has a repetition of 10 Hz which is very slow. A single shot streak camera is used to measure the temporal profile of the laser pulses. This single shot streak camera uses a regular streak tube, but the sweeping voltage will be applied

when a trigger signal is received. The temporal profile of laser light can be measured with a single pulse.

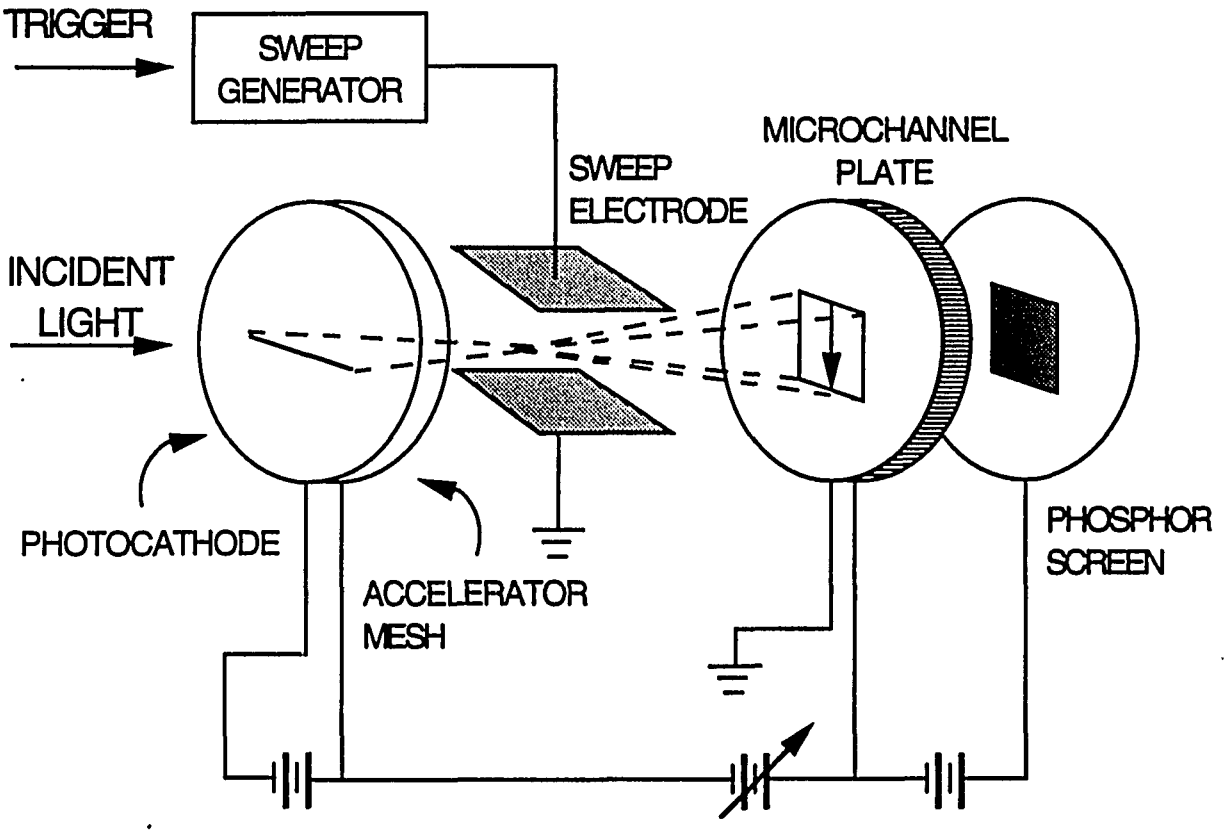

Figure III.10 The schematical diagram of a streak camera tube

IV.8 Auto- and Cross-correlator System for Time-resolved Measurements in Femto-second Regime

A streak camera can measure ultrafast processes up to the picosecond region. For the femtosecond laser pulses, the streak camera can not response properly. A correlation method must used to observe the ultrafast phenomenon in femtosecond region.

Auto-correlation and cross-correlation[12-13] are the standard techniques to measure ultrashort laser pulse duration for femtosecond laser pulses. This is the basic interferometric arrangement as depicted in Figure III.12. In auto-correlation, the two pulses split from one pulse are focused by a positive lens into a nonlinear crystal, such as a KDP crystal, to generate a second harmonic wave which is detected by photomultiplier. Since the second harmonic wave signal can only be detected during temporal overlap in the phase matched direction for absorbing a photon in each beam, the second harmonic signal obtained by varying the delay of one pulse is the pulse auto-correlation. By deconvolution, one can obtain an approximate pulse duration. Assuming a squared hyperbolic secant $sech^2$ pulse profile, the pulse width is the auto-correlation trace width divided by 1.55. If the two pulses have different wavelengths and pulse durations, the sum frequency wave is generated in the nonlinear crystal instead of the second harmonic wave. The measured sum frequency wave signal is the two pulses cross-correlation. An example is that a femtosecond laser pulse is coupled into an optical fiber. The pulse duration and wavelength of the output laser pulse from the optical fiber will change because of the group velocity dispersion and super-continuum generation. This output pulse and the input pulse before fiber can be used to generate the sum frequency. By delaying the fixed frequency pulse (input pulse), the cross-correlation of the two pulses is obtained.

A example is shown in Figure III. 13. Figure III. 13(a) is an auto-correlation trace of CPM laser pulses. The duration of the auto-correlation is 95 fs, corresponding to the laser pulse duration of 60 fs. Figure III. 13(b) is a trace of cross-correlation of two laser beams having different pulse durations. One is the laser beam out of CPM laser system and has a pulse duration of 60 fs. The other beam passed through a half-meter length single-mode optical fiber. Due to the group velocity dispersion in the optical fiber, the output laser pulses at the fiber exit had a much longer pulse duration than the input pulses. The cross-correlation trace shows a temporal duration of 2.8 ps. Because of the great difference between the two pulse durations, the CPM laser pulse with pulse duration of 60 fs just likes a Delta function compared to the duration of the broadening pulses. The cross-correlation trace is actually the temporal profile of the broadening pulses.

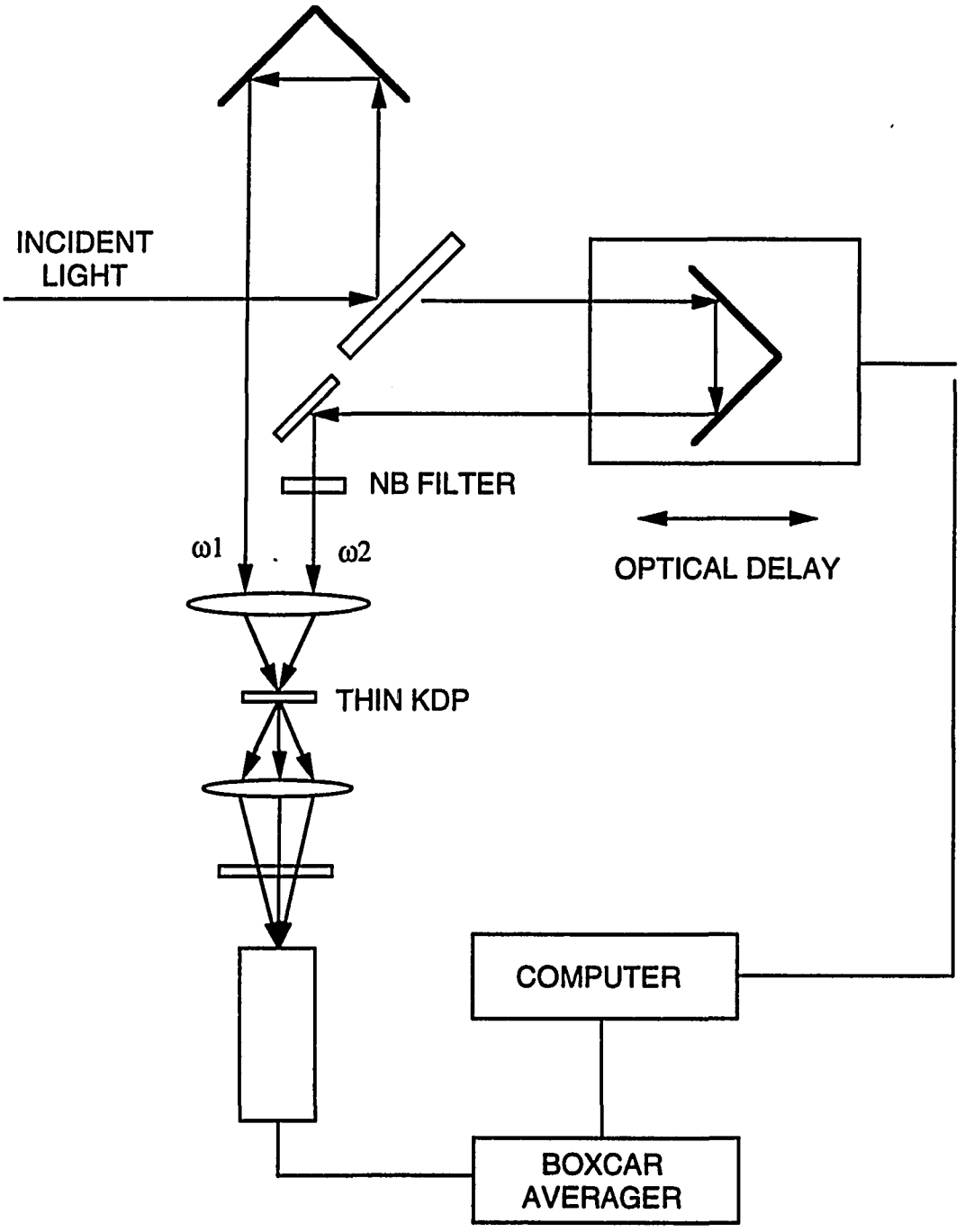

Figure III.11 Pulse duration measurement use correlation method. If $\omega_1=\omega_2$, the HSG obtain from KDP crystal is called auto-correlation and if $\omega_1 \neq \omega_2$, the sum frequency $\omega_s=\omega_1+\omega_2$ is the cross-correlation.

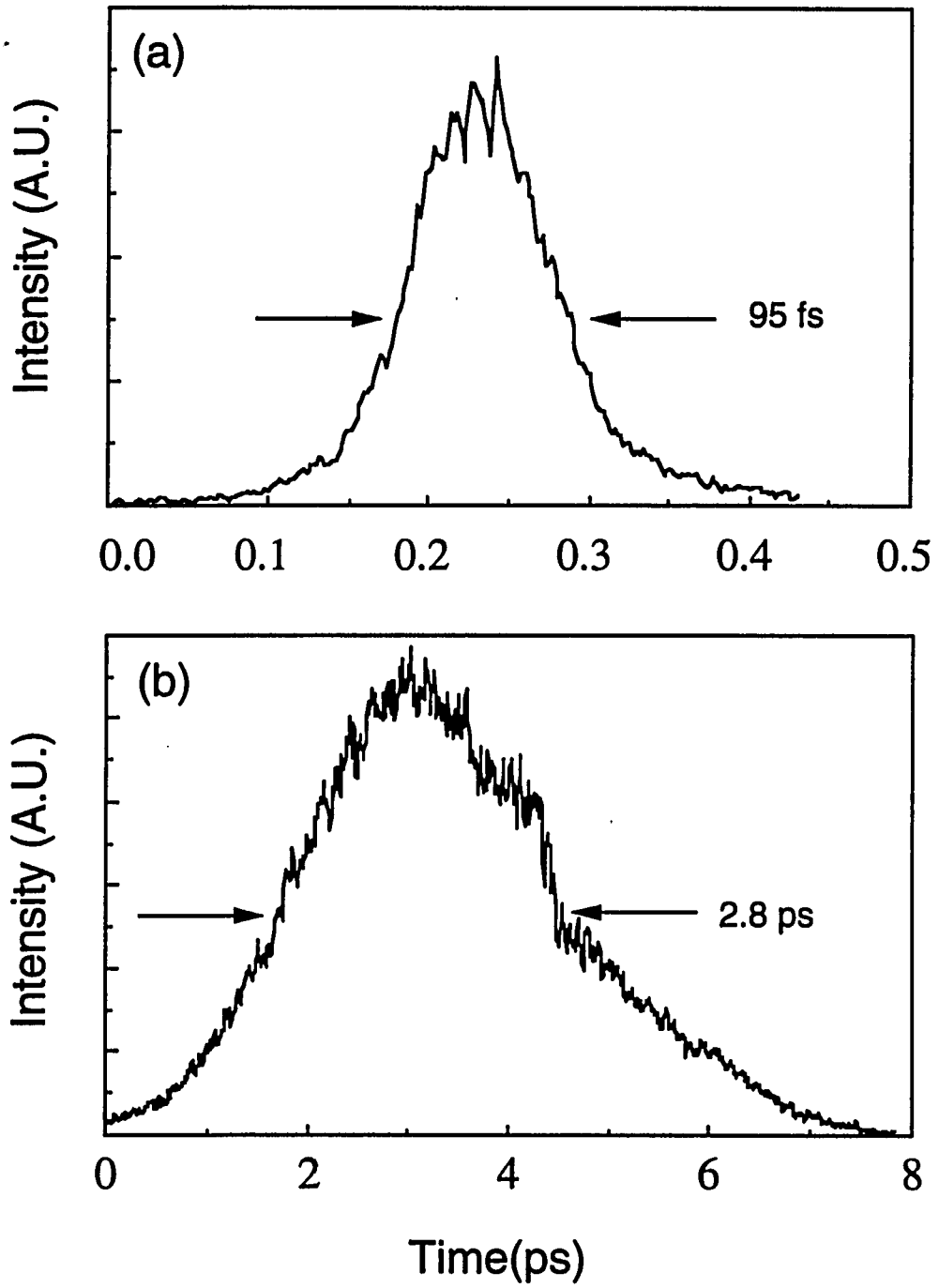

Figure III.13 (a) The auto-correlation trace of CPM laser pulses. (b) cross-correlation trace of CPM laser pulses and the laser pulses passing through a half-meter length single-mode optical fiber.

References:

[1]. W. Kaiser ed., *Topics in Applied Physics, Vol. 60: Ultrashort Laser Pulses* (Springer-Verlag, 1988).

[2]. W. Keochner ed., *Solid-State Laser Engineering,* Springer Verlag Series in Optical Science (Springer-Verlag, 1988).

[3]. Q. Z. Wang, Q. D. Liu, Disa Liu, P. P. Ho, and R. R. Alfano, J. Opt. Soc. Am., **11**, 1084 (1994).

[4]. O. Svelto, *Principles of Lasers,* 2nd edition (Plenum Press, New York and London, 1982).

[5]. J. Wilson, and J. F. B. Hawkes, *Lasers: Principles and applications,* (Prentice Hall,1987).

[6]. Ch. Spielman, P. F. Curley, T. Brabec, E. Wintner, and F. Krausz, Electron. Lett., **28**, 1532 (1992).

[7]. C. P. Huang, M. T. Asaki, S. Backus, M. M. Murnane, H. C. Kapteyn, and H. Nathel, Opt. Lett., **17**, 1289 (1992).

[8]. B. Proctor, and F. Wise, Opt. Lett., **17**, 1295 (1992).

[9]. B. E. Lemoff, and C. P. Barty, Opt. Lett., **17**, 1367 (1992).

[10]. P. J. Delfyett, S. K. Gayen, and R. R. Alfano, Encyclopedia of Physical Science and Technology, **14**, Academic Press Inc., 169 (1987).

[11]. N. Ockman, W. B. Wang, and R. R. Alfano, J. Modern Phys., **B5**, 3165 (1991).

[12]. E. P. Ippen, C. V. Shank in *Ultrashort Light Pulses* ed. by Shapiro (Springer-Verlag, New York, 1977).

[13]. A. G. Doukas, J. Buckett, R. R. Alfano in *Biological Events Probed by Ultrafast Laser Spectroscopy*, ch 17, ed. by R. R. Alfano (Academic Press, San Diego, 1982).

CHAPTER IV

POLARIZATION STABILITIES OF LASER PULSES PROPAGATING IN NON-BIREFRINGENT SINGLE-MODE OPTICAL FIBERS

IV.1 Introduction

A single-mode optical fiber with birefringence can preserve the polarization state of the optical waves[1-6]. When a single-mode optical fiber is non-birefringent, the polarization state of the propagating optical waves will usually be scrambled. Many effects in optical fibers can change the polarization states of the propagating optical waves. Defects and strains that exist either randomly or are introduced by bending or twisting in optical fibers will scatter the light between orthogonal polarization modes. Bending and/or twisting can also cause local fiber birefringence which transfers the light to different polarization states. Linear effects cause depolarization even when optical pulses are weak. Nonlinear effects, such as self-phase modulation (SPM)[7-9], cross-phase modulation (XPM)[8-9] and degenerate four-wave-mixing (DFWM)[10] can affect the polarization state at higher intensity. The polarization instabilities caused by intensity-induced birefringence have been observed in birefringent optical fibers[11-14]. The polarization characteristics for ultrashort optical pulses propagating in non-birefringent single-mode optical fibers has not been experimentally observed and the mechanism for the intensity-induced depolarization has not been described. This thesis addresses this problem.

In this chapter, we will discuss the effect of laser intensity on the polarization state of circularly and linearly polarized optical pulses propagating in non-birefringent

single-mode optical fibers due to nonlinear optical effects. The state of circular polarization has been found to be more stabilized than the state of linear polarization for an intense laser pulse propagating in short ($L < 4m$) non-birefringent single-mode optical fibers. The model using self-phase modulation(SPM) and cross-phase modulation (XPM) which has been developed in chapter II will be used to explain the measured preservation of the circular polarization and the depolarization of linearly polarized laser pulses in the optical fibers.

IV.2 Polarization properties of non-birefringent single-mode optical fibers

A non-birefringent single-mode optical fiber has a symmetrical structure. The core of the fiber is circular and surrounded by the cladding layer. The tension and stress between the core and cladding have been well released during the fabrication process of the fiber. Therefore, there is no any refractive index change induced by stress and tension in the fiber. This type of optical fiber is referred as non-birefringent.

For a perfect non-birefringent single mode optical fiber, the polarization state of the propagating optical waves should be preserved since the light will not be coupled into the orthogonal polarization mode automatically. At the output of a single-mode optical fiber, the polarization state of the exit optical signal should be input one. For a real non-birefringent single-mode optical fiber, there will always be some kind of tension and stress in the fiber. As discussed in the introduction of this chapter, many other effects such as defects, strain, bending, and twisting will also dramatically change the polarization state of the optical waves propagating inside a fiber. Especially for the light propagating in a non-birefringent fiber for a long distance, all these effects will add up to totally scramble the polarization state of the optical wave.

In the experiment, we found that the polarization of optical waves was preserved for short non-birefringent optical fibers (less than 4 m). For longer fibers, the polarization was completely destroyed. This is not surprising at all. Since all the effects that change the polarization of optical wave accumulate with the length of optical fibers. A shorter fiber is much closer to a perfect non-birefringent single-mode fiber than a longer one. Hence, the polarization state can be maintained for the optical waves propagating in short non-birefringent single-mode optical fiber, but not in the long non-birefringent single-mode optical fiber.

IV.3 Polarization instabilities in birefringent optical fibers

To maintain the polarization state of light propagating a fiber over a long propagation distance, optical fibers with birefringence have been designed. Many techniques have been developed for fabricating the birefringent single-mode optical fibers. For example, the cross section of the fiber core has been made to an elliptic shape. By introducing a stress between the fiber core and cladding, a refractive index change was induced[1-6]. This induced refractive index change is not homogenous in every direction since the cross section of the fiber core is elliptic. Along with this birefringence, the optical fiber is anisotropic with two principal optical axes. Optical waves linearly polarized in the principal optical axes of the fiber will remain its linearly polarized state in the propagation no matter for how long the fiber is. To make birefringent single-mode optical fibers more stable to environment, the birefringence was always induced well above the level that introduced by bending, twisting, strain, and other divers effects.

An interesting point is that even for birefringent single-mode optical fibers, the polarization state of propagating optical waves are still instable in some cases. At low optical power or a strongly birefringent fiber, light that is linearly polarized along either of the principal optical axes of the fiber will maintain its state of polarization. At higher intensities in weakly birefringent fibers the birefringence induced through nonlinear processes such as the optical Kerr effect become comparable with the nature fiber birefringence. Under these conditions an asymmetry arises between the fiber principal axes. Induced birefringence adds to the natural birefringence for light polarized along the slow axis, which remains a polarization stable guiding condition. For light polarized along the fast axis the induced and natural birefringence tend to cancel, causing the optical fiber to be a non-birefringent one. Therefore, the fast axis becomes an unstable saddle point. Small deviation from either perfectly linearly polarized light or perfect input

alignment along the fast axis lead to widely different output polarization states. A Signature of this polarization instability is that small changes in input intensity can lead to large changes in the intensity transmitted through a crossed polarizer at the fiber exit.

The nonlinear polarization instability has been observed in single-mode optical fibers with different birefringences[11-14]. Theoretical simulation has made some approach to this nonlinear phenomenon. A calculation of the beat length of a low birefringent single-mode optical fiber as a function of input light power (intensity) is shown in Figure IV.1. At low light power the beat lengths for the light polarized along both the fast and slow axes are the same value of Lo. For higher light power, the beat length of the light oriented along the slow axis does not changes much. It decreases monotonically just a little bit as the dashed curve shown in Figure IV.1. For the light oriented along the fast axis at the higher power, the beat length increases dramatically. At certain input power level, the beat length goes to be very long (to infinity, the instable point). For more higher light power, the beat length decreases as the light power increases. As the demonstration of this figure, the beat length of the fiber is a function of the light power in nonlinear optical regime; so is the birefringence of the fiber. For light oriented along the slow axis of the fiber, the fiber is always birefringent and the light will stay oriented along the slow axis in propagation. There is no light coupled to be polarized along the perpendicular orientation. For light oriented along the fast axis of the fiber, at certain input power the beat length diverges rapidly as the induced birefringence cancels the existing linear birefringence. At this input power, the light equivalently propagates in a non-birefringent fiber. The polarization instability occurs in birefringent fibers when the high light power induces these birefringent fibers to become non-birefringent ones.

When intense light propagates in a non-birefringent single-mode optical fiber, the 'polarization instability' refers to the depolarization of the light in the fiber automatically.

The mechanism of the depolarization has not been investigated yet. In a perfect non-birefringent single-mode optical fiber, the state of the polarization of light should not change itself. In a real fiber, the scattering from the defects inside the fiber may cause light coupled into the other polarization mode. For a short fiber (< 10 m), this scattering effect is small and can be neglected. We will show that the nonlinear effects not only cancels the birefringence at high light intensity, but also cause the depolarization of the linearly polarized light propagating in a non-birefringent single-mode optical fiber.

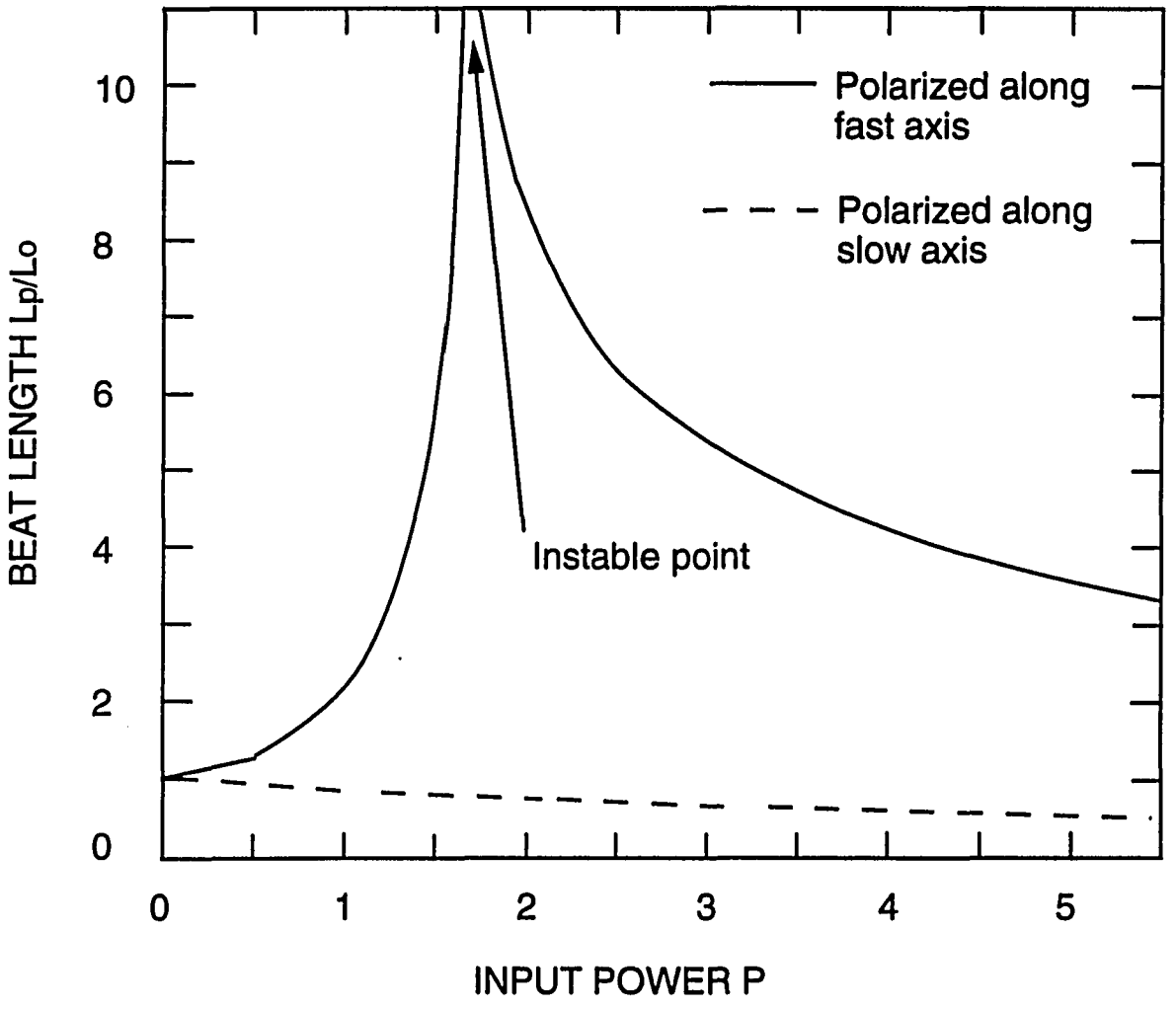

Figure IV.1 Change of beat-length with the power of an intense beam oriented along the fast axis (solid line) or along the slow axis (dashed line).

IV.4 Experimental Setup and Results

The experimental setup is described in Figure IV.2 and IV.3. Details are also given in Chapter III. The optical pulses at 532 nm were obtained from a frequency doubled mode locked Nd:YAG laser at a repetition rate of 10 Hz. Single-mode optical fibers (Newport Corp. Model: FSV-10) at 532 nm are non-birefringent with core diameter of 2.5 μm, cladding thickness of 125μm, and numerical aperture (NA) of 0.11. The fibers were handled very carefully to avoid any induced birefringence by bending and twisting. This induced birefringence will cause the light coupled into the other polarization mode at very low intensity where nonlinear effects are absent. It has been observed that, without the induced birefringence, the states of the polarization of input laser light are preserved at low intensity for both circularly and linearly polarized laser light pulses. Several fibers with different lengths from 0.5m to 4m were used.

(a) Circularly polarized Pluses

The input pulses were linearly polarized to an extinction ratio better than 400 after the polarizer P. The optical axis of P is set at vertical direction. To observe the state of polarization of the circularly polarized laser light pulses propagating in a non-birefringent single-mode optical fiber, these pulses were converted into circularly polarized using a quarter wave plate QWP1 as shown in Figure IV.2. The optical axis (fast or slow axis) of QWP1 is set at 45° to P. By changing the position of fast axis and slow axis of QWP1, it will converts the linearly polarized laser pulses to be either right-handed or left-handed circularly polarized ones. The circularly polarized laser pulses were coupled into and out of a non-birefringent single mode optical fiber with two 10X microscope objective lens. At the fiber exit there maybe not only the input circular polarization state appears, the opposite rotating circular polarization state is also possible as displayed in Figure IV.3 where the polarization states of light and the optical axes of

optical components are shown. The second quarter wave plate QWP2 which is set at the same angle with QWP1 was used at the output to convert two orthogonal circular polarization modes into two linear ones. A beam displacing prism BDP which is alignmented parallel to the optical axis of P was used to spatially separate these two perpendicular linear polarization modes. The energies of the two circularly polarized components can be measured through the two linearly polarized components converted from them.

(b) Linearly Polarized Pulses

To observe the state of polarization of the linearly polarized laser pulses propagating in a non-birefringent single-mode optical fiber, the linearly polarized laser light pulses were directly coupled into and out of an optical fiber as shown in Figure IV.3. The polarization state and the direction of the optical axes of a polarizer and a beam displacement prism (BDP) are also displayed in this figure. The input laser light to a fiber is linearly polarized. The output optical signal at high light intensity maybe depolarized. The two linearly polarized components of the output light are observed using BDP. The optical axis of the BDP is alignmented parallel to that of the polarizer. The energies of the parallel and perpendicular components of the depolarized light pulse can be measured at the exit of BDP.

Depending on the polarization states of the output laser light pulses, one output pulse was divided into two pulses with orthogonal polarization directions by BDP (defined as $\perp$ and $\parallel$). Pulse $\parallel$ is the component parallel to input polarized mode and pulse $\perp$ is the component orthogonally polarized to input pulse. The energies of $\perp$ and $\parallel$ components were measured using a cooled CCD camera system.

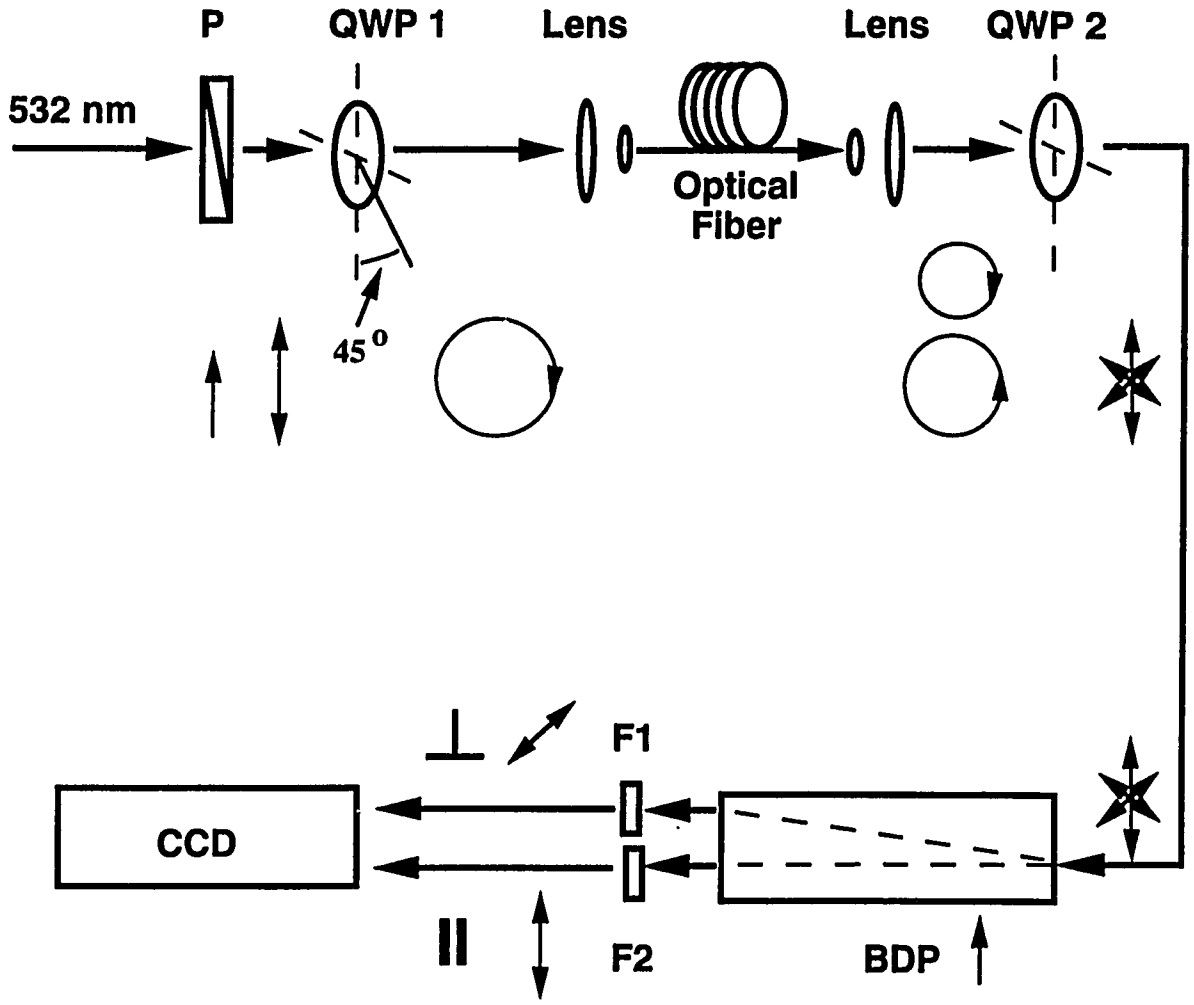

Figure IV.2 Experimental set-up for measuring the polarization stability of circularly polarized laser light pulses, P is a polarizer with the optical axis at vertical direction, QWP's are quarter wave plates with the optical axes at 45° to P, BDP is a beam displacement prism parallel to P.

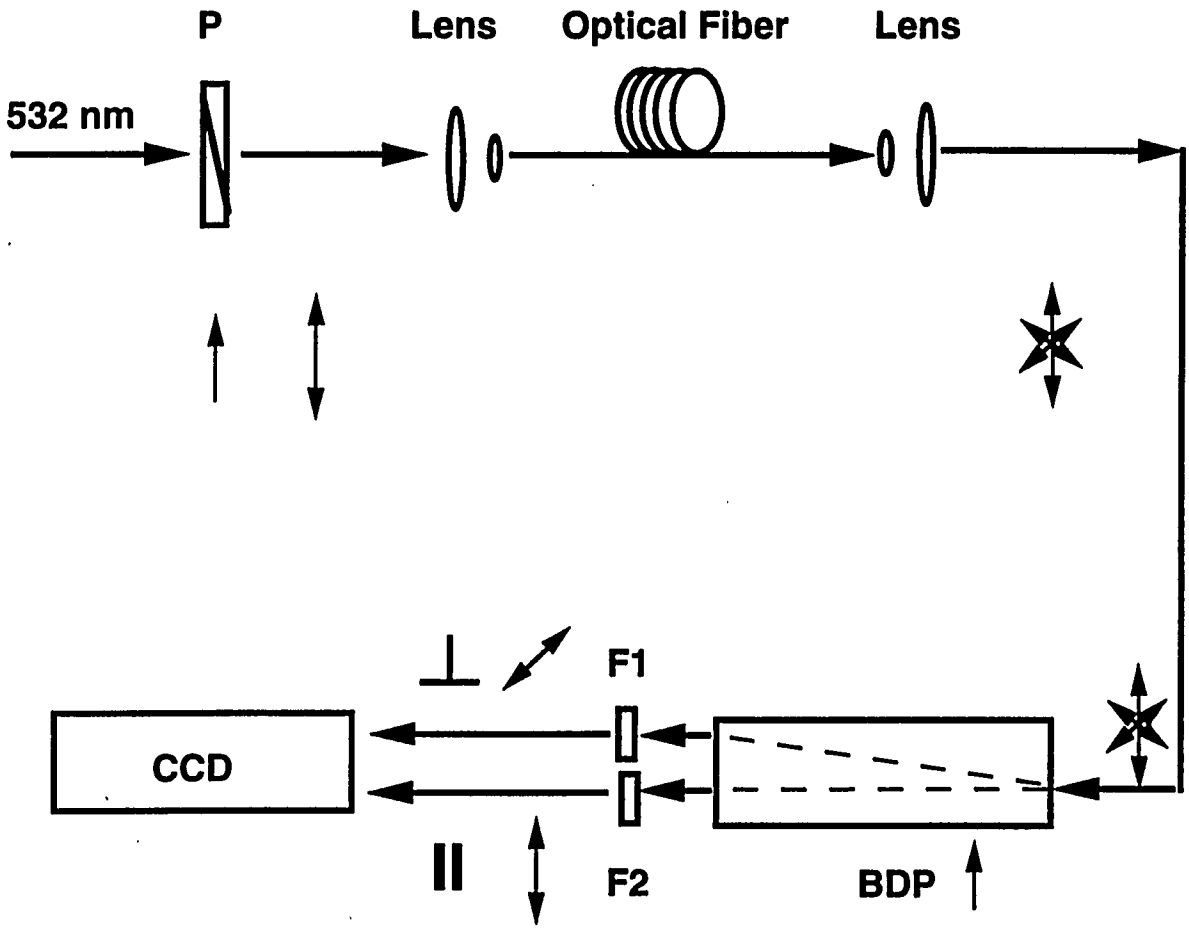

Figure IV.3 Experimental set-up for measuring the polarization stability of linearly polarized laser light pulses, P is a polarizer with the optical axis at vertical direction, BDP is a beam displacement prism parallel to P.

For circularly polarized optical pulses propagating in a fiber, the degree of circular polarization can be calculated through

$$\rho = (|E_R - E_L|) / (E_R + E_L), \qquad \text{(IV.1)}$$

where E_R and E_L are the energies of the right-handed and left-handed components of an optical pulse, respectively. Since these II and $\perp$ components are corresponding to right-handed and left-handed components, respectively, the degree of circular polarization can be expressed as

$$\rho = (|E_{II} - E_{\perp}|) / (E_{II} + E_{\perp}), \qquad \text{(IV.2)}$$

where E_{II} and $E_{\perp}$ are the energies of the linearly polarized components after BDP in measurement. For linearly polarized optical pulses, E_{II} and $E_{\perp}$ are the measured energies of the linearly polarized components at the original input linear polarization direction and its perpendicular direction, respectively. The degree of linear polarization can also be calculated using Eq. (IV.2).

The degree of polarization for circularly and linearly polarized laser pulses propagating in non-birefringent single-mode optical fibers with different lengths for 0.5 m, 1 m, 2 m, and 4 m is plotted from Figure IV.4 to IV.7 as a function of the input laser pulse energy. The dot plots are the measured degree of polarization of the output laser pulses. They have similar characteristics for circularly polarized laser light pulses. The degree of polarization for circularly polarized input laser pulses was preserved to be better than 0.90 when the laser pulse energy was varied from 40 pJ to 100 nJ. The energy range covered three orders of magnitude until the input tip of the optical fiber was damaged because of the high light power. Similar results were observed when the length

of the optical fiber was increased from 0.5 m to 4 m. The states of polarization for circularly polarized laser pulses were preserved in a non-birefringent single mode optical fiber. The degree of polarization of circularly polarized laser pulses dose not depend on the pulse energy.

When linearly polarized laser light pulses were coupled into the same optical fibers, the degree of linear polarization dose depend on the pulse energy. For 0.5 m length fiber in Figure IV.4, the degree of polarization of linearly polarized laser pulses decreases monotonically from 0.97 at very low pulse energy to 0.6 at the pulse energy of 100 nJ. In Figure IV.5, the degree of polarization of linear polarized laser pulses passing through a 1 m length fiber decreases at high pulse energies and displays some kind of oscillation as a function of pulse energy. In Figure IV.6 for a 2 m fiber, the degree polarization of linearly polarized laser pulses drops down as the pulse energy increases. The degree of polarization reaches its minimum value of about 0.2 at the pulse energy of about 70 nJ, then goes up. For a 4 m length optical fiber in Figure IV.7, the linearly polarized laser pulses were depolarized the pulse energy of 10 nJ and the degree of polarization oscillates dramatically as the pulse energy increases. These salient features of the circularly and linearly polarized laser pulses propagating in non-birefringent single-mode optical fibers can be explained using XPM and SPM processes in the non-birefringent single-mode optical fiber.

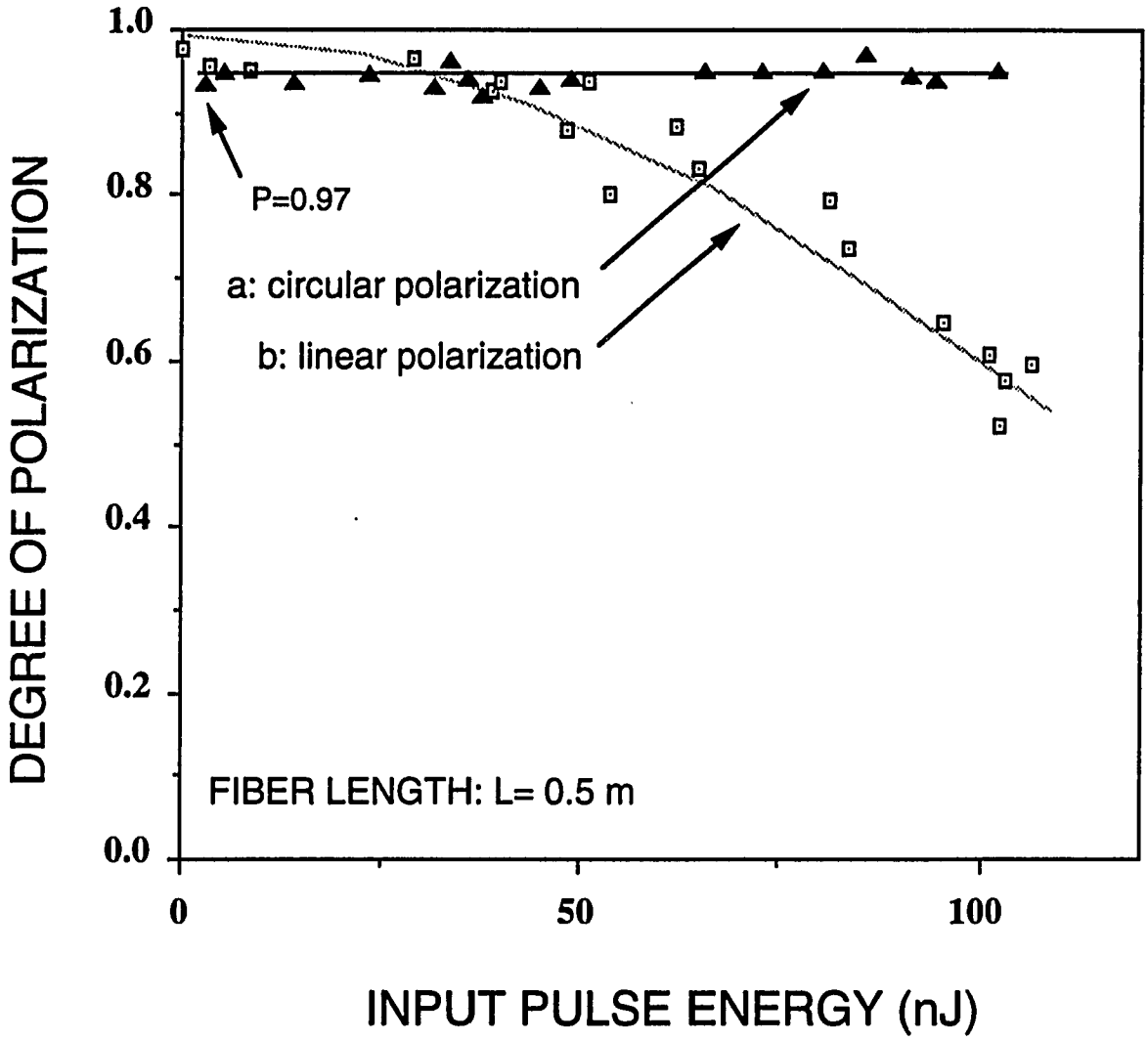

Figure IV.4 The degree of polarization of (a), the circularly polarized and (b), the linearly polarized 35 ps laser pulses after propagated through a 0.5-meter non-birefringent single-mode optical fiber as a function of input 532 nm pulse energy. Dot plots are the experimental results, and solid curves are calculations.

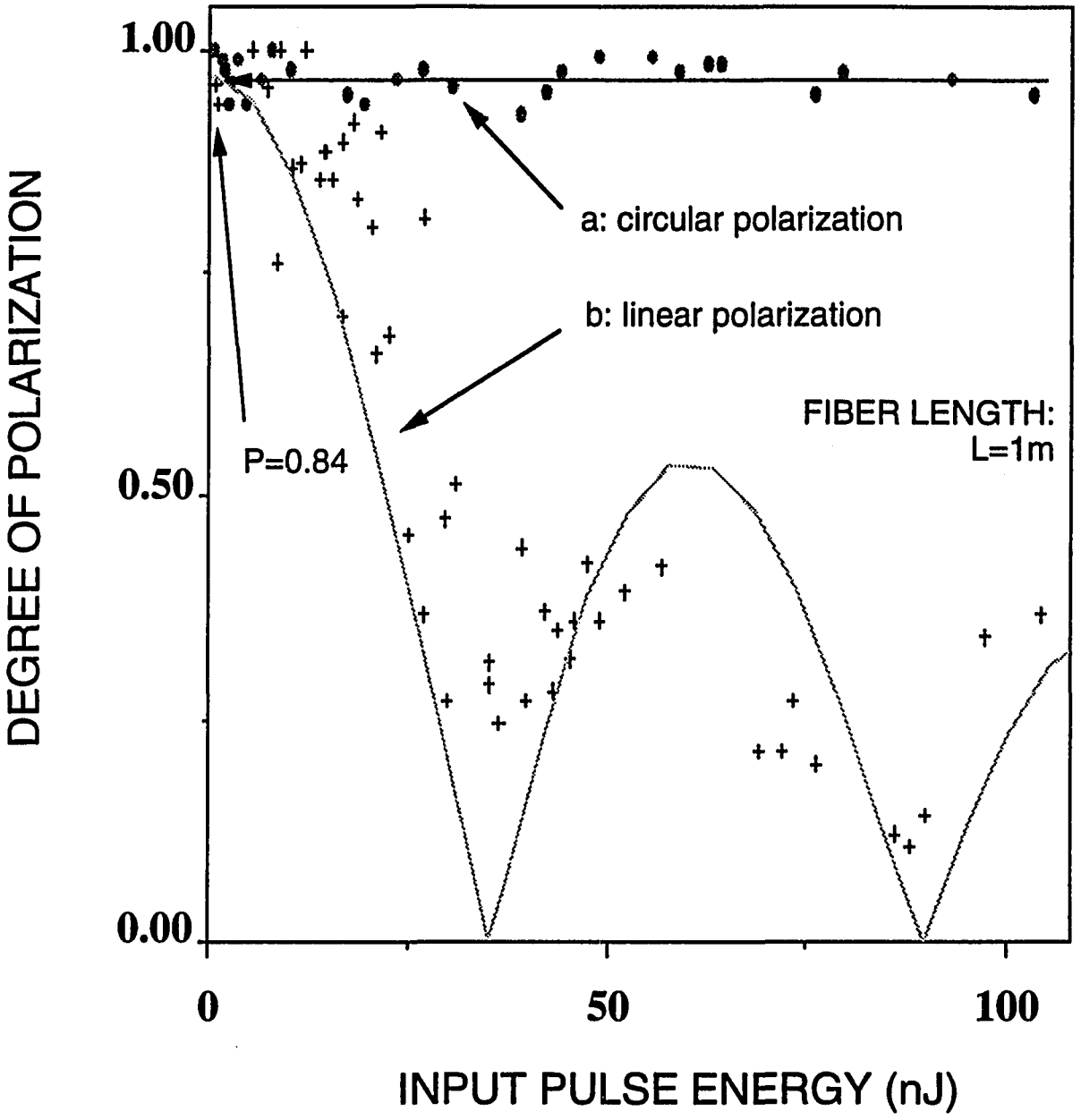

Figure IV.5 The degree of polarization of (a), the circularly polarized and (b), the linearly polarized 35 ps laser pulses after propagated through a 1-meter non-birefringent single-mode optical fiber as a function of input 532 nm pulse energy. Dot plots are the experimental results, and solid curves are calculations.

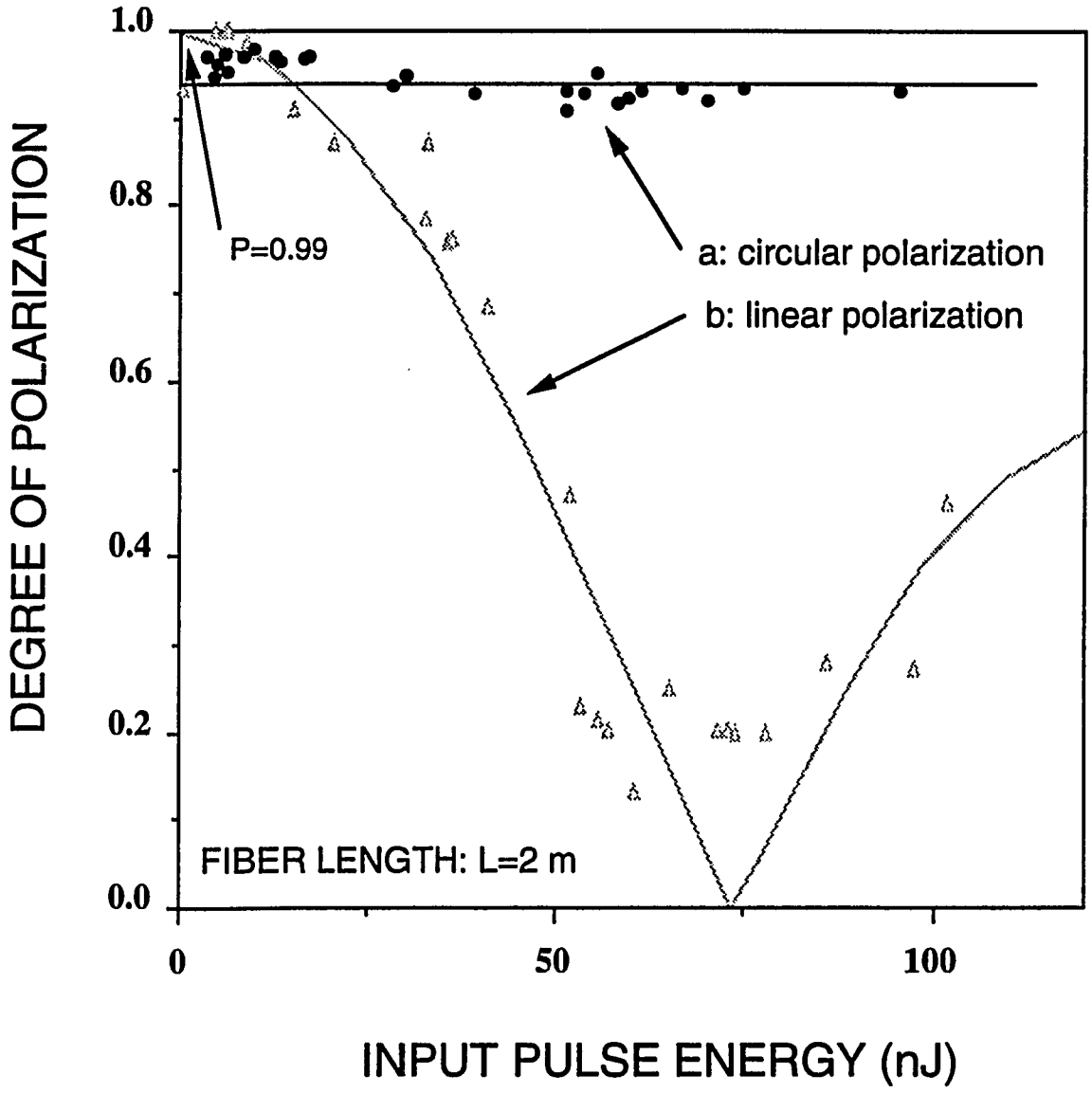

Figure IV.6 The degree of polarization of (a), the circularly polarized and (b), the linearly polarized 35 ps laser pulses after propagated through a 2-meter non-birefringent single-mode optical fiber as a function of input 532 nm pulse energy. Dot plots are the experimental results, and solid curves are calculations.

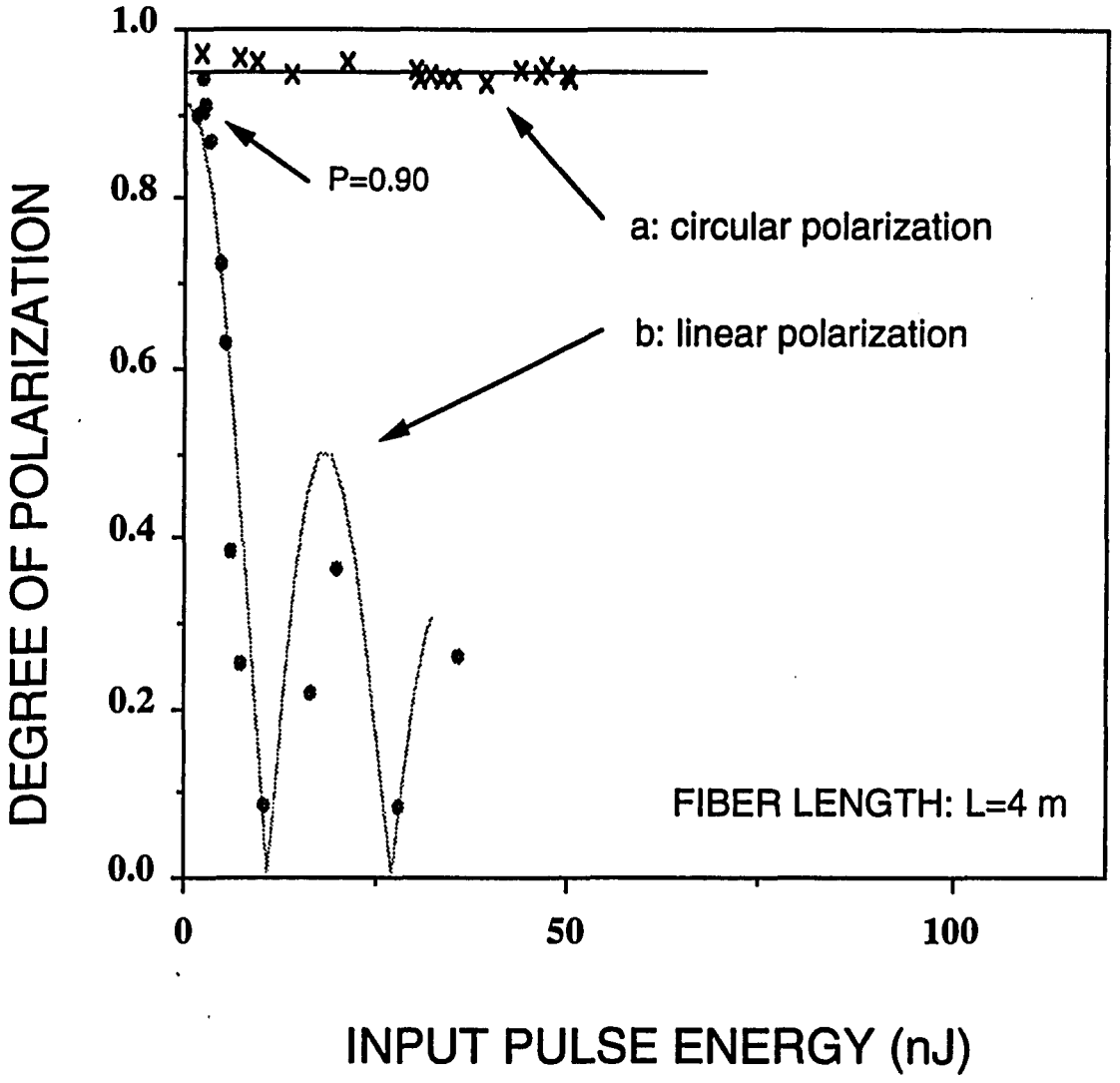

Figure IV.7 The degree of polarization of (a), the circularly polarized and (b), the linearly polarized 35 ps laser pulses after propagated through a 4-meter non-birefringent single-mode optical fiber as a function of input 532 nm pulse energy. Dot plots are the experimental results, and solid curves are calculations.

IV.5 Explanation of Results

To explain the experimental results for the circularly and linearly polarized laser light pulses propagating in short non-birefringent single-mode optical fibers, a theoretical model has been proposed in Chapter II which is used here. Using the slowly varying envelope approximation in circular polarization bases[13], the total electric field of an optical pulse can be expressed as:

$$\vec{E} = \vec{E_R} + \vec{E_L} = \frac{1}{2}\{\vec{e_R} A_{R(r,z,t)} e^{i(\omega t - kz)} + \vec{e_L} A_{L(r,z,t)} e^{i(\omega t - kz)}\} + c.c., \qquad \text{(IV.3)}$$

where $\vec{e}_R = (\vec{e}_x - i\vec{e}_y)/\sqrt{2}$, and $\vec{e}_R = (\vec{e}_x + i\vec{e}_y)/\sqrt{2}$ are the right-handed and left-handed circular polarization unit vectors and A_R, A_L are the amplitudes of two polarization components, respectively. The nonlinear wave equations (Eq. II.42) in an isotropic medium can be expressed as :

$$\frac{\partial A_R}{\partial z} + \frac{1}{v_{gR}}\frac{\partial A_R}{\partial t} + \frac{i}{2}k_R^{(2)}\frac{\partial^2 A_R}{\partial t^2} = i\frac{\omega n_2}{c}\left(\frac{2}{3}|A_R|^2 + \frac{4}{3}|A_L|^2\right)A_R, \qquad \text{(IV.4a)}$$

$$\frac{\partial A_L}{\partial z} + \frac{1}{v_{gL}}\frac{\partial A_L}{\partial t} + \frac{i}{2}k_L^{(2)}\frac{\partial^2 A_L}{\partial t^2} = i\frac{\omega n_2}{c}\left(\frac{2}{3}|A_L|^2 + \frac{4}{3}|A_R|^2\right)A_L, \qquad \text{(IV.4b)}$$

where v_{gR} and v_{gL} are the group velocities for right-handed and left-handed components, respectively, and $v_{gR} = v_{gL}$, $k^{(2)}$'s are the group- velocity dispersion(GVD), and $n_2 = 3\chi^{(3)}/8n$ is the nonlinear refractive index. The amplitudes and phases of the pulse envelope are denoted by A and α, respectively:

$$A_{R(\tau,z)} = A_{R0} e^{i\alpha_{R(\tau,z)}}, \text{ and } A_{L(\tau,z)} = A_{L0} e^{i\alpha_{L(\tau,z)}}, \qquad \text{(IV.5)}$$

where $\tau = (t - z/v_g)/T_0$, T_0 is the 1/e pulse duration, and $A_{R0}(A_{L0})$ is the initial right-handed (left-handed) amplitude.

Substituting expression (IV.5) into Eqs. (IV.4), these nonlinear wave equations can be solved analytically by neglecting the group velocity dispersion from Eqs. (II.57) to (II.59). The solutions for the amplitudes and phases of the two opposite rotating circularly polarized components of a laser light pulse after propagating in an optical fiber with length z are:

$$A_R(\tau,z) = A_{R0}, \tag{IV.6a}$$

$$A_L(\tau,z) = A_{L0}, \tag{IV.6b}$$

and

$$\alpha_R(\tau, z) = \frac{\varpi}{c} n_2 z\left(\frac{2}{3} I_{R0} + \frac{4}{3} I_{L0}\right) e^{-\tau^2}, \tag{IV.6c}$$

$$\alpha_L(\tau, z) = \frac{\varpi}{c} n_2 z\left(\frac{2}{3} I_{L0} + \frac{4}{3} I_{R0}\right) e^{-\tau^2}, \tag{IV.6d}$$

where A_{RO} (A_{LO}) is the amplitude of the right(left)-handed component and I_{R0} (I_{L0}) is the intensity of the right(left)-handed component.

From the solutions (IV.6a) and (IV.6b) of the nonlinear wave equations (IV.4), the amplitudes of two counter rotating circularly polarized components dose not change due to the nonlinear processes which are SPM and DXPM in the fiber. When the laser light pulse propagates in the fiber, the amplitudes of the two circularly polarized components will remain at the values of the initial conditions. There is no exchange of energy caused by nonlinear interaction between these two circularly polarized laser

pulses. These solutions means that circularly polarized laser light pulses are stable in the fiber. The nonlinear processes such as SPM and DXPM in the fiber do not affect the intensities. Conversely, the nonlinear phase changes in solution (IV.6c) and (IV.6d) are sensitive to the intensities of the two components. These nonlinear phase changes will cause spectral broadening of the laser light pulse. They do not affect the polarization state of circularly polarized laser pulse, but they does change the linearly polarized laser pulse.

For a perfect circularly polarized laser pulse which is right or left handed, only SPM exists in this case. From Eqs. (IV.6), the perfect circular polarization will remain circularly polarized after propagating in the fiber. The state of polarization does not change. The only change is the spectral broadening caused by SPM.

When a quasi-circularly polarized laser pulse (defined as elliptically polarized with eccentricity to be almost 0) is coupled into a fiber, nonlinear processes(SPM and DXPM) do not affect the amplitudes of the two circular components as shown by Eq. (IV.6a and 6b). But they do affect the phases of the two opposite circularly polarized components. When the amplitudes of two circularly polarized components were measured at output, the amplitudes of the two circular components are stable. As a result, the degree of polarization of circularly polarized laser pulse does not depend on the pulse energy as shown in Figure IV.4 to IV.7.

When linearly polarized laser pulses were coupled in these optical fibers and the two linearly polarized components were observed at the fiber exit. The results are different with the circularly polarized laser pulses. A perfect linearly polarized laser pulse can be treated as two counter-rotating circularly polarized components with the same amplitudes and phases. From the solution (IV.6), the two circularly polarized components still have stable and equal amplitudes. The nonlinear phase changes are also exactly the

same because of the same intensities of the two circular components. At the fiber exit, the measured linearly polarized components are the superpositions of the two circularly polarized components. These superpositions give the original linearly polarized pulse at fiber output because of the equal amplitudes and equal phases of the two circular components. This perfect linearly polarized laser pulse should not be depolarized from these nonlinear effects.

However, the input linear polarization of laser light was not perfect under our experimental conditions and a small portion of light was scattered into the perpendicularly polarized mode. The most important scattering source is the fiber input surface which was irregular after the fiber cut. A photo picture of the surface of a fiber is shown in Figure IV.8. In this case, the linearly polarized pulses were slightly depolarized with a ratio $r \equiv I_y / I_x$ which resulted in difference in the magnitudes of I_R and I_L. Using the polarization base expressions

$$\vec{e}_x = \frac{1}{\sqrt{2}}(\vec{e}_R + \vec{e}_L), \tag{IV.7a}$$

$$\vec{e}_y = \frac{i}{\sqrt{2}}(\vec{e}_R - \vec{e}_L), \tag{IV.7b}$$

one has

$$\begin{aligned}\vec{E} &= E_x \vec{e}_x + i E_y \vec{e}_y \\ &= E_x \frac{1}{\sqrt{2}}(\vec{e}_R + \vec{e}_L) + i E_y \frac{i}{\sqrt{2}}(\vec{e}_R - \vec{e}_L) \\ &= \frac{1}{\sqrt{2}}(E_x + E_y)\vec{e}_R + \frac{1}{\sqrt{2}}(E_x - E_y)\vec{e}_L\end{aligned} \tag{IV.8}$$

The amplitudes of the two circular components are

$$E_R = \frac{1}{\sqrt{2}}(E_x + E_y), \tag{IV.9a}$$

$$E_L = \frac{1}{\sqrt{2}}(E_x - E_y), \tag{IV.9b}$$

$$\begin{aligned}\Delta I &= |I_R - I_L| \\ &= [\frac{1}{\sqrt{2}}(E_x + E_y)]^2 - [\frac{1}{\sqrt{2}}(E_x - E_y)]^2 \\ \Delta I &= 2E_x E_y,\end{aligned}$$

using $I_y = rI_x$ and $I_x = E_x^2$, we have

$$\Delta I = 2\sqrt{r}\, I_x. \tag{IV.10}$$

For small ratio r, we have $I_x >> I_y$, therefore,

$$\Delta I = 2\sqrt{r}\, I_0, \tag{IV.11}$$

where ΔI is the difference of the intensities of the two circular component and I_0 is the total pulse intensity. When a quasi-linearly polarized(slightly depolarized) laser pulse is undertested and is treated as two circularly polarized components, the nonlinear phases of the two circularly polarized components will be different. The difference can be calculated using Eqs. (IV.6)

$$\Delta\alpha(\tau, z) = |\alpha_R - \alpha_L| = \frac{4\pi}{3\lambda} n_2 z \Delta I e^{-\tau^2} \tag{IV.12}$$

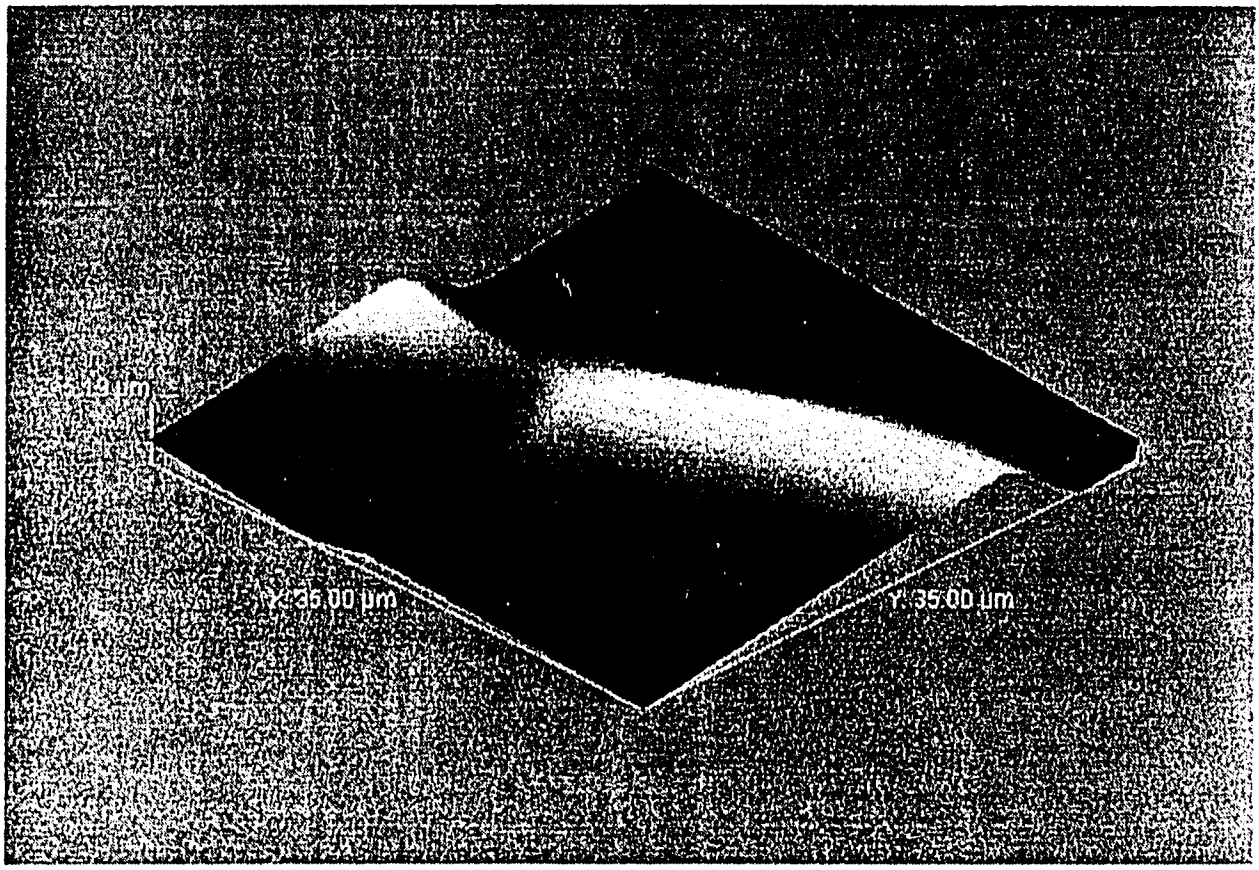

Figure IV.8 The image of the cross section of a single-mode optical fiber under a atomic force microscope (AFM).

where $\Delta I = |I_{R0} - I_{L0}|$ is the intensity difference of the two circular components and $\Delta\alpha$ is the nonlinear phase shift between the two circular components.

At the fiber exit, the measured linearly polarized components are the superpositions of the two circularly polarized components. Since these superpositions are sensitive to the amplitudes as well as the phase of the two circular components, the nonlinear phase shift will cause the linear polarization to change. More accurately, this nonlinear phase shift will cause the quasi-linear polarization to rotate. Consider two opposite circularly polarized lights with equal amplitudes, the superposition is linearly polarized when the phase difference is zero. For a nonlinear phase shift of $\Delta\alpha(\tau, z)$, this superposition remains linearly polarized, but the polarization direction rotates with an angle of $\Delta\alpha(\tau, z)/2$.

Since this nonlinear polarization rotation is proportional to the pulse instantaneous intensity as shown in Eq. (IV.12), the rotation angle within a laser pulse profile will be different at different time. Therefore, when a linearly polarized optical pulse propagated through an optical fiber, the polarization state remained linearly polarized everywhere within the pulse temporal profile but the direction of the polarization changes at different time. The optical pulse appeared to be depolarized at the output of the optical fiber due to the instantaneous intensities in pulse envelope. More details are given in Section 5 of Chapter II from Eqs. (II.66) to (II.69). The two orthogonal linear polarization components after BDP can be denoted as:

$$P_{II} = \int_{-\infty}^{\infty} I_o e^{-\tau^2} \cos^2(k e^{-\tau^2}) d\tau, \qquad \text{(IV.13a)}$$

and

$$P_{\perp} = \int_{-\infty}^{\infty} I_0 e^{-\tau^2} \sin^2(k e^{-\tau^2}) d\tau, \qquad \text{(IV.13b)}$$

where $k = \frac{4\pi}{3\lambda} n_2 z \sqrt{r} I_0$ is a nonlinear phase parameter. The degree of polarization is calculated through: $\rho = |P_{II} - P_{\perp}| / (P_{II} + P_{\perp})$. After simplifying this expression (reference Section 5, Chapter II from Eqs. (II.57) to (II.73)),

$$\rho = \frac{1}{\sqrt{\pi}} \int_{-\infty}^{\infty} e^{-\tau^2} \cos(2k e^{-\tau^2}) d\tau, \qquad \text{(IV.14)}$$

as shown in Eq. (II.73).

The calculation results of the degree of polarization of linearly polarized laser pulses propagating in optical fibers as a function of the input pulse energy are shown from Figure IV.4 to IV.7 as solid curves for r=0.015, 0.086, 0.005, and 0.05 corresponding the fiber length of 0.5 m, 1 m, 2 m, and 4 m, respectively. These calculation curves are in agreement with the experimental measurements.

From the Eq. (IV.14) using the nonlinear phase shift $k = \frac{4\pi}{3\lambda} n_2 z \sqrt{r} I_0$, the degree of polarization of the output laser pulses from an optical fiber is a function of the pulse intensity as well as r which is the small depolarization ratio determined at very low pulse intensity. As discussed before, this small depolarization ratio r arises from the scattering processes introduced by the irregular shape at the fiber input surface which is not intensity related. The typical value of r is between 0.001 and 0.1. It is easy to understand that this depolarization ratio changes from a fiber to another one because of the irregular shape of the fiber end surface. This initial small depolarization ratio will dramatically affect the polarization state of the laser pulses propagating in an optical fiber at high

intensity. As shown in Figure IV.4, the degree of polarization of depolarized output laser pulses for 0.5 m-length optical fiber decreased from the initial value of 0.97 (r=0.015) at very low pulse energy to 0.6 at pulse energy of 100 nJ. For more higher pulse energy, the input tip of the fiber was damaged because of the high laser intensity. For a 1-meter length fiber as shown in Figure IV.5, the initial value of the degree of polarization is 0.84 at low pulse energy (r=0.086), the degree of polarization of the output laser pulses decreased to zero at the input pulse energy of 35 nJ. In Figure IV.6 for a 2-meter length optical fiber, the initial degree of polarization at low pulse energy is 0.99 (r=0.005) which is higher than that for the 1-meter fiber, the degree of polarization decreases to zero at the pulse energy of 74 nJ which is also larger than that of the 1-meter fiber. With a 4-meter length fiber, the initial degree of polarization is 0.90 (r=0.05) at low pulse energy, the degree of polarization dramatically decreases with the pulse energy as shown in Figure IV.7. It arrives zero at the pulse energy of only 11.5 nJ and then oscillates when the pulse energy increases.

To see the effect of the initial depolarization ration more clearly, the degree of polarization of linearly polarized laser light pulses has been measured for the optical fibers having the same length but different values of the initial depolarization ratio r. As shown in Figure IV.9, two optical fibers which cut from one have the same length. The only difference between them is the small depolarization ration at very low laser pulse energy where the nonlinear effects are absent. This difference is from the irregular shape of the fiber end surfaces. The data plots are the measured results. For the fiber with r=0.005, the degree of polarization was 0.99 at low pulse energy and decreased to 0.1 at the pulse energy of 65 nJ. For the fiber with r=0.021, the degree of polarization was 0.96 at low pulse energy and reached the minimum value of 0.2 at the pulse energy of 40 nJ. The solid curves are the theoretical simulations.

The effects of the initial depolarization ratio and the pulse energy have been discussed. From another point of the view for Eq. (IV.14), the degree of polarization of a laser pulse having the Gaussian pulse shape is only a function of the nonlinear phase shift k. This nonlinear phase shift can be calculated through the pulse energy and initial depolarization ratio r. All the measured results can be plotted as a function of k and they should stay on one curve. For various optical fibers having different lengths and initial depolarization ratio, the fit is shown in Figure IV.10 for the degree of polarization of the output laser light pulses as a function of k.

In conclusion, the polarization state of circularly and linearly polarized picosecond laser pulses propagating through non-birefringent single-mode optical fibers have been studied. It was found that circularly polarized laser pulses were less sensitive to the intensity than that of linearly polarized laser pulses. A model using self-phase modulation(SPM) and cross-phase modulation(XPM) has been used to explain the measured preservation of the circular polarization state and the depolarization of linear polarization state in optical fibers. The model is in good agreement with the experimental results.

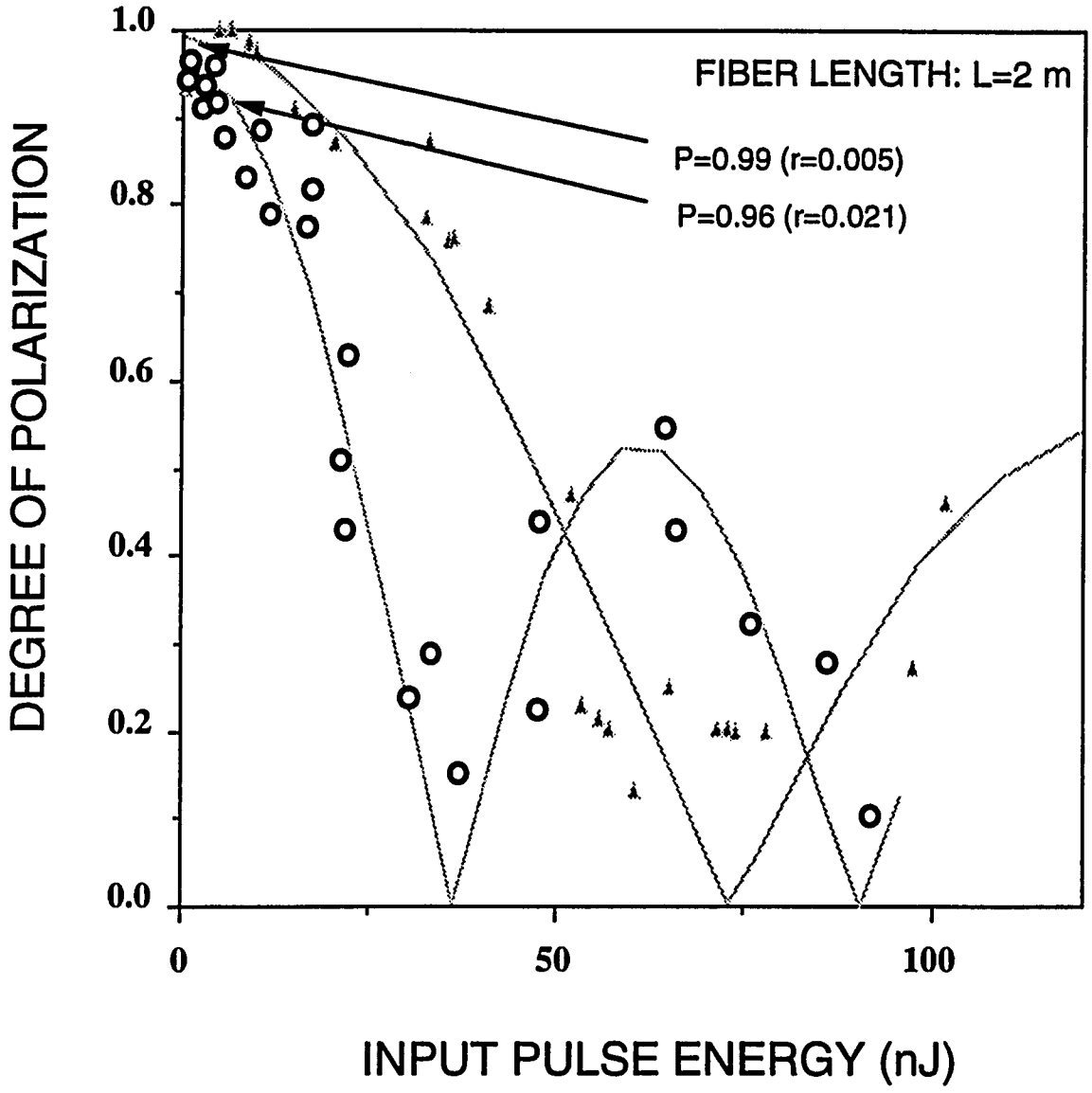

Figure IV.9 The degree of polarization of the linearly polarized 35 ps laser pulses after propagated through a 2-meter non-birefringent single-mode optical fiber as a function of input 532 nm pulse energy. (a) For a fiber with the initial depolarization ratio r=0.005; and (b) r=0.021. Dot plots are the experimental results, and solid curves are calculations.

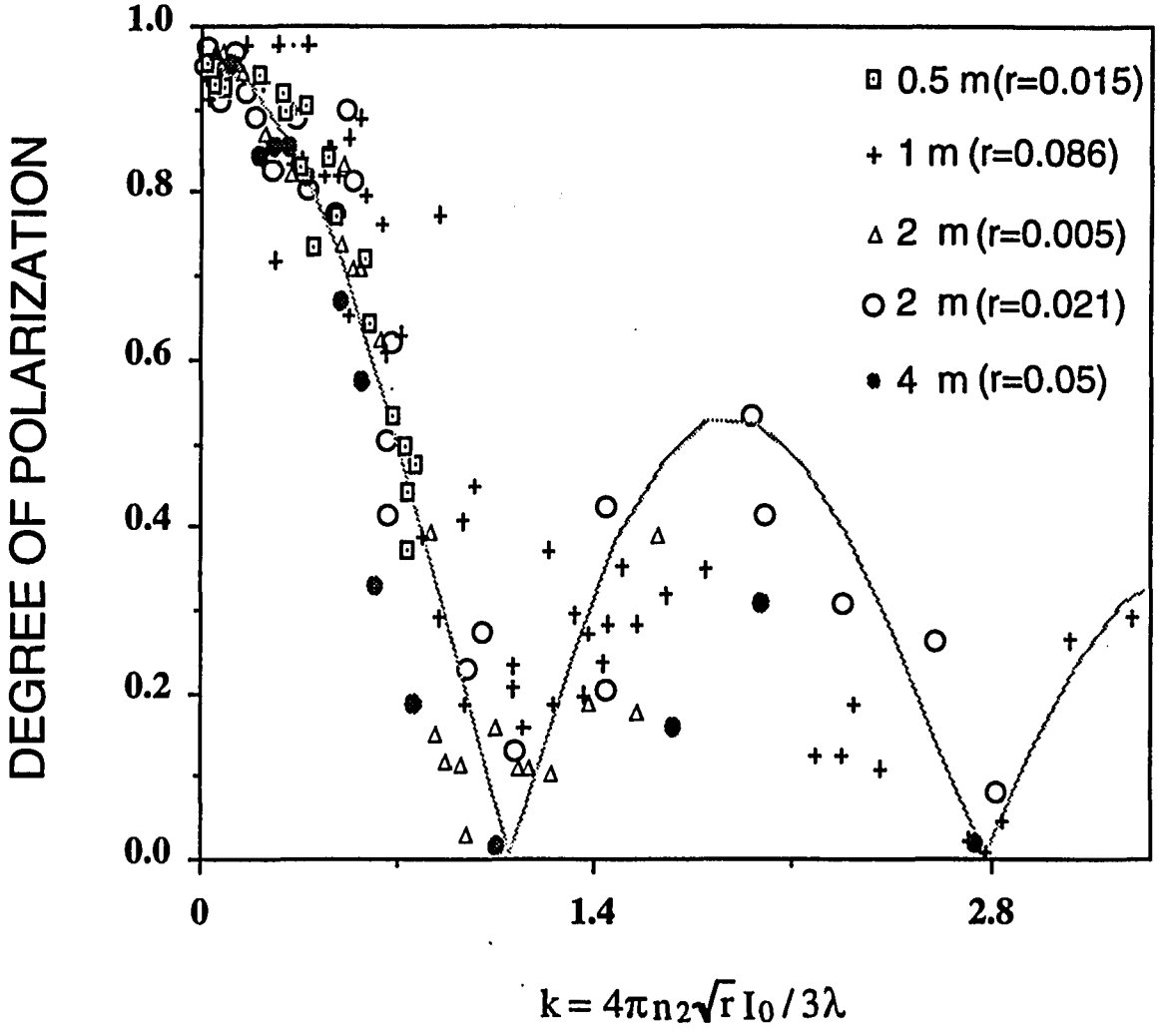

Figure IV.10 The degree of polarization of linearly polarized 35 ps laser pulses after propagated through non-birefringent single-mode optical fibers as a function of nonlinear phase shift k. Dot points are the experimental results for fiber with different lengths, and solid curve is calculations.

References:

[1] I. P. Kaminow, IEEE J. Quantum Electron., QE-**17**, 15 (1981).

[2] N. G. Walker and G. R. Walker, J. of Lightwave Tech., LT-**8**, 438 (1990).

[3] R. H. Stolen, V. Ramaswamy, P. Kaiser, and W. Pleibel, Appl. Phys. Lett., **33**, 699 (1978).

[4] F. M. Sears, J. Lightwave Tech., **8**, 684 (1990).

[5] D. N. Payne, A. J. Barlow, and J. R. Ramskov, IEEE J. Quantum Electron., QE-**18**, 477 (1982).

[6] J. I. Sakai, S. Machida, and T. Kimura, IEEE J. Quantum Electron., QE-**18**, 488 (1982).

[7] R. R.Alfano and S. L. Shapiro, Phys. Rev. Lett., **24**, 592 (1970); Phys. Rev. Lett., **24**, 1219 (1970).

[8] R. Fork, C. Shank, C. Hirliman and R. Yen, Opt. Lett., **8**, 1 (1983).

[9] R. R Alfano and P. P. Ho, IEEE J. Quantum Electron., QE-**24**, 351 (1988).

[10] P. L. Baldeck and R. R. Alfano, IEEE J. Lightwave Tech. LT-**5**, 1712 (1987).

[11] S. F. Feldman, D. A. Weinberger, and H. G. Winful, Opt. Lett., **15**, 311 (1990).

[12] S. Trillo, S. Wabnitz, R. H. Stolen, G. Assanto, C. T. Seaton, and G. I. Stegeman, Appl. Phys. Lett., **49**, 1224 (1986).

[13] H. G. Winful, Opt. Lett., **11**, 33 (1986).

[14] F. Matera, and S. Wabnitz, Opt. Lett., **11**, 467 (1986).

Chapter V

NONLINEAR POLARIZATION TWISTING OF PICOSECOND AND FEMTOSECOND OPTICAL PULSES IN NONBIREFRINGENT SINGLE-MODE OPTICAL FIBERS

V.1 Introduction

Over the past ten years, nonlinear polarization properties of ultrashort laser pulses propagating in birefringent single-mode optical fibers have been studied[1-5] to understand its potential role in various applications in optical communication, switching, and optical amplification. In birefringent single-mode optical fibers, the intensity-dependent linear polarization instabilities have been attributed to an induced refractive index change. This induced index change which depends on light intensity tends to cancel the initial birefringence of optical fibers. At a certain high intensity, this birefringent optical fiber becomes a non-birefringent one. Recently, the polarization state of ultrashort laser pulses propagating in non-birefringent single-mode optical fibers[6] has been investigated. The polarization stabilities of circularly and linearly polarized laser pulses have been measured and theoretically modeled.

In this chapter, the temporal characteristics of the nonlinear depolarization effect for linearly polarized 35 picosecond and 100 femtosecond light pulses propagating through nonbirefringent single-mode optical fibers are investigated. Sub-structures at different polarization modes within linearly polarized input laser pulse profiles after the optical fibers and a polarizer have been observed. This phenomenon arises from Nonlinear Polarization Twisting (NPT). A theoretical model has been developed to explain the NPT in a nonbirefringent single-mode optical fiber (see section II.5, chapter II, Figure II.12). This NPT phenomenon is attributed to the polarization twisting within

the pulse envelope of a linearly polarized laser pulse due to both self-phase modulation (SPM) and degenerate cross-phase modulation (DXPM) processes in the optical fiber.

V.2 Nonlinear Polarization Twisting of 35 Picosecond Laser Pulses in Nonbirefringent Single-mode Optical Fibers

V.2.1 Experimental Setup

The experimental setup to observe the effect of nonlinear polarization twisting (NPT) of picosecond laser light pulses is shown schematically in Figure V.1. Laser pulses with a duration of 35 ps at the wavelength of 532 nm were generated by the second-harmonic generation (SHG) of laser pulses emitted from a mode-locked Nd:YAG laser system. The details of this Nd:YAG laser system were described in the section III.2 of chapter III. After passing through a polarizer P1, these laser pulses were linearly polarized to an extinction ratio of better than 400. The linearly polarized laser pulses were coupled into and out of a 1-m single-mode nonbirefringent optical fiber (Newport Corporation Model: FSA-10). The optical fiber had a symmetric circular cross section without birefringence except the residual birefringence randomly existed in the fiber which was formed during the fabricating process. The beat length (L_B: see chapter I) of this kind of residual birefringence is much longer than the length used in the experiment. Hence, the fiber can be treated as nonbirefringent. For even a single laser pulse propagating in the nonbirefringent optical fiber, both DXPM and SPM processes occurred[7] because of high intensity of the laser pulse. These nonlinear processes usually caused the depolarization of the laser pulse in the fiber. A second polarizer P2 that was parallel to P1 was used at the fiber exit for measuring the parallel component. To measure the perpendicular component, P2 had to set 90° to P1. After the second polarizer P2, a single-shot Hamamatsu streak camera with resolution of 2 ps was used to measure the temporal profiles of the selected polarization component.

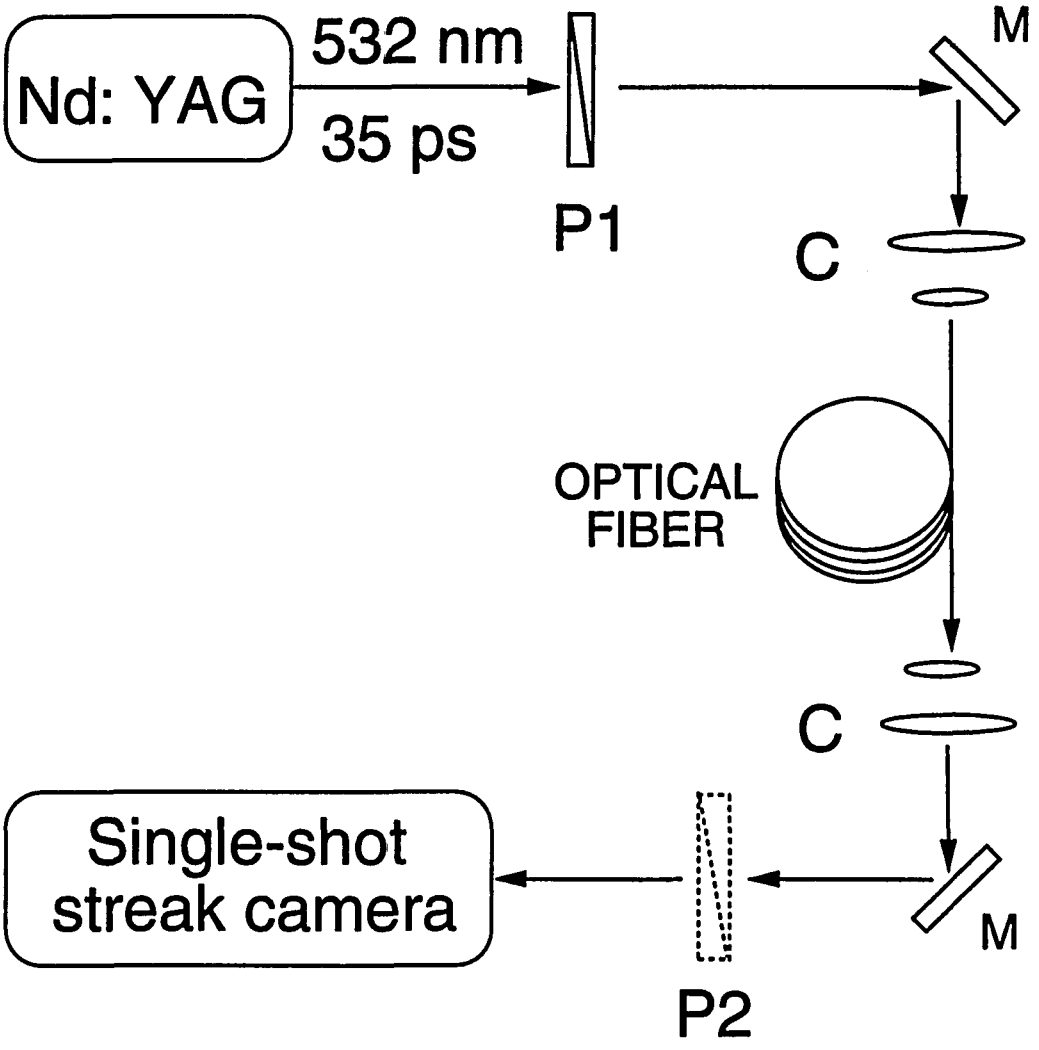

Figure V.1 Schematic diagram of the experimental setup to observe the nonlinear time modulation of picosecond laser light pulses. C: micro-objective lens coupler, P1 and P2: polarizers, M: mirror .

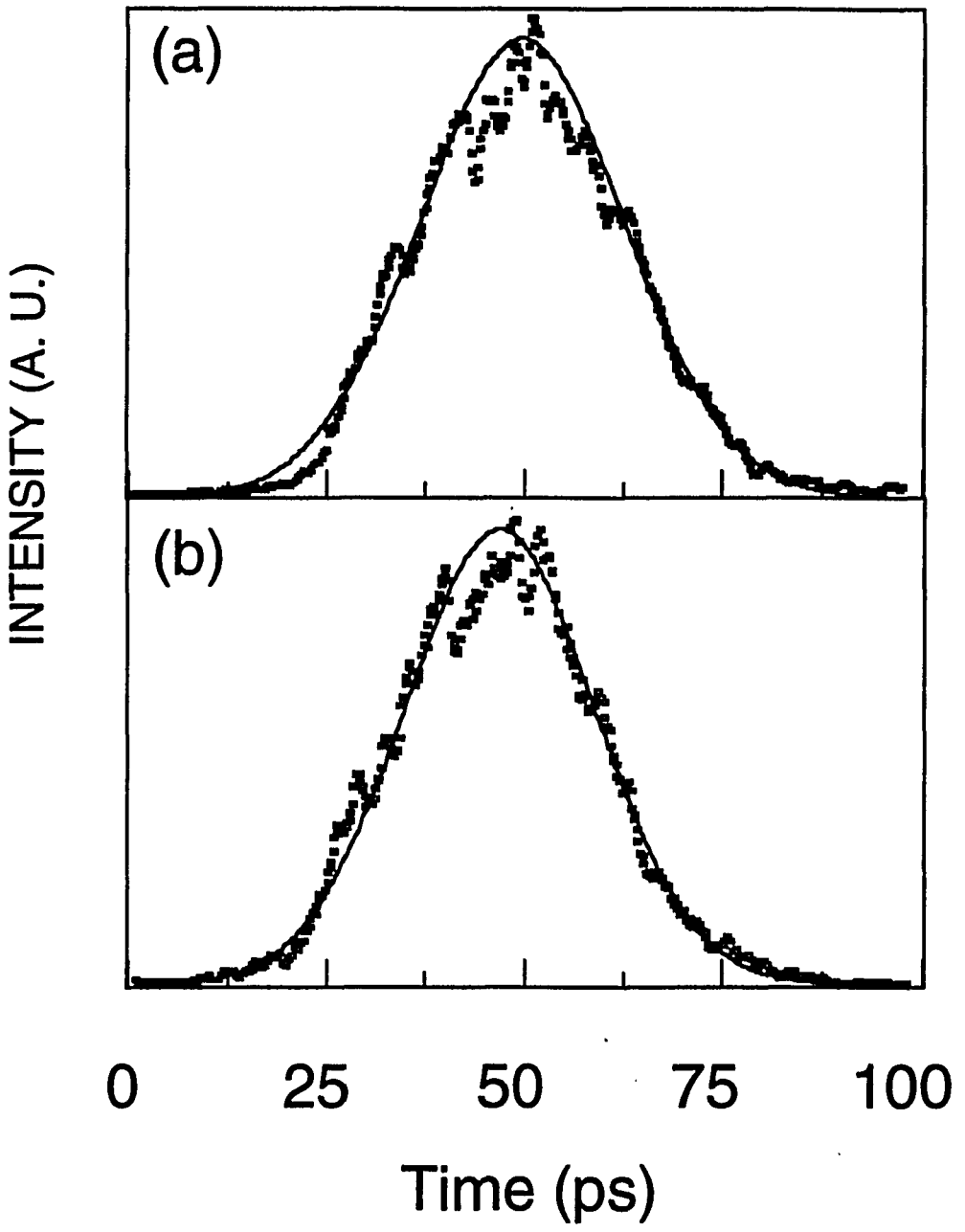

Figure V.2 (a) Temporal profiles of the incident laser pulse, dotted points are measured result and solid curves are theoretical fitting with a 35 ps Gaussian pulse profile. The measured pulse had a small temporal asymmetry where the leading edge is shorter about 4 ps than the trailing edge. (b) Output signal at a fiber exit without passing through polarizer P2 at the pulse energy of 1.5 nJ which has a similar characteristics of the incident laser pulse as shown in (a).

The measured laser light pulse temporal profile from the YAG laser system is displayed in Figure V.2(a) as a dot curve. The temporal profile of the laser light pulse was slightly asymmetric. The leading edge was shorter about 4 ps than the tailing edge. The solid curve shows a Gaussian fitting to the measured pulse shape with a duration of about 35 ps. These laser light pulses were then coupled into a nonbirefringent single-mode optical fiber. The temporal profiles of the output laser pulse at the fiber exit without passing through the polarizer P2 are displayed in Figure V.2(b) as a dot plot for the pulse energy of 0.15 nJ. The output pulse temporal distribution from an optical fiber is similar to the incident pulse as shown in Figure V.2(a) and is independent to the light intensity. This is not surprising because the length of the optical fiber was short. The bandwidth of the picosecond laser light pulse was narrow and the group-velocity dispersion of the optical fiber was small. Hence, the temporal profile of the output laser pulse from an optical fiber was not broadened much.

V.2.2 Results

The temporal profiles of the output laser light pulses from the optical fiber for various pulse energies (pulse intensities) are shown in Figure V.3 for pulse passing through the polarizer P2 set parallel to P1. Six measured temporal profiles are displayed using dot lines for different input pulse energies from 1.5 nJ to 32 nJ. In Figure V.3(a) for a relative low input energy of 1.5 nJ, the output pulse profile became less sharp. A dip appeared in Figure V.3(b) by increasing the input energy up to 6.6 nJ. In Figure V.3(c) for input pulse energy at 12 nJ, sub-pulse structure appeared. The output pulse splits into two pulses. Each one had a duration of about 18 ps. When the input energy was increased further to 19 nJ, the output pulse profile symmetrically developed additional pulse sub-structure. Three pulses were produced as shown in Figure V.3(d). The central one was larger than the side ones. Increasing the input energy to 27 nJ, a complex pulse profile

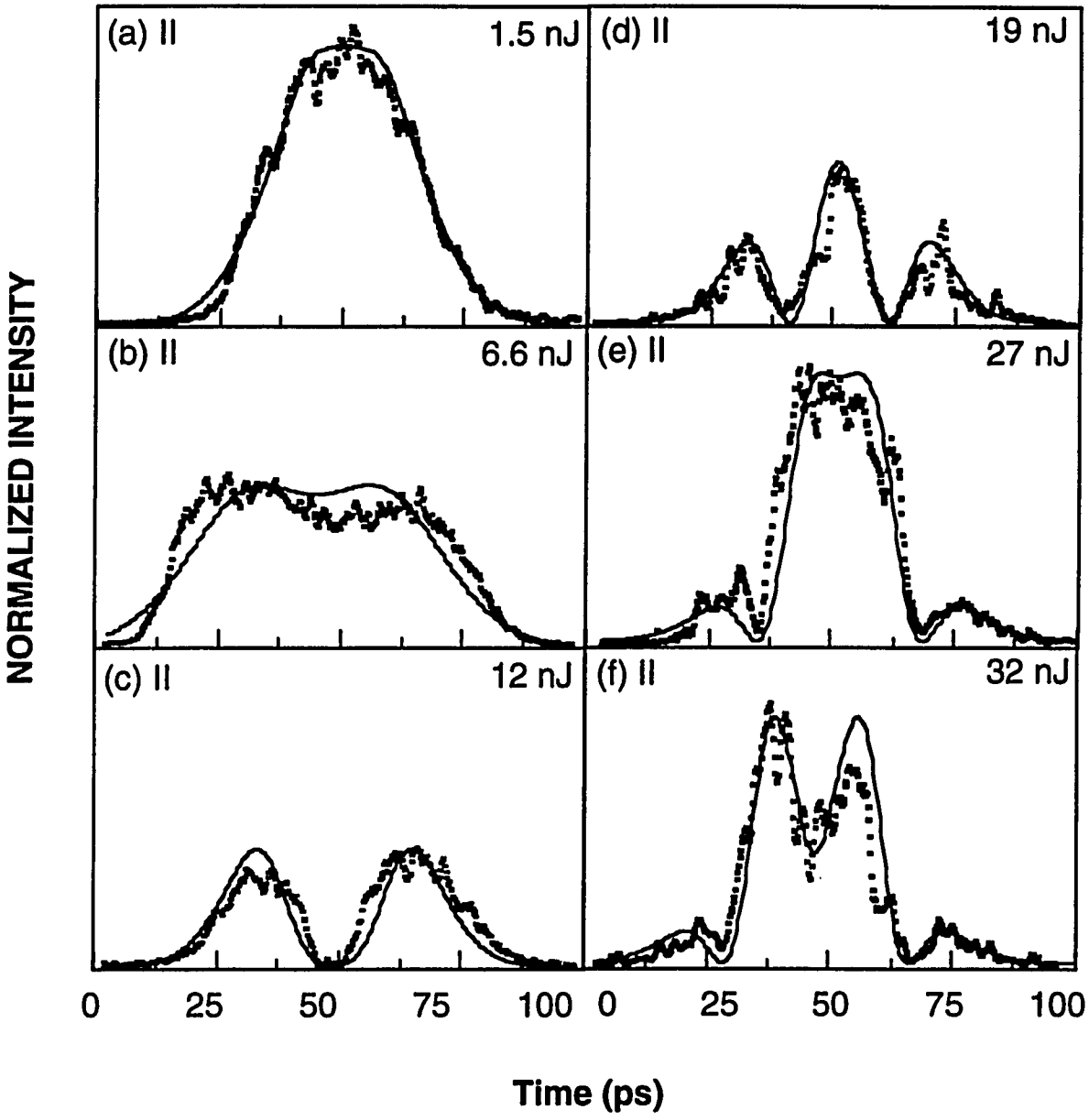

Figure V.3 Temporal profiles of parallel polarized component of the output pulses for different incident pulse intensities. Polarizer P2 was set parallel to P1. The dot plots are the experimental results. The solid curves are fitting for different pulse energies (intensities) and k values (nonlinear phase shift). (a). 1.5 nJ (k=0.2), (b). 6.6 nJ (k=0.8), (c). 12 nJ (k=1.5), (d). 19 nJ (k=2.4), (e). 27 nJ (k=3.4), (f). 32 nJ (k=4.0).

was generated when a low valley appeared on the central pulse to make it look broader in Figure V.3(e). The output pulse has shown four bumps for a higher input pulse energy at 32 nJ as shown in Figure V.3(f). This intensity dependent pulse-splitting phenomenon arises from the nonlinear polarization twisting (NPT).

V.2.3 Discussion

The measured results of NPT is modeled using the nonlinear depolarization in optical fibers[6]. Discussions on NPT effect can also be found in Chapter II. The linearly polarized laser pulses propagating in a nonbirefringent single-mode optical fiber can be analyzed using two orthogonal circular polarization bases. A linearly polarized laser pulse consists of two opposite circularly polarized components. Due to SPM and DXPM between these two circularly polarized components[7], the linear polarization state of the input laser pulse is twisted at different local time in the pulse profile. The nonlinear wave equations of the two circularly polarized components that govern the propagation of the laser pulse in the optical fiber can be expressed as[7]:

$$\frac{\partial A_R}{\partial z}+\frac{1}{v_{gR}}\frac{\partial A_R}{\partial t}+\frac{i}{2}k_R^{(2)}\frac{\partial^2 A_R}{\partial t^2}=i\frac{\omega_R n_2}{c}\left(\frac{2}{3}|A_R|^2+\frac{4}{3}|A_L|^2\right)A_R, \quad \text{(V.1a)}$$

$$\frac{\partial A_L}{\partial z}+\frac{1}{v_{gL}}\frac{\partial A_L}{\partial t}+\frac{i}{2}k_L^{(2)}\frac{\partial^2 A_L}{\partial t^2}=i\frac{\omega_L n_2}{c}\left(\frac{2}{3}|A_L|^2+\frac{4}{3}|A_R|^2\right)A_L, \quad \text{(V.1b)}$$

where υ_{gi} is the group velocity for the wave i, $k_i^{(2)}$ is the group velocity dispersion for the wave i, and $n_2=3\chi^{(3)}/8n$ is the nonlinear refractive index. The first terms in the right-handed side of Eqs. (V.1) are SPM terms and the second terms are the DXPM terms.

These nonlinear wave equations can be solved only using numerical method, but analytical solutions are possible under some approximations. Assuming that the third terms of the left-handed side of Eqs. (V.1) are small enough (meaning that the temporal broadening caused by the group velocity dispersion is neglected, this is true in our case.). Using slowly changing envelope and phase of the pulses with a and α, respectively. we obtain:

$$A_R(\tau,z) = a_{R(\tau,z)} e^{i\alpha_R(\tau,z)}, \tag{V.2a}$$

$$A_L(\tau,z) = a_{L(\tau,z)} e^{i\alpha_L(\tau,z)}, \tag{V.2b}$$

Eqs. (V.1) reduce to

$$\frac{\partial a_R}{\partial z} = 0, \tag{V.3a}$$

$$\frac{\partial a_L}{\partial z} = 0, \tag{V.3b}$$

$$\frac{\partial \alpha_R}{\partial z} = i\frac{\omega}{c} n_2 [\frac{2}{3} a_R^2 + \frac{4}{3} a_L^2], \tag{V.3c}$$

$$\frac{\partial \alpha_L}{\partial z} = i\frac{\omega}{c} n_2 [\frac{2}{3} a_L^2 + \frac{4}{3} a_R^2], \tag{V.3d}$$

where $\tau = (t - z/v_{gl})/\tau_0$ is the pulse local time and τ_0 is the 1/e pulse duration. In addition, Gaussian pulse shapes are chosen at the input z=0:

$$A_R(\tau, z = 0) = a_{R0} e^{-\tau^2/2}, \tag{V.4a}$$

$$A_L(\tau, z = 0) = a_{L0} e^{-\tau^2/2}, \tag{V.4b}$$

where a_{10} and a_{20} is the input peak amplitudes of the laser pulses. With these initial conditions, the solutions for the amplitudes and phases of the pulse after propagating in optical fiber with length z are

$$a_{R(\tau,z)} = a_{R0}, \tag{V.5a}$$

$$a_{L(\tau,z)} = a_{L0}, \tag{V.5b}$$

$$\alpha_R(\tau, z) = \frac{\omega}{c} n_2 z\left(\frac{2}{3} I_{R0} + \frac{4}{3} I_{L0}\right) e^{-\tau^2}, \tag{V.5c}$$

$$\alpha_L(\tau, z) = \frac{\omega}{c} n_2 z\left(\frac{2}{3} I_{L0} + \frac{4}{3} I_{R0}\right) e^{-\tau^2}, \tag{V.5d}$$

where I_{10} and I_{20} are the intensities of the two circular components of input laser pulse. Eqs. (V.5) give the amplitudes and phases caused by SPM and DXPM processes for a single laser pulse propagating in an optical fiber. The amplitudes of the two circular components remain stable during the propagation from the solution (V.5a and V.5b), while the phases depend on the intensities of right- and left-handed components (V.5c and V.5d).

Consider a perfect linearly polarized laser pulse which can be regarded as superposition of two circular polarization components with the same amplitude and zero phase difference. Since these two circularly polarized components have exactly the same intensity, their nonlinear phase changes are equal. At the output of the optical fiber, the superposition of the two equal-phase circular polarization states gives the original linear polarization state. Therefore, the nonlinear depolarization and NPT effects should not occur.

Under practical real world experimental conditions, the input laser pulses was not perfect linearly polarized. The input laser pulses had an extinction ratio of better than 400

before the fiber. At the fiber exit, the output pulse had a typical extinction ratio of 20 (degree of polarization is 0.9). This depolarization is believed to be caused by the scattering of the surfaces of the optical components, more specifically by the fiber input surface which is irregular after the fiber cut. The incident linearly polarized light was scattered into the perpendicular linear polarization mode. As a result, the incident linearly polarized light becomes slightly depolarized. This is true because there is a depolarization background at very low pulse intensity where nonlinear effects are absent. This non-perfectly linear polarization state can be theoretically simulated by an elliptically polarized optical pulse. The intensities of the two circular components became unequal with a difference of $\Delta I = | I_{R0} - I_{L0} | = 2\sqrt{r}\, I_0$, where I_0 is the total intensity, I_{R0} and I_{L0} are the intensities of right- and left-handed components, respectively; and r is the small depolarization ratio defined by $r \equiv I_{\perp} / I_{//}$, where $I_{\perp}$ and $I_{//}$ are the intensities of the perpendicular and parallel linearly polarized components of the incident laser pulse, respectively (see Eq. (IV.10)). The phases of these two circularly polarized components of the high intensity laser pulses are not equal after propagating through an optical fiber. There will be a nonlinear phase shift between these two circular components. The nonlinear phase shift can be calculated using Eqs. (V.5) and expressed as:

$$\Delta\alpha(\tau, z) = | \alpha_R - \alpha_L | = \frac{4\pi}{3\lambda} n_2 z \Delta I e^{-\tau^2} = 2k e^{-\tau^2}, \qquad \text{(V.6)}$$

where $k = 4\pi n_2 z \sqrt{r}\, I_0 / 3\lambda$ is a nonlinear phase parameter. The nonlinear phase shift is a function of pulse instantaneous intensity due to its dependence on pulse local time τ. At the output, the superposition of the two circular components is not the input pulse polarization state because of this nonlinear phase shift $\Delta\alpha$.

After a laser pulse propagated through the optical fiber, the polarization state at the fiber exit is a superposition of the two circularly polarized components. For two

opposite circularly polarized pulses with equal amplitude, the superposition is always a linearly polarized laser pulse. The direction of the linear polarization depends on the phase difference. A zero phase difference between two circularly polarized states will give a linear polarization state at x-axis direction. For a phase difference of $\Delta\alpha(\tau,z)$, the output linear polarization will rotate by an angle of $\Delta\alpha(\tau,z)/2$. Details of the calculation of this polarization rotation can be found in chapter II from Eq. (II.61) to (II.62). After a quasi-linearly polarized ultrashort laser pulse passing through an optical fiber, the state of polarization depends on local time because of the nonlinear phase shift $\Delta\alpha(\tau,z)/2$. The quasi-linearly polarized optical pulse will keep linearly in propagation, but the polarized direction gradually changes at different local time depending on $\Delta\alpha$ within the pulse profile. This nonlinear polarization change at different local time results in a twisting linear polarization state within the pulse envelope.

The three dimensional structures of the evolution of the polarization vector of a quasi-linearly polarized laser pulse at different local time τ are displayed in Figure V.4 after undergoing different nonlinear phase shifts k (for different intensities in the experiment). The intensities of the two linearly polarized components of laser pulses are at x and y directions, respectively, as shown in Figure V.4 where τ is the local time. At low intensity ($k \sim 0$) without any significant nonlinear phase shift, the output laser pulse remains linearly polarized in a x-direction as shown Figure V.4. The electric field profile of the output laser pulse is also in x-τ plane. For k=2, the polarization direction of the laser pulse first shows a rotation at the central region ($\tau \sim 0$). The electric field profile displays a curve which turn to y-direction. For k=4, the electric field profile developed to curve rotating around τ-axis. This curve represented the change of the linear polarization direction in the pulse profile. When k is increased further, the polarized direction of the laser pulse developed into different twisted structures. The polarization change within a

Electric Field Direction Curves of Linearly Polarized Optical Pulses for Different Nonlinear Phase Shift $k=2\pi n_2 z\Delta I/3\lambda$

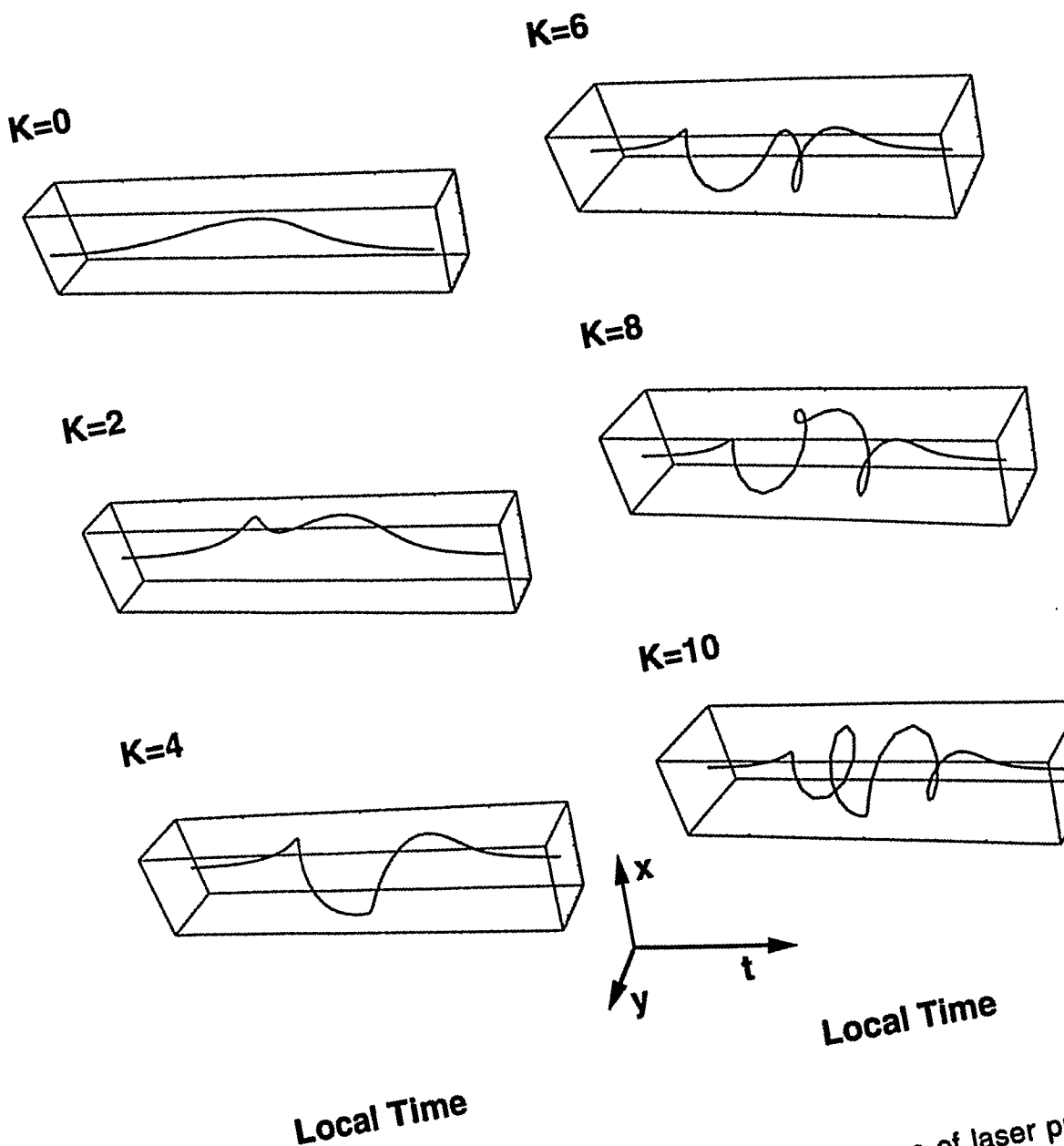

Figure V.4 Three dimensional polarization structures of laser pulses experienced different nonlinear phase shift. The laser pulse is linearly polarized at any local time, but the direction of linear polarization is different at different local time.

pulse profile due to different k can be viewed as polarization-twisted laser pulses in different local time.

For the laser light pulses having Gaussian shape and linearly polarized at x-axis direction. The electric field of the input laser light pulse can be expressed as

$$\vec{A}_{(\tau, z=0)} = \vec{e}_x a_0 e^{-\tau^2/2}. \qquad \text{(V.7)}$$

For the output light pulse having a rotation angle of $\Delta\alpha(\tau,z)/2$, the electric field component at parallel direction (x-axis direction) are

$$A_{x(\tau,z)} = a_0 e^{-\tau^2/2} \cos\{\alpha(\tau,z)/2\}. \qquad \text{(V.8)}$$

The measured intensity temporal distribution of the parallel component of the output laser pulse after polarizer P2 parallel to P1 can be expressed by:

$$I(\tau) = I_o e^{-\tau^2} \cos^2(k e^{-\tau^2}), \qquad \text{(V.9)}$$

where Io is the peak intensity and k(Io) is the nonlinear phase parameter. At high intensities, the $\cos^2(x)$ term will give rise to a high frequency oscillation within the pulse temporal profile. Hence, the input picosecond laser pulse will be split into several narrow small linearly polarized pulses.

Using this model the data fitting are shown in Figure V.3 as solid curves for different pulse energies. These results are in good agreement with the measurements for corresponding values of nonlinear phase parameter k. The temporal profile asymmetry of the incident laser pulses still had a signature in the experimental results and it is clear that

the leading edge was shorter than the trailing edge in Figure V.3(b) at the pulse energy of 6.6 nJ. The output at perpendicularly polarized direction of polarizer P1 is also modulational structures in time but it is a $\sin^2(x)$ function. The output pulse temporal profiles at the perpendicular direction also have been measured for different pulse intensities. The dot plot in Figure V.5(b) is the measured pulse sub-structure at pulse energy of 32 nJ by setting P2 at perpendicular direction of P1. The solid curve is the calculation at the same pulse energy. Figure V.5(a) displays the temporal profile of the parallel component at the pulse energy of 32 nJ to show the differences of these two components. It is easy to understand that the superposition of these two linearly polarized components will give the original pulse shape. At the pulse energy of 32 nJ, the superposition of the parallel component as shown in Figure(a) and the perpendicular one as shown in Figure V.5(b) is displayed in Figure V.5(c) as a dot plot. Indeed, it is similar to the output laser pulse in Figure V.2(b) without passing through the polarizer P2 except that it is much noisy. This noise is caused by the fluctuation of the laser and the jitters of the streak camera. A fitting curve is also shown in Figure V.5(c) as a solid one which has the same pulse duration of the input laser pulse in Figure 2(b). They are in good agreement with each other.

In summary, the nonlinear polarization twisting has been observed arising from nonlinear processes, SPM and DXPM for laser pulses traveling in a nonbirefringent single-mode optical fiber. The theoretical model for NPT is in good agreement with the experimental results. The modulational structures of the temporal profiles of the output linearly polarized components are sensitive to the nonlinear phase shift parameter k. The effect may be used to measure the nonlinear refractive index, n_2, and can be useful in the ultrafast all-optical A/D converters, optical switches, and optical amplifiers.

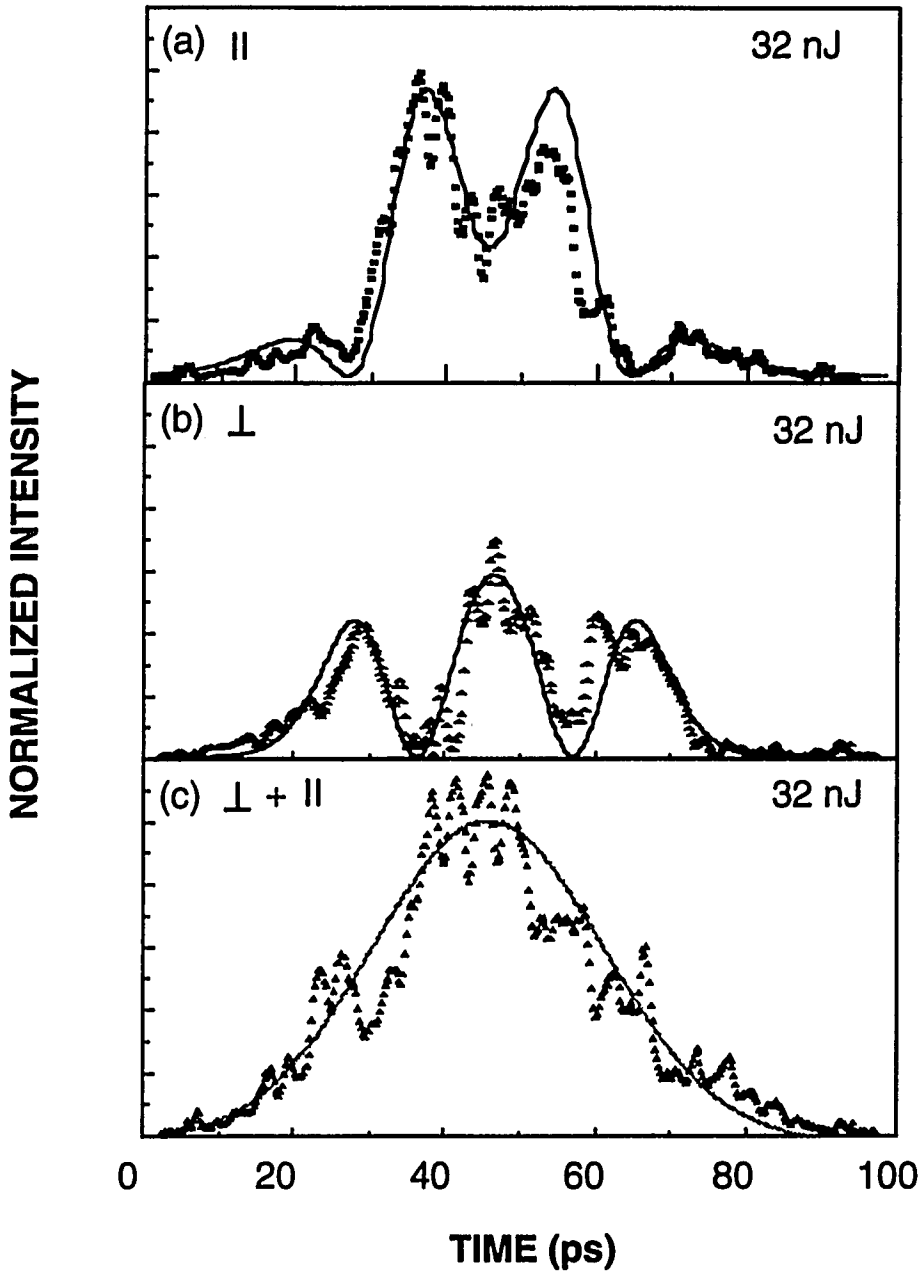

Figure V.5 (a), Output temporal profile of parallel component at the pulse energy of 32 nJ; (b), Temporal profile of perpendicular component (to P1) at the same pulse energy of 32 nJ; (c), The superposition of parallel and the perpendicular component of the output laser pulse. The output pulse is similar to the pulse without passing through the polarizer P2 as shown in Figure V.2 (b). Solid curves are the fittings of the temporal profiles.

V.3 Nonlinear Polarization Twisting of Femtosecond Laser Pulses in Non-birefringent Single-mode Optical Fibers

V.3.1 Experimental Setup

The schematic diagram of the experimental setup for measuring the nonlinear polarization twisting (NPT) for femtosecond laser light pulses is shown in Figure V.6. Ultrashort laser pulses were generated from a colliding-pulse mode-locked dye laser with a power of 5 mW, at the wavelength of 625 nm with a bandwidth of 6 nm, a repetition rate of 82 MHz. These laser light pulses having pulse duration of 60 femtosecond were then amplified to an energy of 1 μJ per pulse by a copper-vapor laser at a pulse repetition rate of 6.5 KHz. These ultrashort laser pulses were linearly polarized at horizontal direction to an extinction ratio of better than 1000. To avoid the temporal broadening caused by group velocity dispersion of the ultrashort laser pulse, a thin glass slide was inserted into the laser beam to select a small portion of the laser light as the reference pulse for the cross correlator which was used to measure the temporal profile of the output optical signal from an optical fiber. The horizontal linearly polarized laser pulses after the glass slide were then coupled into and out of a 0.5-m-length single-mode nonbirefringent optical fiber (Newport Corporation Model: FSA-10). The optical fiber had a symmetric circular cross section without birefringence except the residual birefringence randomly existed in the fiber which was formed during the fabricating process. The beat length of this kind of residual birefringence is much longer than the length used in the experiment. Hence, the fiber can be treated as nonbirefringent. The optical fiber had a core diameter of 4 μm and cladding thickness of 125 μm which can support a single mode at the laser light wavelength of 625 nm. As discussed in last section V.2, both DXPM and SPM processes occurred[7] for even a single laser pulse propagating in the nonbirefringent single-mode optical fiber because of high intensity of

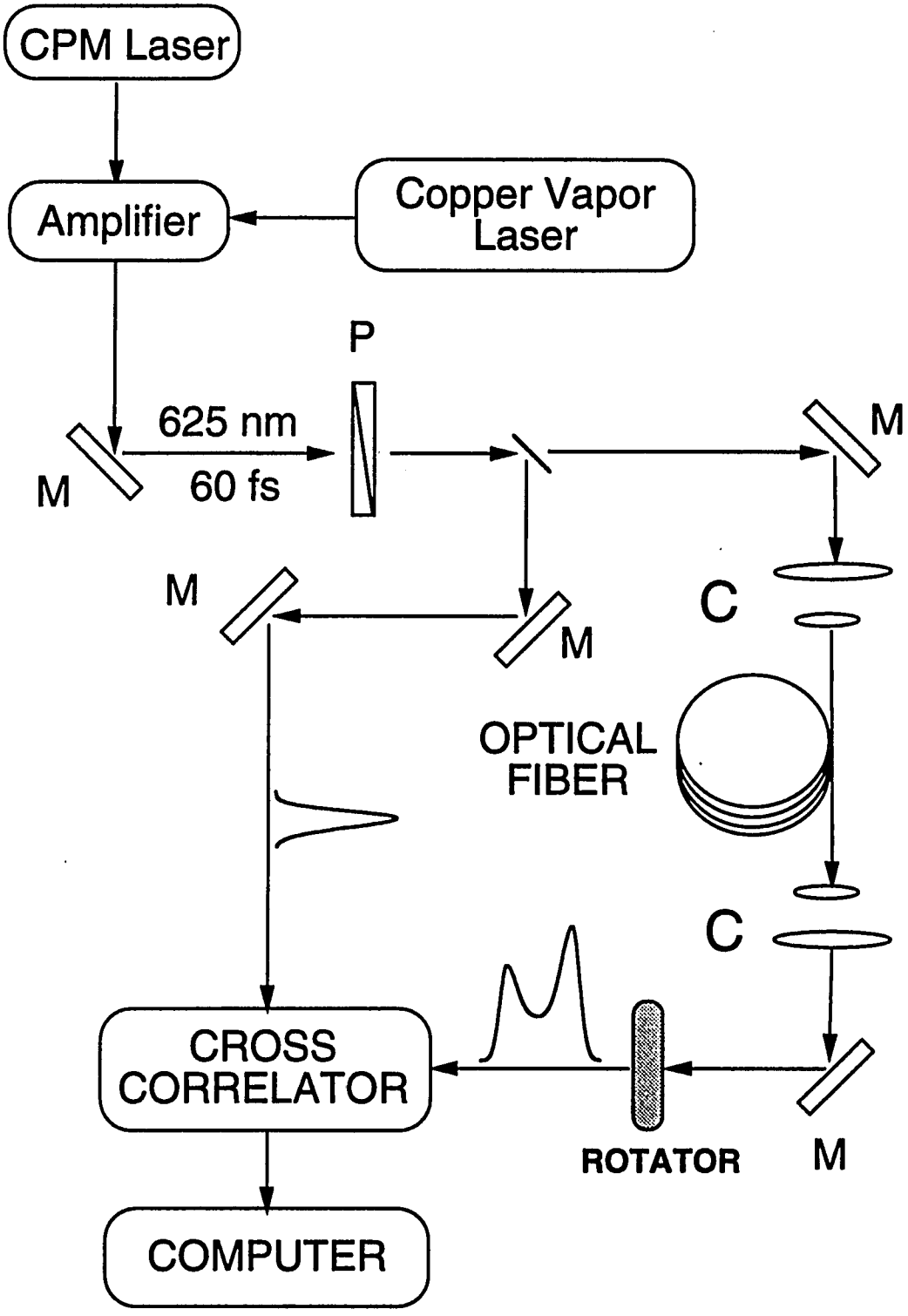

Figure V.6 Schematic diagram of the experimental setup to observe the nonlinear time modulation of femtosecond laser light pulses. C: micro-objective lens coupler, P: polarizers, M: mirror .

the laser pulse. These nonlinear processes usually caused the depolarization of the laser pulse in the fiber. At the fiber exit, the output optical signal was sent to a cross correlator for measuring the temporal profile. The cross correlator has been discussed in section III.8 of Chapter III in great detail. The signal from the cross correlator was collected and analyzed using a computer and displayed on the screen.

An important feature of the cross correlator is that the second harmonic generation (SHG) signal for Type I arrangement is sensitive to the polarization state of the two optical pulses. Since type I SHG (o+o -> e) requires strictly phase match, the SHG signal exists only for two parallel linearly polarized optical pulses. There is no SHG signal for two perpendicular linearly polarized optical pulses. In experiment, the output optical signal pulse from the optical fiber is usually depolarized and has two polarization components. Since the reference pulse is linearly polarized in the horizontal direction, the SHG signal will depend on the horizontal component of the output optical pulse. For the reference pulses at a given intensity, the intensity of SHG is proportional to the intensity of the horizontal components of the output optical plusses from the fiber. By changing the optical delay time between the reference pulse and the signal pulse, the temporal profile of the horizontal component can be measured. To measure the vertical component of the output optical pulses, a 90° rotator was used in front of cross correlator in the signal beam. The optical axis of the rotator was set at 45° to the horizontal direction. After passing through the rotator the direction of polarization of the optical pulse turned 90°. The horizontal and vertical components exchanged their positions. In this case the SHG signal is proportional to the intensity of the vertical component of the output optical pulses from the fiber.

The measured SHG intensities for pulses before and after the fiber as a function of the optical delay for the amplified CPM laser system is displayed in Figure V.7 as solid

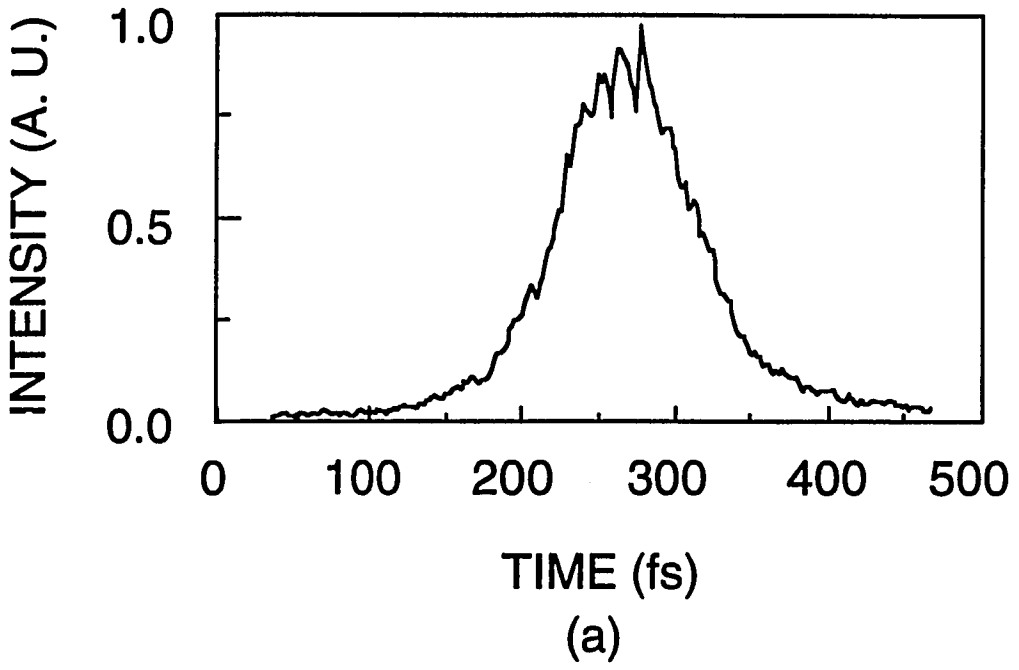

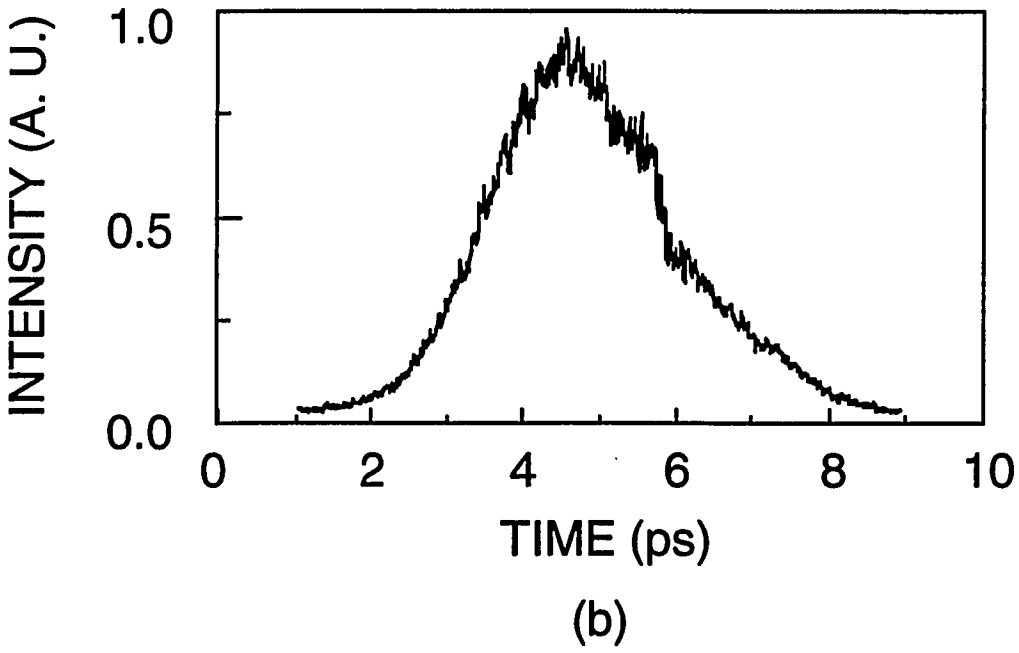

Figure V.7 (a) The auto-correlation curve of the amplified CPM laser light pulses. (b) the cross-correlation curve of the the refrence pulse and the pulses passing through a 0.5-m-length single-mode optical fiber.

curves. The auto-correlation curve of the laser light pulses without passing through the optical fiber is shown in Figure V.7(a). The FWHM of the auto-correlation trace is 95 fs, corresponding to the laser pulse duration of 60 fs for the hyperbolic square secant pulse temporal profile of the laser light pulse. For the laser light pulses passing through the 0.5-m-length nonbirefringent single-mode optical fiber at low pulse energy of 5 nJ, the cross-correlation curve was shown in Figure V.7(b). The cross-correlation has a FWHM of 2.8 ps. This broadening of pulse duration is due to the group velocity dispersion (GVD) in the optical fiber. The input laser light itself has a large bandwidth of 6 nm. When the laser pulses were coupled into the fiber, the supercontinuum generation produced more frequencies due to the high light intensity. The GVD caused the temporal profile of the laser pulse broadened greatly. Because of the large difference between the durations of the reference pulse (60 fs) and the output signal pulse from the fiber. The reference pulse acted just like a Delta function to the signal pulse. The cross-correlation curve is the temporal profile of the horizontal component (without rotator) of the signal light pulse.

V.3.2 Results

The cross-correlation curves (temporal profiles) of the output laser light pulses from the optical fiber for various input pulse energies (pulse intensities) are shown in Figure V.8 for horizontal component without a rotator. Six measured cross-correlation curves are displayed for different input pulse energies from 5 nJ to 45 nJ. Figure V.8(a) shows the output pulse profile of the horizontal component for a relative low input energy of 5 nJ. The intensity of the vertical component of the output light pulses is too weak to be measured at this input pulse energy by using cross-correlation method. It is suffice to say that the light remains linearly polarized at the horizontal direction for the pulse energy of 5 nJ after propagating in the optical fiber. Due to GVD, the temporal profile of the output pulse was much broadened to the FWHM of 2.8 ps. In Figure V.8(b) by

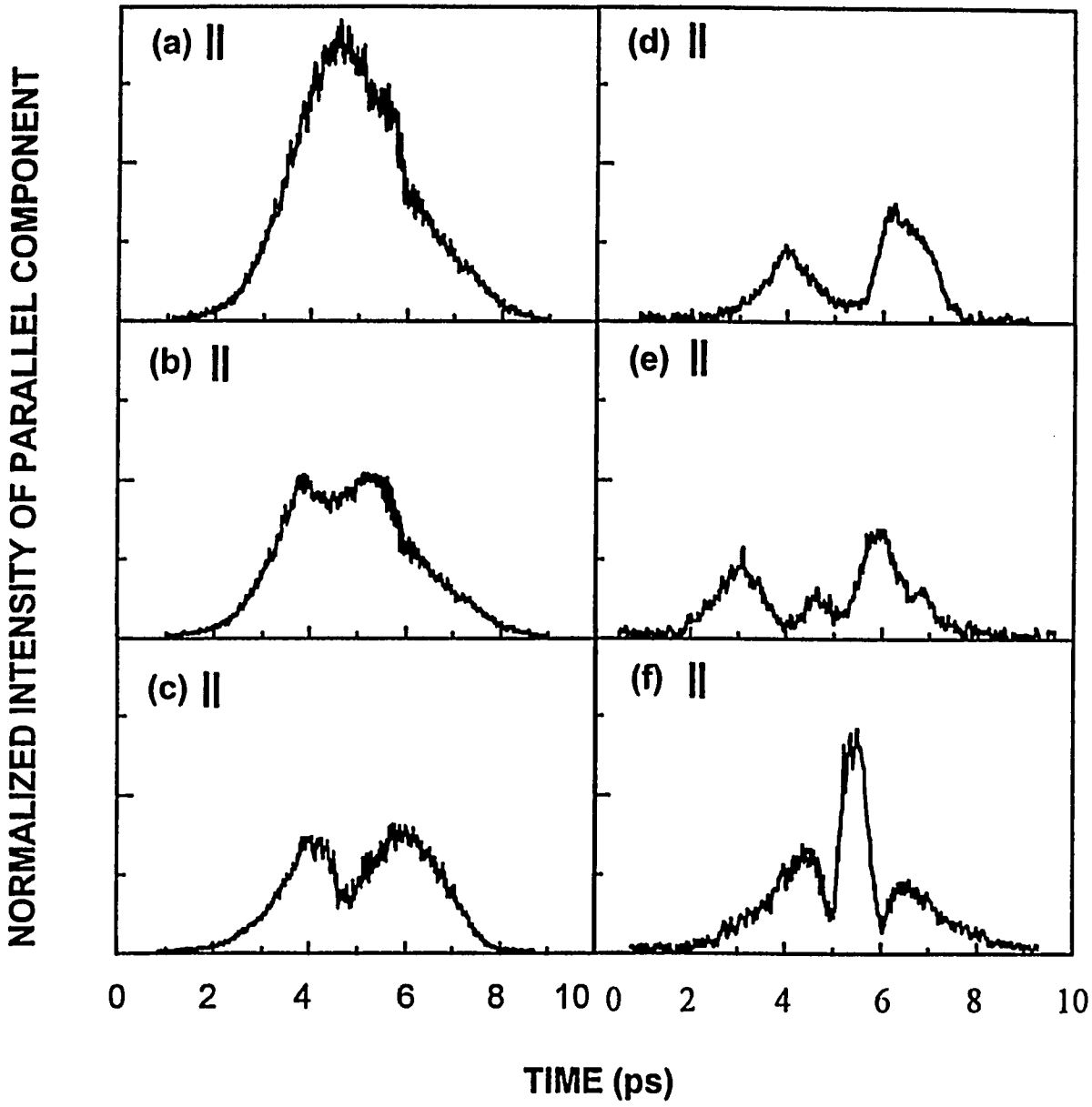

Figure V.8 Temporal profiles of horizontal component of the output pulses for different incident pulse energies. The curves are the experimental results. The input pulse energies (intensities) are (a). 5 nJ, (b). 16 nJ, (c). 21 nJ, (d). 25 nJ, (e). 30 nJ, (f). 45 nJ.

increasing the input pulse energy up to 16 nJ, a dip appears. This dip means that the energy in the dip area is coupled from horizontal polarizing direction to vertical polarizing direction. Increasing the input pulse energy to 21 nJ as shown in Figure V.8(c), the dip develops and is well formed. In Figure V.8(d) for input pulse energy at 25 nJ, sub-pulse structure appeared. The output pulse splits into two pulses. Each one had a duration of about 0.8 ps. When the input energy was increased further to 30 nJ, the output pulse profile symmetrically developed additional pulse sub-structure. Three pulses were produced as shown in Figure V.8(e). The central one was smaller than the side ones. Increasing the input pulse energy to 45 nJ, a complex pulse profile was generated when the central sub-pulse structure became stronger than the side ones and the intensity of the side ones developed asymmetrically as shown in Figure V.8(f). This intensity dependent pulse-splitting phenomenon also arises from the nonlinear polarization twisting (NPT) as we discussed in last section.

V.3.3 Discussion

The experimental measured results of NPT for picosecond laser light pulses has been modeled using the nonlinear depolarization in optical fibers. The nonlinear depolarization can be described using the nonlinear wave equations Eqs. (V.1) of the two circularly polarized components of the laser pulse in the optical fiber. For picosecond laser light pulses, the dispersion terms (third terms on the left-handed side of Eqs. (V.1)) can be neglected since they are small. Analytical solutions have been solved from the nonlinear wave equations for picosecond laser light pulses. The calculation of the NPT has a good agreement with the experimental results. However, the GVD terms can not be neglected for femtosecond laser light pulse since they affected the propagating pulse property strongly. There is no analytical solutions for these nonlinear wave equation.

Fortunately, we can have similar conclusions after analyzing theses nonlinear wave equations (V.1) in detail.

These nonlinear wave equations (V.1) have two terms on the left-handed side which represent for SPM and DXPM. From the solutions of the amplitudes and phases caused by SPM and DXPM processes for a single laser pulse propagating in an optical fiber in Eqs. (V.5). The amplitudes of the two circular components remain stable during the propagation from the solution (V.5a and V.5b), meaning that the right- and left-handed components don not transfer energy from each other. The intensity of the right-handed component remain at the input initial value in the pulse propagation and so dose the left-handed component. The phases of the two components depend on the intensities of right- and left-handed components (V.5c and V.5d). Considering the GVD terms which broadened the pulse dramatically for femtosecond light pulses, as a matter of fact, the only effect of these GVD terms is that the temporal broadening of the laser light pulses. GVD effect does not cause the energy transfer between right-handed component and left-handed component either. The circular polarizations are still stable in this case.

The nonlinear polarization twisting depends on the stable propagation of the circularly polarized components and a nonlinear phase difference between the two circularly polarized components. These conditions are true for femtosecond laser light pulses propagating in the nonbirefringent single-mode optical fiber. The effect of GVD is to broaden the light pulse for which we are not interested. Not surprisingly, the NPT has been observed in the experiment as shown in Figure V.8.

Like picosecond laser light pulses, the femtosecond light pulses were not perfect linearly polarized. The input laser pulses had an extinction ratio of better than 1000 before the fiber. At the fiber exit, the measured output pulse from the fiber had a typical

extinction ratio of 100 (degree of polarization is 0.98) at very low light intensity where the nonlinear effect is absent. This depolarization is believed to be caused by the scattering of the input surfaces of the optical fiber which is irregular after the fiber cut. The incident linearly polarized light was scattered into the perpendicular linear polarization mode. As a result, the incident linearly polarized light becomes slightly depolarized. Again for this not-perfectly linear polarization state, the intensities of the two circular components became unequal with a certain difference. Therefore, the phases of these two circularly polarized components of the high intensity laser pulses are not equal after propagating through an optical fiber. There will be a nonlinear phase shift between these two circular components. The nonlinear phase shift is responsible for the observed NPT.

The nonlinear phase shift can be expressed using Eq. (V.6) for picosecond laser light pulses which is not directively effective for femtosecond laser light pulses. The reason is that the instantaneous light intensity in the pulse temporal profiles changed with the propagating distance in the fiber because of GVD. For picosecond laser light pulses, the temporal broadening has been neglected in the calculation. The instantaneous light intensity in the pulse temporal profile does not the pulse propagation in a fiber. For femtosecond laser pulses, the instantaneous intensity of the light intensity in the pulse temporal profile is always changing due to the GVD effect. The instantaneous intensity in pulse profiles decreases along the fiber, so the nonlinear effect became smaller when the light propagates further in the fiber. The measured NPT effect as shown in Figure V.8 is an total NPT effect for the input laser light pulses with various different nonlinear phase shift k values. In this case, an average nonlinear phase shift <k> can be used to describe the total NPT which is proportional to the input pulse energy. The total nonlinear phase shift can be expressed as

$$\Delta\alpha(\tau,z) = 2 < k > e^{-\tau^2}, \qquad \text{(V.10)}$$

where $< k >= 4\pi n_2 \sqrt{r}\, I_0 z$ is the average nonlinear phase parameter. For light pulses with a Gaussian pulse shape, the theoretical fitting to the measured results as shown in Figure V.8 is displayed in Figure V.9 using Eqs. (V.10), (V.8), and (V.9). Other pulse shape can also be used but the results are similar. It can be seen that this simple simulation is in good agreement with the experimental results. The k value in Figure V.9 is assumed to be an average value of the nonlinear phase shift parameter. The output light pulses with a pulse duration of about 2.5 ps were much broadened than the input light pulse duration which were 100 fs. This is due to strong GVD effect in the fiber. It seems that GVD does not directly affect NPT.

The output pulse temporal profiles for femtosecond input light pulses at the vertical direction also have been measured for different pulse intensities. The curve as shown in Figure V.10(a) is the measured pulse temporal profile at pulse energy of 30 nJ by setting the rotator at 45° to horizontal direction. Figure V.10(b) displays the temporal profile of the horizontal component at the same pulse energy of 32 nJ to show the differences of these two components. It is easy to understand that the superposition of these two linearly polarized components will give the total output pulse shape. At the pulse energy of 32 nJ, the superposition of the horizontal component as shown in Figure V.10(b) and the vertical one as shown in Figure V.10(a) is displayed in Figure V.10(c). A simulation using Gaussian pulse shape is shown in Figure V.11. Figure V.11(a) and V.11(b) are the temporal profiles of the vertical and horizontal components, respectively. Figure V.11(c) is the superposition of the two components. This simulation is in good agreement with measurement as shown in Figure V.10.

The nonlinear polarization twisting has been observed for femtosecond laser pulses traveling in a nonbirefringent single-mode optical fiber. Different temporal profiles of the two polarization components of a laser light pulse output from a nonbirefringent single-mode optical fiber have been observed. The theoretical model for NPT is quantitatively in agreement with the experimental results.

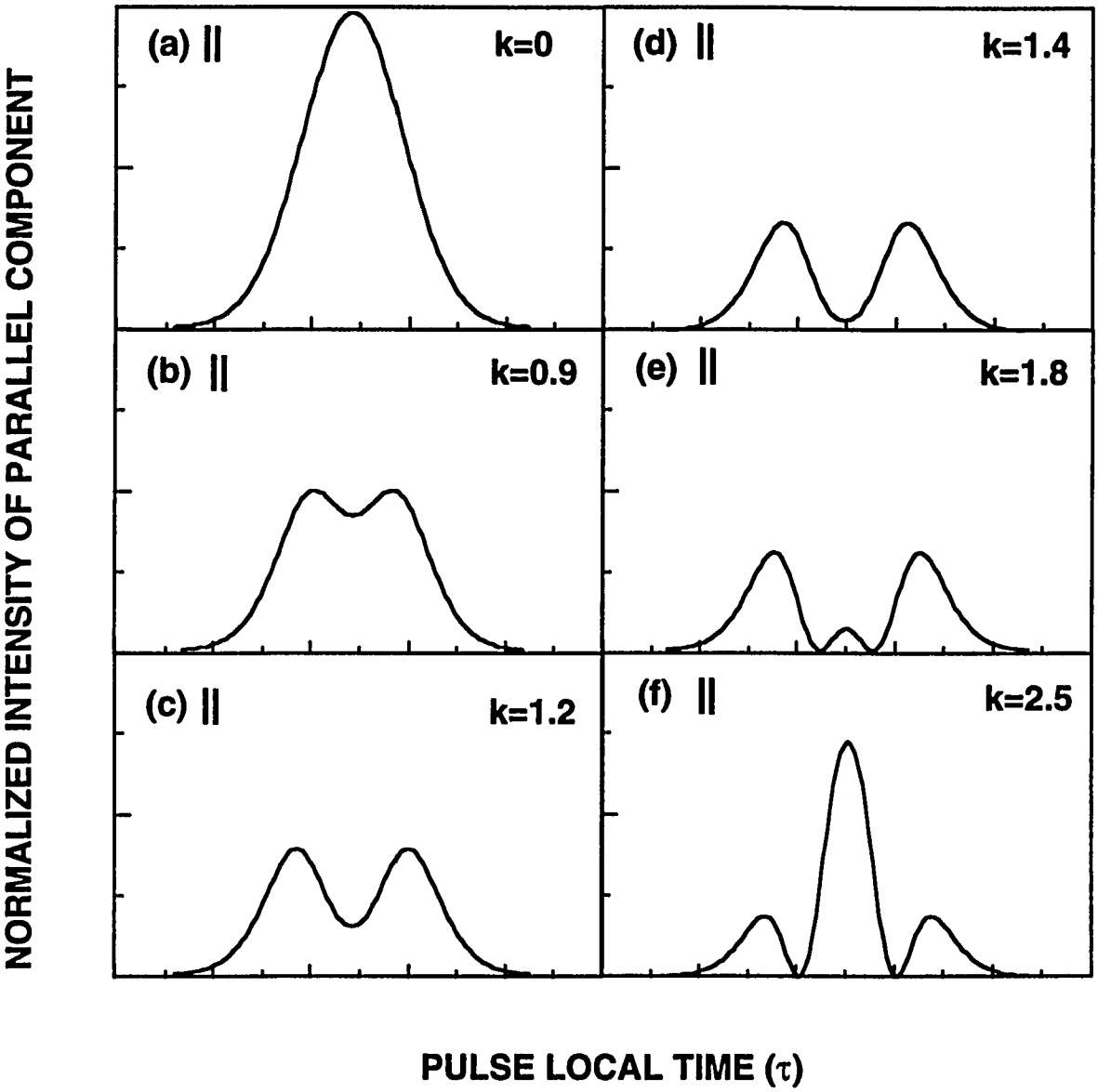

Figure V.9 Temporal profiles of horizontal component of the output pulses for different nonlinear phase shift k for Gaussian pulses .

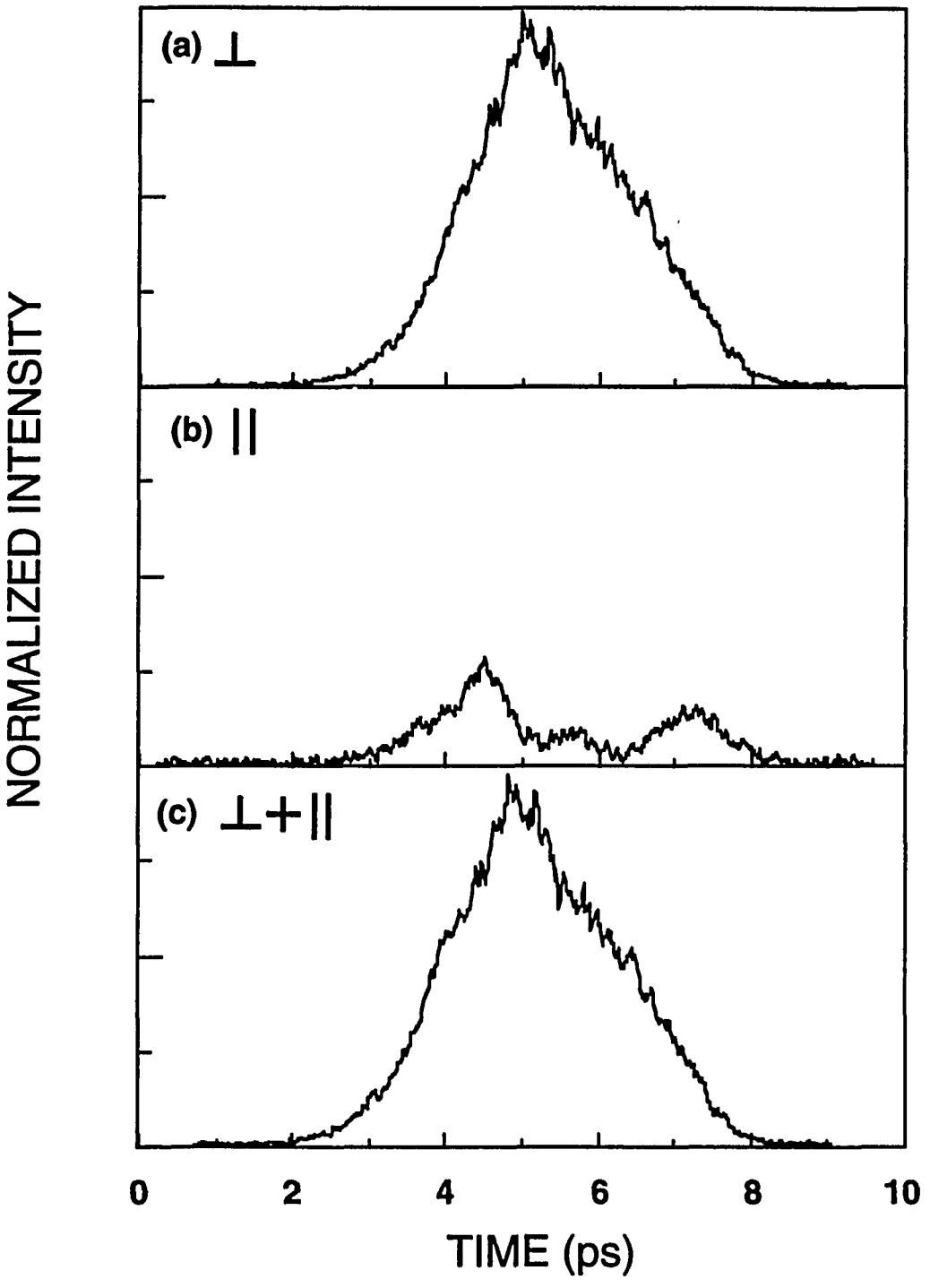

Figure V.10 (a), Output temporal profile of vertical component at the pulse energy of 30 nJ; (b), Temporal profile of horizontal component at the same pulse energy; (c), The superposition of vertical and horizontal components of the output laser pulses. This is the total output pulse shape.

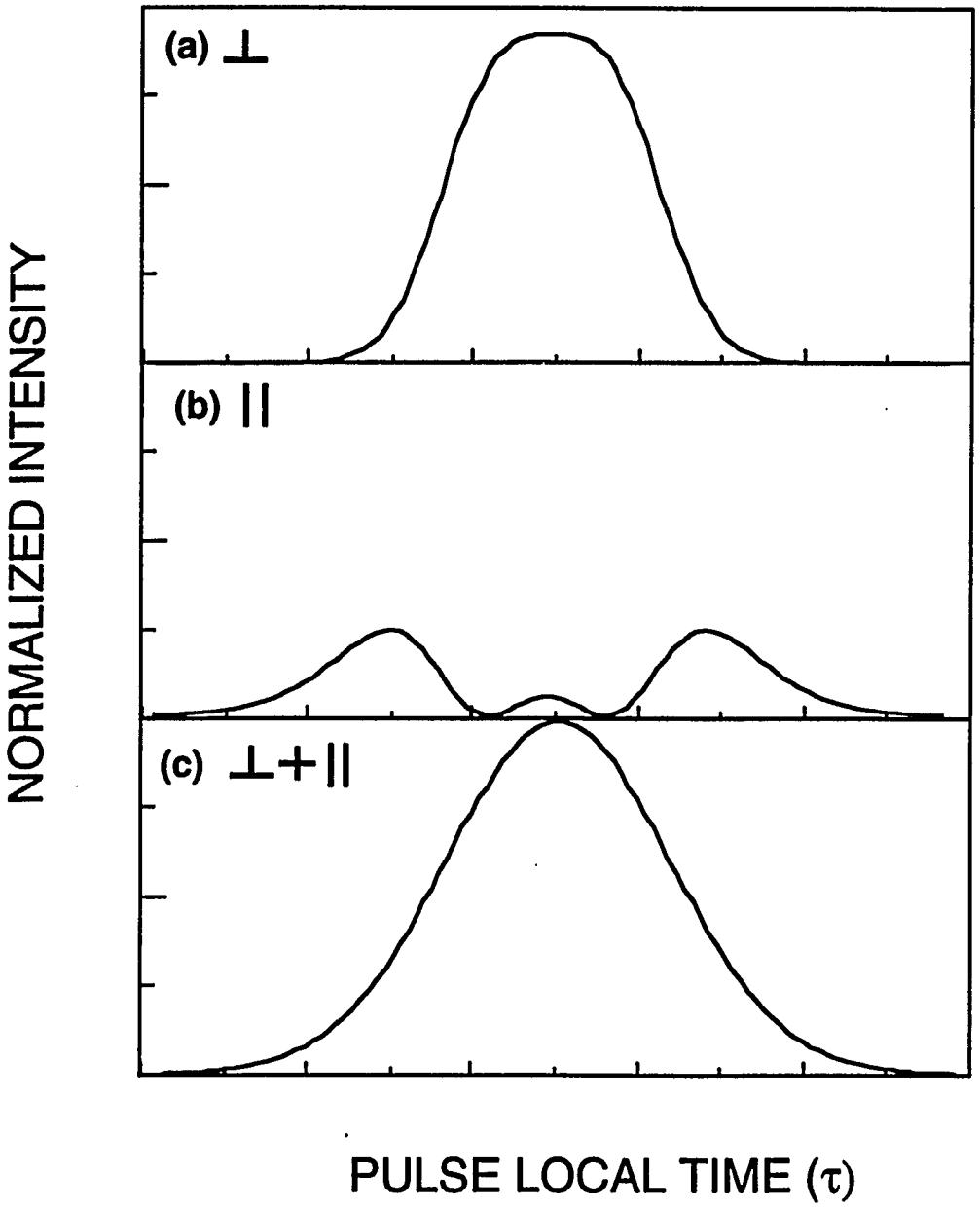

Figure V.11 Simulation of the two polarization components using Gaussian shape pulses for k=1.8, (a), output temporal profile of vertical component; (b), temporal profile of horizontal component; (c), The superposition of vertical and horizontal components of the output laser pulses. This is the total output pulse shape.

References:

[1] S. Trillo, S. Wabnitz, R. H. Stolen, G. Assanto, C. T. Seaton, and G. I. Stegeman, Appl. Phys. Lett.,**49**, 1224 (1986).

[2] S. F. Feldman, D. A. Weinberger, and H. G. Winful, Opt. Lett.,**15**, 311 (1990).

[3] H. G. Winful, Opt. Lett. **11**, 33 (1986).

[4] R. Kashyap, and N. Finlayson, Opt. Lett., **17**, 405 (1992).

[5] E. Lichtman, R. G. Waarts, A. A. Friesem, and S. Tang, Appl. Opt., **28**, 4056 (1989).

[6]. Q. D. Liu, J. T. Chen, Q. Z. Wang, P. P. Ho and, R. R. Alfano, IEEE Phot. Tech. Lett., **7**, 517 (1995).

[7]. Q. D. Liu, J. T. Chen, Q. Z. Wang, P. P. Ho and, R. R. Alfano, Opt. Lett., 20, 542 (1995).

Chapter VI

NONLINEAR VECTOR ROTATION AND DEPOLARIZATION OF FEMTOSECOND LASER PULSES PROPAGATING IN NON-BIREFRINGENT SINGLE-MODE OPTICAL FIBERS

VI. 1 Introduction

Nonlinear effects on the spectral, temporal, and polarization state of high intensity light have been studied intensively[1-11]. Nonlinear polarization rotation was first observed in liquids for high-intensity elliptically polarized light[6]. The change of the polarization state of the output light was attributed to optically induced birefringence. In a solid material, the nonlinear polarization rotation (ellipse rotation) was measured and the results were used to calculate the values of the nonlinear susceptibility of glass[7]. In optical waveguides, nonlinear polarization coupling and instabilities has been demonstrated[8] in a short single-mode liquid-cored birefringent fiber. It has also been found that the nonlinear effect caused the polarization instability[9-11] in birefringent single-mode glass fiber. Recently, the nonlinear depolarization of quasi-linearly (slightly depolarized) polarized picosecond optical pulses propagating in short non-birefringent single-mode optical fibers has been observed[12].

In this chapter, the nonlinear polarization rotation and depolarization is measured for quasi-linearly polarized (slightly depolarized) femtosecond laser pulses propagating in short non-birefringent single-mode optical fibers. The nonlinear polarization rotation and depolarization are attributed to the self-phase modulation (SPM) and cross-phase modulation (XPM) in optical fibers. The experimental results for nonlinear polarization

rotation and depolarization are in good agreement with the estimations using SPM and XPM.

VI. 2 Experimental Setup

The schematic diagram of the experimental setup is shown in Figure VI.1. A Ti:Sapphire laser (Coherent Mira 900-B), operating at the wavelength of 780 nm, was used in the experiment as the light source. The linearly polarized laser pulses had a repetition rate of 76 MHz, duration of 120 fs, and spectral bandwidth of about 4 nm. The mode-locked average output power was 1.5 W. The power fluctuation was less that 3%. The laser pulse train was first launched into an optical isolator (Faraday Rotator) to avoid any reflected light from being fed back to the laser cavity to disturb the mode-locking. Femtosecond laser pulses were coupled into and out of an one-meter long non-birefringent single-mode optical fiber with two 10X micro-objectives. The non-birefringent, single-mode optical fiber (Newport Corp., model: FSV-10) had a core diameter of 4 μm and cladding thickness of 125 μm. The optical fiber was handled very carefully to avoid any environmentally induced birefringence which could couple light into different polarization mode at very low intensity. The output laser pulses from the optical fiber were sent into a beam displacement prism which was mounted on a rotational stage. This prism spatially separated the two perpendicular linearly polarized components while kept them in the same propagating direction.

At different levels of input laser light power, each output light power of the two linearly polarized components at two perpendicular directions was measured with a power meter as shown in Figure VI.1. The output laser pulses from the optical fiber were usually depolarized because of the high light intensity. Rotating the beam displacement prism, the output powers of the two linearly polarized components depended on the direction of the beam displacement prism. The output power of one component was at its maximum while the other was at its minimum when the optical axis of the beam displacement prism was parallel to the main direction of the polarization of the laser

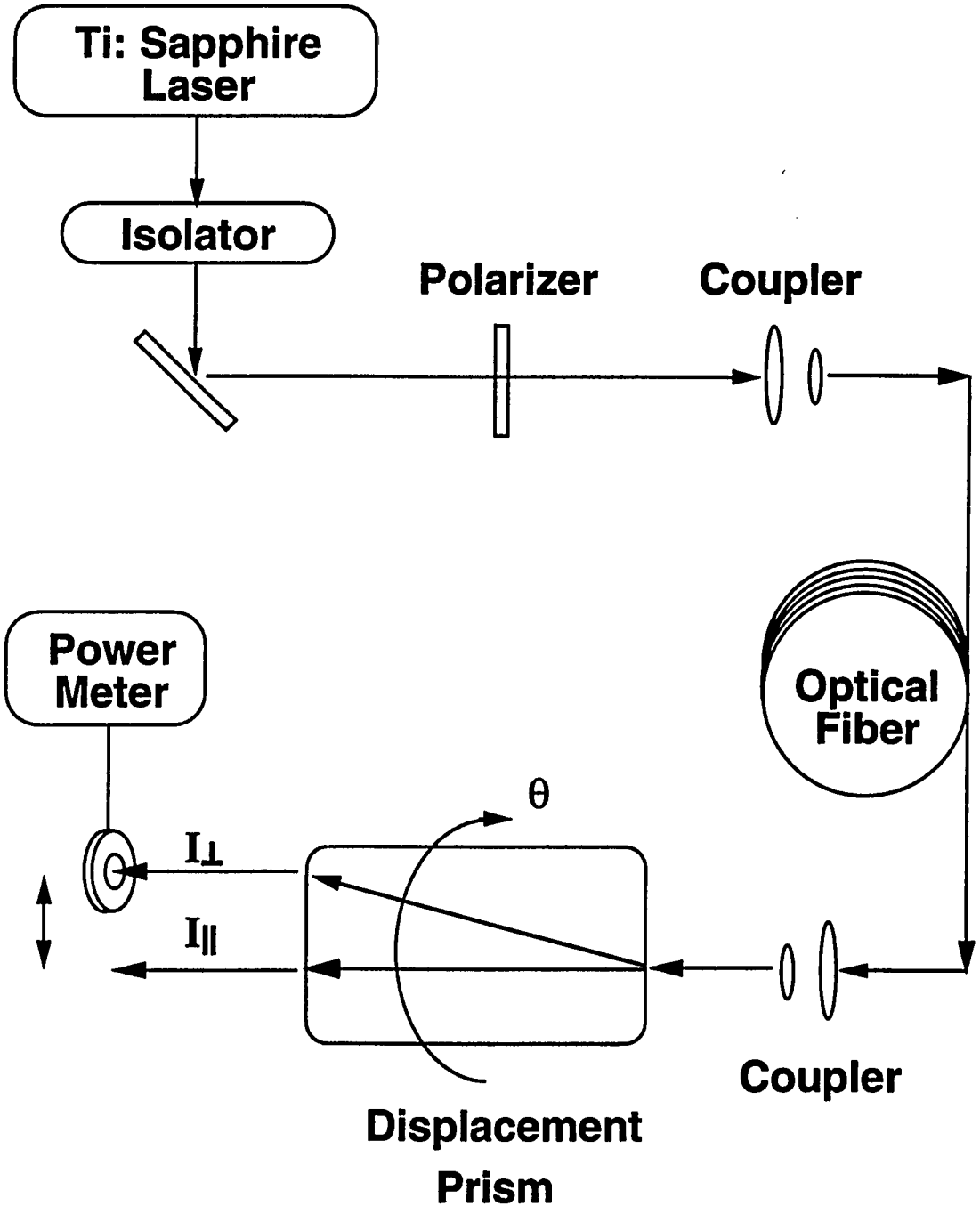

Figure VI.1 The experimental setup for measuring nonlinear polarization rotation and depolarization; the displacement prism was mounted on a rotational stage.

pulses. This main polarization directions of the output laser pulses were measured for different input laser light power. The angle of this main direction of polarization of the output depolarized laser pulses was read out from the rotational stage with an angle resolution of 2°. When the main polarization direction was determined for the input laser light power, the degree of polarization of the output laser pulses was calculated through the power of the two perpendicular linearly polarized components reading from the power meter.

The degree of polarization (ρ) at an angle of θ was calculated using:

$$\rho = (P_{max} - P_{min}) / (P_{max} + P_{min}), \qquad \text{(VI.1)}$$

where P_{max} and P_{min} are the maximum and minimum power of output laser pulses for a given input pulse energy, respectively, and ρ is the degree of polarization. The measured light power is an average power since the output from this Ti:Sapphire laser is pulse train. The input laser pulse energy can be calculated using the measured input power and the pulse repetition rate. The light intensity effects can be investigated through pulse energy which corresponds to laser light intensity.

The input laser pulses were linearly polarized with an extinction ratio better than 10^5 before being coupled into the non-birefringent single-mode fiber. Due to coupling into the fiber, the laser pulses became slightly depolarized. At low pulse energy, the output laser pulses from the optical fiber were linearly polarized along the input polarization. The degree of polarization of output pulses was typically between 0.97 and 0.84. When the pulse energy was slowly increased, the polarization direction of the output pulses rotated and the degree of polarization decreased. Both the polarization

angle and the degree of polarization at this angle were measured as a function of input pulse energy.

VI. 3 Experimental Results

The experimental results are displayed in Figures VI.2 and VI.3 as dot plots for nonlinear polarization rotation and depolarization for two optical fibers, respectively. Fiber 1 and 2 are two non-birefringent single-mode optical fibers of the same type with the same length. Both the polarization rotation angle and the degree of polarization at this rotation angle depend on pulse energy for quasi-linearly polarized input laser pulses. The nonlinear polarization rotation angles were proportional to input pulse energy as shown in Figure VI.2. The degree of polarization was decreased proportionally to input pulse energy as shown in Figure VI.3. Furthermore, the output laser pulses have a nonlinear rotation angle of 30^{o} and a polarization ratio of 0.89 at pulse energy of 3.5 nJ for Fiber 2. At the same pulse energy for Fiber 1, the nonlinear rotation angle is 100^{o} and the polarization ratio is 0.40. These changes in polarization state are not from thermal-effects. This was tested by using continuous wave (CW) laser beam with the same power but without mode-locking from the same laser. The intensity-dependent rotation and depolarization effects disappeared for CW excitation.

It is interesting that the measured results are quite different for the two optical fibers which cut from one and were of the same length. The salient features of the nonlinear polarization rotation and depolarization for optical fibers 1 and 2 can be explained using SPM and XPM and the small depolarization ratio r at the fiber input surface. In fact, they already have been used to explain the nonlinear polarization changes and polarization twisting for picosecond optical pulses propagating in non-birefringent single-mode optical fibers[12,13].

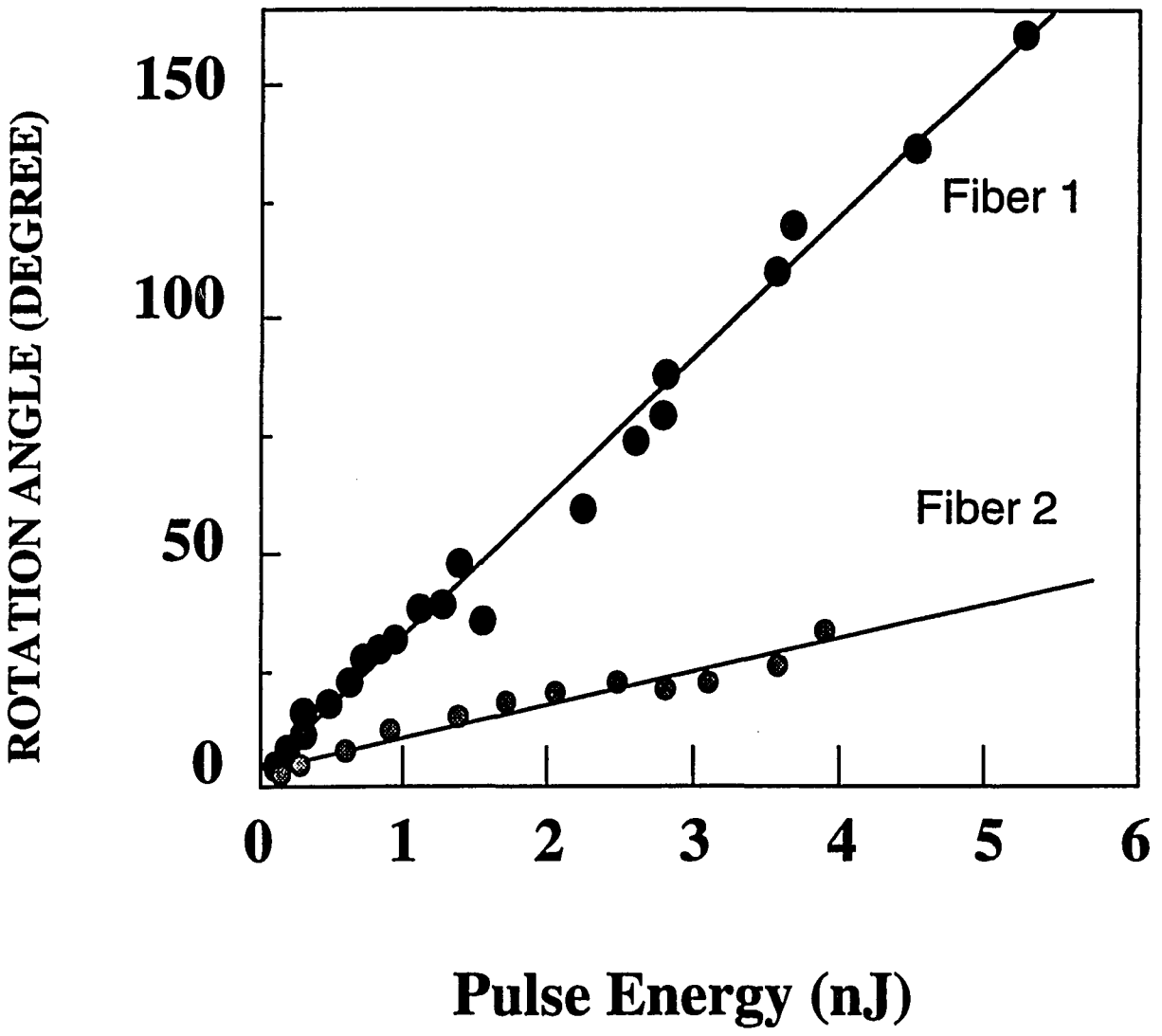

Figure VI.2 The nonlinear polarization rotation for Fibers 1 and 2 as a function of laser pulse energy. Data plot is the experimental results. The solid lines are the least-square fittings.

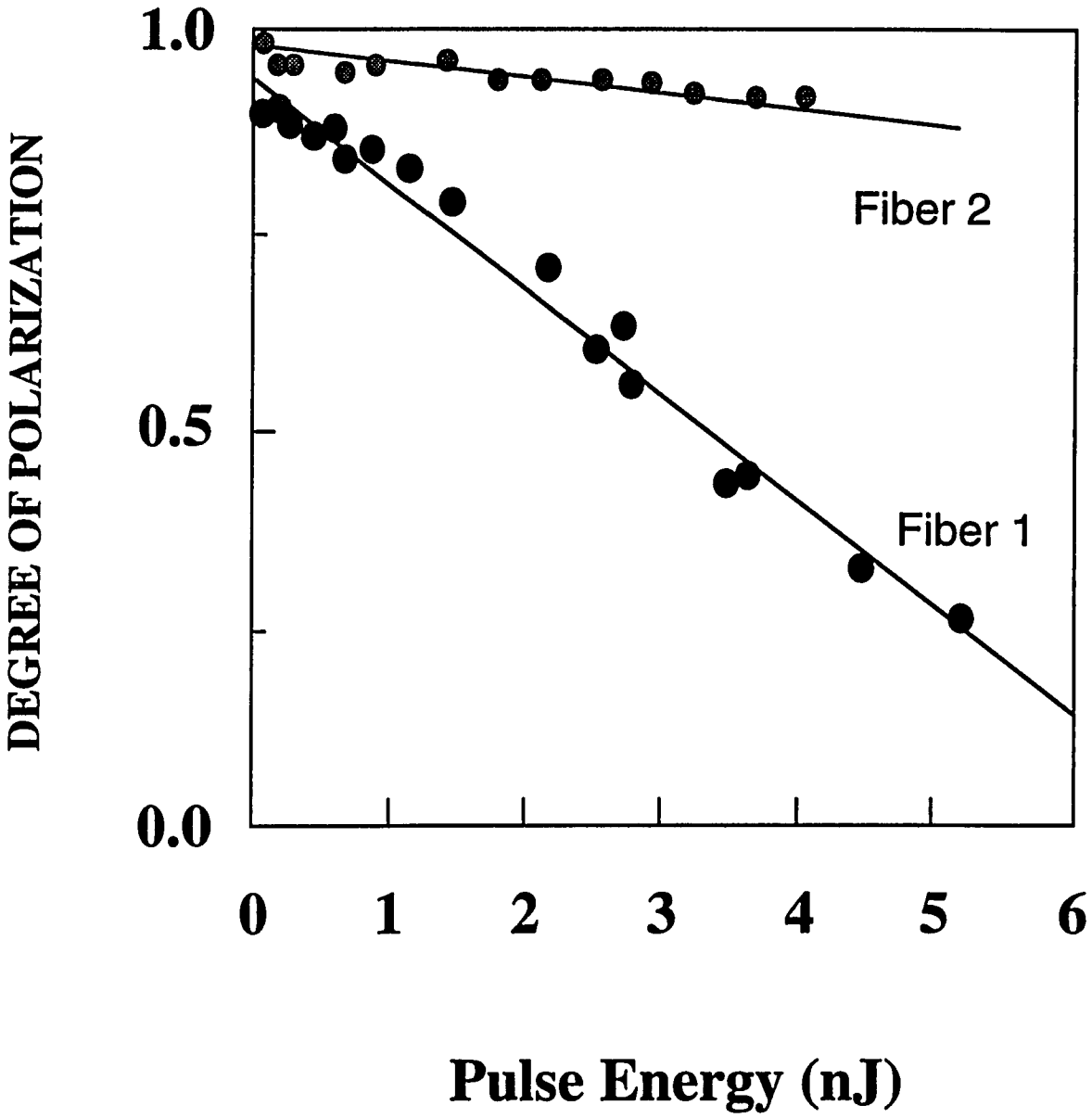

Figure VI.3 The nonlinear depolarization for Fibers 1 and 2 as a function of laser pulse energy. Experimental results are displayed as dots. The solid lines are the least-square fittings.

VI. 4 Discussions

As shown in chapters II, IV, and V, light can be treated as a superposition of two opposite circularly polarized components. From the nonlinear wave equations between two circularly polarized optical waves[12,13], the nonlinear processes are pure phase modulation such as SPM and XPM. There is no energy coupling between these two optical waves which means that the amplitudes of the two optical waves are stable. This is different with the nonlinear processes between two linearly polarized optical waves where the degenerate-four-wave-mixing (DFWM) is important[14]. DFWM will cause the energy transfer in the two optical waves and so the amplitudes are not stable. For a perfect linearly polarized optical pulse, the amplitudes and phase of the two circularly polarized components are equal. These components will remain equal as they propagate down in the fiber and will have exactly same phase modulations (SPM and XPM). Therefore, the two circular components will have the same phase change throughout the propagation. At the output of the fiber the superposition of the two circularly polarized components will give exactly the same polarization state as that at the input. This perfect linear polarization would not intensity-dependently rotate and depolarize.

Under the real experimental conditions, the linear polarization of the input laser pulses is not perfect. This was also discussed in chapter IV and V. Many surfaces of optical devices such as mirror, lens, and filters will affect the polarization state of input optical pulses. The most important is the coupling surface of the optical fiber which had an irregular shape after the fiber cut. The linearly polarized incident light is scattered between the two perpendicular linearly polarized modes. As a result, the incident light is slightly depolarized. This effect is true because there always was a small background in the perpendicular polarizing mode at very low input energy in which the nonlinear effects was absent. As displayed in Figure VI.3, the linearly polarized laser pulses became

slightly depolarized with an extinction ratio between 50 (ρ=0.96) and 13 (ρ=0.85) at low pulse energy after the Fibers 1 and 2, respectively. In this case, the magnitudes of its two circularly polarized components become unequal. Their amplitudes are still stable but the amount of SPM and XPM are not equal. From this effect, there will be a phase shift between the two circularly polarized components after the optical pulse propagated through an optical fiber[12]. This nonlinear phase shift will cause the polarization direction of output optical pulse to rotate.

The superposition of two circularly polarized components with nearly equal amplitudes is always a quasi-linearly polarized state no matter what the phase difference is. For a phase difference $\Delta\alpha$, the linear polarization will rotate with an angle of $\Delta\alpha/2$ which can be expressed as[12]

$$\Delta\alpha / 2 \propto n_2 I\sqrt{r}, \qquad \text{(VI.2)}$$

where n_2 is the nonlinear refractive index, I is the input pulse intensity, and $r \equiv I_{\perp} / I_{\parallel}$ is the depolarization ratio of the input laser pulse at very low intensity for a given fiber. The phase difference is proportional to the pulse intensity[12]. This can explain the nonlinear polarization rotation. The nonlinear depolarization is attributed to the pulse shape; that is, within the pulse envelope, the different intensity in different local time. The linear polarization direction will change at different local time to develop polarization twisted pulses[13] as depicted in Figure VI.4. Figure VI.4(a) displays a linearly polarized (in x-t plane) laser pulse coupled into the optical fiber. After propagating in the fiber, this laser pulse becomes temporally broadened. The polarization direction of the central region of the pulse first rotates as shown in Figure VI.4(b). In Figure VI.4(c), the central region of the pulse completely rotates at the perpendicular direction (y-t plane) of the initial polarization when the pulse propagates further in the

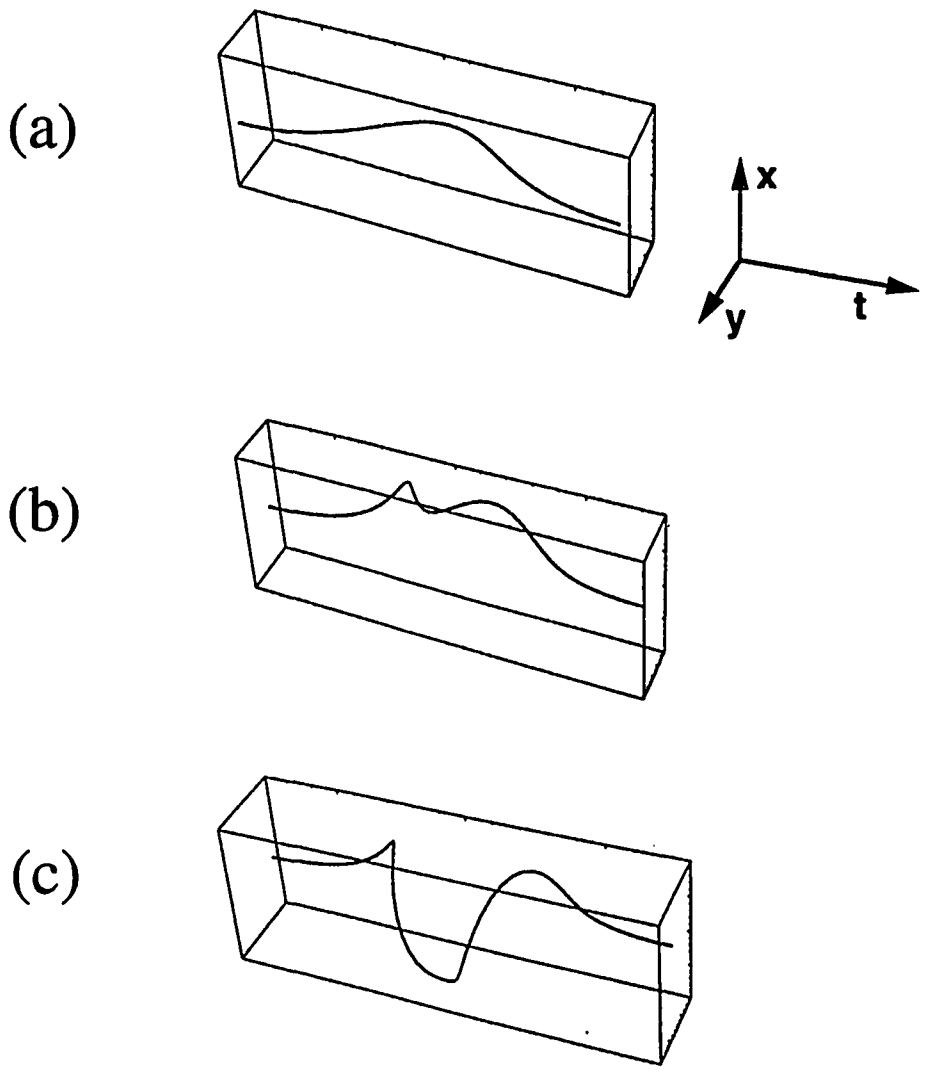

Figure VI.4 The three dimensional schematic diagram of the nonlinear polarization rotation. (a), input linearly polarized (in x-t plane) laser pulse; (b), the polarization direction of the central part of the pulse first shows polarization rotation after propagating a distance inside the fiber; (c), the polarization rotates to the perpendicular direction when the pulse propagates further in the fiber. The polarization rotation depends on the instant intensity in the pulse profile. Although the pulse remain linearly polarized everywhere, the overall effect is a depolarization.

fiber. Although this pulse remains linearly polarized in propagation, the polarization at different time is at different direction. The observed optical pulse is overall depolarized. The measured polarization rotation is an overall effect of the rotation within the laser pulse profile. The solid lines in Figures VI.2 and VI.3 are the linear fitting of the experimental results to the input pulse energies using least-square method. These fits are in good agreement with the experimental results.

The nonlinear vector rotation and depolarization are quite different for the same kinds of Fibers 1 and 2. The rotation in Fiber 1 is about three times larger than that of Fiber 2 as shown in Figure VI.2. The degree of polarization of Fiber 1 is much lower than that of Fiber 2 as shown in Figure VI.3. This observation arises from the small but different depolarizing ratio at very low pulse energy. The depolarizing ratio r which is 0.02 (degree of polarization 0.96) of Fiber 2 at low pulse energy is much smaller than that of Fiber 1 which is 0.081 (degree of polarization 0.85) as shown in Fig. 3. The difference of the amplitudes of the two circularly polarized components for the laser pulses for Fiber 2 is smaller than that for Fiber 1. The smaller amplitude difference will introduce a smaller nonlinear phase shift at the same pulse energy. This means there will be a larger vector rotation and a lower degree of polarization for Fiber 1 than those for Fiber 2. According to Eq. (VI.2) and r, the nonlinear polarization rotation angle is about twice as larger for Fiber 1 than that for Fiber 2. This estimation is near the measurement result which is about 3 times larger as shown in Figure VI. 2.

In conclusion, the nonlinear vector rotation and depolarization have been measured for femtosecond laser pulses propagating in non-birefringent single-mode optical fibers. The change of the small depolarization ratio at the fiber surface can lead to different effects. Significant rotation angles (up to 150°) have been measured for weak input laser pulses with pulse energy as small as 5 nJ. This experiment demonstrates that a

small linear depolarization ratio at low pulse energy is important to the rotating and depolarizing processes of the quasi-linearly polarized optical pulses propagating in single-mode non-birefringent optical fibers.

Reference:

[1] B. Crosignani, B. Daino, P. D. Porto, J. Opt. Am. B, **3**, 1120 (1986).

[2] B. Crosignani, P. D Porto, Opt. Acta, **32**, 1251 (1985).

[3] C. Y. Menyuk, and P. K. A. Wai, J. Opt. Am. B, **11**, 1035 (1994).

[4] H. G. Winful, Appl. Phys. Lett. **47**, 213 (1985).

[5] H. G. Winful, Opt. Lett. **11**, 33 (1986).

[6] P. D. Maker, R. W. Terhune, and C. M. Savage, Phys. Rev. Lett. **12**, 507 (1964).

[7] A. Owyoung, R. W. Hellwarth, and N. George, Phys. Rev. B, **5**, 628 (1972).

[8] R. Kashyap, and N. Finlayson, Opt. Lett. **17**, 405 (1992).

[9] S. Trillo, S. Wabnitz, R. H. Stolen, G. Assanto, C. T. Seaton, and G. I. Stegeman, Appl. Phys. Lett. **49**, 1224 (1986).

[10] S. F. Feldman, D. A. Weinberger, and H. G. Winful, Opt. Lett. **15**, 311 (1990).

[11] E. Lichtman, R. G. Waarts, A. A. Friesem, and S. Tang, Appl. Opt. **28**, 4056, (1989).

[12] Q. D. Liu, J. T. Chen, Q. Z. Wang, P. P. Ho, and R. R. Alfano, IEEE Phot. Tech. Lett., **7**, 517 (1995).

[13] Q. D. Liu, W. L. Sha, P. P. Ho, and R. R. Alfano, " Nonlinear polarization twisting of picosecond laser pulses propagating in nonbirefringent single-mode optical fibers," to be published in JOSA B.

[14] Q. D. Liu, J. T. Chen, Q. Z. Wang, P. P. Ho, and R. R. Alfano, Opt. Lett., **20**, 542 (1995).

Chapter VII

PICOSECOND AND FEMTOSECOND LASER PULSES DEGENERATE-CROSS-PHASE MODULATION (DXPM) IN OPTICAL FIBERS

VII.1 Introduction

When a number of ultrashort laser pulses propagate in a nonlinear medium, an intensity-dependent index is induced in the material[1]. This refractive index change imposes a phase modulation that causes spectral broadening of the propagating pulses[2-7]. When the phase modulation happens to the laser pulse itself, the process is called self-phase-modulation (SPM)[2]. When the phase modulation occurs in the co-propagating pulses, the process is called cross-phase-modulation (XPM)[8-11]. The theoretical understanding and potential applications of SPM and XPM using optical fibers have stimulated great interest among many researchers. For example, the spectral broadening due to SPM and XPM processes in optical fibers has been used in pulse compression to produce ultrashort laser pulses[12]. XPM processes have already been observed using two optical pulses having the same polarization with different wavelengths[10-11] or having the same wavelength but different polarization states[13]. The latter process is called degenerate-cross-phase-modulation (DXPM).

XPM processes have been conventionally observed using two separated laser light pulses propagating in optical fibers. Theoretically, XPM could occur between any light pulse having different wavelengths or different polarization states. One can transfer light wavelength from one spectral region to another. This tuning range can be from UV to IR, maybe even extend to X-ray region. For a single optical pulse, DXPM process should occur between the light at different polarization modes of an optical pulse. When these

polarization modes are not stable, meaning that the polarization modes will transfer energy from each other during the light propagation. At the output optical signal, the spectra of the light at different polarization mode will mix up. In this case, there is no well defined DXPM process recognized from the output spectra of the light at different polarization states. However, when the polarization modes are stable, they will not exchange energy. The light of each polarization component remains at the initial input polarization state without change during the light propagation. The DXPM process should be observable from the spectra of the light with different polarization modes. Therefore, the polarization stability of light propagating in an optical fiber is an important criterion for the observation of the single pulse DXPM, especially for an intense light pulse.

To describe the polarization state of light propagation in optical fibers, either two perpendicularly linearly polarized unit vectors or two opposite rotating circularly polarized unit vectors (right-handed and left-handed) can be used as the polarization eigenmodes[14]. The polarization state of a single optical pulse can be described by the superposition of two orthogonal polarization components. The amplitudes and phases of the components depend on the different types of eigenmodes. For example, an elliptically polarized light with eccentricity ~0(almost circularly polarized) can be treated as two linearly polarized states with a phase difference of $\pi/2$ and almost the same amplitudes, or it can be equivalently expressed as two circular components with zero phase difference with a large disparity of amplitudes. In principal, the two polarization components of a pulse can act as two laser pulses with phase and amplitude differences[15]. The DXPM process between two polarization components in a single laser pulse should occur and be observable if the two polarization states are stable in optical fibers.

Our experimental investigations of the polarization stability of intense laser light pulses in chapter IV suggest that the circular polarization mode in a non-birefringent single-mode optical fiber is stable. It has been found that the circular polarization state of a laser pulse was insensitive to its intensity, whereas a linearly polarized laser pulse was dramatically depolarized at higher laser intensity[16]. Therefore, circularly polarized laser pulses should be used if maintaining the polarization states is desirable. This criterion is true for polarization sensitive processes such as DXPM, XPM, SPM and SRS. For a single light pulse propagating in a nonbirefringent single-mode optical fiber, the DXPM process for the two circularly polarized components should be detectable. For the same reason, since two linear polarization modes are the stable polarization states of light in a birefringent single-mode optical fiber, the DXPM process is active for the two linearly polarized components of single light pulses and should also be detectable.

In this chapter, degenerate-cross-phase modulation (DXPM) has been observed for a single picosecond and femtosecond laser light pulses propagating through short single-mode optical fibers, respectively. Birefringent and non-birefringent single-mode optical fibers were used in the experiments for observing the spectra of the two linearly and circularly polarized components, respectively. The spectral broadening of the two output polarization components of a single laser light pulse was attributed to self-phase modulation (SPM) and degenerate-cross-phase modulation (DXPM) processes under different polarization bases for the single-mode optical fibers with different birefringence. The DXPM of two circularly polarized laser light pulses with different optical delay and pulse energy has also been observed in a nonbirefringent single-mode optical fiber. In a multi-mode optical fiber, the DXPM between different fiber modes has been investigated for different laser light pulse energy. Theoretical simulations for the DXPM of picosecond and femtosecond laser light pulses has made for various experimental configurations. The calculated results are in good agreement with the measured results.

VII.2 DXPM of single picosecond light pulse in a nonbirefringent single-mode optical fiber

VII.2.1 Experimental Method

The experimental arrangement of the single-pulse DXPM is shown in Figure VII.1. A 30 ps laser pulse at 532 nm from a Nd: YAG laser was used. The single-mode, non-birefringent optical fiber(Newport Corp. FSA-10 model) has a core diameter of 2.5 μm and cladding thickness of 125 μm. After the polarizer P, the laser pulse was linearly polarized to a ratio better than 400 to 1. Then, the elliptically polarized laser pulse was obtained by adjusting the relative angle of the optic axes between the quarter wave plate QWP1 and the polarizer P. When this angle was 45°, a circularly polarized laser pulse was produced. The intensities of the two circular polarization components of the single elliptical laser pulse were set with a ratio of 100 to 1. The intense component acted as a pump pulse while the weak one acted as a probe pulse.

The elliptically polarized laser pulse was coupled into and out of a 1-meter single-mode, non-birefringent optical fiber with 5X microscope objectives. Two circularly polarized components co-propagated through the optical fiber and each one remained in its own polarization state without any exchange of energy. After the second quarter wave plate QWP2, these two components were converted into two perpendicular linearly polarized ones. Finally, a polarizing prism BDP was used to separate the two linear polarization components. They were separated while propagating in the same direction. The spectral analysis system with a resolution of 0.02 nm was a 1-meter spectrometer coupled to a CCD camera. In the experiment, the two laser pulse components were sent into the spectrometer at different positions of the slit where the spectra of two

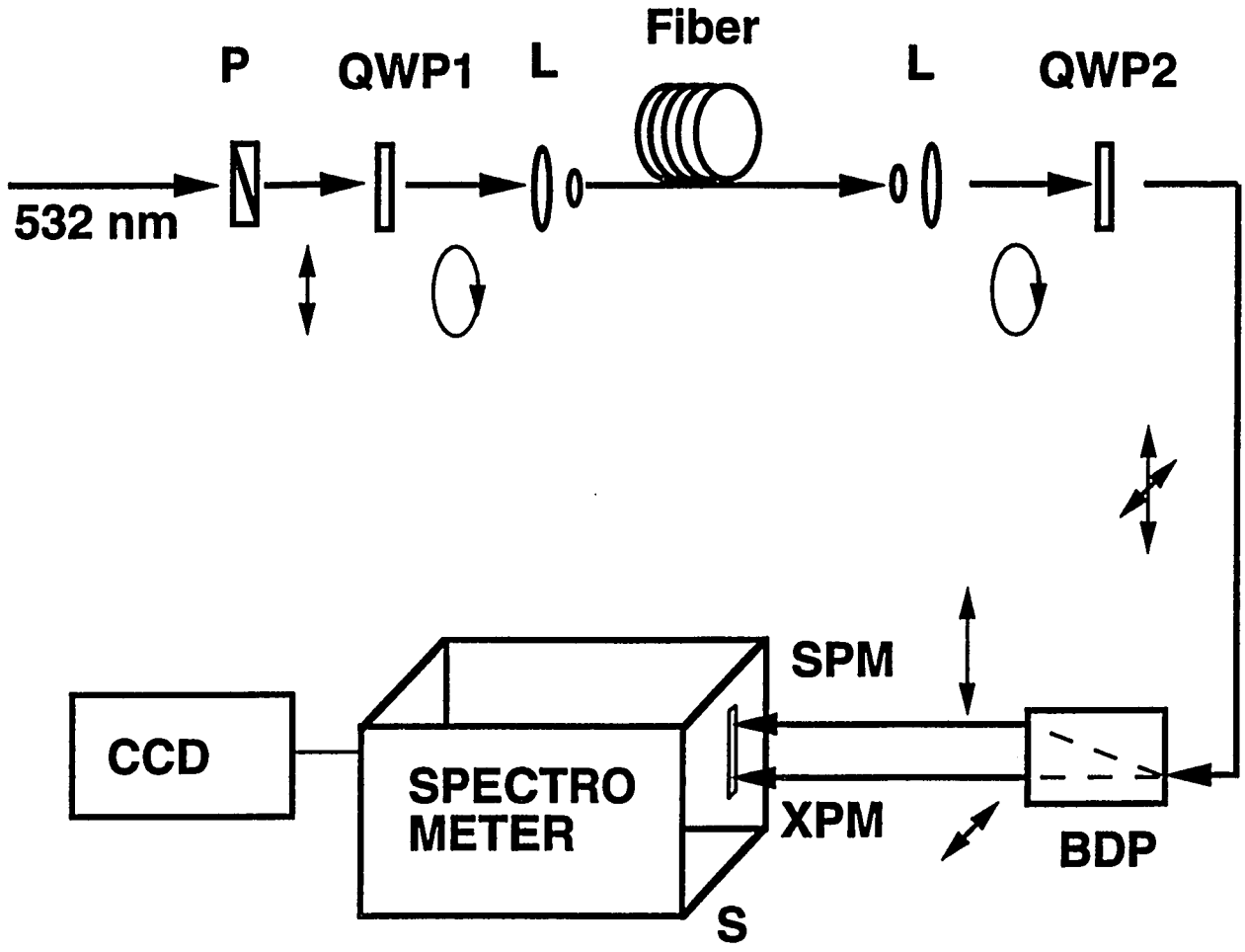

Figure VII.1 Experimental set-up: P is polarizer, QWP's are quarter wave plates, L's are microscope objective lens, BDP is a beam displacing prism, S is slit of spectrometer.

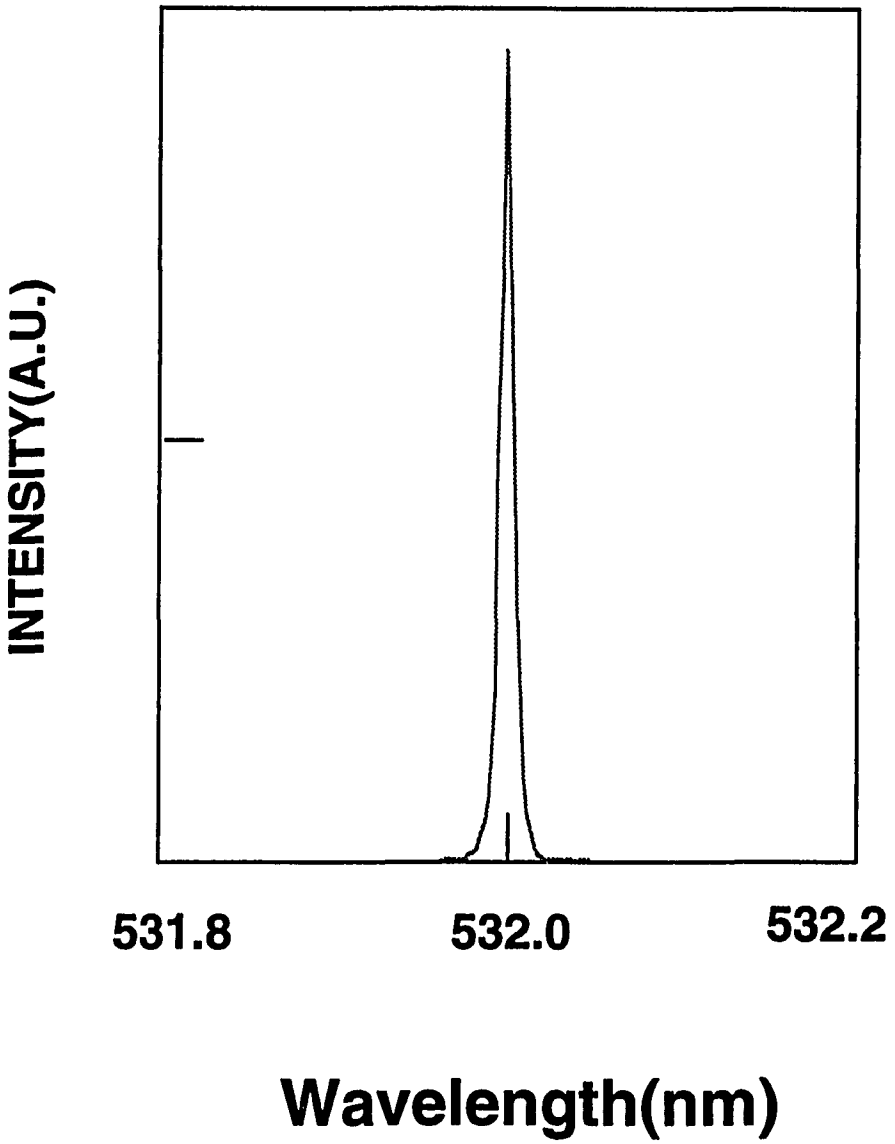

Figure VII.2 The normalized input laser light spectrum from a Nd: YAG laser system with a bandwidth (FWHM) of less than 0.03 nm.

perpendicularly polarized components can be measured simultaneously. The detection area of the CCD camera was large enough to record the spectra of the two components of the output laser pulse at the same time. The input laser light spectrum with a full-width-half-maximum (FWHM) bandwidth less than 0.03 nm is shown in Figure VII.2.

VII.2.2 Results

The spectra of the two output circularly polarized components of a single 35 ps laser light pulse at the wavelength of 532 nm were measured for different coupled pulse energies. Figure VII.3 shows the normalized spectra at an input pulse energy of 30 nJ. Figure VII.3(a) is the output spectrum of the pump component while Figure VII.3(b) is the spectrum of the probe. The spectrum of the pump is attributed to the typical SPM process. Its total width is narrower than that of the probe. Because of a much lower intensity, the spectrum of the probe will not show significant broadening from its own SPM process. The spectral broadening of the probe component was attributed to the XPM process produced by the pump and the interference between the probe and the pump.

VII.2.3 Explanation and Discussion

The difference of the observed spectral broadening in the two polarization components of a single elliptical laser pulse can be explained with SPM and XPM theory. The total electric field of an elliptically polarized laser pulse can be written as:

$$\vec{E} = \vec{E_R} + \vec{E_L} = \frac{1}{2}\{\vec{e}_R A_{R(r,z,t)} e^{i(\omega t - kz)} + \vec{e}_L A_{L(r,z,t)} e^{i(\omega t - kz)}\} + c.c. \qquad \text{(VII.1)}$$

where $\vec{e}_R = (\vec{e}_x - i\vec{e}_y)/\sqrt{2}$ and $\vec{e}_L = (\vec{e}_x + i\vec{e}_y)/\sqrt{2}$ are the right-handed and left-handed unit vectors, respectively. $\vec{E}_{R(L)}$ and $A_{R(L)}$ are the electrical fields and

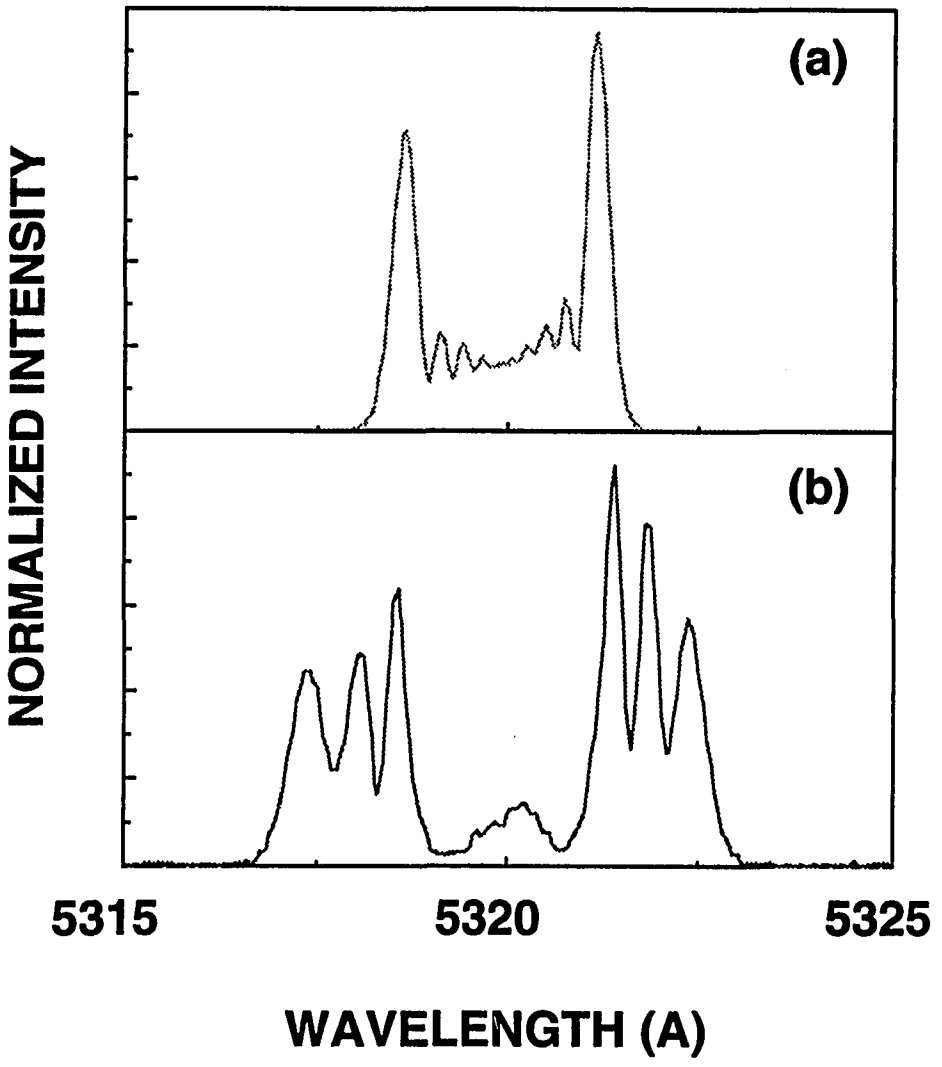

Figure VII.3 The measured spectra of single 30 nJ elliptically polarized laser pulses with a duration of 30 ps propagating in a 1-meter non-birefringent single-mode optical fiber. The intensity ratio of the pump component to the probe was 100 to 1. (a) and (b) correspond to the spectra of pump and probe components, respectively.

amplitudes of right-handed (left-handed) circular components. Applying the slowly varying envelope approximation in Maxwell's equations, the nonlinear wave equations describing light propagation in the optical fibers are:

$$\frac{\partial A_R}{\partial z}+\frac{1}{v_{gR}}\frac{\partial A_R}{\partial t}+\frac{i}{2}k_R^{(2)}\frac{\partial^2 A_R}{\partial t^2}=i\frac{\omega n_2}{c}\left(\frac{2}{3}|A_R|^2+\frac{4}{3}|A_L|^2\right)A_R, \qquad \text{(VII.2a)}$$

$$\frac{\partial A_L}{\partial z}+\frac{1}{v_{gL}}\frac{\partial A_L}{\partial t}+\frac{i}{2}k_L^{(2)}\frac{\partial^2 A_L}{\partial t^2}=i\frac{\omega n_2}{c}\left(\frac{2}{3}|A_L|^2+\frac{4}{3}|A_R|^2\right)A_L \qquad \text{(VII.2b)}$$

where v_{gR} , and v_{gL} are the group velocity for right-handed and left-handed components, respectively; $k^{(2)}$'s are the group- velocity dispersion(GVD), and $n_2=3\chi^{(3)}/8n$ is the nonlinear refractive index of the optical fiber. Because the optical fiber was not optically active, right-handed and left-handed components have the same group velocity i.e. $v_{gR} = v_{gL}$.

Degenerate-four-wave-mixing terms do not exist in the nonlinear coupling equations of the right- and left-handed circularly polarized optical pulses as shown in Eqs.(VII.2). Here, two circular eigenmodes were chosen to describe the polarization state of light and the spectra of the circular polarization components were measured. Third order nonlinear processes affect the phase of the laser pulses and does not cause amplitude or energy exchange between the two orthogonal circular polarization states. This result is in agreement with the investigation of Sylla *et al* [17] for cubic crystal displaying optical activity.

The theoretical simulation was calculated using Eqs.(VII.2). To compare the theoretical calculation with the experimental results, the pump intensity was adjusted to the level where the pump to probe ratio was 100 to 1. Figure VII.4(a) and 4(b) show the

calculated spectra of the pump and probe components at laser pulse energy of 30 nJ. The spectral broadening of the probe is caused by the XPM process of the two components. The SPM process of the pump dominates its own spectrum. There is good agreement between the experimental results and theoretical calculation for the spectrum of the pump component, as shown in Figure VII.3(a) and 4(a). The slight difference is attributed to the limited resolution of our spectral measurement system. The calculated probe spectrum in Figure VII.4(b) show a broader spectrum similar to the measured spectrum displayed in Figure VII.3(b). The theoretical profile qualitatively reproduces the probe spectrum off the central region, but fails to fit the spectrum in the central region. The difference in the middle spectral region is believed to arise from the interference between the probe component and a small pump component that has leaked into the probe polarization direction. Assuming that 0.5 percent of the pump component is coupled into the probe's polarization direction, the calculated spectral profile shown in Figure VII.4(c) appears more like the experimental profile. For an ideal condition, the polarizing prism would completely separate the two polarization components, and no interference should occur. Experimentally, any small misalignment of the polarizing prism or the light scattering from a defect, or a twist in the optical fiber will leak some portion of the pump component into the probe component. The leakage of the pump field will interfere with the probe field and affect the observed probe spectrum. In Figure VII.4(c), the probe spectral distribution considering 0.5% leakage from the pump into probe's polarization direction is in good agreement with the experimental result displayed in Figure VII.3(b).

The DXPM of two orthogonal polarization components has been measured for a single ultrashort optical pulse propagating in a 1-meter non-birefringent single-mode optical fiber. The interference between SPM and DXPM was observed in the probe spectrum. The experimental results are in a good agreement with the theory. For a single

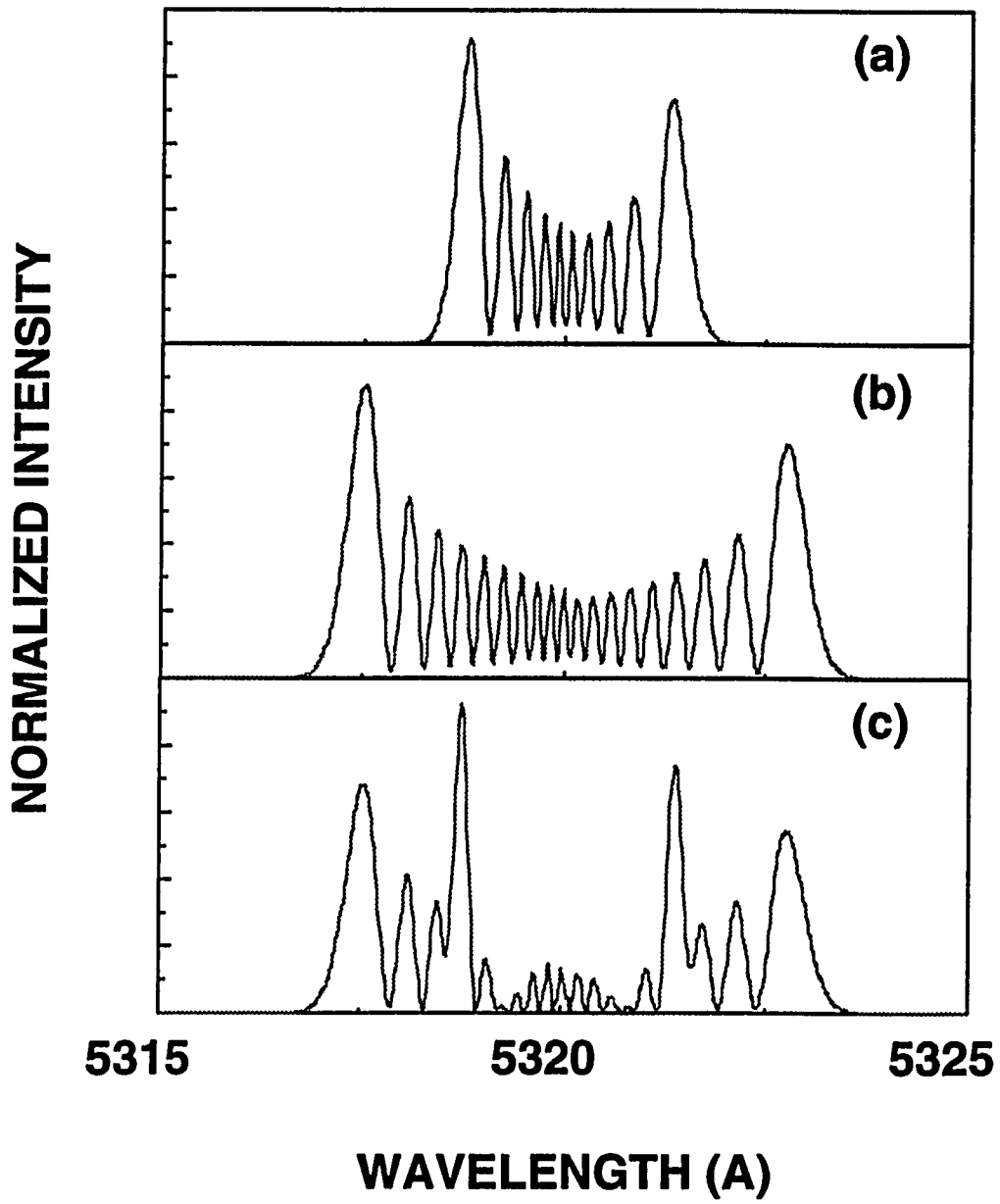

Figure VII.4 The theoretical calculation of SPM and DXPM spectra for a single elliptically polarized laser pulse at the same pulse energy of 30 nJ, n_2=1.3 X 10^{-16} cm^2/w, the fiber length is 1 m, fiber core diameter is 4.0 mm. The intensity ratio of pump to probe is 100 to 1. (a) and (b) are the spectra of pump and probe, respectively. (c) is the spectrum considering interference between the probe and a small portion (0.5%) of the pump.

pulse propagating in optical fibers, self-phase-modulation is not the only source for spectral broadening, degenerate-cross-phase-modulation should also be considered.

VII.3 DXPM of femtosecond laser pulses in a birefringent single-mode optical fiber

VII.3.1 Introduction

Degenerate cross-phase modulation (DXPM) using circularly polarized light pulses has been observed in a non-birefringent single-mode optical fiber which maintained the circular polarization states. In a birefringent single-mode optical fiber, linear polarization states are stable. Therefore, the DXPM process for linearly polarized laser light pulses in the birefringent single-mode optical fiber should be detectable. This experiment is going to report a new observation of DXPM using linearly polarized femtosecond light pulses propagating in a birefringent single-mode fiber.

VII.3.1 Experimental setup

The schematic diagram of the experiment is shown in Figure VII.5. A Titanium: Sapphire laser (Model: Coherent Mira 900-B), operating at the wavelength of 780 nm, was used in the measurement. The laser light pulse train which had a repetition rate of 76 MHz was generated with a pulse duration of 120 fs and spectral bandwidth of about 5 nm. The average output light power of this laser is 1.4 W, corresponding to the laser light pulse energy of 18 nJ. The power fluctuation of this laser is less than 2%. The output laser light pulse train was first launched past an optical isolator (Faraday Rotator) to avoid the reflecting light from the surface of the following optical components back to laser cavity to disturb the mode-locking. The duration of laser pulses was 230 fs after the optical isolator because of group-velocity dispersion. The spectrum of input laser pulse had a bandwidth of 5 nm as shown in the insert of Figure VII.6.

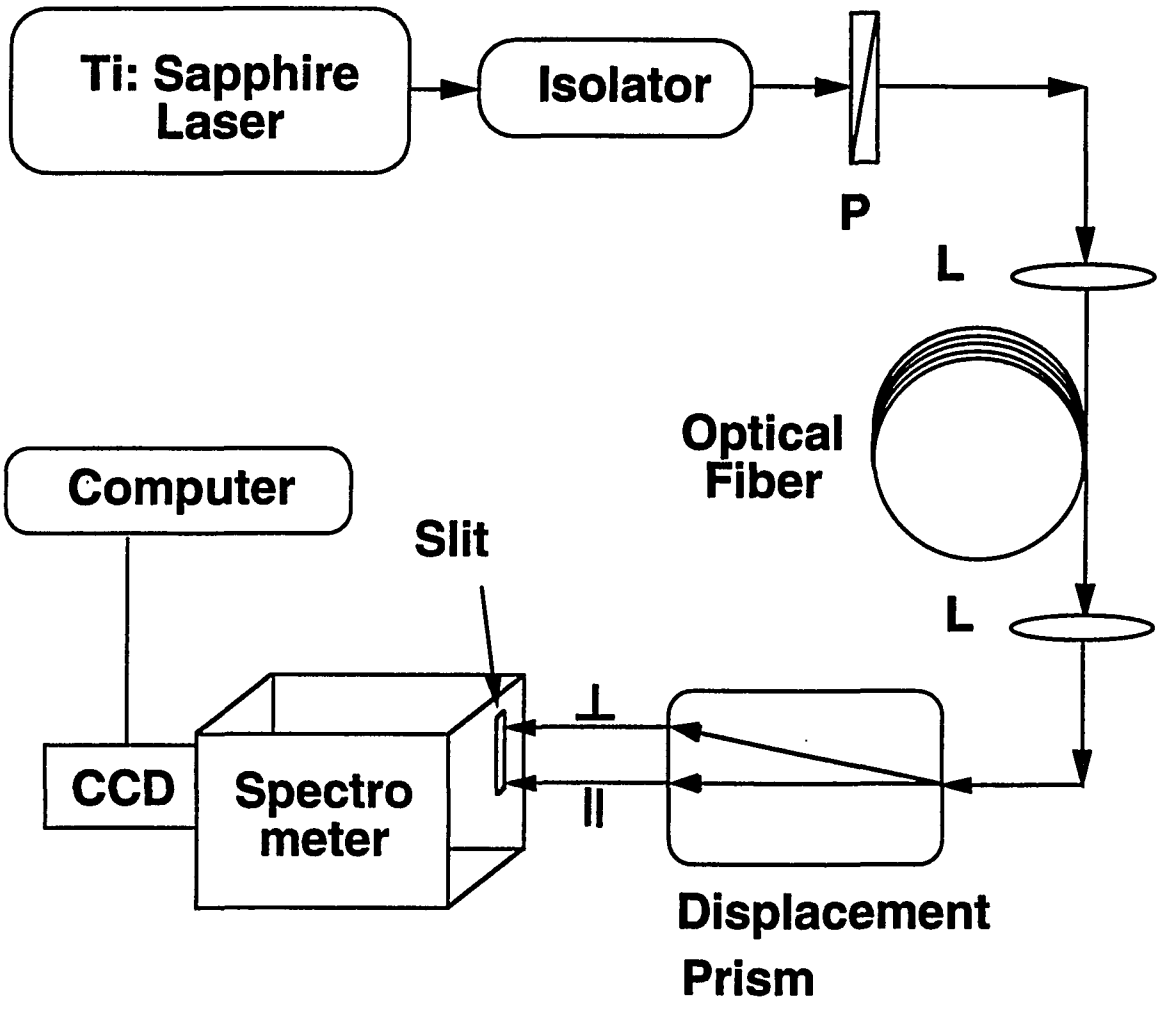

Figure VII.5 Experimental set-up: P is a polarizer, L's are microscope objective lens, a polarizing displacement prism is used to separate two linearly polarized components; the spectral analysis system has a resolution of 1.5 nm with a dispersion of 0.24 nm/pixel.

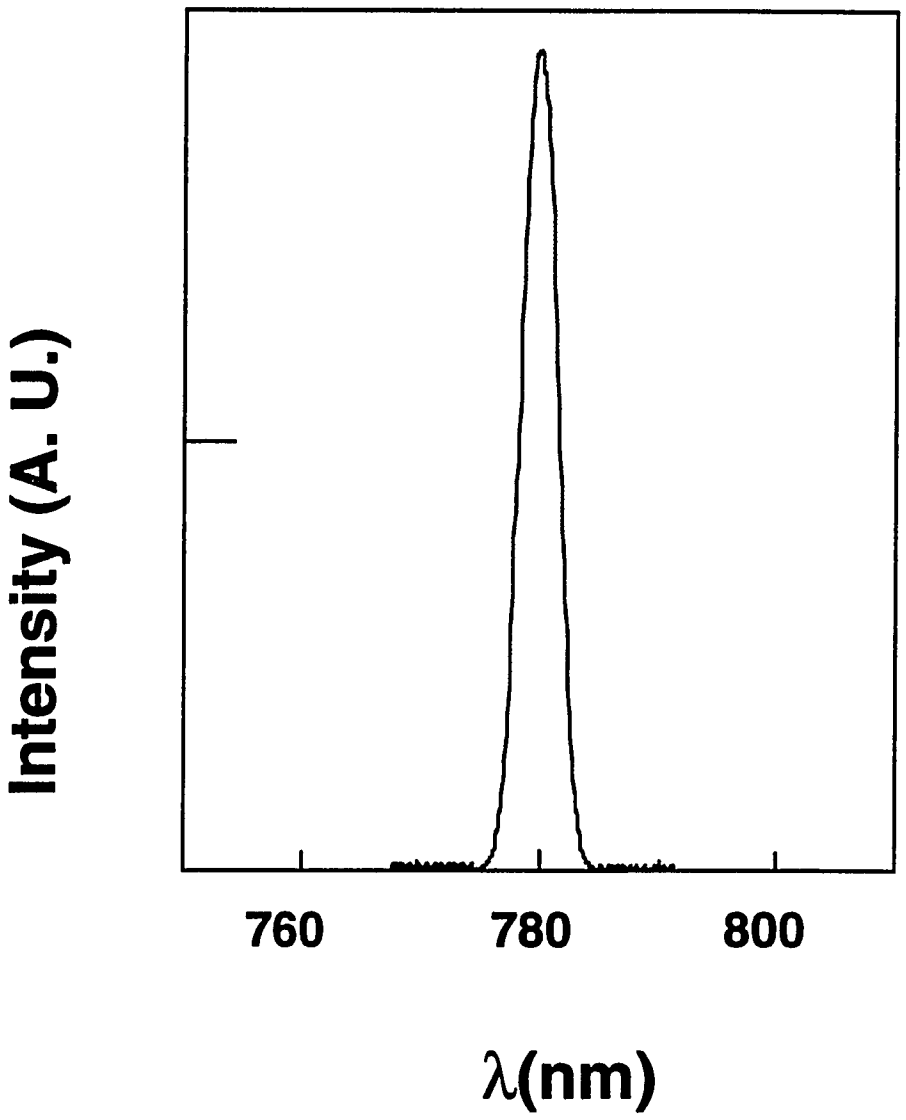

Figure VII.6 The normalized incident laser light spectrum from a Ti:sapphire laser system with a FWHM bandwidth of 5 nm.

A calcite crystal polarizer was used to make the laser beam linearly polarized with a ratio better than 10^5. The 230 femtosecond laser pulses were then coupled into and out of an one-meter-length birefringent single-mode optical fiber with two 10X micro-objective lens. The birefringent (polarization-preserving) single-mode optical fiber (Newport Corp. FSPV-10 model) had a core diameter of 2.6 μm and a cladding thickness of 125 μm. The output laser pulses from the optical fibers passed a polarizing displacement prism. The polarizing displacement prism spatially separated the two perpendicularly linearly polarized components. The spectra of the two linearly polarized components were measured with a spectral analysis system. The spectral measuring system consisted of a spectrometer and a computer controlled charge-coupled-device (CCD) camera. Both polarization components were measured simultaneously by placing the images of beams at different position of slit as shown in Figure VII.5. The images were localized on different positions of CCD camera for wavelength display. The resolution of this system is 1.5 nm with a dispersion of 0.24 nm per pixel.

A polarization-preserving (birefringent) single-mode optical fiber was used in the experiment. Linearly polarized laser pulses were first coupled along one of the optical axis of the optical fiber. The output laser pulses at the fiber exit were preserved to be linearly polarized. The polarizing displacement prism was aligned parallel to the output linear polarization. Hence, there was only one linearly polarized component after the polarizing displacement prism. By rotating the optical fiber with a small angle (6^o), laser light was also coupled into the perpendicularly linearly polarized mode. The intensities of the two linearly polarized components were adjusted to the ratio of 20. The intense component ($\parallel$) is considered as the pump light, and the weak one ($\perp$) is the probe light. DXPM is recognized by the spectral broadening of the weak probe component.

VII.3.2 Results

The spectra of the two linearly polarized components of femtosecond laser pulses propagating through a birefringent single-mode optical fiber were observed at different input laser light pulse energies (intensities). The measured results of the spectra of the two linearly polarized components for a single pulse are shown in Figure VII.7 for input laser light pulse energies of 0.5 nJ, 1.8 nJ, and 3.9 nJ. The right and left columns of Figure VII.7 are the normalized spectra of the pump (parallel) and probe (perpendicular) components, respectively. The spectra of pump component in Figure VII.7($a_{\|}$), ($b_{\|}$), and ($c_{\|}$) were broadened symmetrically with bandwidths of 10 nm, 25 nm, and 45 nm at the central wavelength 780 nm, respectively. This intensity-induced spectral broadening was attributed to SPM process of the pump component itself.

The spectra of the probe($\perp$) component as shown in Figure VII.7(a$\perp$), (b$\perp$), and (c$\perp$) have two peaks. One is at the incident central wavelength of 780 nm, the other was shifted to anti-Stokes side at 777, 770, and 763 nm for pulse energies of 0.5 nJ, 1.8 nJ, and 3.9 nJ, respectively. The intensity of the probe($\perp$) component was too weak to introduce any significant spectral broadening itself through SPM. On the other hand, this asymmetrical spectral broadening could not be possibly caused by SPM which always induces symmetrical spectral broadening. This nonlinear asymmetrical spectral broadening of the probe($\perp$) component which is introduced by the pump($\|$) component is attributed to the DXPM process.

VII.3.3 Theoretical Fitting

The different characteristics of the measured spectra for the two perpendicular linearly polarized components of single femtosecond laser light pulses in a birefringent single-mode fiber can be explained with DXPM and SPM theories with considering the

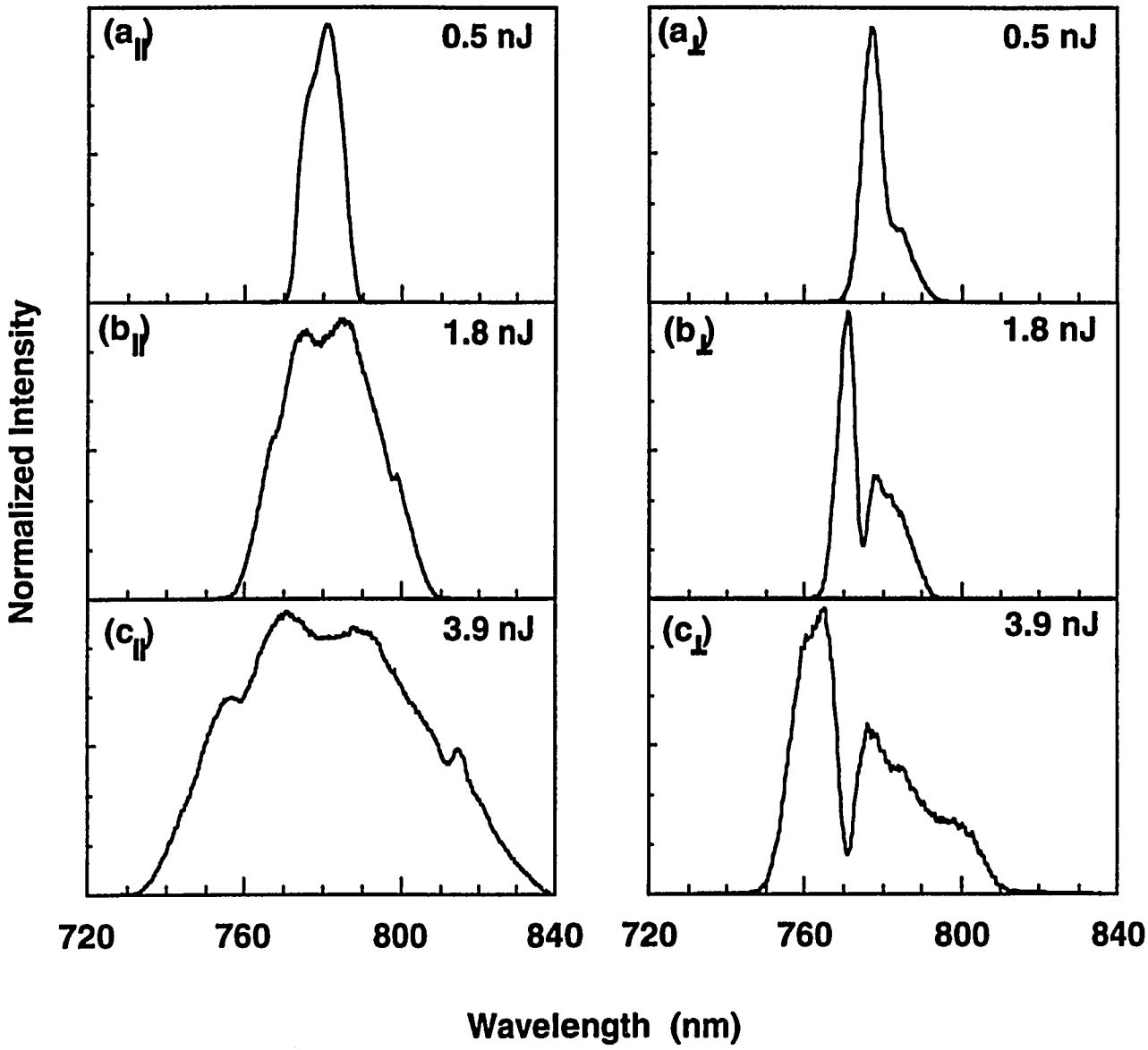

Figure VII.7 The measured spectra of linearly polarized femtosecond laser light pulse propagating in a 1-m-length birefringent single-mode optical fiber. The intensity ratio of the pump(∥) component to the probe(⊥) component was 20. Right and left columns are the spectra of pump and probe components, respectively. ($a_{\parallel}$), ($b_{\parallel}$), and ($c_{\parallel}$) are the pump component spectra for pulse energies of 0.5 nJ, 1.8 nJ, and 3.9 nJ, respectively. ($a_{\perp}$), ($b_{\perp}$), and ($c_{\perp}$) are the corresponding spectra of probe component at the same pulse energies.

polarization properties of the light in optical fibers. In a birefringent fiber, two perpendicular linear polarization are the stable propagation eigen-modes. Hence, linear polarization bases should be used.

Since the laser light pulse had a repetition rate of 76 MHz which is much larger than the response of the shutter of CCD camera, the measured spectral profiles are the overlap of multiple pulses. At this pulse repetition rate and short length of the fiber, there is no inter-pulse interaction. The spectral broadening profiles arise from the two polarization component of a single-pulse. The electric field envelope of a single linearly polarized laser can be expressed as a superposition of the two linearly polarized components with amplitude envelopes of $A_x(z,t)$ and $A_y(z,t)$, respectively. Using the slowly varying envelope approximation, the coupled nonlinear wave equations that govern the two polarization components can be obtained as[1],

$$\frac{\partial A_x}{\partial z}+\frac{1}{v_{gx}}\frac{\partial A_x}{\partial t}+\frac{i}{2}k_x^{(2)}\frac{\partial^2 A_x}{\partial t^2}=i\frac{\omega_x n_2}{c}$$
$$x\ [(|A_x|^2+\frac{2}{3}|A_y|^2)A_x+\frac{1}{3}A_y^{\ 2}A_x^{\ *}\exp(-i2\Delta kz)], \qquad \text{(VII.3a)}$$

$$\frac{\partial A_y}{\partial z}+\frac{1}{v_{gy}}\frac{\partial A_y}{\partial t}+\frac{i}{2}k_y^{(2)}\frac{\partial^2 A_y}{\partial t^2}=i\frac{\omega_y n_2}{c}$$
$$x\ [(|A_y|^2+\frac{2}{3}|A_x|^2)A_x+\frac{1}{3}A_x^{\ 2}A_y^{\ *}\exp(i2\Delta kz)], \qquad \text{(VII.3b)}$$

where V_{gx} and V_{gx} are the group velocities for light polarized along the x axis and y axis, respectively; $k^{(2)}$ is the group-velocity dispersion (GVD), n_2 is the nonlinear refractive index, and $\Delta k=k_x-k_y$ is the propagation constant mismatch between the two orthogonal linear polarization eigen-modes. The first two terms in the right-handed side of Eqs. (VII.3) are the SPM and DXPM which will modulate the phase of the propagating pulses.

The third terms in the equations are the degenerate four-wave mixing (DFWM) terms, which modulated the amplitude as well as the phase of the propagating light pulse.

The observed spectra of different polarization components of a single laser pulse can be explained using Eqs. (VII.3). After a single linearly polarized laser light pulse was coupled into the birefringent optical fiber, the two linearly polarized components propagated like two laser pulses. A key term which will affect the output laser light spectrum caused by DXPM is the walk-off distance between two polarization components. The walk-off distance defined as $Lw = To/(1/Vgx - 1/Vgy)$ is 0.2 m at pulse duration of 230 fs. This means after a light pulse propagates such a distance in the fiber, two linear polarization modes will not spatially overlap. Therefore, no DXPM can occur afterwards. In the experiment, the intense component (pump) was coupled in the fast opto-axis of the fiber. The probe component which was coupled in the slow opto-axis sees only the trailing part of the pump. The phase of the probe component was then modulated by the induced index change caused by the tailing edge of the pump component, the spectrum of the probe component was shifted to the anti-Stokes (blue shifted) side only. This is shown in the left-handed column of Figure VII.7. In equation (VII.3), the coefficient of XPM which is 2/3 is two-third of SPM which is 1. The spectral broadening of DXPM should be 2/3 of SPM. As the result of walk-off effect, the spectral broadening of XPM which are 3 nm, 10 nm, and 17 nm are less than 2/3 of SPM broadening which are 10 nm, 25 nm, and 45 nm (anti-Stokes side only) as shown in Figure VII.7 for pulse energies of 0.5 nJ, 1.8 nJ, and 3.9 nJ, respectively. After a laser light pulse propagated the walk-off distance, the DXPM process vanished since the two polarization components did not overlap. The SPM process still occurred to cause more broadening in the pump component spectra.

The strength of the DFWM process depends on the phase matching between the two orthogonal linear polarization modes characterized by the beat length $L_B=2\pi/(|k_x-k_y|)$. When L, the length of the optical fiber, satisfies $L>>L_B$, the contribution of the DFWM terms in equations (VII.3) can be neglected. This is true for this 1-m-length birefringent fiber with a typical beat-length of $L_B=2$ mm.

Another effect in pulse propagation is GVD. Because the optical fiber has a dispersion of 300 ps/(nm.km) at the central wavelength of 780 nm, GVD must be accounted. The pulse intensity was decreased dramatically in the propagation of the femtosecond laser pulse.

As collaboration with us, G. P. Agrawal *et al.* have simulated the DXPM spectra of femtosecond laser light pulses propagating in the birefringent optical fiber. Figure VII.8 shows the numerical calculation of the spectral broadening of single laser light pulses propagating through a birefringent single-mode optical fiber. The simulation used Eqs. (VII.3) with the last term (DFWM) dropped. The same fiber length was used in the calculation. The GVD parameter $k^{(2)}$, wave vector mismatch Δk, nonlinear refractive index n_2, and chirp of light pulse are 35 ps^2/km, 1.2 ps/m, $3.2x10^{-20}m^2/W$, and 0.5, respectively. Qualitative agreement with the experiment can be seen as shown in Figure VII.8. The spectra of probe and pump components at low input light power (0.5 nJ) show the less agreement with the experiment. We believe that this may be due to an overestimate of the chirp[1] of light pulses combined with the fact that we used a parabolic chirp while the exact chirp profile is unknown. The spectral broadening at high input light power (3.9 nJ) in the simulation is in good agreement with the experiment.

In this section, DXPM process has been observed for the single femtosecond laser light pulses propagating in a birefringent single-mode optical fiber. The difference of the

spectral broadening of the two output polarization components of a single laser light pulse was attributed to self-phase modulation (SPM) and degenerate-cross-phase modulation (DXPM) processes in the optical fiber. Theoretical fittings of the spectral profiles are in reasonable agreement with the measured results. Walk-off, GVD, and chirp effects of the two polarization components are important in the femtosecond pulse propagation.

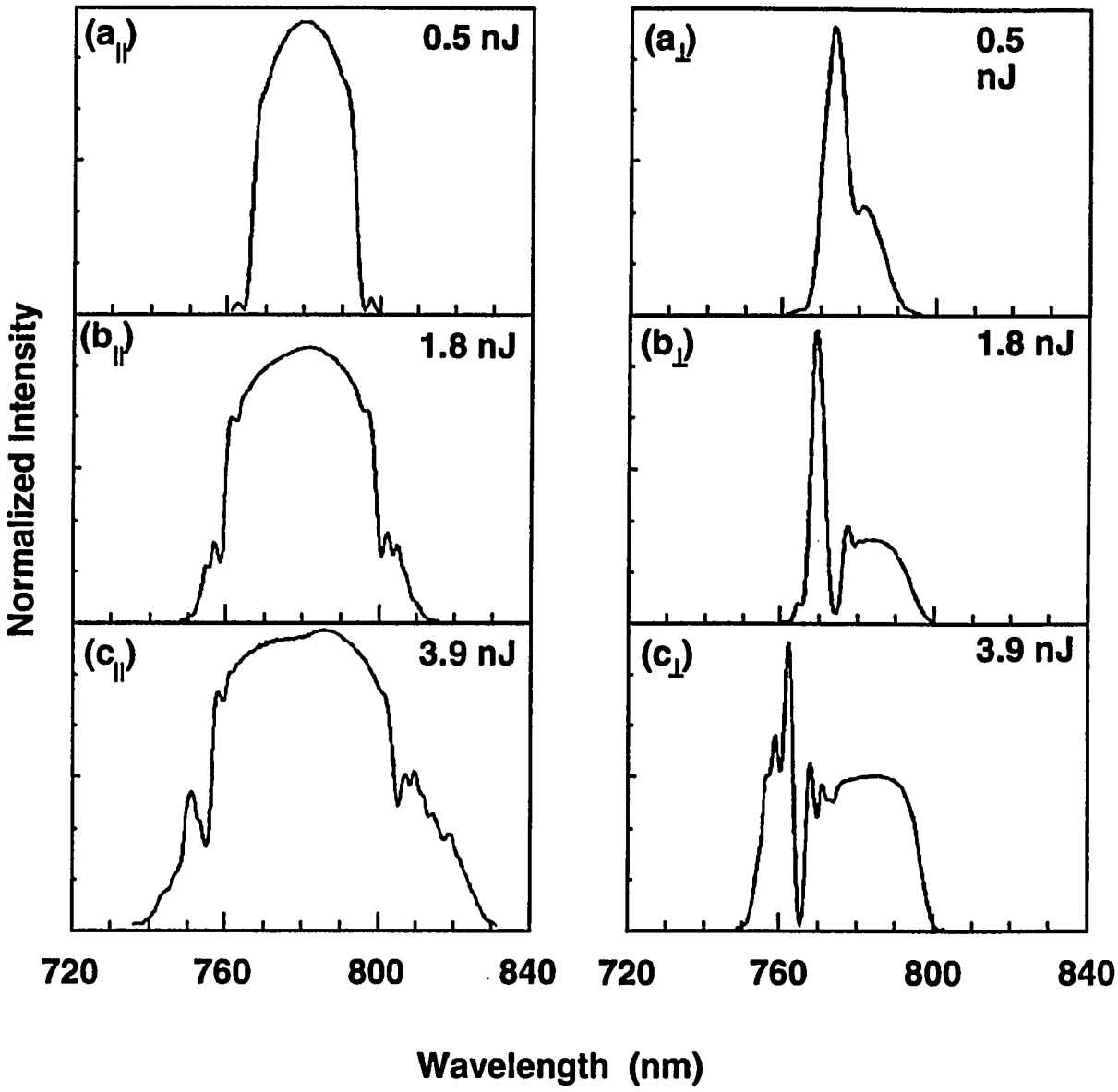

Figure VII.8 The theoretical simulation of the spectra of linearly polarized femtosecond laser light pulses propagating in a 1-m-length birefringent single-mode optical fiber. The intensity ratio of the pump(∥) component to the probe(⊥) component was 20. Fiber length L=1 m. The GVD parameter $k^{(2)}$, wave vector mismatch Δk, nonlinear refractive index n_2, and chirp of light pulse are 35 ps^2/km, 1.2 ps/m, $3.2 \times 10^{-20}\ m^2/W$, and 0.5, respectively. Right and left columns are the spectra of probe and pump components, respectively.

(G. P. Agrawal *et al*)

VII.4 DXPM of circularly polarized femtosecond light pulses in a non-birefringent single-mode optical fiber

VII.4.1 Experimental Method

The experimental setup is shown in Figure VII.9. A Titanium: Sapphire laser (Coherent Mira Model: 900-B), operating at wavelength 780 nm, was used in the experiment. The modelocked laser light pulse train which had a repetition rate of 76 MHz was generated with a pulse duration of 120 fs and spectral bandwidth of about 5 nm. The modelocked output laser light of this laser had an average power of 1.4 W, corresponding 18 nJ per laser light pulse. The power fluctuation is less than 2%. The output laser pulse train was first launched to pass an optical isolator (Faraday Rotator) to avoid the reflecting light from the surface of the following optical devices back to laser cavity to disturb the mode-locking state. The duration of laser pulses was 230 fs after the optical isolator because of group-velocity dispersion. A calcite crystal polarizer was used to make the laser beam linearly polarized with a ratio better than 10^5.

A quarter-wave plate (QWP1) was used after the polarizer. The optical axis of the quarter-wave plate was first set 45° to the optical axis of the polarizer, P. The optical pulses became circularly polarized after passing the quarter-wave plate. By rotating the quarter-wave plate with a small angle (~6°), the circularly polarized optical pulses were converted into slightly elliptically polarized (almost circularly polarized) light pulses. These slightly circularly polarized laser light pulses had two opposite rotating circularly polarized components.

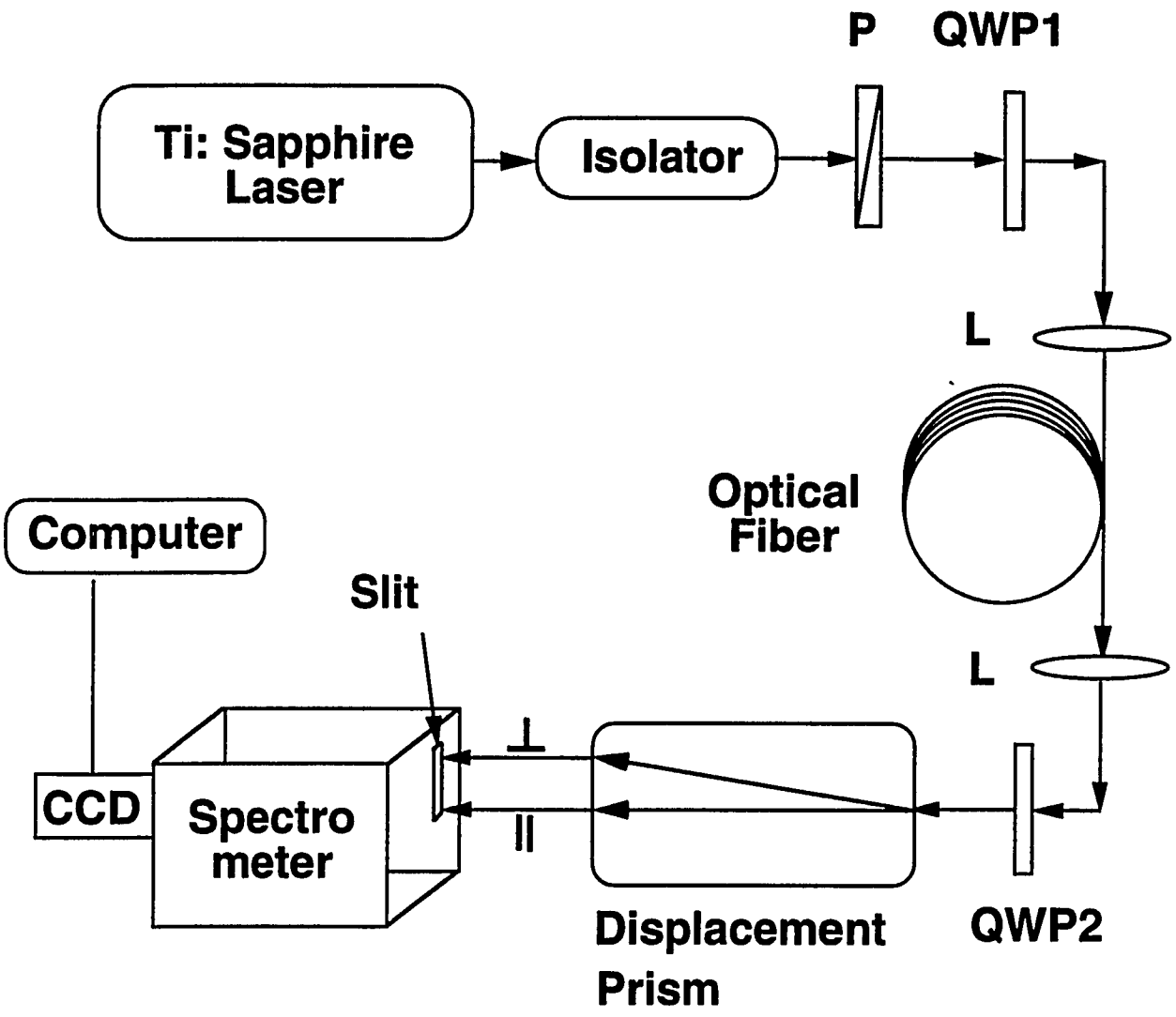

Figure VII.9 Experimental set-up: P is polarizer, QWP's are quarter wave plates, L's are microscope objective lens, a beam displacing prism to separate two circularly polarized components; the spectral analysis system has resolution of 1.5 nm with a dispersion of 0.24 nm/pixel.

The 230 femtosecond slightly circularly polarized laser light pulses were coupled into and out of an one-meter-length nonbirefringent single-mode optical fiber with two 10X micro-objective lens. The optical fiber (Newport Corp. FSV-10 model) had a core diameter of 4 μm and a cladding thickness of 125 μm. This fiber supported a single mode at the wavelength of 780 nm. The regular fiber had a symmetrical circular cross section without any fabricated birefringence. There could be some random micro-birefringence formed inside the fiber. The beat length of this kind of birefringence is much long than the length used in the experiment (1 m). Therefore, the fiber can be treated as nonbirefringent. The output laser pulses from the optical fibers passed a second quarter-wave plate (QWP2) and then a polarizing displacement prism. The optical axis of QWP2 was set parallel to that of the displacement prism. So the circular polarizations were transferred into two perpendicular linear ones and they were spatially separated by the polarizing displacement prism. The ratio of the intensities of the two circularly polarized components was adjusted to 20. The intense component was the pump light while the weak component was the probe light. Then, the spectra of the two linearly polarized components were measured with a spectral analysis system. The spectral measuring system consisted of a spectrometer and a computer controlled charge-coupled-device (CCD) camera. The resolution of this system is 1.5 nm with a dispersion of 0.24 nm per pixel. The spectrum of input laser light pulse has a bandwidth of 5 nm has been shown in Figure VII.6.

VII.4.2 Results

The spectra of the two opposite rotating circularly polarized components have been measured for various incident light pulse energy for the 1-m-length nonbirefringent single-mode fiber. The normalized spectra are displayed in Figure VII.10(a), (b), and (c) for the input laser light energy of 0.5 nJ, 1.8 nJ, and 3.9 nJ, respectively. The right and

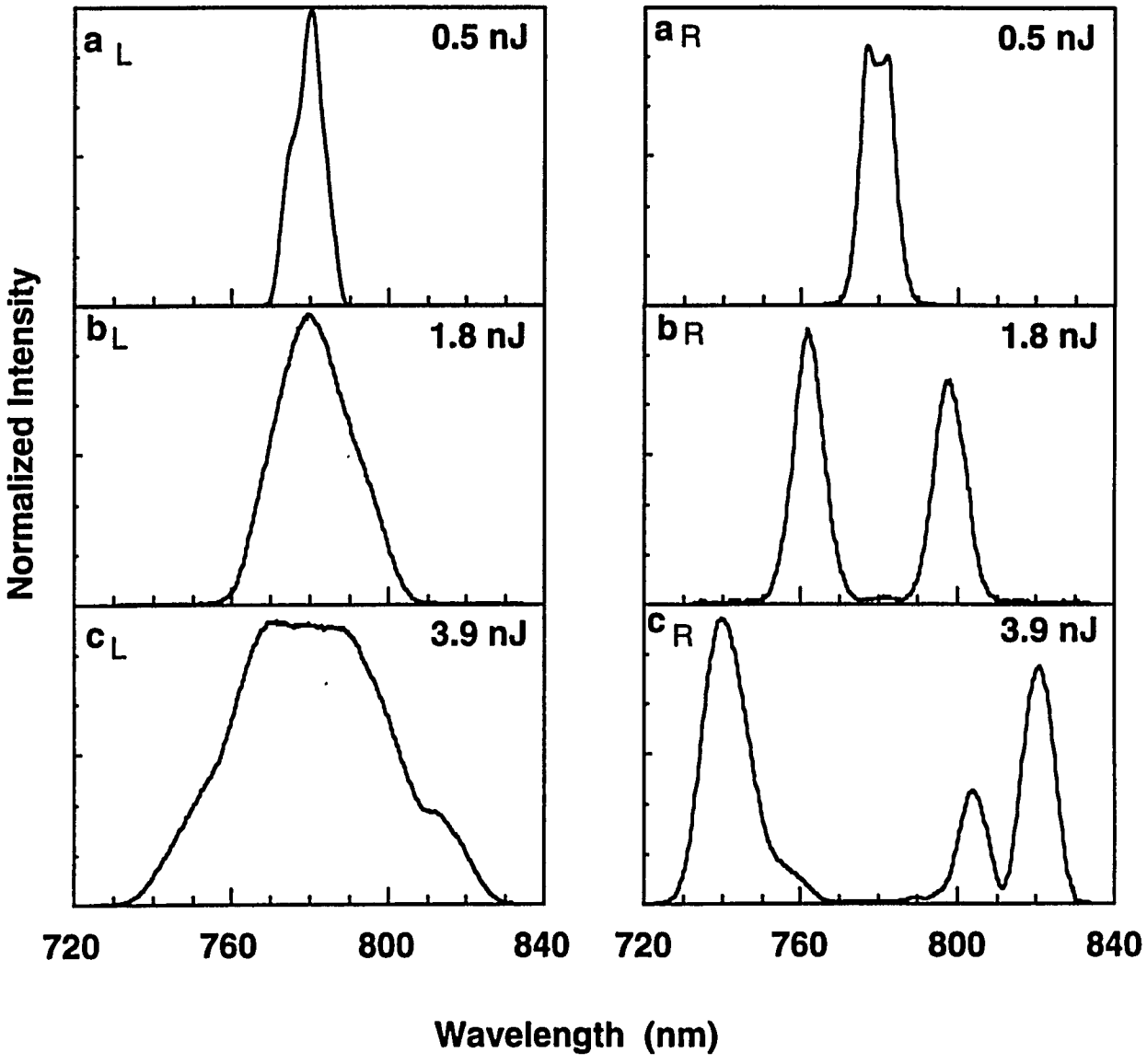

Figure VII.10 The measured spectra of slightly depolarized circular light pulses propagating in a 1-meter nonbirefringent single-mode optical fiber. The intensity ratio of the pump(L) component to the probe(R) component was 20 to 1. Right and left columns are the spectra of probe and pump components, respectively. (a_L), (b_L), and (c_L) are the pump component spectra for pulse energies of 0.5 nJ, 1.8 nJ, and 3.9 nJ, respectively. (a_R), (b_R), and (c_R) are the corresponding spectra of probe component at the same pulse energies.

left columns of Figure VII.10 are the spectra of probe and pump components, respectively. The spectra of the pump component in Figure VII.10(a_L), (b_L), and (c_L) broadened symmetrically with bandwidths of 7 nm, 25 nm, and 45 nm at the central wavelength 780 nm, respectively. This spectral broadening of the pump component is induced by the SPM process of itself.

The spectra of the probe component as shown in Figure VII.10(a_R), (b_R), and (c_R) have two peaks. These peaks symmetrically broadened to Stoke and anti-Stokes sides of the incident central wavelength of 780 nm. The interval of these two peaks are 8 nm, 38 nm, and 80 nm for input pulse energy of 0.5 nJ, 1.8 nJ, and 3.9 nJ, respectively. The intensity of the probe component was too weak to introduce any significant spectral broadening itself through the SPM process. This spectral broadening of the minimum component arise from the DXPM of the two circularly polarized components of the input single laser light pulse.

VII.4.3 Discussion

The laser light pulse had a repetition rate of 76 MHz which is much larger than the response of the shutter of CCD camera, the measured spectral profiles are the overlap of multiple pulses. At this pulse repetition rate and short length of the fiber, there is no inter-pulse interaction. The spectral broadening profiles arise from the two polarization component of a single-pulse. Because of a small power fluctuation from one pulse to another (less than 2%). These overlapped spectra of multiple pulses are the same with those of a single light pulse. The measured spectral of the two circularly polarized components of a single femtosecond laser pulse propagating in the nonbirefringent fiber have different features. These differences can be explained with DXPM and SPM theories with considering the polarization properties of the circularly polarized light in

optical fibers. That is the circular polarization modes are the stable propagation mode of light in a nonbirefringent fiber[14]. Therefore, circular polarization modes should be used. The coupled nonlinear wave equations (VII.2) can also be used to explain the observed spectral broadening as shown in Figure VII.10

When the femtosecond laser light pulses were coupled into the nonbirefringent single-mode fiber, the nonlinear interactions of two circularly polarized light pulses are pure phase modulation processes including SPM and XPM without other adverse effect such as degenerate-four-wave-mixing (DFWM) which will cause amplitude coupling from each other. No energy exchange occurred between the two circularly polarized components due to the nonlinear processes. Furthermore, there is no walk-off effect between the two circularly polarized components since the optical fiber is not optical active. The spectral broadening of DXPM at different pulse energies are about twice of the SPM spectral broadening at different input light pulse energy in Figure VII.10 as expected from Eqs. (VII.2) where the coefficient of DXPM (4/3) is twice larger than that (2/3) of SPM. Another important effect in pulse propagation is GVD. Because the optical fiber has a GVD of 300 ps/(nm.km) at the central wavelength of 780 nm, the intensity was decreased dramatically in the propagation of the femtosecond laser pulse. Since the nonlinear processes of SPM and DXPM are proportional to the intensity of the light, GVD will affect the both SPM and DXPM induced spectral broadening through decreasing light intensity. The spectral broadening is less than that of light propagating in a medium without GVD.

Using Eqs. (VII.2), numerical simulations of the experimental results have been made by G. P. Agrawal *et al.* in collaboration with us. The calculated spectra are shown in Figure VII.11 for the same conditions. Qualitative agreement with the experimental results can be found. At low light pulse energy of 0.5 nJ as shown in Figure VII.11(a), the

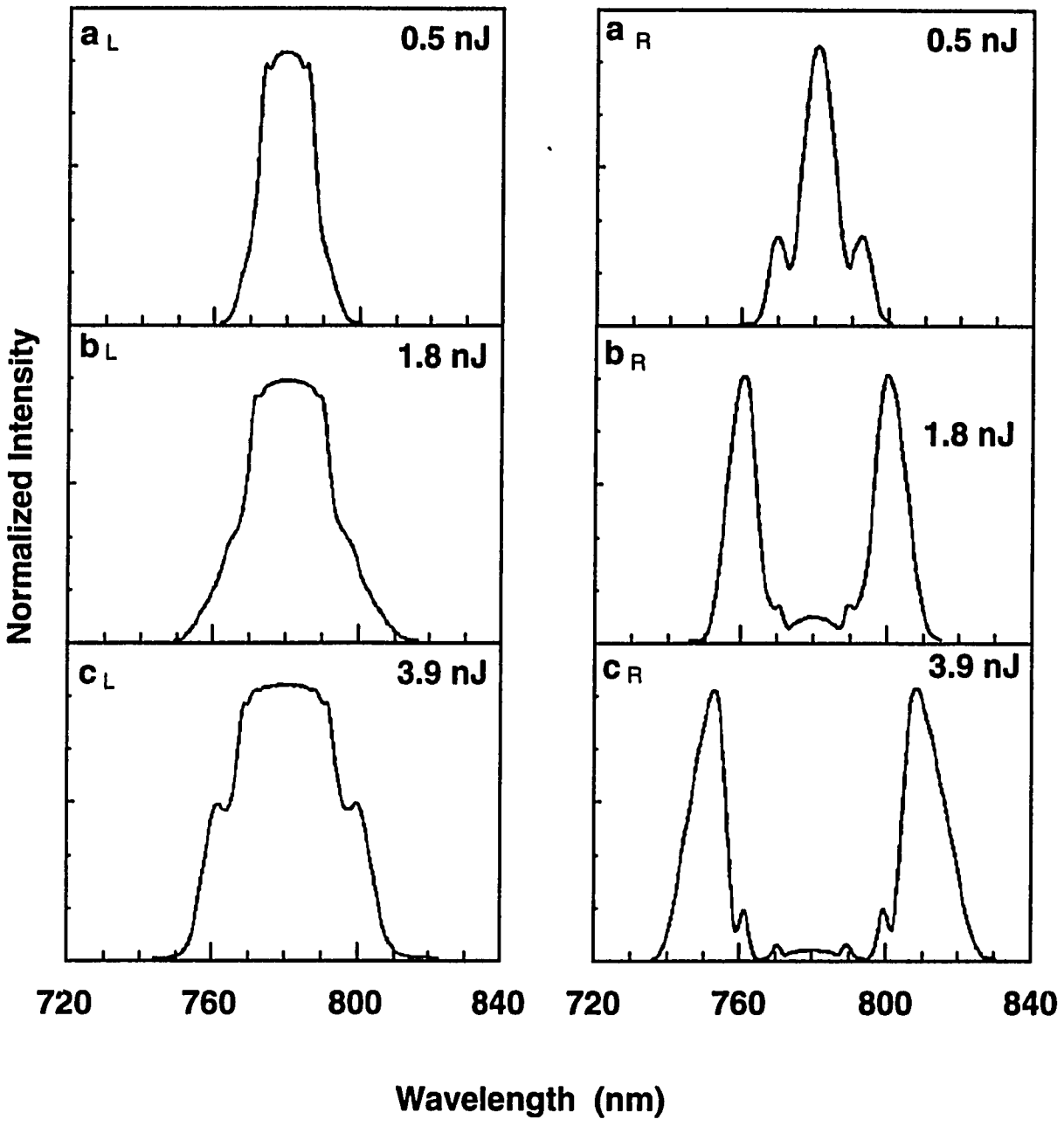

Figure VII.11 The theoretical simulation of the spectra of slight depolarized circular femtosecond laser light pulse propagating in a 1-m-length nonbirefringent single-mode optical fiber. The intensity ratio of the pump(L) component to the probe(R) component was 20. Fiber length L=1 m. The GVD parameter $k^{(2)}$, wave vector mismatch Δk, nonlinear refractive index n_2, and chirp of light pulse are 35 ps^2/km, 1.2 ps/m, $3.2 \times 10^{-20}\ m^2/W$, and 0.5, respectively. Right and left columns are the spectra of probe and pump components, respectively.

(G. P. Agrawal *et al*)

simulated spectra of the two components are broader than the measured results. This is believed due to an overestimate of the chirp[1] of light in the fiber. For middle pulse energy of 1.8 nJ as shown in Figure VII.11(b), the simulations of the spectral broadening of the two circular components are in good agreement with the experimental results. At high input pulse energy of 3.9 nJ displayed in Figure VII.11(c), the calculated spectra for the two components are less broad the measured spectra. This may be due to the nonlinear self-focus effect[18] of light in the fiber which makes light more intense than it looks like. The asymmetrical broadening structure of the probe component may be caused by a slightly asymmetric of the input light pulse temporal profile while symmetrical profile were assumed in the simulations.

In this section, DXPM processes have been observed for the femtosecond laser pulses propagating in a birefringent single-mode optical fiber. Slightly elliptically polarized (almost circular) light pulses were used to measure the spectra of the two circularly polarized components. The experimental results are in reasonable agreement with the theoretical simulations.

VII.5 Temporal DXPM of two circularly polarized 35 picosecond light pulses in a nonbirefringent single-mode optical fiber

VII.5.1 Introduction

In this section, two opposite rotating circularly polarized laser light pulses with different time delays were coupled into a non-birefringent single-mode optical fiber to observe the temporal DXPM effect. Two laser light pulses have the same wavelength, pulse duration, and the same intensity. The spectral broadening of the two light pulses was measured for different optical delays. The spectral broadening of the laser pulses also has been measured as a function of the light intensity.

VII.5.2 Experimental Method

The experimental arrangement for observing the DXPM process of two circularly polarized laser light pulses is shown in Figure VII.12. Laser pulses at the wavelength of 532 nm with a pulse duration of 35 ps from a Nd: YAG laser were used. After the polarizer P1, the laser pulse was linearly polarized to a ratio better than 400 to 1. Then, the linearly polarized laser pulse passed through a polarizing prism (P2). The optical axis of the polarizer P1 was placed at 45° to the optical axis of the polarizing prism P2. The incident laser light pulse was then splitted into two linearly polarized light pulses with perpendicular polarization states (Pulse 1 and 2) and equal intensity. Lets see Pulse 1 first, Pulse 1 which was horizontally polarized passed through a quarter wave plates (QWP1) which was alignment at 45° to horizontal direction. Pulse 1 then became circularly polarized. After certain optical delays and reflected by a mirror (M), Pulse 1 was bounced back and remained circularly polarized. Pulse 1 passed the quarter wave

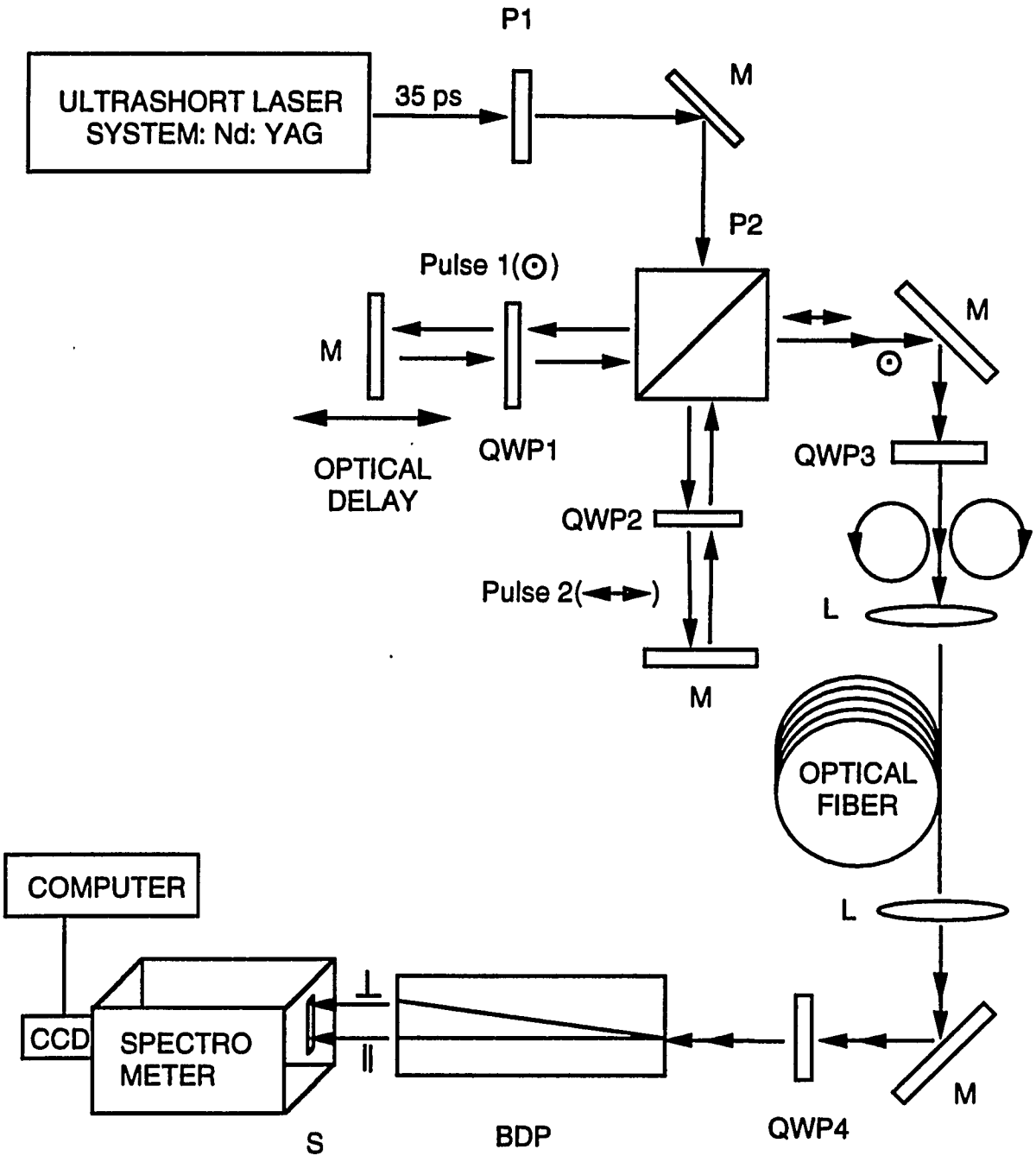

Figure VII.12 The experiemntal setup to observe the degenerate cross-phase modulation of two circularly polarized light pulses propagating in nonbirefringent single-mode optical fiber. M: mirror; P1: polarizer; P2: polarizing prism; QWP's: quarter-wave plate; L's: micro-objective lens; BDP: beam displacement prism; S: slit of the spectrometer.

plate (QWP1) again and became linearly polarized at vertical direction. When Pulse 1 propagated back to the polarizing prism P2, it passed through since its polarization has changed from horizontal to vertical direction. Similarly, Pulse 2 was reflected by polarizing prism P2 since its polarization changed from vertical to horizontal direction.

These two laser light pulses having different optical delays propagated in the same direction. They were linearly polarized and had equal intensity. Their polarization directions were perpendicular to each other. These linearly polarized laser light pulses then passed through another quarter wave plate (QWP3) which the optical axis was at 45^{o} to the horizontal direction.

These laser light pulses became circularly polarized with opposite rotating directions. These circularly polarized laser light pulses were coupled into and out of a nonbirefringent single-mode optical fiber using two micro-objective lenses (L's).

Since the polarization states of circularly polarized light are stable in nonbirefringent single-mode optical fibers, the polarization states of the output light signal from the optical fiber remained in the input circular polarizations. To distinguish these two circular polarization states, another quarter wave plate (QWP4) was used to transfer circular polarization modes into linear ones because the polarizing prism only works for linear polarization states. The two perpendicular linear polarization after QWP4 corresponds the two opposite rotating circularly polarized modes in the optical fiber. Then, the laser light pulses passed through a beam displacement prism (BDP). Two perpendicularly linearly polarized modes were spatially separated. They were sent into a spectrometer at different position of the slit. A computerized CCD camera system was used to record the digitized spectra of the output light signals. The detection area of the CCD camera was large enough to record the spectra of the two components of the output

laser pulses at the same time. The spectral analysis system had a resolution of 0.03 nm and a dispersion of 0.005 nm/pixel. The laser spectrum with a FWHM bandwidth less than 0.03 nm is shown in Figure VII.2.

The same non-birefringent single-mode optical fiber with that in section VII.2 was used in this experiment. The optical fiber (Newport Corp. FSA-10 model) supports a single-mode at the wavelength of 532 nm region with a core diameter of 2.5 μm and cladding thickness of 125 μm.

VII.5.3 Results

The spectra of the two output opposite rotating circularly polarized laser light pulses at the wavelength of 532 nm have been measured for different coupled pulse energies at a given optical delay. Figure VII.13 shows the photo displays of the DXPM spectra from the CCD camera at the optical delay of 52 ps ($\tau_d = t_L - t_R$) for different input laser light pulse energies. The left- and right-handed columns of Figure VII.13 are the spectral photo displays of the left- and right-handed components, respectively. The input laser light spectra for weak light pulse where nonlinear processes were absent were shown in Figure VII.13(a). The laser light spectrum was very narrow and focused to a small spot in the CCD camera. Figure VII.13(b) shows the spectra of the two laser light pulses at the same pulse energy of 5.8 nJ where the left- and right-handed light pulses were blue- and red-shifted, respectively. Since the optical delay between the right- and left-handed laser pulses was 52 ps ($\tau_d = t_L - t_R$), meaning that right-handed pulse was in front of the left-handed one, the left-handed laser pulse saw only the tailing part of the right-handed laser pulse; and obviously, the right-handed pulse saw only the leading part the left-handed pulse. By checking the XPM principle in Figure II.9 of chapter II, one can find that the left-handed laser pulse was blue-shifted and the right-handed pulse was red-

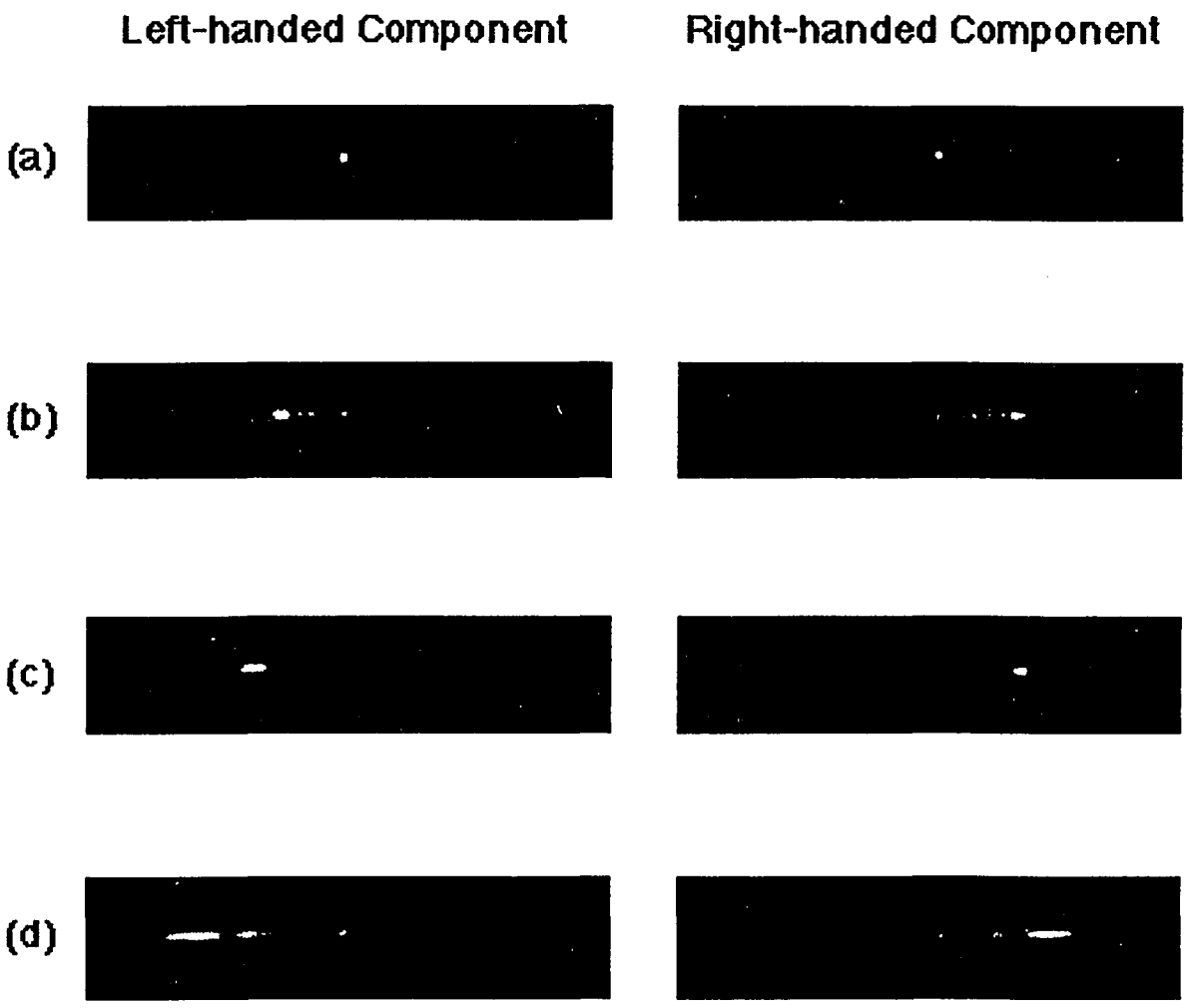

Figure VII.13 The photo displays of the spectral broadening of the two laser light pulses at an optical delay of 52 ps ($\tau_d=\tau_L-\tau_R$). The laser light pulse duratrion was 35 ps. Two pulses had the same pulse energy. The energy of each pulse is: (a) input light; (b) 5.8 nJ; (c) 7.3 nJ; (d) 12.0 nJ.

shifted just like the measured results in Figure VII.13(b). Since two light pulses were at the same pulse energy of 5.8 nJ, the spectral broadening of the two light pulses to anti-Stokes and Stokes sides are about the same.

For the blue-shifted spectral broadening of the left-handed laser pulse in Figure VII.13(b), a weak background on the red-shifted spectral broadening side can be seen in the photo display. This weak background of red-shifted broadening was from the leakage of the right-handed laser pulse. When a circularly polarized laser light pulse was coupled into an optical fiber, many things such as a small misalignment of the polarizer and quarter wave plate or the irregular fiber ending shape after the fiber cut will affect the polarization state of the light. This effect will cause the light coupled to the opposite rotating circularly polarized mode. In our experiment, 8% of the light was found to be coupled into the opposite circularly polarized mode. This leakage of light from one polarization mode to the other is responsible for the weak spectral broadening background on the red-shifted side in Figure VII.13(b) for left-handed laser pulse. The same process happened to the right-handed laser pulse, so a weak background on the blue-shifted spectral broadening can be seen although the spectrum of the right-handed pulse was red-shifted in Figure VII.13(b).

The DXPM spectral broadening for the laser light pulses at the pulse energies of 7.3 nJ and 12 nJ are shown in Figure VII.13(c) and (d), respectively. They have the similar characteristics with those in Figure VII.13(b). From these spectral broadening, one can find that the XPM induced spectral broadening at a given optical delay is proportional to the light pulse energy. The higher the pulse energy, the broader the light spectra. For light pulses with energy high enough, strong Stimulated Raman Scattering (SRS) process will induce a very broad continuum spectrum overlapped with the XPM broadening.

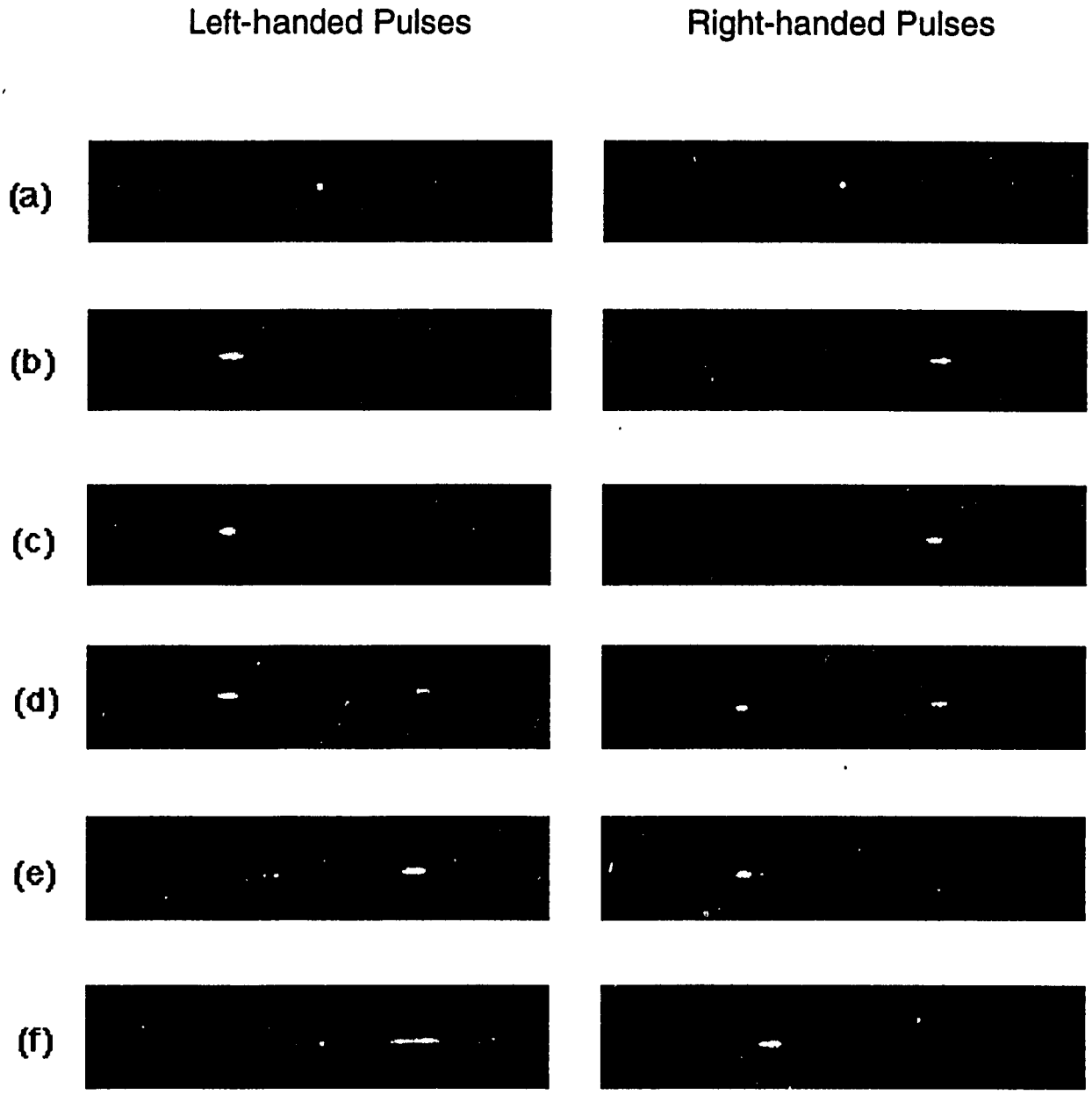

Figure VII.14 The photo displays of the spectral broadening of the two circularly polarized laser light pulses with different optical delays. The laser light pulse duration was 35 ps. Two pulses had the same pulse energy of 6.0 nJ. The optical delay of the two light pulses ($\tau_d=\tau_L-\tau_R$) are: (a) input laser light; (b) 40 ps; (c) 20s; (d) 0 ps; (e) -20 ps; (f) -40ps.

The temporal DXPM spectral broadening have also been measured for light pulses having different optical delays but the same pulse energy. The pulse energies of the left- and right-handed laser pulses were also equal to each other. The measured results were shown in Figure VII.14 as photo display. The left- and right- column are for left- and right-handed laser pulse, respectively. The energy of both left- and right-handed laser pulses remained 6 nJ for all different optical delays. Figure VII.14(a) shows the spectra of the input left- and right-handed pulses at very low pulse energy (<0.1 nJ). The spectrum of input laser light was very narrow and was well focused a fine spot on the CCD screen.

Figure VII.14(b) shows DXPM induced spectral broadening of the left- and right-handed laser pulses with an optical delay of 40 ps ($\tau_d = t_L - t_R$) and the same pulse energy of 6 nJ. The right-handed laser pulse was 40 ps in front of the left-handed one. The spectra of left- and right-handed laser pulses were blue- and red-shifted, respectively. The spectra were shifted equally to blue side (left-handed) and red side (right-handed) since two light pulses had the same energy. The DXPM spectral broadening is shown in Figure VII.14(c) when the right-handed pulse was 20 ps ahead of the left-handed one (τ_d=20 ps). The spectral broadening are very similar to that in (b). For the spectra of left-handed laser pulse in left-column of Figure VII.14, the spectra were blue-shifted for two optical delays in (b) and (c). But it seems there is more light in the red-shifted side in (c) than that in (b), at least more than the leakage from the opposite rotating light that was discussed before. This may arise from the different optical delays. A shorter optical delay (20 ps) will coupled more light to the red-shifted side than a longer optical delay (40 ps).

For τ_d=0 ps, two laser pulses were coupled into the fiber at the same time, the DXPM induced spectral broadening are shown in Figure VII.14(d). The spectra were broadened equally to both blue- and red-shifted sides. This is not surprising because two

light pulses had equal energy, no optical delay, and propagating with the same velocity (without walk-off effect). When the optical delay was τ_d=-20 ps, meaning that the right-handed pulse was 20 ps behind the left-handed one. The spectrum of the left-handed pulse was shifted to Stokes (red) side, and the right-handed pulse was shifted to anti-Stokes (blue) side as shown in Figure VII.14(e). As a matter of fact, this is a reverse effect of Figure VII.14(c) for τ_d=20 ps. For τ_d=-40 ps, the right-handed pulse was 40 ps behind the left-handed one, the spectrum of the left- and right-handed pulses were also shifted to Stokes (red) and anti-Stokes (blue) side, respectively, as shown in Figure VII.14(f). Similarly, these spectral broadening are the reverse effect of the spectral broadening in Figure VII.14(b) for τ_d=40 ps. From the observation of the DXPM induced spectral broadening for different optical delays, it is found that the extending range of the spectral broadening depends on the light pulse energy only. The direction of broadening depends on the optical delay between two light pulses.

VII.5.4 Theoretical Fitting

The measured digitized spectra of the two output laser light pulses for a given optical delay of 52 ps are displayed in Figure VII.15 as solid curves for different input laser pulse energies. These spectral intensity distributions were normalized. The left- and right-column are for the left- and right-handed laser pulses, respectively. Figure VII.15(a) shows the input laser light spectrum which had a full-width-half-maximum (FWHM) bandwidth less than 0.03 nm. Figures VII.13(b), (c), and (d) show the spectral broadening at the input laser pulse energy of 5.8 nJ, 7.3 nJ, and 12 nJ, respectively. The corresponding maximum spectral shifts are 0.13 nm, 0.17 nm, and 0.25 nm, respectively. These two laser light pulses show symmetric shifts around the central initial input wavelength of 532 nm.

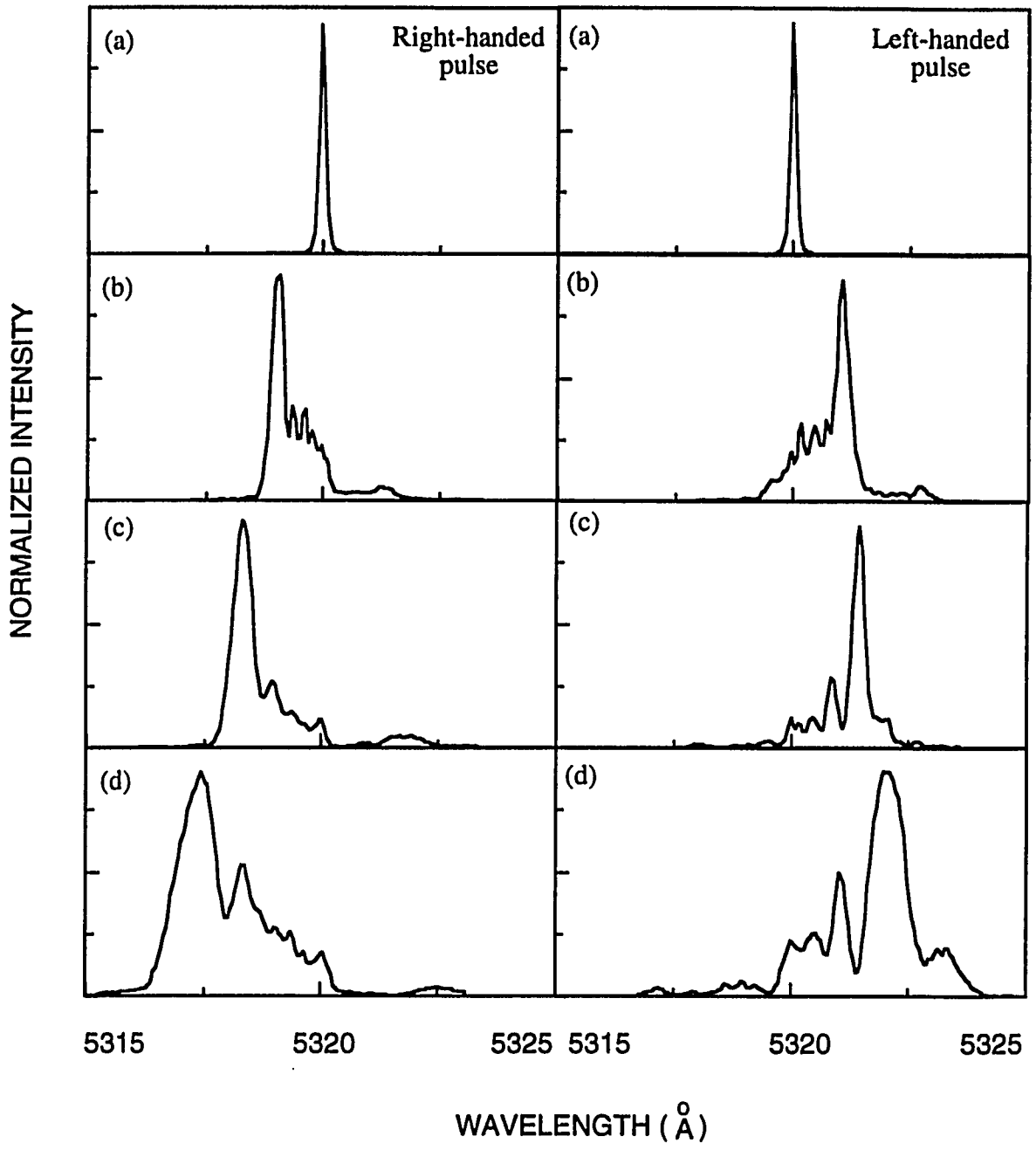

Figure VII.15 The normalized measured spectral of the two circularly polarized laser light pulses at an optical delay of 52 ps ($\tau d=\tau L-\tau R$) with different light pulse energy. The laser light pulse duration was 35 ps. Two pulses had the same pulse energy. The energy of each light pulses are: (a) input laser light; (b) 5.8 nJ; (c) 7.3 nJ; (d) 12.0 nJ.

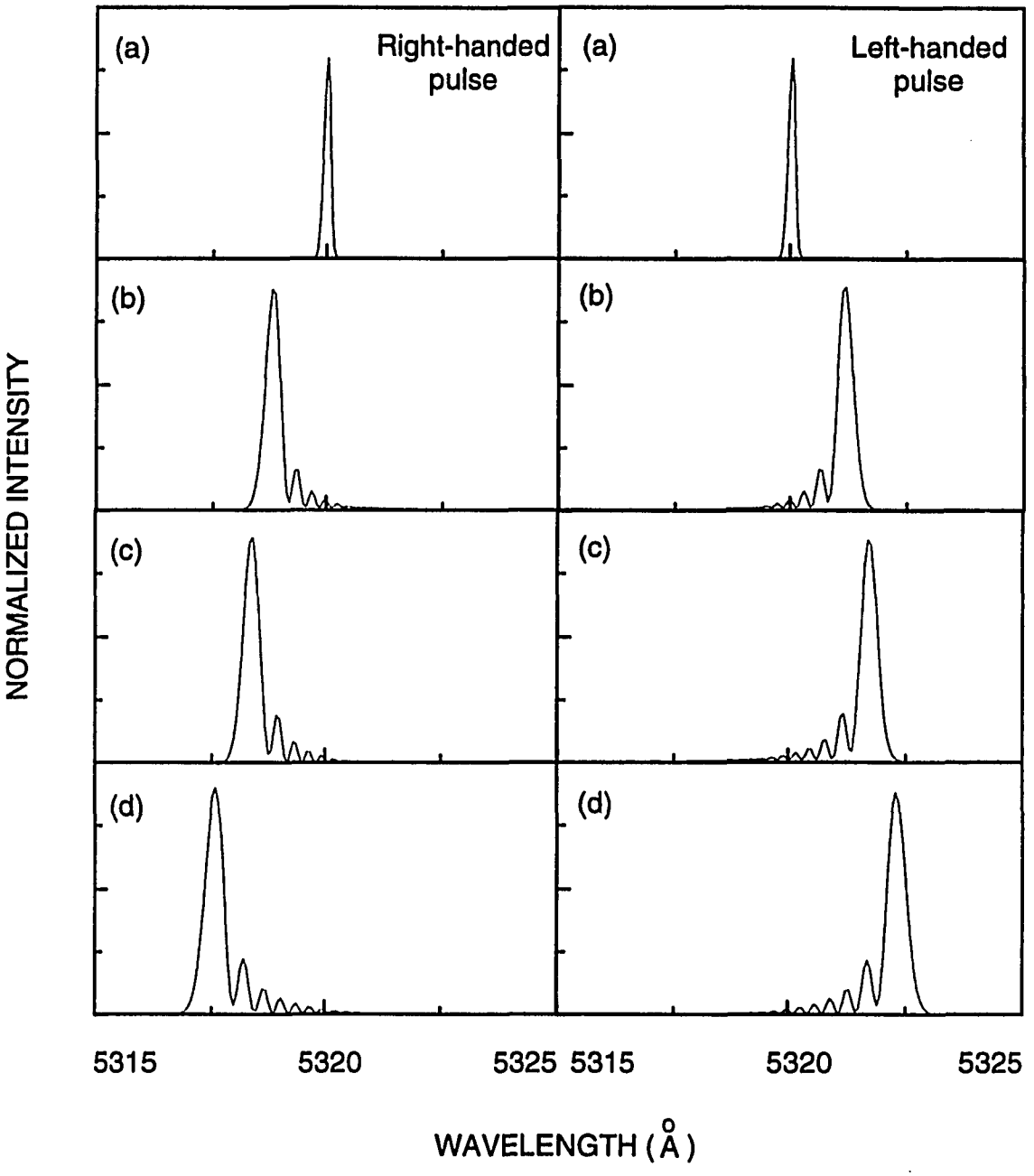

Figure VII.16 The calculated spectra of the two circularly polarized laser light pulses at an optical delay of 52 ps with different light pulse energy. The laser light pulse duration was 35 ps. Two pulses had the same pulse energy of 6.0 nJ. The energy of each light pulses are: (a) input laser light; (b) 5.8 nJ; (c) 7.3 nJ; (d) 12 nJ.

The observed DXPM induced spectral broadening in the two opposite rotating laser light pulses can be explained with DXPM and SPM theory. The nonlinear wave equation (VII.2) for two opposite rotating laser light pulses can be used to simulate the experimental results in Figure VII.15. The theoretical simulation was calculated using Eqs.(VII.2). To compare the theoretical calculation with the experimental results, the energies of the two laser light pulses were assumed to be equal in the calculation. The following parameters were used in the simulation: the fiber length is 1 meter; the nonlinear refractive index $n_2=3.2x10^{-20}m^2/W$. Because of the small bandwidth of the laser light, the dispersion terms in the nonlinear wave equations were neglected (the third terms on the left-handed side of equation VII.2).

The calculated spectra are shown in VII.16 as solid curves for different laser light pulse energies at an optical delay of $\tau_d=52$ ps (right-handed pulse was 52 ps ahead of left-handed pulse). Left- and right-handed columns are for the spectra of left- and right-handed pulses, respectively. Figure VII.16(a) is the calculated spectra of the input laser light. Figure VII.16(b), (c), and (d) are for the laser pulse energy of 5.8 nJ, 7.3 nJ, and 12 nJ, respectively.

At low laser light pulse energies (5.8 nJ and 7.3 nJ for each pulse), the calculated results are in good agreement with the measured spectra as shown in Figure VII.14 for two circularly polarized light pulses having the same pulse energy. The small spectral peaks in the measured results in Figure VII.14(b) and (c) do not separate as clear as they do in the calculation showing in Figure VII.16(b) and (c). This difference is believed due to the limited resolution of the spectral analysis system. At high laser pulse energy (12 nJ for each pulse), the measured spectral for two laser pulses in Figure VII.14(d) are much broader than that of the calculation as shown in Figure VII.16(d). This may be due to the overlap of the spectral broadening caused by the Stimulated Raman Scattering process,

and the additional mixture of broadening since the pump and probe were of the same intensity.

The DXPM induced spectral broadening for two laser light pulses having different optical delays and the same pulse energy were also measured. The normalized spectra are shown in Figure VII.17 as solid curves at pulse energy of 6 nJ for various optical delays. The left- and right-column in Figure VII.17 are for left- and right-handed laser pulses, respectively. Figure VII.17(a) shows the input laser light spectra. Figure VII.17(b), (c), (d), and (e) show the spectral profiles for the optical delay of 0 ps, 20 ps, 27 ps, and 40 ps, respectively. For left-handed laser pulse, the light energy at the output signal was distributed throughout all the broadening spectral range for the 0 ps optical delay as shown in Figure VII.17(b). When the optical delay increased from zero to 40 ps, the normalized spectral profiles of the output left-handed light pulse changed from the broadly distributed light energy as shown in Figure VII.17(b) to transferring most of the light energy to the maximum lobe as shown in Figure VII.17(e). Symmetric development can be seen from the spectral profiles of the right-handed light pulse in the right-column of Figure VII.17.

The DXPM spectra for different optical delays have also been simulated using nonlinear wave equations (VII.2). The calculated results are shown in Figure VII.18. The left- and right-columns are normalized spectra for the left- and right-handed laser pulses, respectively. The calculations of the output spectra are in good agreement with the experimental results except that the measured results are much noisy. From the calculation, it can be seen clearly that most of the light energy is coupled to the main lobe of the DXPM spectra when the optical delay increased from 0 ps to 40 ps. Back to the calculations of the output spectra of the two light pulses having a even larger optical delay of 52 ps as shown in Figure VII.16. One can find that more energy are coupled to

the main lobe in the output DXPM spectra. Neglecting the weak intensity peak in the output spectra, it seems that spectral change caused by DXPM is just a shift effect without any broadening. This may tune out some important applications such as the all-optical A/D converter and amplifier.

In this section, the temporal DXPM spectral broadening of two opposite rotating circularly polarized laser light pulse has been investigated by observing the spectra of the output light pulses from a nonbirefringent single-mode optical fiber. Two laser light pulses had equal pulse energy. The dependence of the spectral broadening of the laser light on the light pulse energy has been measured. The spectral broadening of the laser light for two pulses with various optical delays has also been investigated. The theoretical simulations are in good agreement with the measured results. An important conclusion is that by increasing the optical delay between two laser light pulses, a broadening spectrum due to DXPM process can become a shifted spectrum without broadening. This may be useful for the spectral encoding of the ultrafast XPM analog-to-digital conversion.

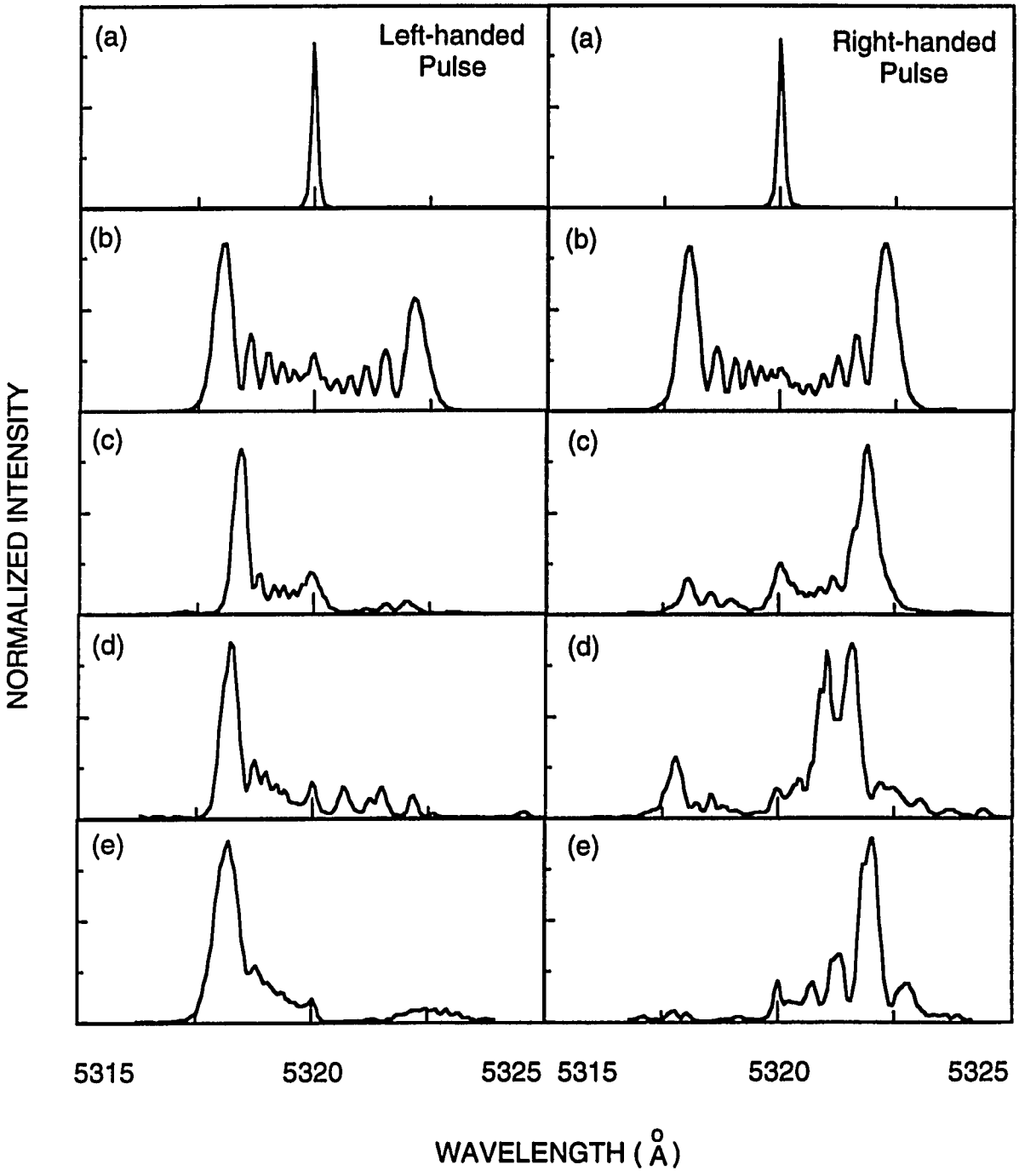

Figure VII.17 The normalized spectra of the two circularly polarized laser light pulses with different optical delays. The laser light pulse duration was 35 ps. Two pulses had the same pulse energy of 6 nJ. The optical delay of the two light pulses ($\tau_d=\tau_R-\tau_L$) are: (a) input laser light; (b) 0 ps; (c) 20s; (d) 27 ps; (e) 40 ps.

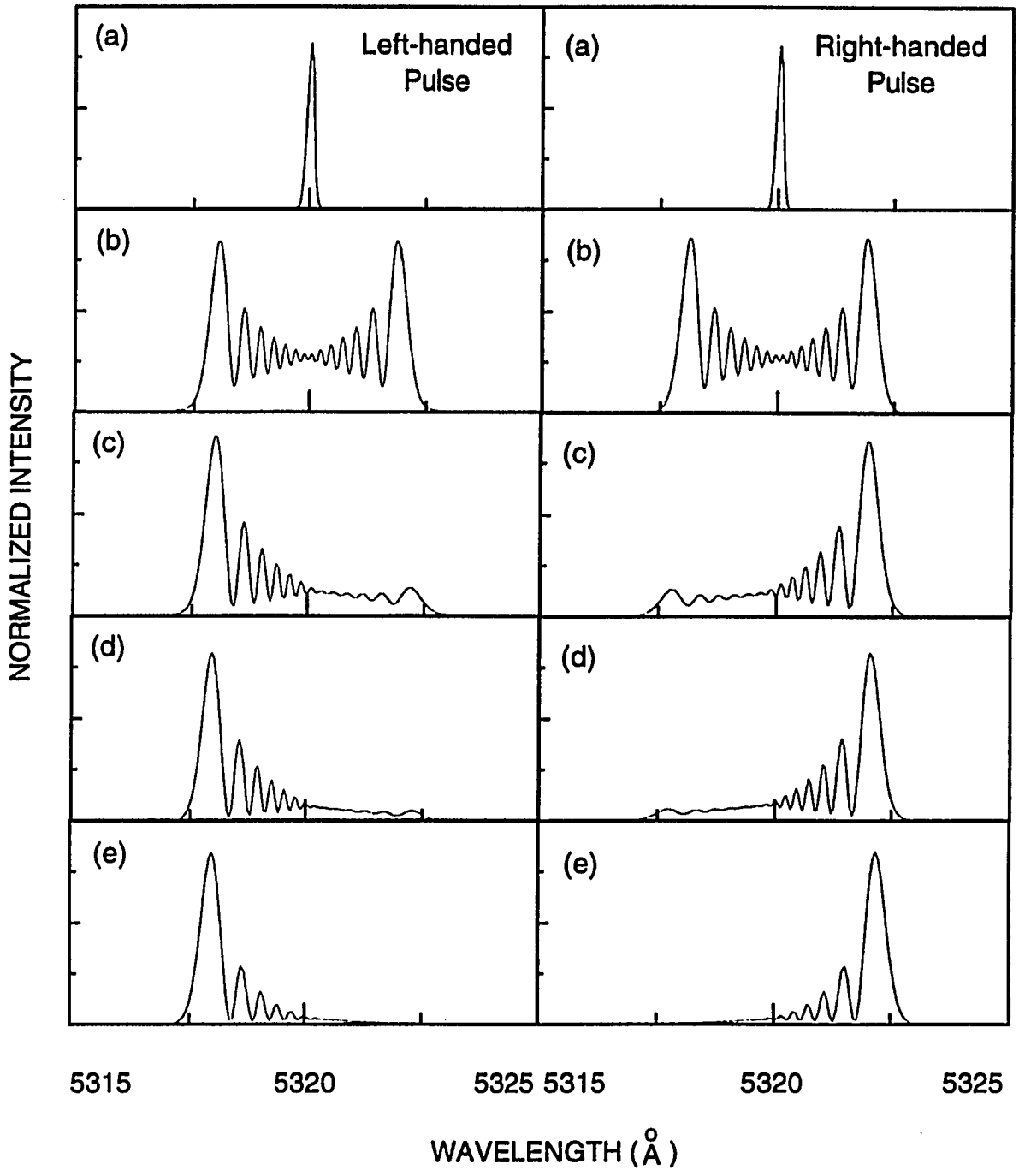

Figure VII.18 The calculated spectra of the two circularly polarized laser light pulses with different optical delays. The laser light pulse duration was 35 ps. Two pulses had the same pulse energy of 6 nJ. The optical delay of the two light pulses ($\tau_d=\tau_L-\tau_R$) is: (a) input laser light; (b) 0 ps; (c) 20s; (d) 27 ps; (e) 40 ps.

VII.6 DXPM of different fiber modes of a 35 ps single-shot laser light pulse in a multi-mode optical fiber

VII.6.1 Introduction

XPM process will occur for optical waves at different states. These different state of light can be different wavelength, polarization, and even different propagation in a multimode optical fiber. The multimode optical fiber used in the experiment was nonbirefringent. The type of optical fiber can support two lowest stable propagation modes. These modes are LP_{01} and LP_{11} modes which have different spatial distribution of light. The mode patterns are shown in Figure VII.19. LP_{01} mode has a symmetric spatial distribution. The light intensity in this mode has a Gaussian distribution. LP_{11} mode spatially separates into two spots with asymmetric intensity distribution.

When laser light is coupled into the multimode optical fiber, light will be coupled into two modes depending on the coupling condition. At the fiber exit, two propagation modes output at the same direction. So two propagation modes spatially overlap with each other and can not be separated. Generally, each mode will carry some light energy. By adjusting the coupling subtlety, most of light can be coupled into one mode such as LP_{01} or LP_{11}. In this experiment, most of the light energy was coupled into the high order mode LP_{11} and very small portion of light was coupled into the LP_{01} mode. Because of its weak intensity, LP_{01} mode hidden between the two lobes of the LP_{11} mode can not be seen at low pulse energy. This was shown in Figure VII.20(a).

VII.6.2 Experimental Method

The experimental arrangement to observe the DXPM between different fiber modes is shown in Figure VII.19. A 35 ps laser pulse at 532 nm from a Nd: YAG laser was used. The multi-mode, non-birefringent optical fiber(Newport Corp. FSV-10 model) has a core diameter of 4 μm and cladding thickness of 125 μm. This optical fiber support two propagation modes at the light wavelength region of 532 nm. These two modes are LP_{01} and LP_{11}. The mode patterns of LP_{01} and LP_{11} are also shown in Figure VII.19. The lowest propagation mode LP_{01} has a circular symmetric intensity distribution on the cross section of the fiber. The first high order mode LP_{11} has two lobes having mirror symmetric distribution. When laser light is coupled into this fiber, light will be coupled into two propagation modes and co-propagate along the fiber. Since this is a multi-mode optical fiber, it dose not maintain any polarization state. There is no favorable polarization direction for the output light signal from the fiber, meaning the light completely depolarized during the propagation in the fiber.

The laser light pulses was coupled into and out of this 1-meter length multi-mode, non-birefringent optical fiber with 5X microscope objective lens (L's). The output light signal was focused to fine points as shown in Figure VII.19. The LP_{11} mode was set parallel to the slit of the spectrometer. Therefore, two lobes of LP_{11} were sent in for spectral analysis. LP_{01} mode is always in the middle of the two lobes of LP_{11} mode. So LP_{01} mode was also sent into the spectrometer. Hence, two modes were sent into the spectrometer at the different position of the slit. The spectra of the output laser light at different fiber propagation modes can be measured for a single shot laser light pulse from the Nd:YAG laser system.

The same spectral analysis system which was used before has a resolution of 0.03 nm was a 1-meter spectrometer coupled to a CCD camera. The detection area of the CCD camera was large enough to record the spectra of the two modes of the output laser pulse

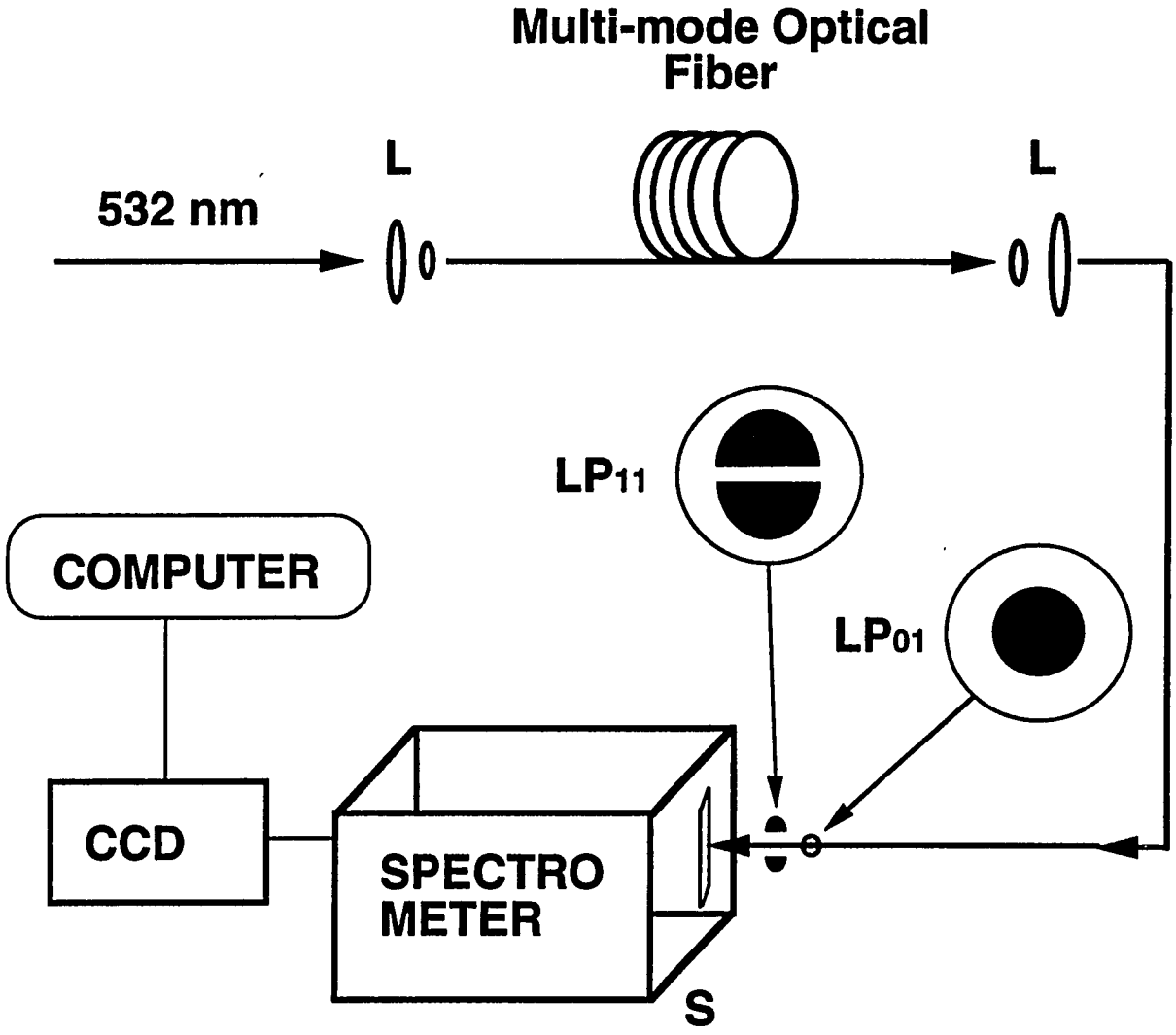

Figure VII.19 Experimental set-up to observe the DXPM between modes of an optical fiber: L's are microscope objective lens, S is slit of spectrometer. The optical fiber surport two modes (LP_{01} and LP_{11})at the wavelength of 532 nm. Most of the light energy was coupled to the mode LP_{11} which was pump mode. LP_{01} mode wasweak which was probe mode.

simultaneously. The input laser light spectrum with a FWHM bandwidth less than 0.03 nm is shown in Figure VII.2.

VII.6.3 Results

The spectra of the two output modes of a single 532 nm laser pulse were measured for different laser light pulse energies. Figure VII.20 shows the photo displays of the output light spectra from the CCD camera. Figure VII.20(a) is the photo display of the laser light spectrum at very low light pulse energy (<0.1 nJ). The image of the two lobes of LP_{11} mode can be seen in the photo display. By adjusting the coupling objective lens and the fiber very subtly, most of the input laser light energy (>90%) was coupled into the LP_{11} mode. The light energy coupled into LP_{01} mode was relatively less (<10%). The image of the LP_{01} mode was located into the middle of the two lobes of LP_{11} mode and it can not be seen clearly.

For a laser light pulse with pulse energy of 7 nJ, the spectral photo display is shown in Figure VII.20(b). The spectra of the two lobes of the LP_{11} mode broadened equally due to SPM of this mode. The spectrum of LP_{01} mode can not be seen in the photo picture since the intensity of light coupled to this mode is too weak. For a higher input light pulse energy at 10 nJ, the spectra of the two modes are shown in Figure VII.20(c). The spectrum of LP_{01} mode was broadened farther than the spectrum of the LP_{11} mode. The broadening of the LP_{01} mode spectrum is larger than that of the LP_{11} mode. The spectral broadening of LP_{11} mode was caused by SPM of the mode itself. For LP_{01} mode, its spectral broadening was induced by the DXPM between two propagation modes. The spectrum of LP_{01} mode is broader than that of LP_{11} mode since most of the light energy was coupled into LP_{11} mode. Approximately, LP_{01} mode spectral broadening is twice larger that of the LP_{11} mode. When the input light pulse energy was

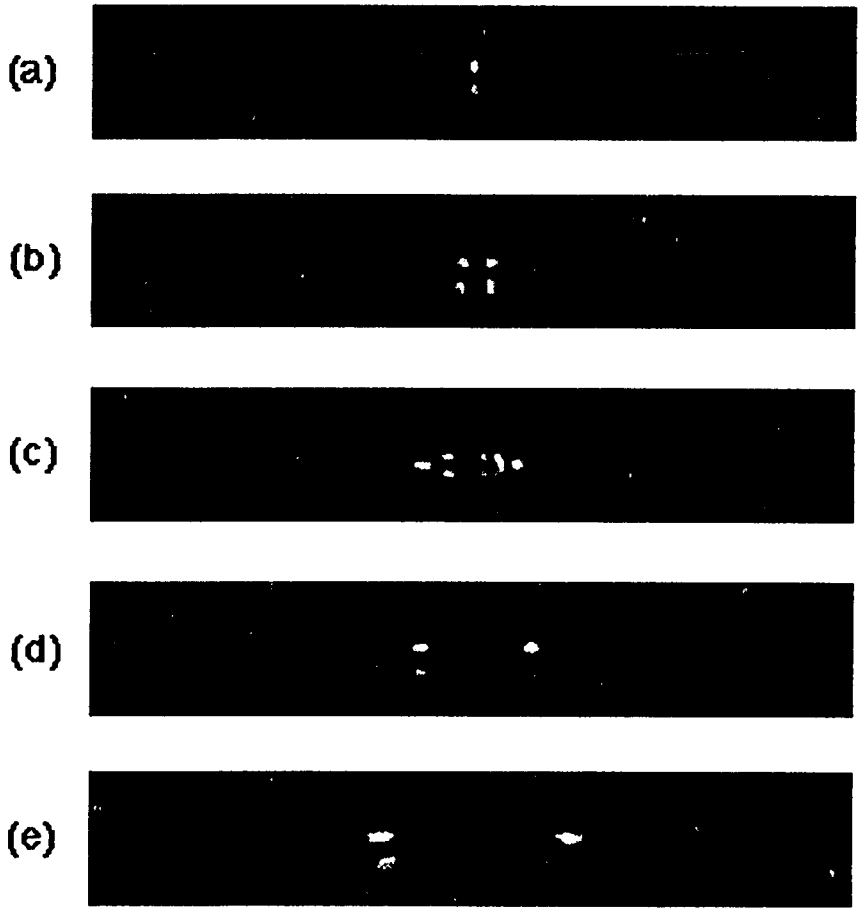

Figure VII.20 The photo displays of the spectral broadening for different fiber mode in a multi-mode optical fiber at different laser light pulse energy. The spectra of two light modes were recorded simultaneously by a CCD camera. (a) the spectra of two light mode at very low light pulse energy (<0.1 nJ), two spots are LP_{11} mode, the weak LP_{01} mode was in the middle of the LP_{11} mode; From (b) to (e) are the spectra of the two light modes at the pulse energy of (b) 7.0 nJ, (c) 10.0 nJ, (d) 25 nJ, and (e) 37 nJ. It can be seen that two fiber modes have different broadening.

increased to 25 nJ, more clear spectrum of DXPM between modes can be seen in Figure VII.20(d).At a very large pulse energy of 37 nJ, the spectral photo displays are shown in Figure VII.20(e). The SPM and DXPM spectra of the two modes gave more broadening for the large input pulse energy. It seems that the spectra were broadened far beyond the DXPM broadening range. This may be induced by the rapidly arising SRS effect at high pulse energy.

The photo images of the spectral broadening of the light at different fiber modes shown in Figure VII.20 can be digitized along the rows of pixels to reduce the mixture of the spectra at different modes. The spectra of LP_{11} mode was digitized by reading the pixel along the row passing through the center of the upper lobe (or the lower one). The spectra of the LP_{01} mode was digitized by reading the pixel of the row passing through the middle of the two lobes of LP_{11} mode. Using this way, the spectra of the two light modes were separated. The normalized spectra at different input pulse energies are shown in Figure VII.21. Left and right column are the spectra of LP_{11} and LP_{01} modes, respectively. Figure VII.21(a) shows the input laser light spectra of the two propagation modes. Figure VII.21(b) and (c) display the normalized spectra of the two modes at the light pulse energy of 10 nJ and 25 nJ, respectively.

VII.6.4 Fitting of Data

In this experiment, linearly polarized laser light pulses were used to observe the DXPM process between different fiber modes. When light was coupled into the multimode fiber into different fiber modes, lights at different modes remain linearly polarized. The nonlinear wave equations for two parallely linearly polarized optical waves were used here for the theoretical simulation. These nonlinear wave equation from Eqs. (II.38) can be expressed as:

$$\frac{\partial A_h}{\partial z}+\frac{1}{v_{gh}}\frac{\partial A_h}{\partial t}+\frac{i}{2}k_h^{(2)}\frac{\partial^2 A_h}{\partial t^2}=i\frac{\omega n_2}{c}(|A_h|^2+2|A_l|^2)A_h, \qquad \text{(VII.4a)}$$

$$\frac{\partial A_l}{\partial z}+\frac{1}{v_{gl}}\frac{\partial A_l}{\partial t}+\frac{i}{2}k_l^{(2)}\frac{\partial^2 A_l}{\partial t^2}=i\frac{\omega n_2}{c}(|A_l|^2+2|A_h|^2)A_l \qquad \text{(VII.4b)}$$

where A_h and A_l are the slow changing amplitudes of the high- and low-order modes, respectively (LP_{11} and LP_{01} modes). V_g and $k^{(2)}$ are the group velocity and GVD, respectively. Eq. (VII.4) have very similar with the Eq. (VII.2) except that the coefficients of XPM and SPM are different. Eq. (VII.4) can be solved using the same method.

The theoretical fittings were calculated using Eqs.(VII.4) at the different input pulse energies. To compare the fittings with the experimental results, the portions of light coupled to LP_{11} mode and the light coupled to LP_{01} mode was adjusted to be 90% and 10%, respectively in the theoretical calculations. The fiber length was 1 meter. Nonlinear refractive index $n_2=3.2\times10^{-20}m^2/W$. Because of the small bandwidth of the laser light, the dispersion terms were dropped in Eqs. (VII.4). The calculated results are shown in Figure VII.22. Figure VII.22(a) shows the calculation of the input laser light spectrum. Figure VII.22(b) and 22(c) show the calculated spectra of the LP_{11} and LP_{01} modes at laser pulse energy of 10 nJ and 25 nJ, respectively.

The spectral broadening of the LP01 mode is attributed to the DXPM process between the two fiber modes. The SPM process of the LP_{11} mode dominates its own spectrum. There are good agreements between the experimental results and theoretical calculations for the spectra of the LP_{11} mode, as shown in left column of Figure

VII.22(b) and 22(c). The slight difference is attributed to the limited resolution of our spectral measurement system.

The calculated spectra of LP_{01} mode as shown in the right column of Figure VII.22(b) and (c) show similar broadening to the measured spectra displayed in Figure VII.21(b) and (c). The theoretical profiles reproduces the LP_{01} mode spectra off the central region, but do not well fit the spectra in the central region. The difference in the middle spectral region is believed to arise from the disturbs of LP_{11} mode. Since the resolution of the spectral analysis system was not high enough, the spectra of the two modes can not be completely separated on the CCD camera screen. When the digitized spectrum of LP_{01} mode was taken along a row of CCD pixels. Some portion of LP_{11} mode spectra was accounted in the LP_{01} mode spectrum. Considering the intensity of LP_{11} mode was much stronger than that of LP_{01} mode, small portion of LP_{11} light will greatly modify the spectral structure of LP_{01} mode in the central region.

In this section, DXPM process between two light propagation modes of LP_{11} and LP_{01} in a multi-mode optical fiber has been observed for a single shot 35 ps laser light pulse. The DXPM induced spectral broadening was observed for different input light pulse energy. The experimental results are in reasonable agreement with the theoretical calculation.

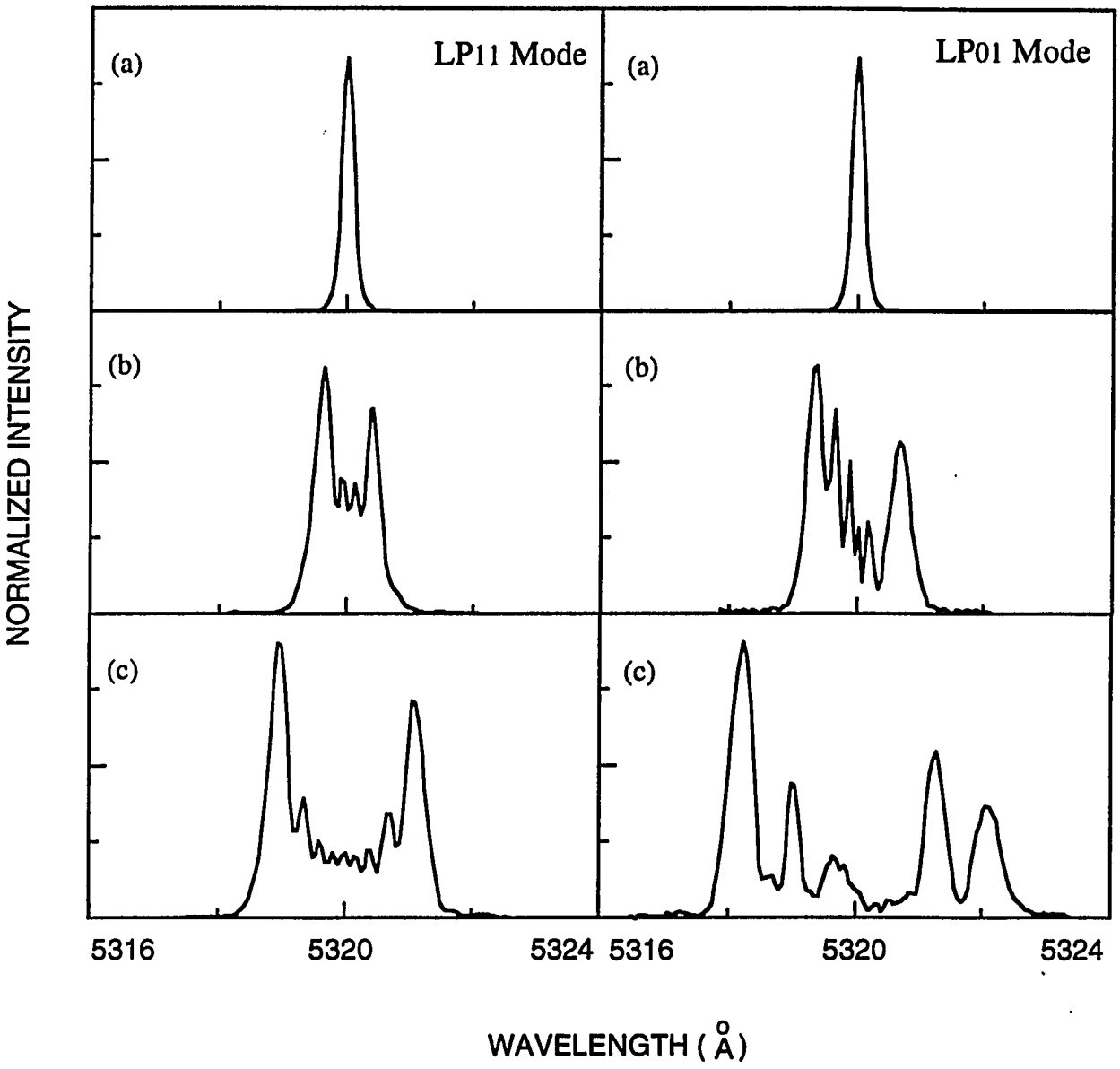

Figure VII.21 The normalized measured spectra of different fiber modes in a multi-mode optical fiber at different laser light pulse energy. (a) the spectra of two light mode at very low light pulse energy (<0.1 nJ); (b) the spectra of the two light modes at the pulse energy of 10 nJ; and (c) 25 nJ.

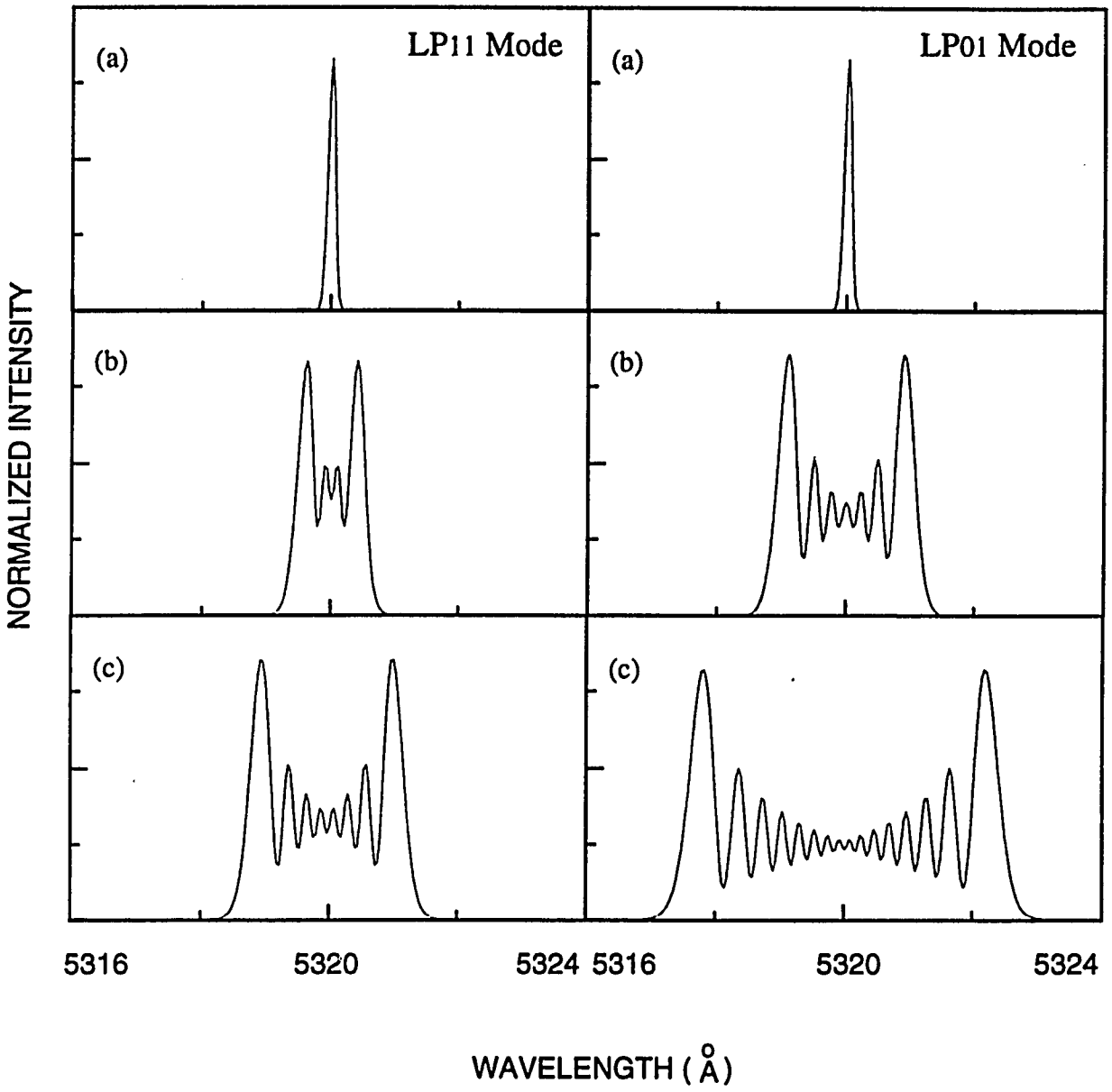

Figure VII.22 The calculated spectra of different fiber modes in a multi-mode optical fiber at different laser light pulse energy. (a) the spectra of input laser light; (b) the spectra of the two light modes at the pulse energy of 10 nJ; and (c) 25 nJ.

References:

[1] G. P. Agrawal, Nonlinear Fiber Optics (Academic Press, Inc., 1989), Chap. 1, p. 15.

[2] R. R. Alfano and Shapiro, Phys. Rev. Lett. **24**, 584, 1217 (1970).

[3] R. Fork, C. Shank, C. Herliman, R. Yen and W. J. Tomlinson, Opt. Lett. **8**, 1 (1983).

[4] G. Yang and Y. R. Shen, Opt. Lett. **9**, 510 (1984).

[5] R. H. Stolen and Chinlon Lin, Phys. Rev. A **17**, 1448 (1978).

[6] E. P. Ippen, C. V. Shank and T. K. Gustafson, Appl. Phys. Lett. **33**, 1765 (1974).

[7] Q. Z. Wang, Q. D. Liu, Disa Liu, P. P. Ho and R. R. Alfano, J. Opt. Soc. Am. B. **11**, 1084-1089 (1994).

[8] R. R. Alfano, Q.X. Li, T. Jimbo, J. T. Manassah, and P. P. Ho, Opt. Lett. **11**, 626 (1986).

[9] C. C. Yang and Alex J. S. Wang, J. Opt. Soc. Am. B 9, 682 (1992).

[10] M. N. Islam, L. F. Mollenauer, R. H. Stolen, J. R. Simpson, H. T. Shang, Opt. Lett. **12**, 625 (1987).

[11] P. L. Baldeck, R. R. Alfano and G. P. Agrawal, Appl. Phys. Lett. **52**, 1939 (1988).

[12] K. J. Blow, N. J. Doran and B. P. Nelson, Opt. Lett. **10**, 393 (1985)

[13] Q. Z. Wang, P. P. Ho and R. R. Alfano, Opt. Lett. **15**, 1023 (1990).

[14] B. Crosignani, B. Daino, P. D. Porto, J. Opt. Soc. Am. B **3**, 1120 (1986)

[15] H. E. Bates, R. R. Alfano and N. Schiller, Appl. Opt. **18**, 947 (1979)

[16] Q. D. Liu, J. T. Chen, P. P. Ho and R. R. Alfano, IEEE Phot. Tech. Lett., **7**, 517 (1995).

[17] M. Sylla, P. X. Nguyen, D. Rouede, and G. Rivoire, J. Appl. Phys. **71**, 5318 (1992).

[18] P. L. Baldeck, F. Raccah, and R. R. Alfano, Opt. Lett., **12**, 588 (1987).

Chapter VIII
FUTURE RESEARCH DIRECTIONS

VIII.1 Introduction:

Optical technology offers many advantages for computation, communication, and signal processing over electronic technology to improve the time and frequency responses of working system. Many electronic devices such as computers, A/D converters and amplifiers which are relatively slow have limited the performance of the electronic system in applications. In optical communication, optical computation, and optical information technology, all optical devices have been drawing considerable interests because of the intrinsic higher speed and wider bandwidth of an optical channel than an electronic one.

For the ultrafast optical signal processing, light can be used to control light. Many applications using third-order nonlinear processes have been developed, such as all optical switches[1], logic-gates[2-3], and multiplexer/demultiplexer[4] based on the optical Kerr effect in nonlinear waveguides. Because of the increased uses of fiber-optic sensors and fiber-optic communications, signals applied to an optical signal processor are often optical, and thus all optical devices (optical amplifiers and A/D converters) should be used to handle ultrafast optical signals (>1 THz). They are also needed to handle real-time data for the optical signal processing applications such as spread spectrum communication, lidar, fiber-optic sensors, etc. Several examples of all optical amplification are stimulated Raman amplifiers[5], erbium-doped fiber amplifiers(EDFA)[6-7], and diode-laser amplifiers[8]. But each of these is limited to the gain bandwidth of the effects used. Using the optical Kerr effect in a lowbirefringent single-mode optical fiber, a modulational gain at the orthogonally polarized direction of

linearly polarized laser input has been observed at high laser intensities[9-10]. An broadband all-optical amplifiers has been proposed by using the optical Kerr effect[9].

Optical analog-to -digital (A/D) conversion has been demonstrated and proposed using an electro-optic waveguide[11], a liquid crystal device[12], and optical logic and a look-up table[13]. an electro-optic guided wave A/D converter has been demonstrated with bandwidths exceeding 10 GHz[14]. Using a nonlinear fiber interferometer, all-optical A/D conversion has been implemented by J.-M, Jeong *et al.*[15]. A more sophisticated design of an all-optical A/D converter based on the cross-phase modulation (XPM) has been proposed for ultrashort intense laser light pulses co-propagating in an optical fiber[16].

In this chapter, the future research is proposed based upon my thesis work. The basic concept of an all-optical amplifier based on the phenomena of SPM and XPM processes in a single-mode optical fiber will be proposed. The basic unit of the all-optical amplifier can be used as the heart of future computers and communication systems. A weak optical signal will be amplified by the all-optical amplifier using an intense pump optical wave copropagating in optical fibers.

VIII.2 All-optical Amplifiers

VIII.2.1 Basic Principle of Optical Amplification

A schematic diagram of an all-optical amplifier is shown in Figure VIII.1, the pump signal (B) and the signal (A) both are linearly polarized. They are perpendicular for the amplification of the weak signal (A). When these linearly polarized laser pulses (A) and (B) are coupled into an single-mode optical fiber, they will co-propagate in the optical fiber like a single pulse having two perpendicular linearly polarized components. Considering nonlinear polarization stabilities of the laser pulse propagating in an optical fiber[11], the two opposite circularly polarized components are used in the theoretical analysis. Assuming the amplitudes of the pump (B) and signal (A) are A_p and A_S, respectively, the amplitudes of the two circularly polarized components are $A_R=A_p+A_S$ and $A_L=A_p-A_S$ for right-handed and left-handed, respectively. When these two circular components copropagate in an optical fiber, both components will have an unbalanced nonlinear phase modulation. The difference of the phase modulation will cause the pump light to be coupled into the signal polarization mode and to be selected as the amplified output by a second polarizer.

The nonlinear wave equations for two circularly polarized light pulses propagating in an optical fiber which is an isotropic medium can be expressed as :

$$\frac{\partial A_R}{\partial z}+\frac{1}{v_{gR}}\frac{\partial A_R}{\partial t}+\frac{i}{2}k_R^{(2)}\frac{\partial^2 A_R}{\partial t^2}=i\frac{wn_2}{c}\left(\frac{2}{3}|A_R|^2+\frac{4}{3}|A_L|^2\right)A_R, \qquad \text{(VIII.1a)}$$

$$\frac{\partial A_L}{\partial z}+\frac{1}{v_{gL}}\frac{\partial A_L}{\partial t}+\frac{i}{2}k_L^{(2)}\frac{\partial^2 A_L}{\partial t^2}=i\frac{wn_2}{c}\left(\frac{2}{3}|A_L|^2+\frac{4}{3}|A_R|^2\right)A_L, \qquad \text{(VIII.1b)}$$

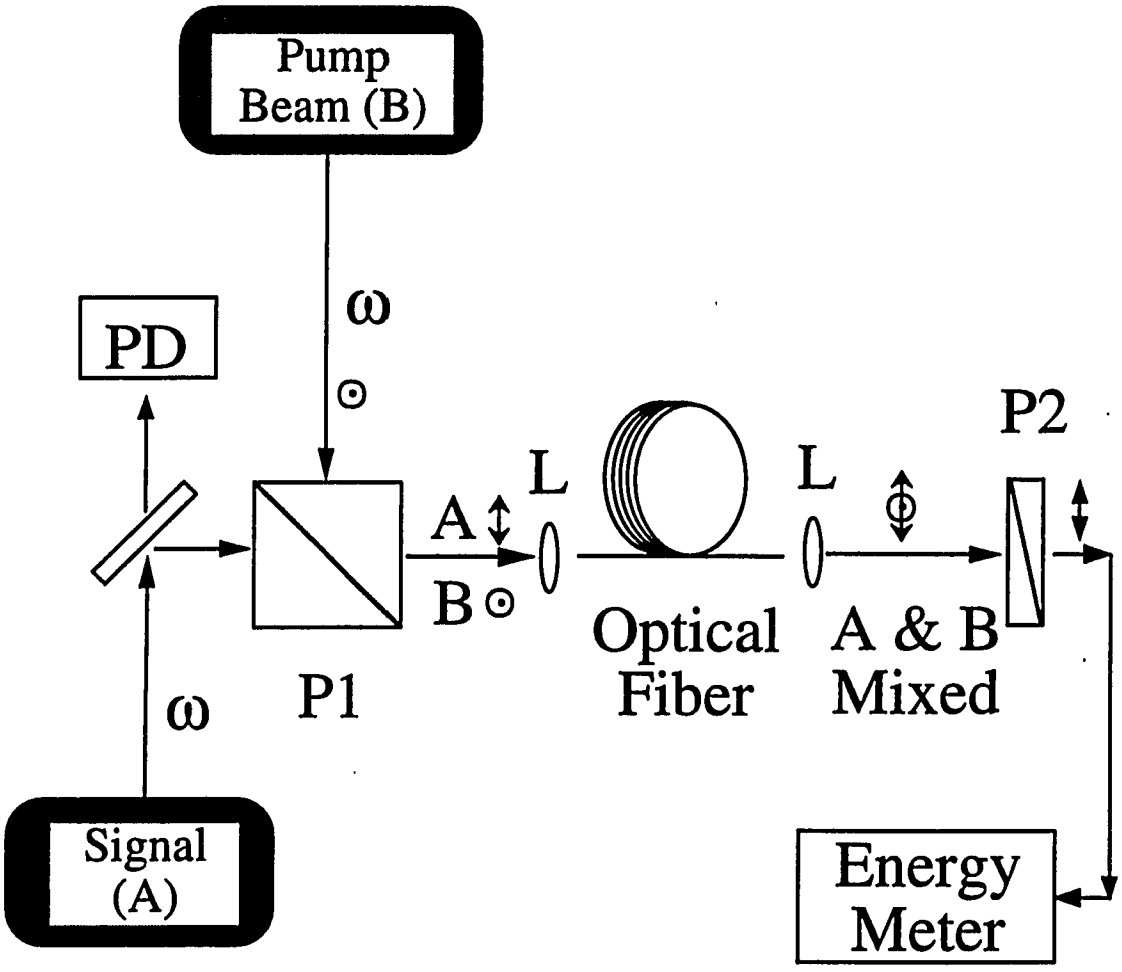

Figure VIII.1 Principle design of the polarization-controlled all-optical amplifier (optical amplifier). P1: polarizing prism; P2: polarizer; L: lens; PD: photo-diode.

where v_{gR} and v_{gL} are the group velocities for right-handed and left-handed components, respectively, and $v_{gR} = v_{gL}$, $k^{(2)}$'s are the group- velocity dispersion(GVD), and $n_2=3\chi^{(3)}/8n$ is the nonlinear refractive index. The amplitudes and phases of the pulse envelope are denoted by A and α, respectively:

$$A_{R(\tau,z)} = a_{R(\tau,z)} e^{i\alpha_{R(\tau,z)}}, \text{ and } A_{L(\tau,z)} = a_{L(\tau,z)} e^{i\alpha_{L(\tau,z)}}, \qquad \text{(VIII.2)}$$

where $\tau = (t - z/v_g)/T_0$ is the local time in the pulse and T_0 is the 1/e pulse duration, and assuming that $k_R^{(2)} = k_L^{(2)} = 0$ Eqs. (VIII.1a) and (VIII.1b) reduce to

$$\frac{\partial a_R}{\partial z} = 0, \qquad \text{(VIII.3a)}$$

$$\frac{\partial \alpha_R}{\partial z} = i\frac{\omega}{c} n_2 \left(\frac{2}{3} a_R^2 + \frac{4}{3} a_L^2\right), \qquad \text{(VIII.3b)}$$

$$\frac{\partial a_L}{\partial z} = 0, \qquad \text{(VIII.3c)}$$

$$\frac{\partial \alpha_L}{\partial z} = i\frac{\omega}{c} n_2 \left(\frac{2}{3} a_L^2 + \frac{4}{3} a_R^2\right). \qquad \text{(VIII.3d)}$$

For a Gaussian pulse at z=0:

$$A_{R(\tau, z=0)} = A_{R0} e^{-\tau^2/2}, \text{ and } A_{L(\tau, z=0)} = A_{L0} e^{-\tau^2/2}, \qquad \text{(VIII.4)}$$

where $A_{R0}(A_{L0})$ is the initial right-handed (left-handed) amplitude. With these initial conditions, the solutions for the phase of the pulse after propagating a distance z in an optical fiber are:

$$A_{R(\tau,z)} = A_{R0}, \text{ and } \quad A_{L(\tau,z)} = A_{L0}, \qquad \text{(VIII.5a)}$$

$$\alpha_R(\tau, z) = \frac{\varpi}{c} n_2 z \left(\frac{2}{3} I_{R0} + \frac{4}{3} I_{L0}\right) e^{-\tau^2}, \qquad \text{(VIII.5b)}$$

$$\alpha_L(\tau, z) = \frac{\varpi}{c} n_2 z(\frac{2}{3} I_{L0} + \frac{4}{3} I_{R0}) e^{-\tau^2}, \qquad \text{(VIII.5c)}$$

where $I_{R0}(I_{L0})$ is the intensity of the right(left)-handed component. Taking $\Delta I = | I_{R0} - I_{L0} |$ is the intensity difference for the two components. The induced phase shift is:

$$\Delta\alpha(\tau, z) = |\alpha_R - \alpha_L| = \frac{4\pi}{3\lambda} n_2 z \Delta I e^{-\tau^2}, \qquad \text{(VIII.6)}$$

From the solutions of (VIII.5) and (VIII.6), the amplitudes of any two counter-rotating circularly polarized laser pulses are stable. There is no exchange of energy caused by nonlinear interaction between these two circularly polarized laser pulses. There will be a phase shift between the two pulses when their amplitudes are not equal. The nonlinear phase modulations can change the polarization state of propagating laser pulses. When there is only the linearly polarized pump laser pulse, this laser pulse can be regarded as superposition of two circularly polarized components with the same amplitude and their nonlinear phase changes are equal.

At the exit of an optical fiber, the result of the superposition of the two circular polarization states is the original linear polarization state. When a weak signal pulse which is perpendicularly linearly polarized is sent into this optical amplifier, the incident laser pulses have two linearly polarized components. We can also use two circularly polarized components to describe this polarization state. The relations between linear and circular polarization bases are:

$$\vec{e}_X = \frac{1}{\sqrt{2}}(\vec{e}_R + \vec{e}_L), \qquad \text{(VIII.7a)}$$

$$\vec{e}_Y = \frac{i}{\sqrt{2}}(\vec{e}_R - \vec{e}_L), \qquad \text{(VIII.7b)}$$

The total electric field of the input optical wave is:

$$\begin{aligned}\vec{E} &= E_X \vec{e_X} + i E_X \vec{e_X} \\ &= E_X \frac{1}{\sqrt{2}}(\vec{e_R} + \vec{e_L}) + i E_Y \frac{i}{\sqrt{2}}(\vec{e_R} - \vec{e_L}) \\ &= \frac{1}{\sqrt{2}}(E_X + E_Y)\vec{e_R} + \frac{1}{\sqrt{2}}(E_X - E_Y)\vec{e_L}, \end{aligned} \qquad \text{(VIII.8)}$$

The magnitudes of I_{R0} and I_{L0} which are the intensities of the right-handed and left-handed circularly polarized components, respectively became unequal with a difference:

$$\Delta I = \frac{1}{2}(E_X+E_Y)^2 - \frac{1}{2}(E_X-E_Y)^2 = 2E_X E_Y, \qquad \text{(VIII.9)}$$

In this device, the pump is along x-direction and signal is along y-direction, therefore, $E_s \equiv E_X$ and $E_p \equiv E_Y$. In this arrangement, we have $I_s=E_x^2$, $I_p=E_Y^2$; substituted into equation (VIII.9):

$$\Delta I = 2\sqrt{I_p}\sqrt{I_s}, \qquad \text{(VIII.10)}$$

where I_p and I_s are the intensities of the two linearly polarized components which are corresponding to the intensities of the pump pulse and the weak signal pulse, respectively. The phases of the two circular polarization are shifted after propagating through an optical fiber. The induced phase shift is given by:

$$\Delta\alpha(\tau,z) = |\alpha_R - \alpha_L| = \frac{8\pi}{3\lambda} n_2 z \sqrt{I_p}\sqrt{I_s}\, e^{-\tau^2} . \qquad \text{(VIII.11)}$$

The phase shift is a function of time due to its dependence on the local time τ. The superposition of the two circularly polarized components with equal amplitude will always give rise to a linear polarization state no matter what the phase difference is. For a phase shift of $\Delta\alpha(\tau,z)$, the linearly polarized output will rotate by an angle of $\Delta\alpha(\tau,z)/2$. Therefore, the output optical pulse at the fiber exit will keep to be almost linearly polarized in propagation, but the polarization direction will change at different local time. The output is a polarization twisted optical pulse. After the polarizing prism which was set at the orthogonally polarized direction with that of the pump pulses, the pulse intensity is modulated with a $\sin^2(\Delta\alpha/2)$ function, the optical amplifier output energy is:

$$P_{out} = \int_{-\infty}^{\infty} I_p e^{-\tau^2} \sin^2(k e^{-\tau^2}) d\tau \quad , \qquad \text{(VIII.12)}$$

where $k = 4\pi n_2 z \sqrt{I_p}\sqrt{I_s}/3\lambda$ is a nonlinear phase parameter.

Amplification effect of a weak optical signal can be observed by analyzing these equations from (VIII.6) to (VIII.12). When there is only the linearly polarized pump beam, this pump laser beam will propagate in the optical fiber without any change on its polarization state. At the fiber exit, the output laser beam is at its input linear polarization and it can not pass a polarizer which is perpendicular to the input polarization state. There will be no output. When the linearly polarized pump laser beam is coupled into the optical fiber with a linearly polarized weak signal optical beam which is at the perpendicular polarization of the pump beam, the nonlinear phase shift in equation (VIII.11) will cause the linear polarizing direction of the pump laser beam rotates with an certain angle which depends on the pump intensity and pulse local time. At the fiber exit, the output pulse energy for laser pulses after a polarizer which is perpendicular to the

input pump polarizing direction (parallel to the weak signal polarizing direction) are given by equations (VIII.12). The polarization rotation of the pump beam will lead the pump energy coupled into the output polarizing direction. The energy of the input weak signal light pulse will be amplified.

VIII.2.2 Characteristic curves of the Optical Amplifier:

The output pulse energy of the optical amplifier can be calculated by using the equation (VIII.7) for pumping with laser pulses (B). The calculations of the optical amplifier output energy are shown in Figure VIII.2 for five different pump pulse (B) energies which are 20, 40, 60 80 and 100 nJ, respectively, at pulse durations of 35 ps for different input signal energies. When the energy of input signal (A) is increased under a given pump energy, the output is also increased. At low input signal energy, the optical pulse is almost linearly amplified. There is a saturation effect of amplification for a high input energy of signal pulse (A). This is not surprising because most of the pump energy (up to 80 %) is coupled into the output laser pulse at high input pulse energy. To increase the input signal energy further, there is no more energy can be coupled. If the input pulse energy is large enough, the output pulse energy will decrease and then will show an oscillating characteristic because of nonlinear phase modulations which is not displayed in Figure VIII.2. For the same input signal pulse energy, the higher the pump energy, the larger the output energy. The calculations in Figure VIII.2 for different pump energies show that an optical amplifier with higher pump energy has a lower input signal energy at which the amplification saturation happens. On other words, an optical amplifier with a lower pump energy will yield a larger dynamic range for the input signal energy. One problem is if the pump pulse energy is set too low, the gain of amplification will be small.

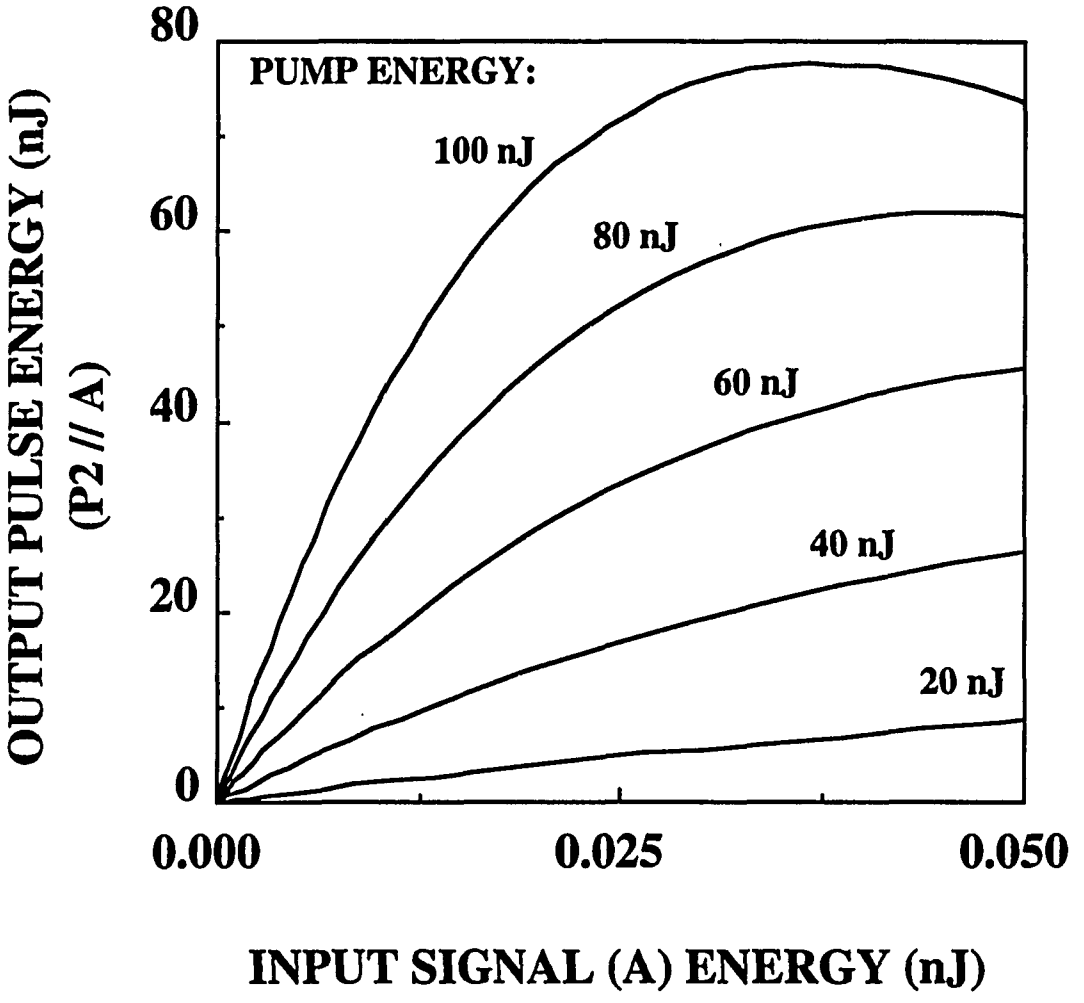

Figure VIII.2 The output energies of an optical amplifier under different pump pulse energies.

The percentage (T) of the transferred energy from the polarization state of pump pulse (B) to that of signal pulse (A) is calculated by using:

$$T = P_{\perp} / P_0, \qquad \text{(VIII.13)}$$

where P_0 is the energy of the pump pulse and $P_{\perp}$ is the output of the amplifier. The calculated results for T are shown in Figure VIII.3. At the same input signal pulse energy of (A), higher pump pulse energy of (B) will give a higher coupling efficiency for small input signal energies of (A). The saturation will appear for large input signals.

The gain factor for the weak signal pulse (A) under the different energies of pump pulse (B) can also be calculated by:

$$G = \frac{\Delta I_{out}}{\Delta I_{in}}, \qquad \text{(VIII.14)}$$

where ΔI_{in} is the change of the input signal pulse energy and ΔI_{out} is the corresponding change of the output pulse energy of this all-optical amplifier. The output energy gain factors versus signal energies of signal (A) are displayed in Figure VIII.4 for five different pump pulse energies from 20 to 100 nJ. For the same input pulse signal energy of (A), higher pump energy of (B) will give a higher energy gain factor. For the same pump pulse energy of (B), the gain factor keep constant at low input signal pulse energy of (A). At the area where the saturation effect happens, the energy gain factor will decrease dramatically. A trade-off effect can also be seen here which is a lower gain factor (lower pump energy) combining with a larger dynamic range of input signal energy, but a higher gain factor (higher pump energy) combining with a smaller dynamic range of input signal energy.

The temporal profile of the output laser pulse (mixed with A and B) can be calculated by using the same expression (9) without the integration of local time. The temporal profiles of the optical amplifier output laser pulse were calculated for different nonlinear phase shifts as shown in Figure VIII.5. The calculations have shown that the output laser pulse was slightly-off Gaussian distribution for Gaussian pump pulse (B) and signal pulse (A). The output pulse duration was about 0.75 times of that of the incident signal pulse. In Fig. 6, (a) is the incident Gaussian pulse; (b) is the temporal profile for k=0.1 which is for very weak input signal pulse; and (c) is the output pulse profile for k=1.5 which is for relative strong input signal pulse (A).

In application, the pump laser pulses and the weak signal pulses were orthogonally linearly polarized. Hence, the sensitivity of this all-optical amplifier depends on the extinction ratio of pump pulse (B). Any depolarization from pump pulse (B) will decrease the sensitivity of the optical amplifier.

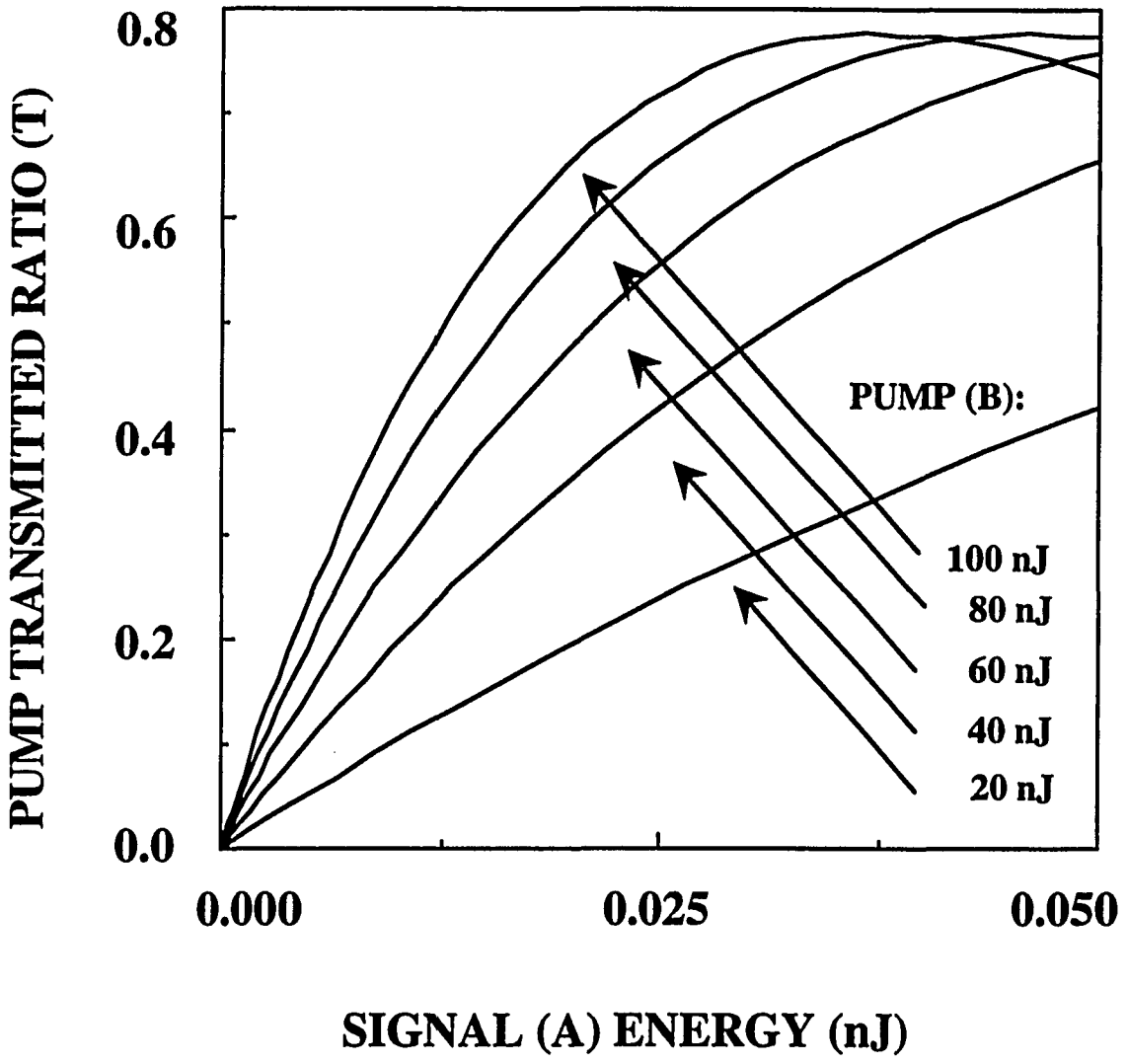

Figure VIII.3 The transmission ratio of an optical amplifier for different pump pulse energies.

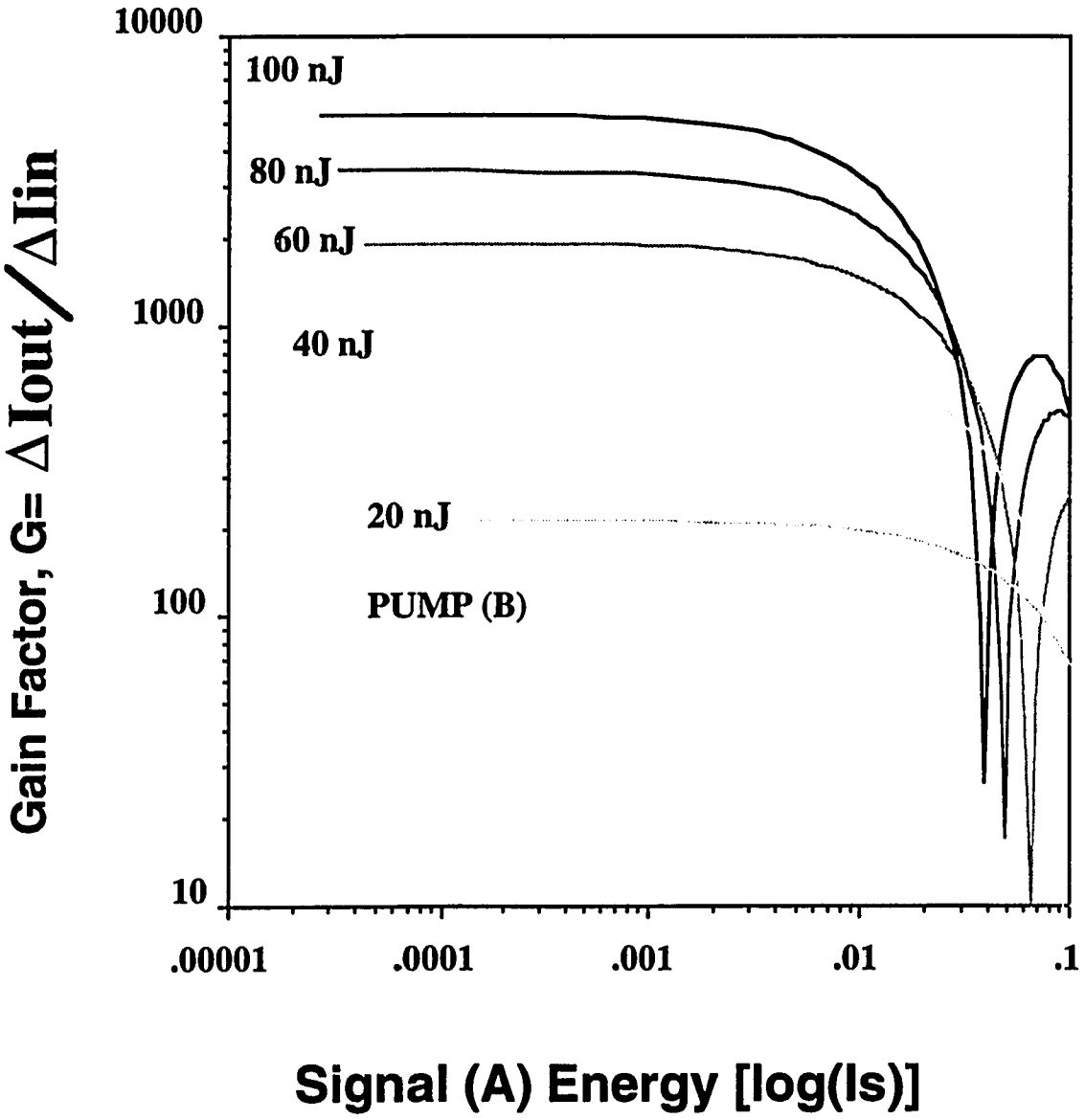

Figure VIII.4 The gain characteristic curves of an optical amplifier for different optical pump pulse energy.

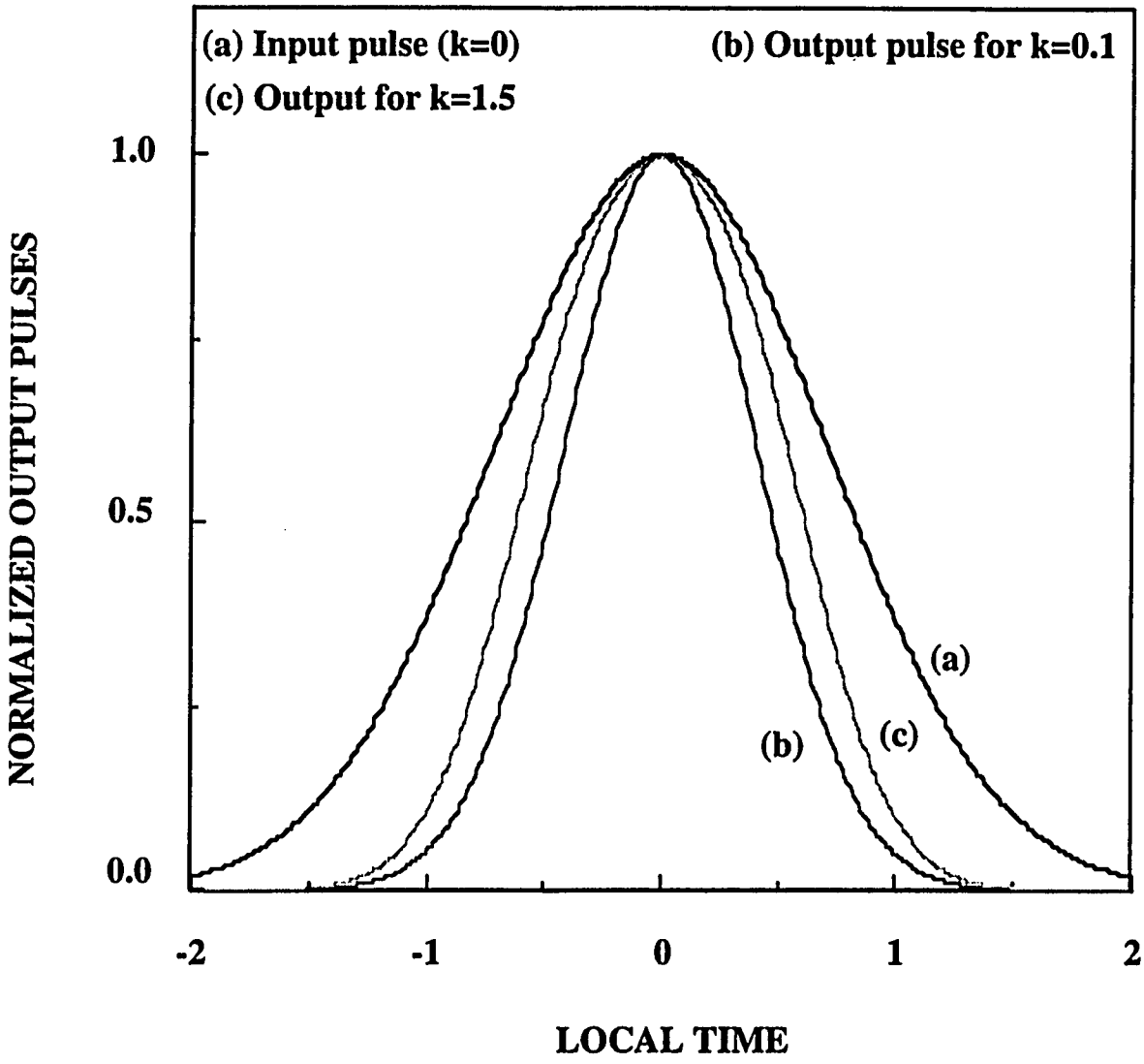

Figure VIII.5 optical amplifier output pulse compression effect. (a). incident laser pulse with a Gausain distribution; (b). output pulse temporal profile for a small signal of nonlinear phase shift k=0.1; (c). output pulse temporal profile for a relatively high intensity signal of k=1.5.

References:

[1]. M. J. lagers, D. Liu-wong, J. G. and H. A. Has, Opt. Lett. **14**, 311-313, (1989).

[2]. Y. Kimura, K. I. Kitayama, N. Shibata and S. Seikai, Electron. Lett. **22**, 277 (1986).

[3]. J. -M. Jeong and M. E. Marhic, Opt. Comm. **85**, 430 (1991).

[4]. T. Morioka, M. Saruwatari and A. Takada, Electron. Lett. **27**, 210 (1991).

[5]. M. Nakazawa, Appl. Phys. Lett. **46**, 628 (1985).

[6]. R. J. Mears, L. Reekie, I. M. Jauncey, and D. N. Payne, Electron. Lett. **23**, 1026 (1987).

[7]. M. Nakazawa, K. Kurokawa, H. Kubota, K. Suzuki, and Y. Kimura, Appl. Phys. Lett. **57**, 653 (1990).

[8]. M. J. Mahony, in Digest of Conference on Integrated Optics and Optical Fiber Communication (Istituto Internazionale Delle Communicazioni, Venice, Italy, (1985), Vol. **2**, p. 39.

[9]. A. S. Davison, and I. H. White, Opt. Lett. **14**, 802 (1989).

[10]. S. F. Feldman, D. A. Weinberger, and H. G. Winful, Opt. Lett. **15**, 311 (1990).

[11]. R. A. Becker, C. E. Woodward, F. J. Leonberger, and R. C. Williamson, IEEE Proc., **72**, 802 (1984).

[12]. A. Armand, A. A. Sawchuck, T. C. Strand, D. Boswell, andB. H. Soffer, Opt. Lett., **5**, 129 (1980).

[13]. A. D. McAulay, Opt. Lett., **29**, 114 (1990).

[14]. R. G. Walker, and I. Bennion, SPIE, **1141**, 138 (1989).

[15]. J.-M, Jeong, and M. E. Marhic, Opt. Commu., **91**, 115 (1992).

[16]. P. P. Ho, Q. Z. Wang, Q. D. Liu, Disa Liu, and R. R. Alfano, SPIE, **2155**, 37 (1994).

APPENDIX

Nonlinear Wave Equations and Solutions of Optical Waves in Optical Fibers

In chapter II, the general form of the nonlinear wave equations of an optical wave propagating in a nonlinear medium has been studied. The time-dependent nonlinear wave equation can be expressed as:

$$i\left(\frac{\partial A_{(z,t)}}{\partial z}+\frac{1}{\upsilon_g}\frac{\partial A_{(z,t)}}{\partial t}\right)-\frac{1}{2}k_0^{(2)}\frac{\partial^2 A_{(z,t)}}{\partial t^2}=-\frac{2\pi\omega_0}{k_0c^2}P_{NL}(z,t) \times\exp[-i(k_0z-\omega_0t)]. \qquad \text{(II.22)}$$

where υ_g is the group velocity and $k_0^{(2)}$ is the group-velocity dispersion (GVD). In Eq. (II.22), the first two terms on the left side describes the developing propagation at the group velocity; the third term determines the temporal pulse broadening due to the group velocity dispersion; and the term which contains nonlinear polarization P_{NL} on the right side characterizes the nonlinear polarization which is responsible for different kinds of nonlinear phenomena. P_{NL} depends on different conditions such as for SPM and XPM under different polarization bases.

The nonlinear polarization P_{NL} can be expressed as

$$\vec{P}_{NL}=\sum_i P_i\vec{e}_i, \qquad \text{(A.1)}$$

where Pi is the nonlinear polarization component at the i direction (i=x, y, z). In a nonlinear medium possessing third-order nonlinearity, these nonlinear polarization components are:

$$P_i = \sum_{jkl} \chi^{(3)}_{ijkl} E_j E_k E_l, \qquad i=x, y, z; \tag{A.2}$$

where $\chi^{(3)}_{ijkl}$ is the third-order nonlinear suceptibility of the material which is a tensor and has 81 components in all. In an isotropic nonlinear medium, most of the components are zero. The non-zero components of the third-order nonlinear suceptibility are listed as follows:

$$\chi_{xxxx} = \chi_{yyyy} = \chi_{zzzz} = \chi, \tag{A.3a}$$

$$\chi_{xxxx} = \chi_{yyyy} = \chi_{zzzz} = \chi, \tag{A.3b}$$

$$\chi_{xxyy} = \chi_{yyxx} = \chi_{zzxx} = \chi_{xxzz} = \chi_{yyzz} = \chi_{zzyy} = \frac{1}{3}\chi, \tag{A.3c}$$

$$\chi_{xyxy} = \chi_{xyyx} = \chi_{yzyz} = \chi_{yzzy} = \chi_{zxzx} = \chi_{zxxz} = \frac{1}{3}\chi, \tag{A.3d}$$

$$\chi_{yxyx} = \chi_{yxxy} = \chi_{zyzy} = \chi_{zyyz} = \chi_{xzxz} = \chi_{xzzx} = \frac{1}{3}\chi. \tag{A.3e}$$

By calculating the nonlinear polarization through the Eqs. (A.1) to (A.3), the nonlinear wave equations for SPM and XPM can be derived.

A.1 Nonlinear Wave Equation of Self-phase Modulation (SPM)

There only one optical wave for SPM, this optical wave is assumed to be linearly polarized at the x-axis direction. The electric field of this optical wave is;

$$\vec{E} = E_x \vec{e_x}, \tag{A.4}$$

where the amplitude Ex is

$$E_x = \frac{1}{2} A_{(z,t)} e^{-i(\omega t - \beta z)} + c.c.. \tag{A.5}$$

where $A_{(z,\,t)}$ is the slow-changing amplitude envelope of the optical wave. Substituting Eq. (A.5) into (A.2), one can find

$$P_x = \chi E_x^3, \text{ and } P_y = P_z = 0, \tag{A.6}$$

expanding E_x^3 using (A.5), one obtains

$$P_x = \frac{1}{8}\chi\{A_{(z,t)}^3 e^{-3i(\omega t-\beta z)} + 3A_{(z,t)}^2 A_{(z,t)}^* e^{-i(\omega t-\beta z)} + 3A_{(z,t)} A_{(z,t)}^{*2} e^{i(\omega t-\beta z)} + A_{(z,t)}^{*3} e^{3i(\omega t-\beta z)}\}, \tag{A.6a}$$

keeping only the terms at the same frequency with the incident optical wave, one has:

$$P_x = \frac{3}{8}\chi |A_{(z,t)}|^2 A_{(z,t)} e^{-i(\omega\, t-\beta z)} + c.c.. \tag{A.7}$$

Substituting (A.7) into the nonlinear wave equation (II.22), one has the nonlinear wave equation for SPM:

$$\frac{\partial A_{(z,t)}}{\partial z} + \frac{1}{\upsilon_g}\frac{\partial A_{(z,t)}}{\partial t} + \frac{i}{2} k_0^{(2)} \frac{\partial^2 A_{(z,t)}}{\partial t^2} = \frac{i\omega n_2}{c} |A_{(z,t)}|^2 A_{(z,t)}, \tag{A.8}$$

where $n_2 = 3\chi / 8n$ is the nonlinear refractive index. This equation can be further reduced by neglecting the group-velocity dispersion and expressed as:

$$\frac{\partial A}{\partial z} + \frac{1}{\upsilon_g}\frac{\partial A}{\partial t} = i\frac{\omega_o n_2}{c}|A|^2 A. \tag{A.9}$$

By changing the variables with:

$$\tau = t - z/\upsilon_g, \quad \text{and} \quad z'=z, \tag{A.10}$$

where t is real time, and τ is defined as the pulse local time. Therefore, one has

$$\partial\tau/\partial t = 1,\ \partial\tau/\partial z = -1/\vartheta_g; \text{ and}$$
$$\partial z'/\partial z = 1 \quad \partial z'/\partial t = 0, \tag{A.11}$$

substituting (A.11) into next variable change relation, one has

$$\frac{\partial}{\partial t} = \frac{\partial}{\partial \tau}\frac{\partial \tau}{\partial t} + \frac{\partial}{\partial z'}\frac{\partial z'}{\partial t} = \frac{\partial}{\partial \tau}, \tag{A.12a}$$

$$\frac{\partial}{\partial z} = \frac{\partial}{\partial z'}\frac{\partial z'}{\partial z} + \frac{\partial}{\partial \tau}\frac{\partial \tau}{\partial z} = \frac{\partial}{\partial z'} - \frac{1}{\vartheta_g}\frac{\partial}{\partial \tau}, \tag{A.12b}$$

putting (A.12) into nonlinear wave equation (A.9), that is

$$\left(\frac{\partial}{\partial z'} - \frac{1}{\vartheta_g}\frac{\partial}{\partial \tau} + \frac{1}{\vartheta_g}\frac{\partial}{\partial \tau}\right)A = i\frac{\omega_o n_2}{c}|A|^2 A,$$

i.e.

$$\frac{\partial A}{\partial z'} = i\frac{\omega_o n_2}{c}|A|^2 A. \tag{A.13}$$

Since z'=z, the equation can be expressed as

$$\frac{\partial A}{\partial z} = i\frac{\omega_o n_2}{c}|A|^2 A. \tag{A.14}$$

Denoting by $a_{(z,\tau)}$ and $\alpha_{(z,\tau)}$ the amplitude and the phase of the electric envelope of the laser pulse, respectively, the pulse slowly varying profile $A_{(z,t)}$ can be written as

$$A_{(z,\tau)} = a_{(z,\tau)}\exp[i\,\alpha_{(z,\tau)}]; \tag{A.15}$$

substituting (A.15) into (A.14), one has

$$\frac{\partial}{\partial z}(a\,e^{i\alpha}) = i\frac{\omega_o n_2}{c}a^2 a\,e^{i\alpha}, \tag{A.16}$$

expanding (A.16),

$$e^{i\alpha}\frac{\partial a}{\partial z} + ia\,e^{i\alpha}\frac{\partial \alpha}{\partial z} = i\frac{\omega_o n_2}{c}a^2 a\,e^{i\alpha}, \tag{A.17}$$

(A.17) is

$$\frac{\partial a}{\partial z} + ia\frac{\partial \alpha}{\partial z} = i\frac{\omega_o n_2}{c}a^2 a, \tag{A.18}$$

separating the real and imagine terms of (A.18), Eq. (A.18) reduces to

$$\frac{\partial a}{\partial z} = 0, \tag{A.19a}$$

$$\frac{\partial \alpha}{\partial z} = \frac{\omega_o n_2}{c}\alpha^2. \tag{A.19b}$$

The analytical solutions of Eqs. (A.19) for the nonlinear phase modulation and the slowly changing amplitude of a light pulse can be obtained as

$$a_{(z,\tau)} = a_0 F_{(\tau)}, \tag{A.20a}$$

$$\alpha_{(z,\tau)=}\frac{\omega_o n_2}{c} a_o^2 z F_{(\tau)}^2. \tag{A.20b}$$

where a_o is the peak amplitude of the laser pulse and $F_{(\tau)}$ is the envelope of the light pulse.

From the solution (A.20), the main physics of SPM is that the phase of an optical pulse propagating in a nonlinear medium becomes time dependent in the pulse profile, and results in SPM. The frequency of the electric field will be continuously shifted in time. The electric field at each given τ within the pulse has a specific local instantaneous frequency that is given by

$$\omega_{(\tau)} = \omega_o + \delta\omega_{(\tau)}, \tag{A.21}$$

where

$$\delta\omega_{(\tau)} = -\frac{\partial \alpha}{\partial \tau} = -\frac{\omega_o n_2}{c} a_o^2 \frac{\partial F_{(\tau)}^2}{\partial \tau}. \tag{A.22}$$

where $\delta\omega(\tau)$ is the frequency shift generated at a particular local time τ within the pulse envelope. This frequency shift is proportional to the derivative of the pulse envelope with respect to τ, the nonlinear index, and the intensity of the pulse.

The complex-field spectral profiles $E(z, \omega-\omega_0)$ of the optical pulse after SPM process can be obtained by computing the Fourier transformation of its temporal pulse distribution as

$$E(z, \omega-\omega_0) = \frac{1}{2\pi}\int A(\tau,z)\exp(-i\omega_0\tau)\exp(-i\omega\tau)d\tau$$
$$= \frac{1}{2\pi}\int a(\tau,z)\exp[i\alpha(\tau,z)]\exp[i(\omega-\omega_0)\tau]d\tau. \qquad (A.23)$$

The spectral intensity distribution of the pulse due to SPM induced spectral broadening is given by

$$|E(z,\omega-\omega_0)|^2. \qquad (A.24)$$

The spectral intensity distribution of SPM has to be calculated numerically using Eq.(A.24). A few softwares such as FORTRAN and Matlab are able to complete this calculation. By using Matlab, this calculation is especially simple. All one needs to do is to input the analytical solution of the light in Eq. (A.23).

A.2 Nonlinear Wave Equation of Cross-phase Modulation (XPM) for two Parallel linearly polarized optical waves

When more than one optical waves propagate in a nonlinear medium, one optical wave will affect another optical wave at high intensity. A typical condition is the nonlinear interaction for two optical waves. For linearly polarized optical waves propagating in a nonlinear medium, these two optical waves are assumed to be parallel polarized in the x-axis direction, and these optical waves propagate along the z-axis direction. The total electric field can be expressed as:

$$\vec{E}(z,t) = \frac{1}{2}\vec{e}_x\{A_1(z,t)e^{-i(\omega_1 t-\beta_1 z)} + A_2(z,t)e^{-i(\omega_2 t-\beta_2 z)} + c.c.\}, \qquad (A.25)$$

where $A_{1(z,t)}$ ($A_{2(z,t)}$), ω_1 (ω_2), and β_1 (β_2) are the slow changing amplitude, frequency, and propagation constant of these optical waves, respectively. This case just likes the condition for SPM except there are two optical waves here. So, nonlinear polarization has the same components as shown in Eq. (A.6)

$$P_x = \chi E_x^3, \text{ and } P_y = P_z = 0, \qquad (A.6)$$

Substituting the total electric field in Eq. (A.25) into (A.6)

$$P_x = \frac{1}{8}\chi\{A_1(z,t)e^{-i(\omega_1 t-\beta_1 z)} + A_2(z,t)e^{-i(\omega_2 t-\beta_2 z)} + c.c.\}^3. \qquad (A.26)$$

Expanding (A.26)

$$\begin{aligned} P_x = \frac{1}{8}\chi\{&A_1^3 e^{-3i(\omega_1 t-\beta_1 z)} + A_2^3 e^{-3i(\omega_2 t-\beta_2 z)} \\ &+ A_1^{*3} e^{3i(\omega_1 t-\beta_1 z)} + A_2^{*3} e^{3i(\omega_2 t-\beta_2 z)} \\ &+3A_1^2 A_2 e^{-i[(2\omega_1+\omega_2)t-(2\beta_1+\beta_2)z]} + 3A_1^{*2} A_2^* e^{i[(2\omega_1+\omega_2)t-(2\beta_1+\beta_2)z]} \\ &+3A_1 A_2^2 e^{-i[(\omega_1+2\omega_2)t-(\beta_1+2\beta_2)z]} + 3A_1^* A_2^{*2} e^{i[(\omega_1+2\omega_2)t-(\beta_1+2\beta_2)z]} \end{aligned}$$

$$+3A_1^2A_2^*e^{-i[(2\omega_1-\omega_2)t-(2\beta_1-\beta_2)z]}+3A_1^{*2}A_2e^{i[(2\omega_1-\omega_2)t-(2\beta_1-\beta_2)z]}$$
$$+3A_1^*A_2^2e^{-i[(-\omega_1+2\omega_2)t-(-\beta_1+2\beta_2)z]}+3A_1A_2^{*2}e^{i[(-\omega_1+2\omega_2)t-(-\beta_1+2\beta_2)z]}$$
$$+3A_1^2A_1^*e^{-i(\omega_1t-\beta_1z)}+3A_1A_1^{*2}e^{i(\omega_1t-\beta_1z)}$$
$$+3A_2^2A_2^*e^{-i(\omega_2t-\beta_2z)}+3A_2A_2^{*2}e^{i(\omega_2t-\beta_2z)}$$
$$+6A_1|A_2|^2e^{-i(\omega_1t-\beta_1z)}+6A_1^*|A_2|^2e^{i(\omega_1t-\beta_1z)}$$
$$+6A_2|A_1|^2e^{-i(\omega_2t-\beta_2z)}+6A_2^*|A_1|^2e^{i(\omega_2t-\beta_2z)}\}. \qquad \text{(A.27)}$$

Keeping only the terms synchronized with ω_1 and ω_2 in Eq. (A.27), one obtains

$$P_x(z,t)=P_{x1}(z,t)+P_{x2}(z,t), \qquad \text{(A.28a)}$$
$$P_{x1}(z,t)=\frac{3}{8}\chi\,(|A_{1(z,t)}|^2+2|A_{2(z,t)}|^2)A_1e^{-i(\omega_1t-\beta_1z)}, \qquad \text{(A.28b)}$$
$$P_{x2}(z,t)=\frac{3}{8}\chi\,(|A_{2(z,t)}|^2+2|A_{1(z,t)}|^2)A_2e^{-i(\omega_2t-\beta_2z)}. \qquad \text{(A.28c)}$$

where P_{x1} and P_{x2} are the nonlinear polarizations at frequencies ω_1 and ω_2, respectively. Substituting Eqs. (A.28) into Eq. (II.22) and separating the equations which describe the propagation of the optical waves at different frequencies ω_1 and ω_2, one obtains the nonlinear wave equations for XPM process:

$$\frac{\partial A_1}{\partial z}+\frac{1}{v_{g1}}\frac{\partial A_1}{\partial t}+\frac{i}{2}k^{(2)}\frac{\partial^2A_1}{\partial t^2}=i\frac{\omega_1n_2}{c}(|A_1|^2+2|A_2|^2)A_1, \qquad \text{(A.29a)}$$
$$\frac{\partial A_2}{\partial z}+\frac{1}{v_{g2}}\frac{\partial A_2}{\partial t}+\frac{i}{2}k^{(2)}\frac{\partial^2A_2}{\partial t^2}=i\frac{\omega_2n_2}{c}(|A_2|^2+2|A_1|^2)A_2, \qquad \text{(A.29b)}$$

where υ_{gi} is the group velocity for the wave i, $k_i^{(2)}$ is the group velocity dispersion for the wave i, and $n_2=3\chi^{(3)}/8n$ is the nonlinear refractive index. The first terms in the right sides of Eqs. (A.29) are SPM terms and the second terms are the XPM terms. Eqs. (A.29) also

show that XPM terms are twice larger than SPM terms for two optical waves at the same linear polarization state.

In the most general case, numerical methods have to be used to solve these nonlinear coupling equations. However, the analytical solutions can be obtained when the group velocity dispersion temporal broadening can be neglected. In this case, the nonlinear wave equations are

$$\frac{\partial A_1}{\partial z}+\frac{1}{v_{g1}}\frac{\partial A_1}{\partial t}=i\frac{\omega_1 n_2}{c}(|A_1|^2+2|A_2|^2)A_1, \tag{A.30a}$$

$$\frac{\partial A_2}{\partial z}+\frac{1}{v_{g2}}\frac{\partial A_2}{\partial t}=i\frac{\omega_2 n_2}{c}(|A_2|^2+2|A_1|^2)A_2. \tag{A.30b}$$

By changing the variables with:

$$\tau = t - z/\upsilon_{g1}, \text{ and } z'=z, \tag{A.31}$$

where t is real time, and τ is defined as the pulse local time. Therefore, one has

$$\partial\tau/\partial t = 1,\ \partial\tau/\partial z = -1/\vartheta_{g1};\ \text{and}$$
$$\partial z'/\partial z = 1\ \ \partial z'/\partial t = 0, \tag{A.32}$$

substituting (A.32) into next variable change relation, one has

$$\frac{\partial}{\partial t}=\frac{\partial}{\partial\tau}\frac{\partial\tau}{\partial t}+\frac{\partial}{\partial z'}\frac{\partial z'}{\partial t}=\frac{\partial}{\partial\tau}, \tag{A.33a}$$

$$\frac{\partial}{\partial z}=\frac{\partial}{\partial z'}\frac{\partial z'}{\partial z}+\frac{\partial}{\partial\tau}\frac{\partial\tau}{\partial z}=\frac{\partial}{\partial z'}-\frac{1}{\vartheta_{g1}}\frac{\partial}{\partial\tau}, \tag{A.33b}$$

putting (A.33) into nonlinear wave equations (A.30), they are

$$(\frac{\partial}{\partial z'}-\frac{1}{\vartheta_{g1}}\frac{\partial}{\partial \tau}+\frac{1}{\vartheta_{g1}}\frac{\partial}{\partial \tau})A_1 = i\frac{\omega_1 n_2}{c}(|A_1|^2+2|A_2|^2)A_1, \qquad \text{(A.34a)}$$

$$(\frac{\partial}{\partial z'}-\frac{1}{\vartheta_{g1}}\frac{\partial}{\partial \tau}+\frac{1}{\vartheta_{g2}}\frac{\partial}{\partial \tau})A_2 = i\frac{\omega_2 n_2}{c}(|A_2|^2+2|A_1|^2)A_2, \qquad \text{(A.34b)}$$

i.e.

$$\frac{\partial A_1}{\partial z'} = i\frac{\omega_1 n_2}{c}(|A_1|^2+2|A_2|^2)A_1, \qquad \text{(A.35a)}$$

$$\frac{\partial A_2}{\partial z'}+(\frac{1}{\vartheta_{g2}}-\frac{1}{\vartheta_{g1}})\frac{\partial A_2}{\partial \tau} = i\frac{\omega_2 n_2}{c}(|A_2|^2+2|A_1|^2)A_2, \qquad \text{(A.35b)}$$

Since z'=z, the equation can be expressed as

$$\frac{\partial A_1}{\partial z} = i\frac{\omega_1 n_2}{c}(|A_1|^2+2|A_2|^2)A_1. \qquad \text{(A.36a)}$$

$$\frac{\partial A_2}{\partial z}+(\frac{1}{\vartheta_{g2}}-\frac{1}{\vartheta_{g1}})\frac{\partial A_2}{\partial \tau} = i\frac{\omega_2 n_2}{c}(|A_2|^2+2|A_1|^2)A_2. \qquad \text{(A.36b)}$$

By denoting the slowly changing envelope and phase of the pulses with A and α, we obtain:

$$A_1(\tau,z) = a_{1(\tau,z)}e^{i\alpha_1(\tau,z)} \quad \text{and} \quad A_2(\tau,z) = a_{2(\tau,z)}e^{i\alpha_2(\tau,z)}. \qquad \text{(A.37)}$$

Substituting (A.37) into Eqs. (A.36), one has

$$\frac{\partial}{\partial z}(a_1 e^{i\alpha_1}) = i\frac{\omega_1 n_2}{c}(a_1^2+2a_2^2)a_1 e^{i\alpha_1}, \qquad \text{(A.38a)}$$

$$\{\frac{\partial}{\partial z}+(\frac{1}{\vartheta_{g2}}-\frac{1}{\vartheta_{g1}})\frac{\partial}{\partial \tau}\}(a_2 e^{i\alpha_2})=i\frac{\omega_2 n_2}{c}(a_2^2+2a_1^2)a_2 e^{i\alpha_2}, \qquad \text{(A.38b)}$$

Hence,

$$e^{i\alpha_1}\frac{\partial a_1}{\partial z}+i a_1 e^{i\alpha_1}\frac{\partial \alpha_1}{\partial z}=i\frac{\omega_1 n_2}{c}(a_1^2+2a_2^2)a_1 e^{i\alpha_1}, \qquad \text{(A.39a)}$$

$$e^{i\alpha_2}\frac{\partial a_2}{\partial z}+i a_2 e^{i\alpha_2}\frac{\partial \alpha_2}{\partial z}+(\frac{1}{\vartheta_{g2}}-\frac{1}{\vartheta_{g1}})(e^{i\alpha_2}\frac{\partial a_2}{\partial \tau}+ia_2 e^{i\alpha_2}\frac{\partial \alpha_2}{\partial \tau})$$
$$=i\frac{\omega_2 n_2}{c}(a_2^2+2a_1^2)a_2 e^{i\alpha_2}, \qquad \text{(A.39b)}$$

(A.39) can be simplified as

$$\frac{\partial a_1}{\partial z}+i a_1\frac{\partial \alpha_1}{\partial z}=i\frac{\omega_1 n_2}{c}(a_1^2+2a_2^2)a_1, \qquad \text{(A.40a)}$$

$$\frac{\partial a_2}{\partial z}+(\frac{1}{\vartheta_{g2}}-\frac{1}{\vartheta_{g1}})\frac{\partial a_2}{\partial \tau}+i a_2\{\frac{\partial \alpha_2}{\partial z}+(\frac{1}{\vartheta_{g2}}-\frac{1}{\vartheta_{g1}})\frac{\partial \alpha_2}{\partial \tau}\}$$
$$=i\frac{\omega_2 n_2}{c}(a_2^2+2a_1^2)a_2, \qquad \text{(A.40b)}$$

separating the real and part, Eqs. (A.40) reduce to

$$\frac{\partial a_1}{\partial z}=0, \qquad \text{(A.41a)}$$

$$\frac{\partial \alpha_1}{\partial z}=\frac{\omega_1}{c}n_2[a_1^2+2a_2^2], \qquad \text{(A.41b)}$$

$$\frac{\partial a_2}{\partial z}+(\frac{1}{\upsilon_{g2}}-\frac{1}{\upsilon_{g1}})\frac{\partial a_2}{\partial \tau}=0, \qquad \text{(A.41c)}$$

$$\frac{\partial \alpha_2}{\partial z}=\frac{\omega_2}{c}n_2[a_2^2+2a_1^2], \qquad \text{(A.41d)}$$

where $\tau = (t - z/\upsilon_{g1})/\tau_0$ is the local time and τ_0 is the 1/e pulse duration. In addition, Gaussian pulse shapes are chosen at the input z=0:

$$A_{1(\tau, z=0)} = A_{10} e^{-\tau^2/2}, \tag{A.42a}$$

$$A_{2(\tau, z=0)} = A_{20} e^{-(\tau-\tau_d)^2/2}, \tag{A.42b}$$

where A_{10} and A_{20} is the input peak amplitudes of the laser pulses, and $\tau_d=t_d/\tau_0$ is the normalized time delay between pulses at z=0. With these initial conditions, the equations of the amplitudes and phases of the optical pulses after propagating in an optical fiber with length z can be solved as following. To solve equation (A.41c), one has to change the variables with

$$\tau' = \tau - z(\frac{1}{\upsilon_{g2}} - \frac{1}{\upsilon_{g1}})/\tau_0,, \text{ and } z'=z, \tag{A.43}$$

where t is local time. Therefore, one has

$$\partial\tau'/\partial\tau = 1, \partial\tau'/\partial z = -(\frac{1}{\upsilon_{g2}} - \frac{1}{\upsilon_{g1}}); \text{ and}$$

$$\partial z'/\partial z = 1 \quad \partial z'/\partial t = 0, \tag{A.44}$$

substituting (A.43) into next variable change relation, one has

$$\frac{\partial}{\partial\tau} = \frac{\partial}{\partial\tau'}\frac{\partial\tau'}{\partial\tau} + \frac{\partial}{\partial z'}\frac{\partial z'}{\partial\tau} = \frac{\partial}{\partial\tau'}, \tag{A.45a}$$

$$\frac{\partial}{\partial z} = \frac{\partial}{\partial z'}\frac{\partial z'}{\partial z} + \frac{\partial}{\partial\tau'}\frac{\partial\tau'}{\partial z} = \frac{\partial}{\partial z'} - (\frac{1}{\upsilon_{g2}} - \frac{1}{\upsilon_{g1}})\frac{\partial}{\partial\tau'}, \tag{A.45b}$$

putting (A.44) into nonlinear wave equation (A.41c), that is

$$\{\frac{\partial}{\partial z'}-(\frac{1}{\upsilon_{g2}}-\frac{1}{\upsilon_{g1}})\frac{\partial}{\partial \tau'}+(\frac{1}{\upsilon_{g2}}-\frac{1}{\upsilon_{g1}})\frac{\partial}{\partial \tau'}\}a_2=0, \tag{A.46}$$

i.e.

$$\frac{\partial}{\partial z'}a_2=0. \tag{A.47}$$

The solution of (A.47) is:

$$a_{2(z',\tau')}=c_{(\tau')}, \tag{A.48}$$

where $c_{(\tau')}$ can be determined by initial condition (A.42b) as

$$c_{(\tau')}=A_{20}e^{-(\tau'-\tau_d)^2/2}, \tag{A.49}$$

the solution of the amplitude for the second optical wave is

$$a_{2(z',\tau')}=A_{20}e^{-(\tau'-\tau_d)^2/2}, \tag{A.50}$$

using propagation distance z and pulse local time τ, substituting (A.43) into (A.50), the solution is

$$a_{2(z,\tau)}=A_{20}\exp\{-[\tau-z(\frac{1}{\upsilon_{g2}}-\frac{1}{\upsilon_{g1}})/\tau_0-\tau_d]^2/2\}. \tag{A.51}$$

defining that $L_w = \tau_0 / (\frac{1}{\upsilon_{g2}} - \frac{1}{\upsilon_{g1}})$ as a walk-off length, (A.51) can be expressed as

$$a_{2(z,\tau)} = A_{20} \exp\{-[\tau - z / L_w - \tau_d]^2 / 2\}. \quad \text{(A.52)}$$

Equation (A.41a) can be solved with solution as

$$a_{1(z,\tau)} = A_{10} \exp(-\tau^2 / 2). \quad \text{(A.53)}$$

The nonlinear phase changes of the two optical waves can be calculated through the equations (A.41c) and (A.41d), the solutions are integrals such as

$$\alpha_{1(z,\tau)} = \int_0^z \frac{\omega_1}{c} n_2 [a_1^2 + 2a_2^2] dz, \quad \text{(A.54a)}$$

$$\alpha_{2(z,\tau)} = \int_0^z \frac{\omega_1}{c} n_2 [a_2^2 + 2a_1^2] dz, \quad \text{(A.54b)}$$

substituting the solutions of amplitudes (A.52) and (A.53) into (A.54), the nonlinear phase can be calculated. Putting all the solution together, the amplitudes and phases of two optical waves after XPM process are

$$a_{1(z,\tau)} = A_{10} \exp(-\tau^2 / 2), \quad \text{(A.55a)}$$

$$a_{2(z,\tau)} = A_{20} \exp\{-[\tau - z(\frac{1}{\upsilon_{g2}} - \frac{1}{\upsilon_{g1}}) / \tau_0 - \tau_d]^2 / 2\}, \quad \text{(A.55b)}$$

$$\alpha_1(\tau, z) = \frac{\omega_1}{c} n_2 z I_{10} e^{-\tau^2} + 2\sqrt{\pi} \frac{\omega_1}{c} n_2 L_w I_{20} * [\mathrm{erf}(\tau - \tau_d) - \mathrm{erf}(\tau - \tau_d - \frac{z}{L_w})], \quad \text{(A.55c)}$$

$$\alpha_2(\tau, z) = \frac{\omega_2}{c} n_2 z I_{20} e^{-(\tau-\tau_d-z/L_w)^2} + 2\sqrt{\pi}\frac{\omega_2}{c} n_2 L_w I_{20},$$
$$*[\mathrm{erf}(\tau) - \mathrm{erf}(\tau - \frac{z}{L_w})], \qquad \text{(A.55d)}$$

where I_{10} and I_{20} are the input intensities of the laser pulses, and $L_w=\tau_o/(1/v_{g1}-1/v_{g2})$ is defined as the walk-off length. Eqs. (A.55) give the nonlinear phase changes for laser pulses propagating in a nonlinear medium. This phase modulation will generate new frequencies as SPM does. The first terms on the right-handed side of Eqs. (A.55c and A.55d) are the SPM induced phase changes which will broaden the spectrum of the optical pulse itself. The second terms on the right-handed side of Eqs. (A.55c and A.55d) are the XPM induced phase changes which will broaden the spectrum of the other copropagating optical pulse. The nonlinear phase change coefficient of XPM is twice of the SPM. The instantaneous nonlinear frequency changes are obtained by differentiating the phase changes in (A.55c) and (A.55d) according to

$$\delta\omega_{(\tau)} = -\partial\alpha / \partial\tau. \qquad \text{(A.56)}$$

The instantaneous nonlinear frequency changes are:

$$\Delta\omega_1(\tau, z) = 2\frac{\omega_1}{c} n_2 I_{10} \frac{z}{\tau_0} \tau e^{-\tau^2} + 4\frac{\omega_1}{c} n_2 I_{20} \frac{L_w}{\tau_o}$$
$$*[(\tau-\tau_d)e^{-(\tau-\tau_d)^2} - (\tau-\tau_d-z/L_w)e^{-(\tau-\tau_d-z/L_w)^2}], \qquad \text{(A.56a)}$$
$$\Delta\omega_2(t, z) = 2\frac{\omega_2}{c} n_2 I_{20} \frac{z}{\tau_0} (\tau-\tau_d-z/L_w) e^{-(\tau-\tau_d-z/L_w)^2}$$
$$+4\frac{\omega_2}{c} n_2 I_{20} \frac{L_w}{\tau_o} [\tau e^{-\tau^2} - (\tau-z/L_w)e^{-(\tau-z/L_w)^2}], \qquad \text{(A.56b)}$$

where $\Delta\omega_1=\omega-\omega_1$ and $\Delta\omega_2=\omega-\omega_2$. The first and second terms on the right-handed side of Eqs. (A.56) are the contributions of SPM and XPM, respectively. The XPM induced frequency change is twice of that induced by SPM. The XPM induced frequency shift also depends on the initial optical delay τ_d and the walk-off distance L_W. Finally, the spectral profiles can be studied by computing the Fourier transform as shown in Eqs. (A.23) and (A.24).

A.3 Nonlinear Wave Equation of Cross-phase Modulation (XPM) for two Perpendicular linearly polarized optical waves

For two optical waves which are linearly polarized at the perpendicular direction, the nonlinear wave equations for XPM are different. Assuming these two optical waves are polarized at the x- and y-axis direction, respectively. the total electric field is:

$$\vec{E}(z,t)=\frac{1}{2}\{A_x(z,t)e^{i(\omega_x t-\beta_x z)}\vec{e_x}+A_y(z,t)e^{i(\omega_y t-\beta_y z)}\vec{e_y}\}+c.c., \qquad (A.57)$$

the nonlinear polarization can be calculated through all the non-zero components of the third order suceptibility for an isotropic material;

$$\begin{aligned} P_x &= \sum_{ijk}\chi^{(3)}_{xijk}E_iE_jE_k \\ &= \chi_{xxxx}E_x^3+\chi_{xxyy}E_xE_y^2+\chi_{xyyx}E_xE_y^2+\chi_{xyxy}E_xE_y^2, \end{aligned} \qquad (A.58a)$$

$$\begin{aligned} P_y &= \sum_{ijk}\chi^{(3)}_{yijk}E_iE_jE_k \\ &= \chi_{yyyy}E_y^3+\chi_{yyxx}E_yE_x^2+\chi_{yxxy}E_yE_x^2+\chi_{yxyx}E_yE_x^2. \end{aligned} \qquad (A.58b)$$

substituting (A.3) for the values of the third order suceptibility tensor into (A.28), we have

$$P_x = \chi(E_x^3 + E_x E_y^2), \tag{A.59a}$$

$$P_y = \chi(E_y^3 + E_y E_x^2). \tag{A.59b}$$

Substituting Eq. (A.57) into (A.59) and expanding Px and Py, one has

$$\begin{aligned}
P_x &= \frac{1}{8}\chi\{[A_x e^{-i(\omega_x t-\beta_x z)} + A_x^* e^{i(\omega_x t-\beta_x z)}]^3 \\
&\quad +[A_x e^{-i(\omega_x t-\beta_x z)} + A_x^* e^{i(\omega_x t-\beta_x z)}]\,[A_y e^{-i(\omega_y t-\beta_y z)} + A_y^* e^{i(\omega_y t-\beta_y z)}]^2\} \\
&= \frac{1}{8}\chi\{A_x^3 e^{-3i(\omega_x t-\beta_x z)} + A_x^{*3} e^{3i(\omega_x t-\beta_x z)} \\
&\quad +3A_x^2 A_x^* e^{-i(\omega_x t-\beta_x z)} + 3A_x A_x^{*2} e^{i(\omega_x t-\beta_x z)} \\
&\quad +[A_x e^{-i(\omega_x t-\beta_x z)} + A_x^* e^{i(\omega_x t-\beta_x z)}] \\
&\quad *[A_y^2 e^{-2i(\omega_y t-\beta_y z)} + 2A_y A_y^* + A_y^{*2} e^{2i(\omega_y t-\beta_y z)}]\} \\
&= \frac{1}{8}\chi\{A_x^3 e^{-3i(\omega_x t-\beta_x z)} + 3A_x^2 A_x^* e^{-i(\omega_x t-\beta_x z)} + 2A_y A_y^* A_x e^{-i(\omega_x t-\beta_x z)} \\
&\quad + A_x^* A_y^2 e^{-i(\omega_x t-\Delta\beta z)}\} + \text{c.c.},
\end{aligned} \tag{A.60a}$$

$$\begin{aligned}
P_y &= \frac{1}{8}\chi\{[A_y e^{-i(\omega_y t-\beta_y z)} + A_y^* e^{i(\omega_y t-\beta_y z)}]^3 \\
&\quad +[A_y e^{-i(\omega_y t-\beta_y z)} + A_y^* e^{i(\omega_y t-\beta_y z)}]\,[A_x e^{-i(\omega_x t-\beta_x z)} + A_x^* e^{i(\omega_x t-\beta_x z)}]^2\} \\
&= \frac{1}{8}\chi\{A_y^3 e^{-3i(\omega_y t-\beta_y z)} + A_y^{*3} e^{3i(\omega_y t-\beta_y z)} \\
&\quad +3A_y^2 A_y^* e^{-i(\omega_y t-\beta_y z)} + 3A_y A_y^{*2} e^{i(\omega_y t-\beta_y z)} \\
&\quad +[A_y e^{-i(\omega_y t-\beta_y z)} + A_y^* e^{i(\omega_y t-\beta_y z)}] \\
&\quad *[A_x^2 e^{-2i(\omega_x t-\beta_x z)} + 2A_x A_x^* + A_x^{*2} e^{2i(\omega_x t-\beta_x z)}]\} \\
&= \frac{1}{8}\chi\{A_y^3 e^{-3i(\omega_y t-\beta_y z)} + 3A_y^2 A_y^* e^{-i(\omega_y t-\beta_y z)} + 2A_x A_x^* A_y e^{-i(\omega_y t-\beta_y z)}
\end{aligned}$$

$$+A_y^* A_x^2 e^{-i(\omega_y t+\Delta\beta z)}\} + c.c., \qquad \text{(A.60b)}$$

keeping only the terms synchronized with ω_x and ω_y, one obtains

$$P_x(z,t) = \frac{3}{8}\chi\{(|A_{x(z,t)}|^2 + \frac{2}{3}|A_{y(z,t)}|^2)A_x + A_{y(z,t)}^2 A_{x(z,t)}^* e^{-i2\Delta\beta z}\}e^{-i\omega_x t}, \text{(A.61a)}$$

$$P_y(z,t) = \frac{3}{8}\chi\{(|A_{y(z,t)}|^2 + \frac{2}{3}|A_{x(z,t)}|^2)A_y + A_{x(z,t)}^2 A_{y(z,t)}^* e^{i2\Delta\beta z}\}e^{-i\omega_y t}, \quad \text{(A.61b)}$$

where $\Delta\beta=\beta_x-\beta_y$. For two optical waves at the x- and y-axis direction the nonlinear wave equations can be derived by the substituting the nonlinear polarization components in Eqs. (A.61) into (II.22) for different optical waves at the frequencies of ω_x and ω_y, one obtains the nonlinear wave equations for XPM process:

$$\frac{\partial A_x}{\partial z} + \frac{1}{v_{gx}}\frac{\partial A_x}{\partial t} + \frac{i}{2}k_x^{(2)}\frac{\partial^2 A_x}{\partial t^2} = i\frac{\omega_x n_2}{c}$$

$$x\ [(|A_x|^2 + \frac{2}{3}|A_y|^2)A_x + \frac{1}{3}A_y{}^2 A_x{}^* \exp(-i2\Delta\beta z)], \qquad \text{(A.62a)}$$

$$\frac{\partial A_y}{\partial z} + \frac{1}{v_{gy}}\frac{\partial A_y}{\partial t} + \frac{i}{2}k_y^{(2)}\frac{\partial^2 A_y}{\partial t^2} = i\frac{\omega_y n_2}{c}$$

$$x\ [(|A_y|^2 + \frac{2}{3}|A_x|^2)A_y + \frac{1}{3}A_x{}^2 A_y{}^* \exp(i2\Delta\beta z)], \qquad \text{(A.62b)}$$

where $\Delta\beta=\beta_x-\beta_y$ is the wave vector mismatch for the two optical waves. The first and second terms in the right sides of Eqs. (A.62) are the SPM and XPM. The XPM coefficient is smaller (only 2/3) than SPM. The third terms in the right sides of Eqs. (A.62) are known as the degenerate four-wave mixing (DFWM) terms.

When the frequencies of the two optical waves are not equal, means $\omega_x \neq \omega_y$ and the wave vector mismatch $\Delta\beta>>0$, these terms will oscillate and then vanish. There is no net effect in this case. Therefore, the DWFM terms in the nonlinear wave equations can be neglected. Eqs. (A.62) will reduce to the similar form to Eqs. (A.29) except that the coefficients of SPM and XPM are different. Using exactly the same way for Eq. (A.29), Eqs. (A.62) can be solved for which we do not repeat here.

When two optical wave are at these same frequency which is called degenerate case. The DFWM terms is steady because of the wave vector mismatch $\Delta\beta=0$. DFWM processes will modulate the phase and cause the amplitudes of the two optical waves coupling with each other during nonlinear interactions of the optical waves. In this case, the nonlinear wave equations (A.62) can not be solved analytically even when the GVD terms are neglected. Numerical method must be used to solve these equations.

A.4 Nonlinear Wave Equation of Cross-phase Modulation (XPM) for two opposite rotating circularly polarized optical waves

Mathematically, either two perpendicularly linearly polarized unit vector or two opposite rotating circularly polarized unit vector can be used as the polarization eigen-modes for optical wave propagating in a material. For two opposite-rotating circularly polarized optical waves with slow changing amplitudes of E_r and E_l at the frequencies of ω_r or ω_l for right- and left-handed waves, respectively, the total electric field is the superposition of the right-handed wave and the left-handed wave:

$$\begin{aligned}\vec{E} &= E_r\vec{e}_r + E_l\vec{e}_l \\ &= E_r\frac{1}{\sqrt{2}}(\vec{e}_x - i\vec{e}_y) + E_l\frac{1}{\sqrt{2}}(\vec{e}_x + i\vec{e}_y)\end{aligned}$$

$$= \frac{1}{\sqrt{2}}(E_r + E_l)\vec{e_x} + \frac{i}{\sqrt{2}}(E_r - E_l)\vec{e_y}. \tag{A.63}$$

The complex expressions of the x and y components are;

$$E_x = \frac{1}{2\sqrt{2}}(E_l e^{-i\omega_l t} + E_r e^{-i\omega_r t} + c.c.), \tag{A.64a}$$

$$E_y = \frac{1}{2\sqrt{2}}(i E_l e^{-i\omega_l t} - i E_r e^{-i\omega_r t} + c.c.), \tag{A.65b}$$

i.e.

$$E_x = \frac{1}{2\sqrt{2}}(E_l e^{-i\omega_l t} + E_r e^{-i\omega_r t} + E_l^* e^{i\omega_l t} + E_r^* e^{i\omega_r t}), \tag{A.66a}$$

$$E_y = \frac{i}{2\sqrt{2}}(E_l e^{-i\omega_l t} - E_r e^{-i\omega_r t} - E_l^* e^{i\omega_l t} + E_r^* e^{i\omega_r t}). \tag{A.66b}$$

We have:

$$\begin{aligned} E_x^3 = \frac{1}{16\sqrt{2}}\{ & E_l^3 e^{-i3\omega_l t} + 3E_l^2 E_r e^{(-i2\omega_l t - i\omega_r t)} + 3E_l E_r^2 e^{(-i\omega_l t - 2i\omega_r t)} \\ & + E_r^3 e^{-3i\omega_r t} + 3E_l^2 E_l^* e^{-i\omega_l t} + 6E_l^* E_l E_r e^{-i\omega_r t} + 3E_r^2 E_l^* e^{(-i2\omega_r t + i\omega_l t)} \\ & + 3E_l E_l^{*2} e^{i\omega_l t} + 3E_r E_l^{*2} e^{(i2\omega_l t - i\omega_r t)} + 3E_l^{*3} e^{3i\omega_l t} \\ & + 3E_l^2 E_r^* e^{(-i2\omega_l t + i\omega_r t)} + 6E_l E_r E_r^* e^{-i\omega_l t} + 3E_r^2 E_r^* e^{-i\omega_r t} \\ & + 6E_l E_l^* E_r^* e^{i\omega_r t} + 6E_l^* E_r E_r^* e^{i\omega_l t} + 3E_l^{*2} E_r^* e^{(i2\omega_l t + i\omega_r t)} \\ & + 3E_l E_r^{*2} e^{(i2\omega_r t - i\omega_l t)} + 3E_r E_r^{*2} e^{i\omega_r t} + 3E_l^* E_r^{*2} e^{(i2\omega_r t + i\omega_l t)} \\ & + 3E_r^{*3} e^{i3\omega_r t}\}, \end{aligned} \tag{A.67a}$$

$$E_y^3 = \frac{i}{16\sqrt{2}}\{-E_l^3 e^{-3i\omega_l t} + 3E_l^2 E_r e^{(-2i\omega_l t - i\omega_r t)} - 3E_l E_r^2 e^{(-i\omega_l t - 2i\omega_r t)}$$
$$+E_r^3 e^{-3i\omega_r t} + 3E_l^2 E_l^* e^{-i\omega_l t} - 6E_l^* E_l E_r e^{-i\omega_r t} + 3E_r^2 E_l^* e^{(-i2\omega_r t + i\omega_l t)}$$
$$-3E_l E_l^{*2} e^{i\omega_l t} + 3E_r E_l^{*2} e^{(i2\omega_l t - i\omega_r t)} + 3E_l^{*3} e^{3i\omega_l t}$$
$$-3E_l^2 E_r^* e^{(-i2\omega_l t + i\omega_r t)} + 6E_l E_r E_r^* e^{-i\omega_l t} - 3E_r^2 E_r^* e^{-i\omega_r t}$$
$$+6E_l E_l^* E_r^* e^{i\omega_r t} - 6E_l^* E_r E_r^* e^{i\omega_l t} - 3E_l^{*2} E_r^* e^{(i2\omega_l t + i\omega_r t)}$$
$$-3E_l E_r^{*2} e^{(i2\omega_r t - i\omega_l t)} + 3E_r E_r^{*2} e^{i\omega_r t} + 3E_l^* E_r^{*2} e^{(i2\omega_r t + i\omega_l t)}$$
$$-3E_r^{*3} e^{i3\omega_r t}\}, \qquad \text{(A.67b)}$$

and

$$E_y^2 E_x = \frac{1}{16\sqrt{2}}\{-E_l^3 e^{-3i\omega_l t} + E_l^2 E_r e^{(-2i\omega_l t - i\omega_r t)} + E_l E_r^2 e^{(-i\omega_l t - 2i\omega_r t)}$$
$$-E_r^3 e^{-3i\omega_r t} + E_l^2 E_l^* e^{-i\omega_l t} + 2E_l^* E_l E_r e^{-i\omega_r t} - 3E_r^2 E_l^* e^{(-i2\omega_r t + i\omega_l t)}$$
$$+E_l E_l^{*2} e^{i\omega_l t} - 3E_r E_l^{*2} e^{(i2\omega_l t - i\omega_r t)} - E_l^{*3} e^{3i\omega_l t}$$
$$-3E_l^2 E_r^* e^{(-i2\omega_l t + i\omega_r t)} + 2E_l E_r E_r^* e^{-i\omega_l t} + E_r^2 E_r^* e^{-i\omega_r t}$$
$$+2E_l E_l^* E_r^* e^{i\omega_r t} + 2E_l^* E_r E_r^* e^{i\omega_l t} + E_l^{*2} E_r^* e^{(i2\omega_l t + i\omega_r t)}$$
$$-3E_l E_r^{*2} e^{(i2\omega_r t - i\omega_l t)} + E_r E_r^{*2} e^{i\omega_r t} + E_l^* E_r^{*2} e^{(i2\omega_r t + i\omega_l t)}$$
$$-E_r^{*3} e^{i3\omega_r t}\}, \qquad \text{(A.67c)}$$

$$E_x^2 E_y = \frac{i}{16\sqrt{2}}\{E_l^3 e^{-3i\omega_l t} + E_l^2 E_r e^{(-2i\omega_l t - i\omega_r t)} - E_l E_r^2 e^{(-i\omega_l t - 2i\omega_r t)}$$
$$-E_r^3 e^{-3i\omega_r t} + E_l^2 E_l^* e^{-i\omega_l t} - 2E_l^* E_l E_r e^{-i\omega_r t} - 3E_r^2 E_l^* e^{(-i2\omega_r t + i\omega_l t)}$$
$$-E_l E_l^{*2} e^{i\omega_l t} - 3E_r E_l^{*2} e^{(i2\omega_l t - i\omega_r t)} - E_l^{*3} e^{3i\omega_l t}$$
$$+3E_l^2 E_r^* e^{(-i2\omega_l t + i\omega_r t)} + 2E_l E_r E_r^* e^{-i\omega_l t} - E_r^2 E_r^* e^{-i\omega_r t}$$
$$+2E_l E_l^* E_r^* e^{i\omega_r t} - 2E_l^* E_r E_r^* e^{i\omega_l t} - E_l^{*2} E_r^* e^{(i2\omega_l t + i\omega_r t)}$$
$$+3E_l E_r^{*2} e^{(i2\omega_r t - i\omega_l t)} + E_r E_r^{*2} e^{i\omega_r t} + E_l^* E_r^{*2} e^{(i2\omega_r t + i\omega_l t)}$$
$$+E_r^{*3} e^{i3\omega_r t}\}. \qquad \text{(A.67d)}$$

Substituting (A.35) into (A.29), the nonlinear polarization is

$$P_x = \frac{1}{4\sqrt{2}}\{E_l^2 E_r e^{(-2i\omega_l t - i\omega_r t)} + E_l E_r^2 e^{(-i\omega_l t - 2i\omega_r t)} + E_l^2 E_l^* e^{-i\omega_l t}$$
$$+2E_l^* E_l E_r e^{-i\omega_r t} + E_l^{*2} E_l e^{i\omega_l t} + 2E_l E_r E_r^* e^{-i\omega_l t} + E_r^2 E_r^* e^{-i\omega_r t}$$
$$+2E_r^* E_l E_l^* e^{i\omega_r t} + 2E_r E_r^* E_l^* e^{i\omega_r t} + E_l^{*2} E_r^* e^{(2i\omega_l t + i\omega_r t)} + E_r E_r^{*2} e^{i\omega_r t}$$
$$+E_l^* E_r^{*2} e^{(i\omega_l t + 2i\omega_r t)}\}, \qquad \text{(A.68a)}$$

$$P_y = \frac{i}{4\sqrt{2}}\{E_l^2 E_r e^{(-2i\omega_l t - i\omega_r t)} - E_l E_r^2 e^{(-i\omega_l t - 2i\omega_r t)} + E_l^2 E_l^* e^{-i\omega_l t}$$
$$-2E_l^* E_l E_r e^{-i\omega_r t} - E_l^{*2} E_l e^{i\omega_l t} + 2E_l E_r E_r^* e^{-i\omega_l t} - E_r^2 E_r^* e^{-i\omega_r t}$$
$$+2E_r^* E_l E_l^* e^{i\omega_r t} - 2E_r E_r^* E_l^* e^{i\omega_r t} - E_l^{*2} E_r^* e^{(2i\omega_l t + i\omega_r t)} + E_r E_r^{*2} e^{i\omega_r t}$$
$$+E_l^* E_r^{*2} e^{(i\omega_l t + 2i\omega_r t)}\}. \qquad \text{(A.68b)}$$

After simplifying (A.68) and leaving only those terms which are at the frequencies of ω_r or ω_l, we have

$$P_x = \frac{1}{4\sqrt{2}}\{E_l |E_l|^2 e^{-i\omega_l t} + 2|E_l|^2 E_r e^{-i\omega_r t} + 2E_l |E_r|^2 e^{-i\omega_l t}$$
$$+E_r |E_r|^2 e^{-i\omega_r t}\} + \text{c.c.}, \qquad \text{(A.69a)}$$

$$P_y = \frac{i}{4\sqrt{2}}\{E_l |E_l|^2 e^{-i\omega_l t} - 2E_r |E_l|^2 e^{-i\omega_r t} + 2E_l |E_r|^2 e^{-i\omega_l t}$$
$$-E_r |E_r|^2 e^{-i\omega_r t}\} + \text{c.c.}. \qquad \text{(A.69b)}$$

Finally, the total nonlinear polarization can be expressed as:

$$\vec{P}_{NL} = P_x \vec{e}_x + P_y \vec{e}_y$$

$$= \frac{1}{4\sqrt{2}}\{|E_l|^2 + 2|E_r|^2\}E_l e^{-i\omega_l t}(\vec{e_x} + i\vec{e_y})$$
$$+ \frac{1}{4\sqrt{2}}\{|E_r|^2 + 2|E_l|^2\}E_r e^{-i\omega_r t}(\vec{e_x} - i\vec{e_y}) + c.c.. \quad (A.70)$$

i.e.

$$\vec{P}_{NL} = \frac{1}{4}\{|E_l|^2 + 2|E_r|^2\}E_l e^{-i\omega_l t}\vec{e_l} + \frac{1}{4}\{|E_r|^2 + 2|E_l|^2\}E_r e^{-i\omega_r t}\vec{e_r}. \quad (A.70)$$

Right- and left-handed components are:

$$P_r = \frac{1}{4}\{|E_r|^2 + 2|E_l|^2\}E_r e^{-i\omega_r t}, \quad (A.71a)$$
$$P_l = \frac{1}{4}\{|E_l|^2 + 2|E_r|^2\}E_l e^{-i\omega_l t}. \quad (A.71b)$$

Substituting (A.71) into the nonlinear wave equations (II.22), we have the nonlinear wave equations for XPM of the two opposite rotating circularly polarized optical waves:

$$\frac{\partial A_r}{\partial z} + \frac{1}{v_{gr}}\frac{\partial A_r}{\partial t} + \frac{i}{2}k^{(2)}\frac{\partial^2 A_r}{\partial t^2} = i\frac{\omega_r n_2}{c}(\frac{2}{3}|A_r|^2 + \frac{4}{3}|A_l|^2)A_r, \quad (A.72a)$$
$$\frac{\partial A_l}{\partial z} + \frac{1}{v_{gl}}\frac{\partial A_l}{\partial t} + \frac{i}{2}k^{(2)}\frac{\partial^2 A_l}{\partial t^2} = i\frac{\omega_l n_2}{c}(\frac{2}{3}|A_l|^2 + \frac{4}{3}|A_r|^2)A_l. \quad (A.72b)$$

where $A_1(z,t)$ and $A_2(z,t)$ are the amplitude envelopes of the laser pulses, and ω_r, ω_l are their frequencies. The first and second terms in the right sides of the Eqs. (A.72) are

SPM and XPM processes, respectively. The coefficient of DXPM which is 3/4 is twice of that for SPM which is 2/3.

Assuming that the group velocity dispersion temporal broadening can be neglected, and the nonlinear medium is not optical active, $V_{gl}=V_{gr}$. These equations (A.72) can be solved by using the same method from (A.30) to (A.55). By denoting the slowly changing envelope and phase of the pulse with A and α, we obtain:

$$A_R(\tau,z) = a_{R(\tau,z)} e^{i\alpha_R(\tau,z)}, \tag{A.73a}$$

$$A_L(\tau,z) = a_{L(\tau,z)} e^{i\alpha_L(\tau,z)}, \tag{A.73b}$$

Eqs. (A.72) reduce to

$$\frac{\partial a_R}{\partial z} = 0, \tag{A.74a}$$

$$\frac{\partial a_L}{\partial z} = 0, \tag{A.74b}$$

$$\frac{\partial \alpha_R}{\partial z} = i\frac{\omega}{c} n_2 [\frac{2}{3} a_R^2 + \frac{4}{3} a_L^2], \tag{A.74c}$$

$$\frac{\partial \alpha_L}{\partial z} = i\frac{\omega}{c} n_2 [\frac{2}{3} a_L^2 + \frac{4}{3} a_R^2], \tag{A.74d}$$

where $\tau = (t - z/\upsilon_{gl})/\tau_0$ is defined as the pulse local time and τ_0 is the 1/e pulse duration. In addition, Gaussian pulse shapes are chosen at the input z=0:

$$A_R(\tau, z=0) = a_{R0} e^{-\tau^2/2}, \tag{A.75a}$$

$$A_L(\tau, z=0) = a_{L0} e^{-\tau^2/2}, \tag{A.75b}$$

where a_{10} and a_{20} is the input peak amplitudes of the laser pulses. With these initial conditions, the solutions for the amplitudes and phases of the pulse after propagating in optical fiber with length z are

$$a_{R(\tau,z)} = a_{R0}, \tag{A.76a}$$

$$a_{L(\tau,z)} = a_{L0}, \tag{A.76b}$$

$$\alpha_R(\tau, z) = \frac{\omega}{c} n_2 z\left(\frac{2}{3} I_{R0} + \frac{4}{3} I_{L0}\right) e^{-\tau^2}, \tag{A.76c}$$

$$\alpha_L(\tau, z) = \frac{\omega}{c} n_2 z\left(\frac{2}{3} I_{L0} + \frac{4}{3} I_{R0}\right) e^{-\tau^2}, \tag{A.76d}$$

where I_{10} and I_{20} are the intensities of the two circularly polarized input laser pulses. Eqs. (A.76) give the amplitudes and phases caused by SPM and DXPM processes for two circularly polarized laser pulses propagating in an optical fiber or any other nonlinear medium. Finally, the spectral profiles of the XPM and SPM processes can be studied by computing the Fourier transform as shown in Eqs. (A.23) and (A.24).

A.5 Nonlinear Wave Equation of Cross-phase Modulation (XPM) for two circularly polarized optical waves at the same rotating direction

For two circularly polarized optical waves at the same rotating direction, the total electric field can be expressed as:

$$\vec{E} = (E_1 + E_2)\vec{e}_r, \tag{A.77}$$

where two right-handed circularly polarized optical waves were used (we also can used two left-handed circularly polarized optical waves, the results are the same). We have

$$E_x = \frac{1}{\sqrt{2}}(E_1 + E_2), \tag{A.78a}$$

$$E_y = -\frac{i}{\sqrt{2}}(E_1 + E_2), \tag{A.78b}$$

for two optical waves at different frequencies, the electric fields are:

$$E_{x(z,t)} = \frac{1}{2\sqrt{2}}\{E_1 e^{-i(\omega_1 t - \beta_1 z)} + E_2 e^{-i(\omega_2 t - \beta_2 z)}\} + c.c., \tag{A.79a}$$

$$E_{y(z,t)} = -\frac{i}{2\sqrt{2}}\{E_1 e^{-i(\omega_1 t - \beta_1 z)} + E_2 e^{-i(\omega_2 t - \beta_2 z)}\} + c.c.. \tag{A.79b}$$

Using (A.59) which is

$$P_x = \chi(E_x^3 + E_x E_y^2), \tag{A.59a}$$

$$P_y = \chi(E_y^3 + E_y E_x^2). \tag{A.59b}$$

One has

$$(a + a_{c.c.})^2 = a^2 + a a^* + c.c, \tag{A.80a}$$

$$(a + a_{c.c.})^3 = a^3 + 3a^2 a^* + c.c, \tag{A.80b}$$

$$(a + a_{c.c.})(b + b_{c.c.}) = ab + a b^* + c.c, \tag{A.80c}$$

Assuming

$$a = E_1 e^{-i(\omega_1 t - \beta_1 z)}, \tag{A.81a}$$

$$b = E_2 e^{-i(\omega_2 t - \beta_2 z)}, \tag{A.81b}$$

one has

$$E_{x(z,t)} = \frac{1}{2\sqrt{2}}(a+b+a^*+b^*), \tag{A.82a}$$

$$E_{y(z,t)} = -\frac{i}{2\sqrt{2}}(a+b-a^*-b^*), \tag{A.82b}$$

and

$$\begin{aligned}
E_x E_y^2 &= \frac{1}{16\sqrt{2}}(a+b+c.c.)(-ia-ib+c.c.)^2 \\
&= \frac{1}{16\sqrt{2}}(a+b+c.c.)[(-ia-ib)^2+(-ia-ib)(ia^*+ib^*)+c.c] \\
&= \frac{1}{16\sqrt{2}}(a+b+c.c)[(a+b)\ (a^*+b^*-a-b)+c.c] \\
&= \frac{(a+b)}{16\sqrt{2}}[(a+b)\ (a^*+b^*-a-b)+(a+b)^*(-a^*-b^*+a+b)+c.c] \\
&= \frac{(a+b)}{16\sqrt{2}}[(a+b)\ (a^*+b^*-a-b)+(a+b)^*(-a^*-b^*+a+b)]+c.c \\
&= -\frac{1}{16\sqrt{2}}[(a+b)\ (a+b+-a^*-b^*)^2]+c.c,
\end{aligned} \tag{A.83a}$$

and

$$\begin{aligned}
E_x^3 &= \frac{1}{16\sqrt{2}}(a+b+c.c)^3 \\
&= \frac{1}{16\sqrt{2}}\{(a+b)^3+3(a+b)^2(a+b)^*+c.c\},
\end{aligned} \tag{A.83b}$$

substituting (A.83) into (A.59) and leaving only those terms which are at the frequencies of ω_1 or ω_2, we have

$$P_x = \frac{1}{8\sqrt{2}}\{2|a|^2a\ +2|b|^2b\ +|a|^2b\ +|b|^2a\ +c.c\}. \tag{A.84}$$

Substituting Eq. (A.81) into (A.84) for Px, one has

$$P_x = \frac{1}{8\sqrt{2}}\{[2|E_2|^2 + |E_1|^2]E_2 e^{-i(\omega_2 t - \beta_2 z)} + [2|E_2|^2 + |E_1|^2]E_2 e^{-i(\omega_2 t - \beta_2 z)}\}\vec{e_x} + c.c., \quad \text{(A.85a)}$$

P_y which is very similar to P_x (only difference is 90 degree phase, i) can be calculated using the same method and the result are also similar as following

$$P_y = -\frac{i}{8\sqrt{2}}\{[2|E_2|^2 + |E_1|^2]E_2 e^{-i(\omega_2 t - \beta_2 z)} + [2|E_2|^2 + |E_1|^2]E_2 e^{-i(\omega_2 t - \beta_2 z)}\}\vec{e_y} + c.c.. \quad \text{(A.85b)}$$

Finally, the total nonlinear polarization can be expressed as:

$$\begin{aligned}\vec{P_{NL}} &= P_x\vec{e_x} + P_y\vec{e_y} \\ &= \frac{1}{8\sqrt{2}}[2|E_1|^2 + |E_2|^2]E_1 e^{-i(\omega_1 t - \beta_1 z)}(\vec{e_x} - i\vec{e_y}) \\ &+ \frac{1}{8\sqrt{2}}[2|E_2|^2 + |E_1|^2]E_2 e^{-i(\omega_2 t - \beta_2 z)}(\vec{e_x} - i\vec{e_y}) + c.c.. \quad \text{(A.86)}\end{aligned}$$

i.e.

$$\vec{P_{NL}} = \frac{1}{8}\{[2|E_1|^2 + |E_2|^2]E_1 e^{-i(\omega_1 t - \beta_1 z)} + [2|E_2|^2 + |E_1|^2]E_2 e^{-i(\omega_2 t - \beta_2 z)}\}\vec{e_r}.$$

The components synchronized with frequencies at ω_1 and ω_2,are:

$$P_1 = \frac{1}{8}\{2|E_1|^2 + |E_2|^2\}E_1 e^{-i(\omega_1 t - \beta_1 z)}, \quad \text{(A.87a)}$$

$$P_2 = \frac{1}{8}\{2|E_2|^2 + |E_1|^2\}E_2 e^{-i(\omega_2 t - \beta_2 z)}, \quad \text{(A.87b)}$$

substituting the nonlinear polarization components in Eqs. (A.87) into (II.22) for different optical waves at the frequencies of ω_1 and ω_2, one obtains the nonlinear wave equation for the XPM process of two circularly polarized optical waves having the same rotating direction are;

$$\frac{\partial A_1}{\partial z} + \frac{1}{v_{g1}}\frac{\partial A_1}{\partial t} + \frac{i}{2}k^{(2)}\frac{\partial^2 A_1}{\partial t^2} = i\frac{\omega_1 n_2}{c}\left(\frac{2}{3}|A_1|^2 + \frac{1}{3}|A_2|^2\right)A_1, \quad \text{(A.88a)}$$

$$\frac{\partial A_2}{\partial z} + \frac{1}{v_{g1}}\frac{\partial A_2}{\partial t} + \frac{i}{2}k^{(2)}\frac{\partial^2 A_2}{\partial t^2} = i\frac{\omega_2 n_2}{c}\left(\frac{2}{3}|A_2|^2 + \frac{1}{3}|A_1|^2\right)A_2. \quad \text{(A.88b)}$$

where υ_{gi} is the group velocity for the wave i (i=1,2), $k_i^{(2)}$ is the group velocity dispersion for the wave i, A_i is the amplitude envelope of the optical wave i, ω_i is the frequency, and $n_2=3\chi^{(3)}/8n$ is the nonlinear refractive index. The first terms in the right sides of Eqs. (A.88) are SPM terms and the second terms are the XPM terms. Eqs. (A.88) also show that SPM terms are twice larger than XPM terms for two optical waves at the same circular polarization state.

THESIS PUBLICATIONS, PRESENTATIONS AND PROCEEDING OF Q. D. LIU

PUBLICATIONS:

[1]. Q. D. Liu, W. L. Sha, P. P. Ho, and R. R. Alfano, "Intensity dependent polarization twisting within the temporal profiles of optical pulses in a nonbirefringent single-mode optical fiber", accepted, to be published in JOSA B, may, 96.

[2]. Q. D. Liu, L. Shi, P. P. Ho, and R. R. Alfano, "Nonlinear vector rotation and depolarization of femtosecond laser pulses propagating in nonbirefringent single-mode optical fibers", to be published in Opt. Lett..

[3]. Q. D. Liu, L. Shi, P. P. Ho, R. R. Alfano, R. -J. Essiambre, and G. P. Agrawal, "Degenerate-cross-phase modulation of femtosecond laser pulses in a birefringent single-mode optical fiber", submitted to Opt. Lett..

[4]. Q. D. Liu, J. Qureshi, P. P. Ho, R. R. Alfano, "Polarization stability of laser pulses propagating in nonbirefringent single-mode optical fibers", to be submitted to JOSA B.

[5]. Q. D. Liu, L. Shi, P. P. Ho, R. R. Alfano, R. -J. Essiambre, and G. P. Agrawal, "Degenerate-cross-phase modulation of femtosecond laser pulses in a nonbirefringent single-mode optical fiber", to be submitted to Opt. Lett..

[6]. J. T. Chen, Q.D. Liu, P. P. Ho, and R. R. Alfano, "Comparison of nonlinear effects of linearly and circularly polarized picosecond pulses propagating in optical fibers", J. Opt. Sc. Am. B, **12**, 907 (1995).

[7]. I. Zeylikovich, Q. D. Liu, G. Bai, N. Zhadin, A. Gorokhovsky, and R. R. Alfano, "Interferometric 2D imaging amplitude correlator for ultrafast pulses", Opt. Commun., **115**, 485 (1995).

[8]. Q. Z. Wang, Q. D. Liu, P. P. Ho, E. Walge, and R. R. Alfano, "High resolution spectra of cross-phase modulation in optical fibers", Opt. Lett., 19, 1636 (1994).

[9]. Q. Z. Wang, Q. D. Liu, Disa, P. P. Ho, and R. R. Alfano, "High resolution spectra of self-phase modulation in optical fibers", J. Opt. Soc.Am. B, **11**, 1084 (1994).

[10]. Q.D. Liu, J. T. Chen, Q. Z. Wang, P. P. Ho, and R. R. Alfano, "Polarization stability of circularly polarized laser pulses propagating in nonbirefringent single-mode optical fibers", IEEE Phot. Tech. Lett., **7**, 517 (1995).

[11]. Q. D. Liu, J. T. Chen, Q. Z. Wang, P. P. Ho, and R. R. Alfano, "Single-pulse degenerate-cross-phase modulation in nonbirefringent single-mode optical fibers", Opt. Lett., **20**, 542 (1995).

PRESENTATIONS AND PROCEEDING:

[1]. Q. D. Liu, L. Shi, W. L. Sha, P. P. Ho, and R. R. Alfano, "Vector characteristics of femtosecond laser pulses propagating in single-mode optical fibers", CLEO/QELS'95, **QELS-16**, 179 (1995).

[2]. Q. Z. Wang, Q. D. Liu, P. P. Ho, E. Walge, and R. R. Alfano, "Wavelength multiplexer signal encoding for ultrafast XPM A/D converter", OSA'94 Annual Meeting.

[3]. P. P. Ho, Q. Z. Wang, Q. D. Liu, Disa Liu, and R. R. Alfano, "High resolution spectra of cross-phase modulation for A/D converter", Optoelectronic Signal Processing for Phased-array Antennas IV, SPIE Proc. vol **2155**, 37 (1994).

[4]. P. P. Ho, Q. Z. Wang, Q. D. Liu, Disa Liu, and R. R. Alfano, "Induced beam deflection for ultrafast low-signal level optical waveform digitization", Optoelectronic Signal Processing for Phased-array Antennas IV, SPIE Proc. vol **2155**, 157 (1994).

BIBLIOGRAPHY

Chapter 1

[1]. A. C. S. Van Heel, Nature **173**, 39 (1954).

[2]. N. S. Kapany, J. Opt. Soc. Am. **49**, 779 (1959).

[3]. N. S. Kapany, *Fiber Optics: Principles and Applications* (Academic, New York, 1967)

[4]. D. N. Payne and W. A. Gambling, Electron. Lett., **10**, 289 (1974).

[5]. W. G. French, J. B. McChesney, P. B. O'Connor and G. W. Tasker, Bell Sys. Tech. J., **53**, 951 (1974).

[6]. T. Miya, Y. Terunuma, T. Hosaka and T. Miyoshita, Electron. Lett., **15**, 106 (1979).

[7]. Y. Suematsu, Proc. IEEE **71**, 692 (1983).

[8]. T. Li, IEEE J. Sel. Areas Commun. **SAC-1**, 356 (1983).

[9]. E. E. Basch, ed., *Optical Fiber Transmission* (Sams, Indianapolis, 1986).

[10]. S. E. Miller and I. P. Kaminow, eds., *Optical Fiber Telecommunications II* (Academic, Boston, 1989).

[11]. Y. Suemastu, Proc. IEEE, **71**, 692 (1983).

[12]. T. Li, IEEE, J. Sel. Areas Commun., **SAC-1**, 356 (1983).

[13]. E. E. Basch, ed., *Optical Fiber Transmission*, (Sams, Indianapolis, 1986).

[14]. S. E. Miller, and I. P. Kaminow, eds., *Optical Fiber Telecommunication II*, (Academic, Boston, 1988).

[15]. G. P. Agrawal, ed., *Nonlinear Fiber Optics* (Academic Press, New York, 1989).

[16]. R. R. Alfano and Shapiro, Phys. Rev. Lett. **24**, 584, (1970).

[17]. R. R. Alfano and Shapiro, Phys. Rev. Lett. **24**, 592, (1970).

[18] Q. Z. Wang, Q. D. Liu, P. P. Ho and R. R. Alfano, J. Opt. Soc. Am. B **11**, 1084 (1994).

[19]. M. N. Islam, L. F. Mollenauer, R. H. Stolen, J. R. Simpson, H. T. Shang, Opt. Lett. **12**, 625 (1987).

[20]. P. L. Baldeck, R. R. Alfano and G. P. Agrawal, Appl. Phys. Lett. **52**, 1939 (1988).

[21]. Q. Z. Wang, P. P. Ho and R. R. Alfano, Opt. Lett. **15**, 1023 (1990).

[22]. R. H. Stolen, E. P. Ippen and A. R. Tynes, Appl. Phys. Lett., **20**, 62 (1972).

[23]. E. P. Ippen and R. H. Stolen, Appl. Phys. Lett., **21**, 539 (1972).

[24]. R. G. Smith, Appl. Opt., **11**, 2489 (1972).

[25]. R. H. Stolen and A. Ashkin, Appl. Phys. Lett., **22**, 294 (1973).

[26]. R. H. Stolen, J. E. Bjorkholm and A. Ashkin, Appl. Phys. Lett., **24**, 308 (1974).

[27]. R. H. Stolen, IEEE J. Quantum Electron. **QE-11**, 100 (1975).

[28]. L. F. Mollenauer, R. H. Stolen and J. P. Gordon, Phys. Rev. Lett., **45**, 1095 (1980).

[29]. H. G. Winful, Opt. Lett., **11**, 33 (1986).

[30]. S. F. Feldman, D. A. Weinberger, and H. G. Winful, Opt. Lett., **15**, 311 (1990).

[31]. S. Trillo, S. Wabnitz, R. H. Stolen, G. Assanto, C. T. Seaton, and G. I. Stegeman, Appl. Phys. Lett., **49**, 1224 (1986).

[32]. L. F. Mollenauer, R. H. Stolen, and J. P. Gordon, Phys. Rev. Lett., **45**, 1095 (1980).

[33]. L. F. Mollenauer, and R. H. Stolen, Opt. Lett., **9**, 13 (1984).

[34]. L. F. Mollenauer, J. P. Gordon, and M. N. Islam, IEEE J. Quantum Electron., **QE-22**, 157 (1986).

[35]. M. N. Islam, L. F. Mollenauer, R. H. Stolen, and J. R. Simpson, and H. T. Shang, Opt. Lett., **12**, 814 (1987).

[36]. A. S. Gouveia-Neto, A. S. L. Gomes, and J. R. Taylor, Opt. Quantum Electron., **20**, 165 (1988).

[37]. J. D. Kafka, and T. Baer, Opt. Lett., **12**, 181 (1987).

[38]. P. J. Dean ed., *Optical Communication Systems* (Prentice Hall International, UK, 1984)

[39]. R. H. Stolen, V. Ramaswamy, P. Kaiser and W. Pleibel, Appl. Phys. Lett., **33**, 699 (1978).

[40]. I. P. Kaminow, IEEE J. Quantum Electron. **QE-17**, 15 (1981).

[41]. Q. Z. Wang, Q. D. Liu, P. P. Ho and R. R. Alfano, Opt. Lett. **19**, 1636 (1994).

[42]. Q. D. Liu, J. T. Chen, Q. Z. Wang, P. P. Ho and R. R. Alfano, IEEE Photon. Tech. Lett., 7, 517 (1995).

[43]. M. J. LaGasse, D. Liu-wong, J. G. Fujimoto and H. A. Haus, Opt. Lett. **14**, 311 (1989).

[44]. Y. Kimura, K. I. Kitayama, N. Shibata and S. Seikai, Electron. Lett. **22**, 277 (1986).

[45]. J. -M. Jeong and M. E. Marhic, Opt. Comm. **85**, 430 (1991).

[46]. A. S. Davison and I. H. White, Opt. Lett. **14**, 802 (1988).

[47]. M. E. Marhic, C. H. Hsia and J. -M. Jeong, Electron. Lett. **27**, 27 (1991).

[48]. T. Morioka, M. Saruwatari and A. Takada, Electron. Lett. **27**, 210 (1991).

[49]. J. -M. Jeong and M. E. Marhic, Opt. Comm. **91**, 115 (1992).

[50]. A. M. Weiner, J. P. Heritage and J. A. Salehi, Opt. Lett. **13**, 300 (1988).

[51]. M. A. Flavin and J. L. Horner, Appl. Opt. **28**, 1692 (1989).

[52]. B. L. Shoop and J. W. Goodman, Appl. Opt. **31**, 5654 (1992).

[53]. P. P. Ho, Q. Z. Wang, Q. D. Liu , Disa Liu, and R. R. Alfano, Optoelectronic Signal Processing for Phased-array Antennas IV, SPIE Proc. Vol. **2155**, 157 (1994).

[54]. P. P. Ho, Q. Z. Wang, Q. D. Liu , Disa Liu, and R. R. Alfano, Optoelectronic Signal Processing for Phased-array Antennas IV, SPIE Proc. Vol. **2155**, 37 (1994).

[55]. N. Nakazawa, Appl. Phys. Lett., **46**, 628 (1985).

[56]. M. J. Mohony, in Digest of Conference on Integrated Optics and Optical Fiber Communication (Istituto Internazionale Delle Conmmunicazioni, Venice, Italy, 1985).

[57]. R. J. Mears, L. Reekie, I. M. Jauncey and D. N. Payne, Electron. Lett., **23**, 1026 (1987).

[58]. M. Nakazawa, K. Kurokawa, H. Kubota, K. Suzuki and Y. Kimura, Appl. Phys. Lett., 57, 653 (1990).

[59]. A. S. Davison and I. H. White, Opt. Lett., **14**, 802 (1989).

Chapter 2

[1]. P. L. Baldeck, R. R. Alfano, and G. P. Agrawal, Ultrafast Phenomena **6**, p 53-55 (Springer-Verlag, Berlin, Heilderberg 1988).

[2]. J. T. Manassah, P. L. Baldeck, and R. R. Alfano, Opt. Lett., **13**, 1090 (1988).

[3]. P. L. Baldeck, P. P. Ho, and R. R. Alfano, Rev. Phys. Appl., **22**, 1677 (1987).

[4]. R. R. Alfano, P. L. Baldeck, and P. P. Ho, J. Opt. Soc. Am **B 6**, 824 (1989).

[5]. P. L. Baldeck, P. P. Ho, and R. R. Alfano, *The Supercontinuum Laser Source*, pp 117, chapter 4 (Springer-Verlag, Berlin, 1989).

[6]. P. L. Baldeck, R. Garuthara, F. Raccah, and R. R. Alfano, Proceeding paper #TuC4, ILS-III, Atlantic City, N. J. (1987).

[7]. P. L. Baldeck, R. R. Alfano, and G. P. Agrawal, Appl. Phys. Lett., **52**, 1939 (1988).

[8]. R. R. Alfano, P. L. Baldeck, F. Raccah, and P. P. Ho, Appl. Opt., **26**, 3491 (1987).

[9]. J. T. Manassah, P. L. Baldeck, and R. R. Alfano, Appl. Opt., **27**, 3586 (1988).

[10]. P. L. Baldeck, F. Raccah, and R. R. Alfano, Opt. Lett., **12**, 588 (1987).

[11]. Y. R. Shen, *The Principles of Nonlinear Optics*, (Wiley, New York, 1971).

[12]. J. A. Amstrong, N. Bloembergen, J. Ducuining, and P. S. Pershan, Phys. Rev., **127**, 1918 (1962).

[13]. N. Bloembergen, *Nonlinear Optics* (Benjamin, New York, 1965).

[14]. N. Bloembergen, P. S. Pershan, Phys. Rev., **128**, 606 (1965).

[15]. S. A. Akmanov, A. S. Chirkin, K. N. Drabovich, A. I. Kovrigin, R. V. Khokholov, and A. P. Sukhorukov, IEEE J. Quantum Electron., **QE-4**, 598 (1968).

[16]. R. R. Alfano ed., *The Supercontinuum Laser Source*, chapter 2 (Springer-Verlag, New York, 1990).

[17]. F. Shimisu, Phys. Rev. Lett., **19**, 1097 (1967).

[18]. R. R. Alfano, and S. L. Shapiro, Phys. Rev. Lett., **24**, 584, 592, and 1219 (1970).

[19]. R. R. Alfano, Interaction of picosecond pulses with matter, GTE Technical Report TR-72-330.1 (1972) and Ph. D. Thesis, New York University (1972).

[20]. R. H. Stolen, and C. Lin, Phys. Rev., A **17**, 1448 (1978).

[21]. Q. Z. Wang, Q. D. Liu, Disa Liu, P. P. Ho, and R. R. Alfano, J. Opt. Soc. Am., B **11**, 1084 (1994).

[22]. S. De Silvestri, P. Laporta, and O. Svelto, IEEE, J. Quantum Electron., **QE-20**, 533 (1984).

[23]. W. Rudolph, and B. Wilhelmi, ed., *Light Pulse Compression*, (Char: Harwood), (1989).

[24]. W. J. Tomlinson, R. H. Stolen, and C. V. Shank, J. Opt. Soc. Am. B, **1**,139 (1984).

[25]. A. S. L. Gomes, A. S. Gouveia-Neto, and J. R. Taylor, Opt. Quantum Electron., **20**, 95 (1988).

[26]. H. Nakatsuka, D. Grischkowsky, and A. C. Balant, Phys. Rev. Lett., **47**, 1910 (1988).

[27]. C. V. Shank, R. L. Fork, R. Yen, R. H. Stolen, Appl. Phys. Lett., **40**, 761 (1982).

[28]. R. Fork, C. Shank, C. Hirliman, and R. Yen, Opt. Lett., **8**, 1 (1983).

[29]. G. Yang, and Y. R. Shen, Opt. Lett., **9**, 510 (1984).

[30]. T. Jimbo, V. L. Caplan, Q. X. Li, Q. Z. Wang, P. P. Ho, and R. R. Alfano, Opt. Lett., **12**, 477 (1987).

[31]. T. K. Gustafson, J. Taran, P. Kelley, and R. Chiao, Opt. Commun., **2**, 17 (1970).

[32]. R. R. Alfano, Q. X. Li, T. Jimbo, T. Manassah, and P. P. Ho, Opt. Lett., **11**, 626 (1986).

[33]. R. R. Alfano, P. L. Baldeck, F. Raccah, and P. P. Ho, Appl. Opt., **26**, 3491 (1987).

[34]. P. L. Baldeck, R. R. Alfano, and G. P. Agrawal, Appl. Phys. Lett., **52**, 1939 (1988).

[35]. R. R. Alfano, Q. Z. Wang, T. Jimbo, and P. P. Ho, Phys. Rev., A **35**, 459 (1987).

[36]. J. E. Rothenberg, Opt. Lett., **15**, 495 (1990).

[37]. J. Gersten, R. R. Alfano, and M. Beli, Phys. Rev., A **21**, 1222 (1980).

[38]. Q. Z. Wang, Q. D. Liu, P. P. Ho, E. K. Walge, and R. R. Alfano, Opt. Lett., **19**, 1638 (1994).

[39]. P. P. Ho, and R. R. Alfano, IEEE J. Quantum Electron., **24**, 351 (1988).

[40]. Q. Z. Wang, P. P. Ho, and R. R. Alfano, Opt. Lett., **15**, 1023 (1990).

[41]. I. P. Kaminow, IEEE J. Quantum Electron., QE-**17**, 15 (1981).

[42]. N. G. Walker and G. R. Walker, J. of Lightwave Tech., LT-**8**, 438, (1990).

[43]. R. H. Stolen, V. Ramaswamy, P. Kaiser, and W. Pleibel, Appl. Phys. Lett., **33**, 699 (1978).

[44]. F. M. Sears, J. Lightwave Tech., **8**, 684 (1990).

[45]. D. N. Payne, A. J. Barlow, and J. R. Ramskov, IEEE J. Quantum Electron., QE-**18**, 477 (1982).

[46]. J. I. Sakai, S. Machida, and T. Kimura, IEEE J. Quantum Electron., QE-**18**, 488 (1982).

[47]. S. F. Feldman, D. A. Weinberger, and H. G. Winful, Opt. Lett., **15**, ,311 (1990).

[48]. H. G. Winful, Opt. Lett., **11**, 33 (1986).

[49]. F. Matera, and S. Wabnitz, Opt. Lett., **11**, 467 (1986).

[50]. B. Crosignani, P. D Porto, Opt. Acta, **32**, 1251 (1985).

[51]. B. Crosignani, B. Daino, P. D. Porto, J. Opt. Am. B, **3**, 1120 (1986).

[52]. H. G. Winful, Appl. Phys. Lett. **47**, 213 (1985).

[53]. P. D. Maker, R. W. Terhune, and C. M. Savage, Phys. Rev. Lett. **12**, 507 (1964).

[54]. A. Owyoung, R. W. Hellwarth, and N. George, Phys. Rev. B, **5**, 628 (1972).

[55]. R. Kashyap, and N. Finlayson, Opt. Lett. **17**, 405 (1992).

[56]. S. Trillo, S. Wabnitz, R. H. Stolen, G. Assanto, C. T. Seaton, and G. I. Stegeman, Appl. Phys. Lett. **49**, 1224 (1986).

[57]. E. Lichtman, R. G. Waarts, A. A. Friesem, and S. Tang, Appl. Opt. **28**, 4056 (1988).

[58]. Q. D. Liu, J. T. Chen, Q. Z. Wang, P. P. Ho, and R. R. Alfano, Opt. Lett., **20**, 542 (1995).

Chapter 3

[1]. W. Kaiser ed., *Topics in Applied Physics, Vol. 60: Ultrashort Laser Pulses* (Springer-Verlag, 1988).

[2]. W. Keochner ed., *Solid-State Laser Engineering,* Springer Verlag Series in Optical Science (Springer-Verlag, 1988).

[3]. Q. Z. Wang, Q. D. Liu, Disa Liu, P. P. Ho, and R. R. Alfano, J. Opt. Soc. Am., **11**, 1084 (1994).

[4]. O. Svelto, *Principles of Lasers,* 2nd edition (Plenum Press, New York and London, 1982).

[5]. J. Wilson, and J. F. B. Hawkes, *Lasers: Principles and applications,* (Prentice Hall,1987).

[6]. Ch. Spielman, P. F. Curley, T. Brabec, E. Wintner, and F. Krausz, Electron. Lett., **28**, 1532 (1992).

[7]. C. P. Huang, M. T. Asaki, S. Backus, M. M. Murnane, H. C. Kapteyn, and H. Nathel, Opt. Lett., **17**, 1289 (1992).

[8]. B. Proctor, and F. Wise, Opt. Lett., **17**, 1295 (1992).

[9]. B. E. Lemoff, and C. P. Barty, Opt. Lett., **17**, 1367 (1992).

[10]. P. J. Delfyett, S. K. Gayen, and R. R. Alfano, Encyclopedia of Physical Science and Technology, **14**, Academic Press Inc., 169 (1987).

[11]. N. Ockman, W. B. Wang, and R. R. Alfano, J. Modern Phys., **B5**, 3165 (1991).

[12]. E. P. Ippen, C. V. Shank in *Ultrashort Light Pulses* ed. by Shapiro (Springer-Verlag, New York, 1977).

[13]. A. G. Doukas, J. Buckett, R. R. Alfano in *Biological Events Probed by Ultrafast Laser Spectroscopy*, ch 17, ed. by R. R. Alfano (Academic Press, San Diego, 1982).

Chapter 4

[1] I. P. Kaminow, IEEE J. Quantum Electron., QE-**17**, 15 (1981).

[2] N. G. Walker and G. R. Walker, J. of Lightwave Tech., LT-**8**, 438 (1990).

[3] R. H. Stolen, V. Ramaswamy, P. Kaiser, and W. Pleibel, Appl. Phys. Lett., **33**, 699 (1978).

[4] F. M. Sears, J. Lightwave Tech., **8**, 684 (1990).

[5] D. N. Payne, A. J. Barlow, and J. R. Ramskov, IEEE J. Quantum Electron., QE-**18**, 477 (1982).

[6] J. I. Sakai, S. Machida, and T. Kimura, IEEE J. Quantum Electron., QE-**18**, 488 (1982).

[7] R. R.Alfano and S. L. Shapiro, Phys. Rev. Lett., **24**, 592 (1970); Phys. Rev. Lett., **24**, 1219 (1970).

[8] R. Fork, C. Shank, C. Hirliman and R. Yen, Opt. Lett., **8**, 1 (1983).

[9] R. R Alfano and P. P. Ho, IEEE J. Quantum Electron., QE-**24**, 351 (1988).

[10] P. L. Baldeck and R. R. Alfano, IEEE J. Lightwave Tech. LT-**5**, 1712 (1987).

[11] S. F. Feldman, D. A. Weinberger, and H. G. Winful, Opt. Lett., **15**, 311 (1990).

[12] S. Trillo, S. Wabnitz, R. H. Stolen, G. Assanto, C. T. Seaton, and G. I. Stegeman, Appl. Phys. Lett., **49**, 1224 (1986).

[13] H. G. Winful, Opt. Lett., **11**, 33 (1986).

[14] F. Matera, and S. Wabnitz, Opt. Lett., **11**, 467 (1986).

Chapter 5

[1] S. Trillo, S. Wabnitz, R. H. Stolen, G. Assanto, C. T. Seaton, and G. I. Stegeman, Appl. Phys. Lett.,**49**, 1224 (1986).

[2] S. F. Feldman, D. A. Weinberger, and H. G. Winful, Opt. Lett.,**15**, 311 (1990).

[3] H. G. Winful, Opt. Lett. **11**, 33 (1986).

[4] R. Kashyap, and N. Finlayson, Opt. Lett., **17**, 405 (1992).

[5] E. Lichtman, R. G. Waarts, A. A. Friesem, and S. Tang, Appl. Opt., **28**, 4056 (1989).

[6]. Q. D. Liu, J. T. Chen, Q. Z. Wang, P. P. Ho and, R. R. Alfano, IEEE Phot. Tech. Lett., **7**, 517 (1995).

[7]. Q. D. Liu, J. T. Chen, Q. Z. Wang, P. P. Ho and, R. R. Alfano, Opt. Lett., 20, 542 (1995).

Chapter 6

[1] B. Crosignani, B. Daino, P. D. Porto, J. Opt. Am. B, **3**, 1120 (1986).

[2] B. Crosignani, P. D Porto, Opt. Acta, **32**, 1251 (1985).

[3] C. Y. Menyuk, and P. K. A. Wai, J. Opt. Am. B, **11**, 1035 (1994).

[4] H. G. Winful, Appl. Phys. Lett. **47**, 213 (1985).

[5] H. G. Winful, Opt. Lett. **11**, 33 (1986).

[6] P. D. Maker, R. W. Terhune, and C. M. Savage, Phys. Rev. Lett. **12**, 507 (1964).

[7] A. Owyoung, R. W. Hellwarth, and N. George, Phys. Rev. B, **5**, 628 (1972).

[8] R. Kashyap, and N. Finlayson, Opt. Lett. **17**, 405 (1992).

[9] S. Trillo, S. Wabnitz, R. H. Stolen, G. Assanto, C. T. Seaton, and G. I. Stegeman, Appl. Phys. Lett. **49**, 1224 (1986).

[10] S. F. Feldman, D. A. Weinberger, and H. G. Winful, Opt. Lett. **15**, 311 (1990).

[11] E. Lichtman, R. G. Waarts, A. A. Friesem, and S. Tang, Appl. Opt. **28**, 4056, (1989).

[12] Q. D. Liu, J. T. Chen, Q. Z. Wang, P. P. Ho, and R. R. Alfano, IEEE Phot. Tech. Lett., **7**, 517 (1995).

[13] Q. D. Liu, W. L. Sha, P. P. Ho, and R. R. Alfano, " Nonlinear polarization twisting of picosecond laser pulses propagating in nonbirefringent single-mode optical fibers," to be published in JOSA B.

[14] Q. D. Liu, J. T. Chen, Q. Z. Wang, P. P. Ho, and R. R. Alfano, Opt. Lett., **20**, 542 (1995).

Chapter 7

[1] G. P. Agrawal, Nonlinear Fiber Optics (Academic Press, Inc., 1989), Chap. 1, p. 15.

[2] R. R. Alfano and Shapiro, Phys. Rev. Lett. **24**, 584, 1217 (1970).

[3] R. Fork, C. Shank, C. Herliman, R. Yen and W. J. Tomlinson, Opt. Lett. **8**, 1 (1983).

[4] G. Yang and Y. R. Shen, Opt. Lett. **9**, 510 (1984).

[5] R. H. Stolen and Chinlon Lin, Phys. Rev. A **17**, 1448 (1978).

[6] E. P. Ippen, C. V. Shank and T. K. Gustafson, Appl. Phys. Lett. **33**, 1765 (1974).

[7] Q. Z. Wang, Q. D. Liu, Disa Liu, P. P. Ho and R. R. Alfano, J. Opt. Soc. Am. B. **11**, 1084-1089 (1994).

[8] R. R. Alfano, Q.X. Li, T. Jimbo, J. T. Manassah, and P. P. Ho, Opt. Lett. **11**, 626 (1986).

[9] C. C. Yang and Alex J. S. Wang, J. Opt. Soc. Am. B 9, 682 (1992).

[10] M. N. Islam, L. F. Mollenauer, R. H. Stolen, J. R. Simpson, H. T. Shang, Opt. Lett. **12**, 625 (1987).

[11] P. L. Baldeck, R. R. Alfano and G. P. Agrawal, Appl. Phys. Lett. **52**, 1939 (1988).

[12] K. J. Blow, N. J. Doran and B. P. Nelson, Opt. Lett. **10**, 393 (1985)

[13] Q. Z. Wang, P. P. Ho and R. R. Alfano, Opt. Lett. **15**, 1023 (1990).

[14] B. Crosignani, B. Daino, P. D. Porto, J. Opt. Soc. Am. B **3**, 1120 (1986)

[15] H. E. Bates, R. R. Alfano and N. Schiller, Appl. Opt. **18**, 947 (1979)

[16] Q. D. Liu, J. T. Chen, P. P. Ho and R. R. Alfano, IEEE Phot. Tech. Lett., **7**, 517 (1995).

[17] M. Sylla, P. X. Nguyen, D. Rouede, and G. Rivoire, J. Appl. Phys. **71**, 5318 (1992).

[18] P. L. Baldeck, F. Raccah, and R. R. Alfano, Opt. Lett., **12**, 588 (1987).

Chapter 8

[1]. M. J. lagers, D. Liu-wong, J. G. and H. A. Has, Opt. Lett. **14**, 311-313, (1989).

[2]. Y. Kimura, K. I. Kitayama, N. Shibata and S. Seikai, Electron. Lett. **22**, 277 (1986).

[3]. J. -M. Jeong and M. E. Marhic, Opt. Comm. **85**, 430 (1991).

[4]. T. Morioka, M. Saruwatari and A. Takada, Electron. Lett. **27**, 210 (1991).

[5]. M. Nakazawa, Appl. Phys. Lett. **46**, 628 (1985).

[6]. R. J. Mears, L. Reekie, I. M. Jauncey, and D. N. Payne, Electron. Lett. **23**, 1026 (1987).

[7]. M. Nakazawa, K. Kurokawa, H. Kubota, K. Suzuki, and Y. Kimura, Appl. Phys. Lett. **57**, 653 (1990).

[8]. M. J. Mahony, in Digest of Conference on Integrated Optics and Optical Fiber Communication (Istituto Internazionale Delle Communicazioni, Venice, Italy, (1985), Vol. **2**, p. 39.

[9]. A. S. Davison, and I. H. White, Opt. Lett. **14**, 802 (1989).

[10]. S. F. Feldman, D. A. Weinberger, and H. G. Winful, Opt. Lett. **15**, 311 (1990).

[11]. R. A. Becker, C. E. Woodward, F. J. Leonberger, and R. C. Williamson, IEEE Proc., **72**, 802 (1984).

[12]. A. Armand, A. A. Sawchuck, T. C. Strand, D. Boswell, andB. H. Soffer, Opt. Lett., **5**, 129 (1980).

[13]. A. D. McAulay, Opt. Lett., **29**, 114 (1990).

[14]. R. G. Walker, and I. Bennion, SPIE, **1141**, 138 (1989).

[15]. J.-M, Jeong, and M. E. Marhic, Opt. Commu., **91**, 115 (1992).

[16]. P. P. Ho, Q. Z. Wang, Q. D. Liu, Disa Liu, and R. R. Alfano, SPIE, **2155**, 37 (1994).